Synthesis, Characterization and Evaluation of Aza-dipyrromethenes and other Small Molecules for Organic Photovoltaics

A thesis presented in partial fulfilment of the requirements for the degree of

Doctor of Philosophy

In

Chemistry

MASSEY UNIVERSITY
TE KUNENGA KI PŪREHUROA
UNIVERSITY OF NEW ZEALAND

Palmerston North, New Zealand

Emad Mohamed Abdulrazaq Al-Imarah

2014

For Mum, Dad and Huda

“anyone who has never made a mistake
has never tried anything new”

Albert Einstein, 1879-1955
theoretical physicist

Abstract

A designed series of novel boron-difluoride chelated aza-dipyrromethenes with particular physical properties have been synthesized for the purpose of exploring their usefulness as donors in organic photovoltaic (OPV) cells. Boron-difluoride chelated aza-dipyrromethenes are commonly referred in the literature as aza-BODIPYs, and this convention has been adopted in this thesis. The aza-BODIPYs synthesised were symmetrically substituted with aryl groups on the pyrrole rings. The synthesised aza-BODIPYs were: terthiophene-BF_2-aza-dipyrromethene (87), methoxy-terthiophene-BF_2-aza-dipyrromethene (88), triphenylamine-BF_2-aza-dipyrromethene (100), thiophene-triphenylamine-BF_2-aza-dipyrromethene (106), benzothiadiazole-BF_2-aza-dipyrromethene (111), benzothiadiazole-thiophene-BF_2-aza-dipyrromethene (112), benzothiadiazole-triphenylamine-BF_2-aza-dipyrromethene (113), ethylenedioxythiophene-BF_2-aza-dipyrromethene (125), thiophene-phenothiazine-BF_2-aza-dipyrromethene (132), thiophene-methylpyrrole-BF_2-aza-dipyrromethene (139), thiophene-carbazole-BF_2-aza-dipyrromethene (145), fluorenone-BF_2-aza-dipyrromethene (150), and thiophene-fluorenone-BF_2-aza-dipyrromethene (151). The numbers are used to refer to individual compounds in this thesis. Ruthenium dyes, terthiophene monomers and silicon quantum dots were also synthesised, again with a view to discovering novel donors for OPV cells.

The aza-BODIPYs were characterized spectroscopically by ultraviolet-visible (UV-VIS) absorption spectroscopy, fluorescence and time-correlated single-photon counting (TCSPC). Benzothiadiazole-triphenylamine-BF_2-aza-dipyrromethene (referred to as compound (113) in this thesis) was found to exhibit significant red-shifts in absorption (λ_{max}=855 nm) and emission (λ_{em}=953 nm). This compound showed a large bathochromic shift (205 nm) in absorption, in comparison with the standard BF_2-tetra-aryl aza-dipyrromethene (compound (4), λ_{max}=650 nm). Evidence has been found of strong intramolecular-charge-transfer (ICT) character in the excited state. It has been demonstrated how absorption and emission of aza-BODIPYs can be fine-tuned by manipulating the ICT between variously electronic donating and withdrawing substituents in the aza-BODIPY structure. Fluorescence and time-correlated single-photon counting (TCSPC) on the aza-BODIPYs in the presence of fullerenes supported the conclusion that there were charge transfer processes.

Time-dependent density functional theory (TD-DFT) has been successfully used to provide a guide to the structure-property relationships and electronic structures of the aza-BODIPYs. Absorption energies, calculated for the aza-BODIPYs using the B3LYP (Becke, three-parameter, Lee-Yang-Parr) exchange-correlation functional with a split-valence basis set of 6-311++G (2d, P). The B3LYP/6-311++G (2d, P) level of calculation delivered reasonable estimates of the absorption wavelengths for a number of the aza-BODIPYs, although the calculations did give poor estimates for the absorption wavelengths of others.

Photovoltaic devices were fabricated, using primarily carbon-60 fullerene as acceptor in conjunction with the aza-BODIPYs as donors, and successfully generated current on exposure to simulated solar radiation. Using a xenon arc lamp as a solar simulator, external photon-to-current quantum efficiencies (EQE) and overall power conversion efficiencies (η) were measured for these devices with a variety of layer structures, film compositions and film-processing conditions. Compound (106) and compound (113) gave EQEs of 3.89% and 3.01%, and overall power conversion efficiencies of 0.88% and 0.031% respectively. Current density-voltage (J-V) curves exhibit a significant inflection, which was reflected in the low fill factors (FF). The low values of EQE and η are attributed to low open-circuit voltage (V_{OC}) (0.32 V and 0.55 V in compounds (106) and (113)) and low fill factors (FF) (0.312 and 0.0147 in compounds (106) and (113)). The low V_{OC} and FF are possibly the result of an interfacial extraction barrier at one of the active layer interfaces, possibly between the active layer and the metal cathode. Avoiding the possibility of oxide and other layers through encapsulating the devices in an inert environment might remove the charge extraction barrier. The conclusion drawn is efficiencies of devices based on aza-BODIPYs might be improved significantly through further studies of interfaces and defects in devices.

Acknowledgements

Firstly, I would like to thank my supervisors Professor Peter Derrick, Associate Professor Ashton Partridge and Associate Professor Eric Ainscough for their support and assistance throughout the duration of this thesis. Especially Peter Derrick for the enthusiastic leadership he showed towards the project and Eric Ainscough for his kind support at the latest stages of my PhD. Thanks to Dr. Justin Hodgkiss for his assistance with the time-correlated single-photon counting (TCSPC) spectroscopy, solar cell device fabrication and testing. Also, I'd like to thanks Hannah Stern for her assistance with device fabrication and testing. Dr. Richard Tilly for providing and testing silicon quantum dots.

Thanks to all my colleagues in the Institute of Fundamental Sciences for their support, especially Adam Stephenson. I am also grateful for Ross Davidson for his help with TD-DFT calculations. I'd like also to thank the assistance of Departmental technical and administrative staff within the Institute over the years I have been at Massey. I would like also to thank the Graduate Research School at Massey.

I would like to acknowledge important financial support from the Ministry of Business, Innovation and Employment (MBIE).

Finally, a big thanks to family and friends, especially my wife for her unlimited support over the past few years.

Table of Contents

List of Figures

List of Tables

Abbreviations

ACN	acetonitrile
Ar	aromatic
$CDCl_3$	deuterated chloroform
conc	concentrated
Da	daltons
DBU	1,8-diazabicyclo[5.4.0]undec-7-ene
DCM	dichloromethane
DDQ	2,3-dichloro-5,6-dicyanobenzoquinone
DFT	density functional theory
DEA	Diethylamine
DIEA	*N*,*N*-Diisopropylethylamine
DME	Dimethyl ether
DMF	*N*,*N*-dimethylformamide
DSSC	dye sensitised solar cell
ESI	electrospray ionisation
EtOH	ethanol
FF	fill factor
ITO	indium tin oxide
J_{sc}	short circuit current
L	litres
LDA	Lithium diisopropylamide
MALDI	matrix assisted laser desorption ionisation
MeOH	methanol
min	minute
mL	millilitres
mmol	millimole
NBS	*N*-bromosuccinimide
NMP	N-methyl-2-pyrrolidone
NMR	nuclear magnetic resonance
Ph	phenyl
ppm	parts per million
R_f	retention factor
TFA	Trifluoroacetic acid
THF	tetrahydrofuran
TLC	thin layer chromatography

TMS	tetramethylsilane
TOF	time of flight
UV-Vis	ultraviolet-visible spectroscopy
V_{oc}	open circuit voltage

Chapter 1

Introduction

Chapter 1

1.1 Introduction

The global demand for energy is increasing. On the other hand, the atmospheric concentrations of carbon dioxide, which rise as a result of human efforts to produce energy, are responsible for global warming.[1,2] Photovoltaic technology potentially offers a solution to this conundrum.

Photovoltaic (PV) technology offers several advantages over traditional energy sources such as oil and coal. The most important advantage of PV technology is the potential to provide clean and sustainable sources of energy without pollution. PV technology, in which solar energy is converted into electricity, is the most promising of the possibilities in the field of renewable energy. The word "*photovoltaic*" comes from the two terms: "*photo"*, derived from a Greek word means *light*, and "*voltaic"*, from the name of one of the innovators in the electricity field of study, Alessandro Volta (1745-1827). A photovoltaic device can be defined as a device having the ability to convert light into electricity.[3] Photovoltaic cells are also "solar cells". Organic photovoltaics are based on the same principles as the photosynthesis process in plants. Photosynthesis involves absorption of sunlight by the chlorophyll (dye), followed by charge separation, which leads to conversion of carbon dioxide, water and minerals into oxygen and organic compounds.

The photovoltaic effect was observed for the first time by Henri Becquerel almost 200 years ago (1839).[4] He illuminated a silver chloride thin-layer coated on a platinum sheet in an electrolytic solution, and connected the platinum to a counter electrode. This arrangement would now be known as a photo-electrochemical cell (PEC). Modern photovoltaic devices tend to incorporate *pn* junctions in semiconductor layers, where the photovoltaic potential is developed.[5]

1.2 Types of Solar Cells

1.2.1 Crystalline-Silicon and Gallium Arsenide (GaAs) Solar Cells

Silicon solar cells constitute about 85% of the total world PV share-market, because of the ready availability of the necessary feedstock materials.[6] Crystalline-silicon solar cells are made of single silicon crystals. The high cost and time consumption of making a single pure crystal, not to mention the possibility of damage to the PV panels due to falling objects, have led to the emergence of other types of PV technology.

Thin-film solar cells are made by the deposition of a thin layer of PV material on a substrate. The thicknesses of layers can vary from nanometers to micrometers. Examples of this type of solar cell are thin-film silicon, cadmium-telluride (CdTe) thin-film and chalcopyrite-based solar cells. Thin-film silicon solar cells offer some advantages such as the use of non-toxic raw materials, the energy required for device fabrication being very low and the fabrication temperature being around 200°C,[7] which is a much lower temperature than those used in fabrication of other solar cells. The disadvantage of these cells is the low conversion efficiency compared with other types of PV technology.
The energy gap (1.45 ev) and the strong light absorption (10^5 cm^{-1} at $\lambda < 800nm$) of CdTe, as well as the low cost of production (when using a simple deposition technique) favour the use of CdTe in thin-film solar cells.[8] Efficiencies of above 16% have been achieved in CdTe solar cells. The main disadvantages of CdTe thin-film solar cells are environmental pollution and the health hazards of Cd.[9]

A gallium arsenide (GaAs) based solar cell is one of a number of solar cells which have been developed for use in space by the National Renewable Energy Laboratory (NREL).[10] The high efficiency, temperature stability and high radiation-resistance are the main advantages behind the development of these GaAs solar cells. Groups 13-15 semiconductor-based solar cells, also called 13-15 multi-junction solar cells, have reached the highest efficiencies (above 40%) of any PV technology. For example, a GaInP/GaInAs/Ge triple-junction solar cell has achieved 41.6% efficiency.[10] These solar cells are already widely used in space applications. At the moment, these cells are very expensive to produce, and they would need to be much more cost-effective for use on Earth.

1.2.2 Dye-Sensitized Solar Cells (DSSC)

The first known electrochemical cell was introduced by Fujishima and Honda.[11] They reported the use of a titanium dioxide (TiO_2) photo-anode in an electrochemical cell to split water into hydrogen and oxygen. Subsequent research in photo-electrochemistry for solar energy conversion did not produce much progress until the early 1990's, when Grätzel and colleagues succeeded in increasing the performances of dye-sensitized solar cells (DSSC) through the use of high surface-area electrodes.[12] The basic structure of dye-sensitized solar cells (DSSC) involves a working electrode (semiconductor), an electrolyte and a counter-electrode (usually a metallic material). The core of the cell is the semiconductor-electrolyte interface (SEI) of the working electrode.[13] Light is absorbed by a sensitizer, and charge separation occurs at the interface via photo-induced electron injection from the dye into the conduction band of the solid. Carriers are transported in the conduction band of the charge collector. DSSC have reached solar conversion efficiencies of over 10% according to Grätzel et al.[14]

The major downside of a DSSC is the use of liquid electrolytes, which typically are not stable if the temperature changes. The electrolyte freezes at low temperatures, leading to physical damage. The electrolyte expands at high temperatures, and keeping the panels sealed becomes a serious problem. In addition, the ruthenium dye and the platinum catalyst, which typically are used to produce this type of solar cell, are very costly.

1.2.3 Organic Solar Cells

An organic solar cell (also called organic photovoltaic (OPV) cell) usually consists of a p-type (donor) and an n-type (acceptor) semiconductor. The contact area between them is the heterojunction. Absorption of light creates excitons, which diffuse to this donor-acceptor interface and dissociate into free holes and electrons. These are transferred into the electrodes.[15] Given the impressive performances of OPV devices, the prospects of having cheap OPV cells in the near future are good. Small OPV devices are already commercially available.[13] New organic photovoltaic (OPV) devices are discussed in more detail below.

A breakthrough in the emerging field of photovoltaics appears to have been achieved with the introduction of solid-state hybrid solar cells based on organometal trihalide perovskite absorbers.[16] These perovskite solar cells are believed to combine both low cost and high

efficiency. Perovskite solar cells were reported for the first time in 2009.[17] Hybrid perovskites are mixed-halide organic-inorganic compounds (e.g. chemical formula $CH_3NH_3PbX_3$, where X = I, Cl, Br), which have shown impressively high performances in converting solar light into electrical power. Power-conversion efficiencies (η) have exceeded 15%.[18-22]

1.3 Organic Photovoltaic Devices

1.3.1 Device Architecture

1.3.1.1 Single-Layer Devices

The architecture of a basic organic solar cell consists of a layer of organic material in between two metallic electrodes, as depicted in Fig. (1.1). In this architecture, a single organic layer is typically sandwiched between an Al electrode and a transparent indium tin oxide (ITO) substrate. Following transmission, photons are absorbed in the organic layer and excitons are created. An exciton is a bound state of an electron and a hole which are attracted to each other by the Coulomb force. The photo-active volume in these single-layer devices is restricted to small volumes near the metal contacts, as a consequence of the diffusion path-length of the excitons. The diffusion path-length is a measure of the average distance a carrier will diffuse before recombining. Dyes and polymers have been used in single layers in this kind of solar cell. A single-layer polyacetylene-based solar cell has been reported with an efficiency of 0.3%; other single-layer cells have been based on polythiophene derivatives.[23,24]

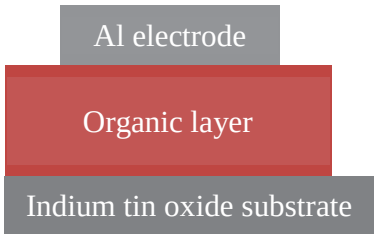

Figure 1.1 Single-layer solar cell device architecture

1.3.1.2 Bi-Layer Heterojunction Devices

Fig. (1.2) illustrates the typical structure of a bi-layer type of solar cell. Bi-layer devices with a fullerene derivative (see below) as an electron acceptor have been reported as achieving 5% efficiency.[25-27] The donor and acceptor layers in a bi-layer device can be deposited either as one layer onto the other layer by lamination or a stamp transfer process, or using spin coating or vacuum deposition.

The major disadvantage of the bi-layer type of solar cell device is that charge separation occurs only in a small interfacial region between the two layers. A thick active layer affording greater light absorption could not be used in this type of device.

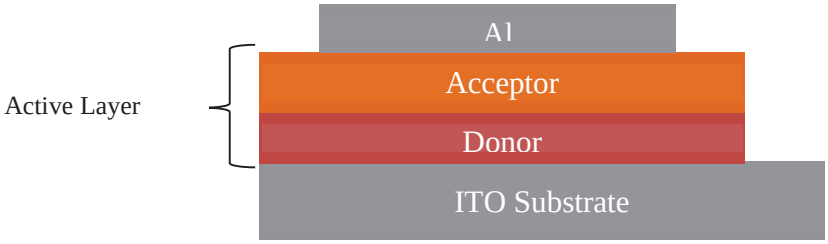

Figure 1.2 Bi-layer heterojunction solar cell device architecture.

1.3.1.3 Bulk Heterojunction Devices

In bulk heterojunction devices, the donor and acceptor are mixed in a single layer in order to increase the interfacial surface area. This approach has been used widely with organic-fullerene and polymer-polymer blends. Fig. (1.3) illustrates the typical structure of this type of solar cell device. The high interfacial surface area between the donor and acceptor in bulk heterojunction devices increases the probability of exciton creation and light absorption can be increased by using a thicker active layer.

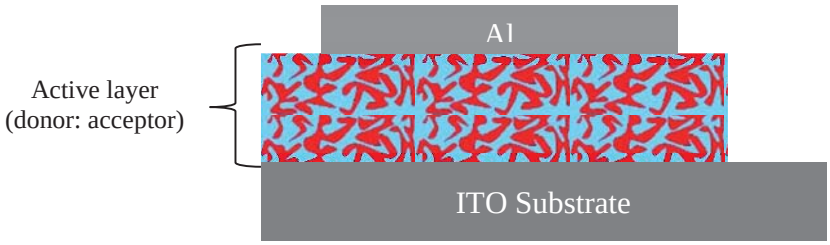

Figure 1.3 Bulk heterojunction solar cell device architecture.

1.3.2 Properties and Operation of Organic Photovoltaic Devices

The operation of an organic solar cell involves three processes: light absorption, charge separation, and charge transport. A close investigation of these processes will give us an understanding of the functions of the OPV materials inside the solar device, and draws out the characteristic properties of the materials themselves. Fig. (1.4) shows a schematic representation of the basic operation of an organic solar cell, consisting of a donor and an acceptor in the active layer. Light is absorbed by the donor generating the exciton which leads either to charge separation (dissociation to electron and hole) or decay (relaxation back to the ground state). Charge separation will form polarons (a polaron is a quasiparticle which is composed of a charge and its accompanying polarization field) which can produce current if they reach the electrodes before recombining with each other. The charge separation process is restricted to the interface between donor and acceptor, so that the morphology of the active layer is very important and must be considered in order to achieve an efficient device.

Generation of photocurrent is the essential function of a solar cell, and current generation is determined by a balance between light absorption, charge carrier generation and recombination. The initial electronic excitation process leads to production of charge carriers, while recombination, an electronic relaxation process, reduces the number of free charge carriers. Upon absorption of a photon, charge carrier generation occurs as a result of the promotion of an electron from the HOMO (highest occupied molecular orbital) to the LUMO (lowest unoccupied molecular orbital), subsequent electron transfer from donor to acceptor and charge separation.[28]

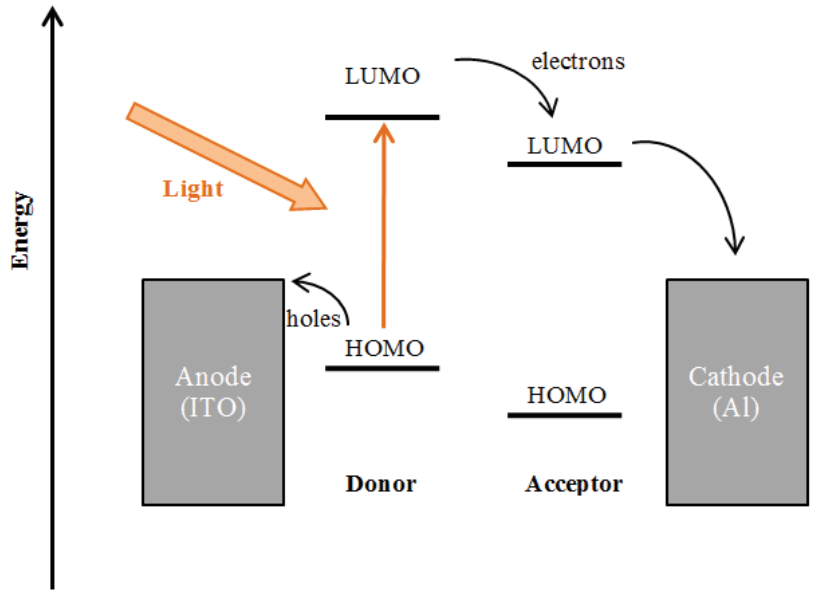

Figure 1.4 Bulk heterojunction band structure with a donor-acceptor blend as an active layer.[29]

Recombination is an undesirable process, in which an electron and a hole will be lost through the decay of an electron to a lower energy state. Energy is released as heat by phonon emission (non-radiative recombination), as a photon (radiative recombination) or into kinetic energy of another free carrier (Auger recombination).

Two types of recombination process can be distinguished: [28]

(i) Unavoidable recombination which occurs as a result of physical processes such as spontaneous and stimulated emission. Auger recombination is another form of unavoidable recombination process, in which an interaction of an electron or hole with a second similar carrier results in an increase in the kinetic energy of one carrier by an amount equal to the band gap and recombination of the other carrier across the band gap (see Fig. 1.5 (c)). Auger recombination is important in materials which have low band-gaps, strong carrier-carrier interactions and high carrier-densities.[28,30-35]

(ii) Avoidable recombination process, which is due to imperfect material. In this type of recombination, a relaxation occurs by way of a localized trap state, due to impurities or defects in the crystal structure, see Fig. 1.5 (a) and (b).[36]

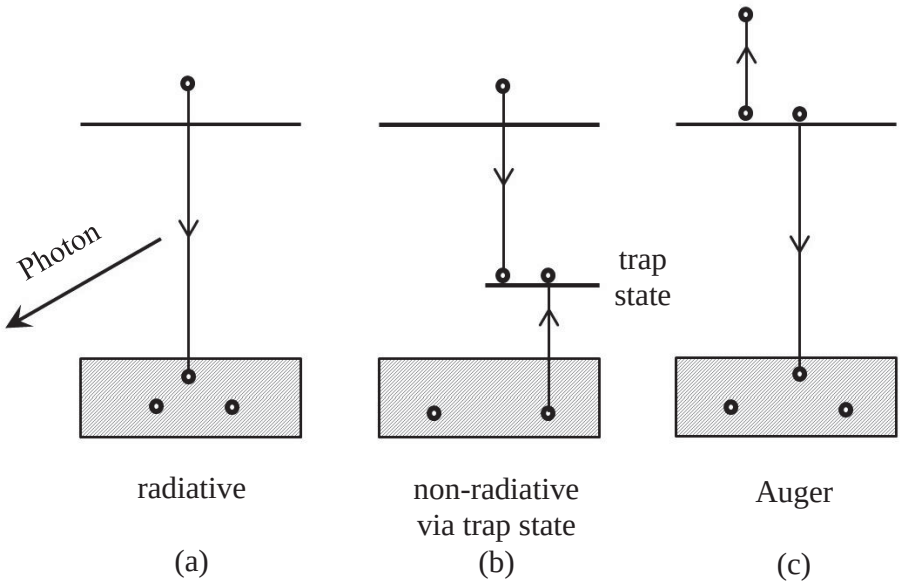

Figure 1.5 (a) Radiative, (b) non-radiative and (c) Auger recombination.[28]

The principles of operational heterojunction devices can be described on the basis of Fig. (1.4). Upon light absorption, an electron from the highest-occupied molecular orbital (HOMO) of the donor is promoted to the lowest-unoccupied molecular orbital (LUMO) of the donor. Following charge separation at donor-acceptor interfaces, free charge carriers will be transported through the semi-conducting materials of the active layer: the holes reach the anode (ITO) and the electrons reach the cathode (Al).

From a practical point of view, the photovoltaic properties can be obtained from current-voltage curves, (Fig. (1.6)). A cell is exposed to light and a photo-current is generated as a result of free charge carriers being transferred to the electrodes. The performance of a solar cell is described by the power conversion efficiency (η), which is the ratio of the maximum power (P_m) generated by the device to the incident power (P_{in}).

Considering Fig. (1.6), there are three key parameters which determine the power conversion efficiency (η): open circuit voltage (V_{OC}), which is the maximum voltage difference between the two electrodes; short-circuit current density (J_{SC}), which is the maximum current which can run through the cell; fill factor (FF), which is defined as the ratio:

$$FF = \frac{J_{max}V_{max}}{J_{sc}V_{oc}} \qquad \text{Eq. 1.1}$$

J_{max} and V_{max} are respectively the current density and voltage at the maximum power point (MPP) (see Fig. 1.6).

The relationships among these factors are given by the following equations:[37]

$$\eta = \frac{P_{max}}{P_{in}} = \frac{J_{max}\,V_{max}}{P_{in}} \qquad \text{Eq. 1.2}$$

The power conversion efficiency (η) is related to J_{SC}, V_{OC} and FF:

$$\eta = \frac{FF\,J_{sc}\,V_{oc}}{P_{in}} \qquad \text{Eq. 1.3}$$

The Standard Test Condition (STC) for solar cells is the Air Mass 1.5 spectrum, an incident power density of 100 mW cm^{-2}, and a temperature of 25°C. Air Mass 1.5 is the solar spectrum, corresponding to the sun being at an elevation of 42°. separation.[28]

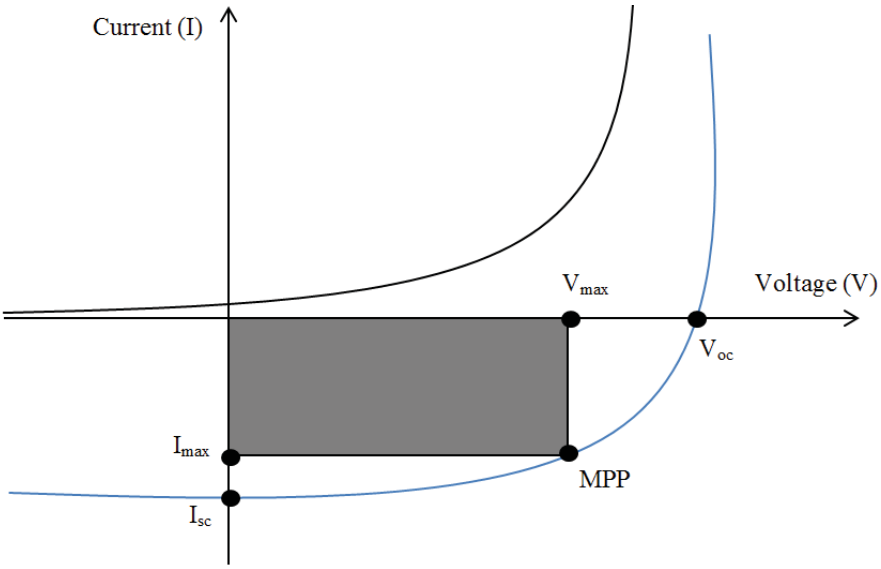

Figure 1.6 Current-voltage characteristics of an organic solar cell in the dark (black line) and under illumination (blue line).

Photocurrent generated by a solar cell is dependent on the wavelength, or energy, of the photons, and the short-circuit current density (J_{SC}) represents an integration over the spectrum of incident light.[28,38] External quantum efficiency (EQE) (also sometimes called simply "quantum efficiency")[28] of a solar cell is the amount of current produced by the cell upon irradiation of photons at a particular wavelength or energy. The short-circuit current density (J_{SC}) therefore depends upon the spectrum of light incident on the solar cell. EQE depends on the efficiency of charge separation, on the efficiency of charge collection, and on the absorption coefficient of the OPV material.[28,38]

1.3.3 Optimizing the Performance of Organic Photovoltaics

The P3HT: PCBM bulk heterojunction solar cell is used as an example in discussing different ways to increase efficiency (P3HT is poly (3-hexylthiophene), see Fig. (1.9); and PCBM is a fullerene derivative, see Fig. (1.11)). The strategies described are generally valid for organic-fullerene bulk-heterojunction solar cells. Figure (1.7) shows energy levels for a typical cell, taken from the literature.[39,40]

Energy loss in electron transfer between donor (P3HT) and acceptor (PCBM) will impact adversely on the open circuit voltage (V_{OC}), which in turn can affect the efficiency of the cell (Equation 1.1). V_{OC} is determined by the difference in energy between the HOMO of the donor and the LUMO of the acceptor. Typically, the electron transfer from the donor to the acceptor is enhanced by tuning the offset value between the LUMO(donor) and the LUMO(acceptor).[41] It has been found with organic-fullerene cells that V_{OC} is also influenced by the morphology of the active layer.[42]

To achieve high efficiency in a photovoltaic device, the ideal requirements are: [28]

(i) OPV materials with an optimal band gap in the range 0.5 to 3.0 eV, which can absorb visible light to excite electrons across the band gap. For example, gallium arsenide (GaAs) has a band gap close to optimum (1.42 eV at 300 K), which is very favorable for high performance devices, while silicon used in the most popular type of solar cells has a less favorable band gap (1.1 eV).

(ii) Increase the absorption of the incident light by OPV materials. This can be achieved by controlling the thickness of the active layer.

(iii) Each absorbed photon should generate exactly one electron-hole pair.

(iv) The excited charges should not combine.

(v) The excited states should be completely separated.

(vi) The charges should be transported to the electrodes without loss.

The main reasons behind the low performance of a solar cell are incomplete absorption of the incident light, the non-radiative recombination of photogeneration carriers and the voltage drop due to a series resistance between the point of photogeneration and the external circuit. The incomplete absorption occurs because the photons are reflected from the surface without being absorbed, which reduces the photocurrent. Non-radiative recombination causes the excited charges to be trapped at defect sites and to recombine before being collected, which reduces both the photocurrent and the voltage.[28,43] For a highly efficient OPV device, an optimum band gap, efficient charge separation and efficient charge transport are required.

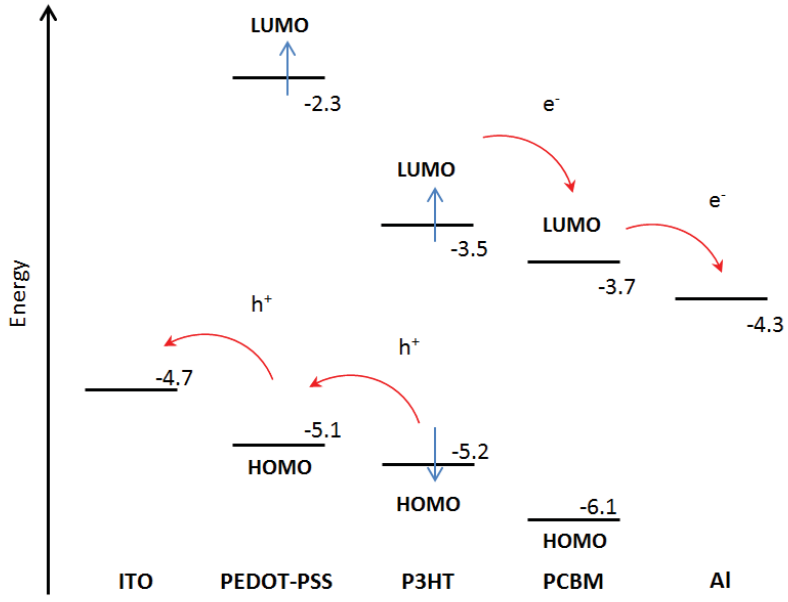

Figure 1.7 The energy levels (eV) (HOMO and LUMO) of donor (P3HT) and acceptor (PCBM) in a bulk heterojunction device. (PEDOT:PSS is an additional layer, which facilitates the efficient extraction of charges generated in the active layer, see Fig. (1.9) for structure)

In a typical bulk heterojunction solar cell (Fig. (1.8)), there are ways to enhance charge transfer by changing differences in energy levels between donor and acceptor. The difference between the LUMO(acceptor) and LUMO(donor) is the energy offset.[44] The power conversion efficiency of the cell has reached 8% by tuning the LUMO level of PCBM[45,46] or by finding another acceptor with a more favorable LUMO level such that the LUMO(acceptor)-LUMO(donor) offset is vicinity of 0.5 eV (Fig. (1.8) (a)). Through lowering the donor band gap combined with good charge transporting properties (Fig. (1.8) (b)), organic fullerene bulk-heterojunction solar cells have reached power conversion efficiencies of above 10%.[46-48]

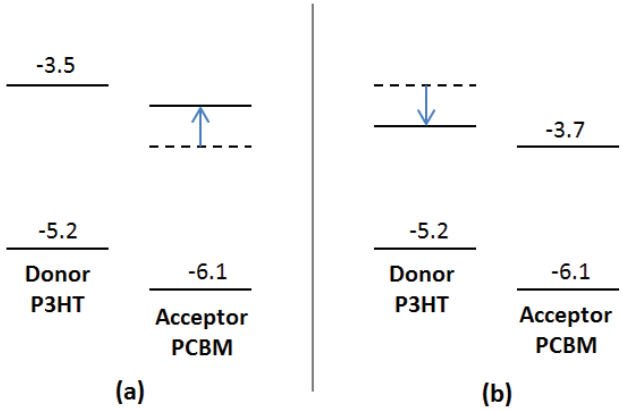

Figure 1.8 The influence of the energy offset between the LUMO(donor) and the LUMO(acceptor).

1.4 Organic Photovoltaic Materials

1.4.1 Donor Materials

Materials that have the ability to absorb light and conduct charges through the molecular structure are known as organic semi-conductors. These materials can be classified as p-type (hole transporting) or n-type (electron transporting). Conjugated polymers such as PPV (poly(*p*-phenylenevinylene)),[49-52] MEH-PPV (poly[2-methoxy-5-(2'-ethylhexyloxy)-*p*-phenylenevinylene]),[53-58] MDMO-PPV (poly[2-methoxy-5-(3′,7′-dimethyloctyloxy)-1,4-phenylenevinylene]),[59-63] P3HT (poly(3-hexylthiophene)),[64-68] P3OT (poly(3- Octyl thiophene)),[69-73] PEDOT-PSS (poly(3,4-ethylenedioxythiophene) poly

(styrenesulfonate)),[74,75] and PCPDTBT (poly[2,6-(4,4-bis-(2-ethylhexyl)-4H-cyclopenta [2,1-b;3,4-b′]dithiophene)-alt-4,7(2,1,3-benzothiadiazole)]) have been used as p-type organic semi-conductors.[76-82] The structures of these polymers are depicted in Fig. (1.9).

A variety of small molecules have also been used as dyes in solar cells, the most well-known being are phthalocyanine (Pc),[83-89] pentacene,[90-94] merocyanine (MC),[95,96] diketopyrrolopyrroles (DPP),[97-102] perylene diimides (PDI),[103-106] and quinacridone (QD).[107-109] There have been few studies on the use of derivatives of dipyrromethene (BODIPY),[110-114] and fewer still on derivatives of aza-dipyrromethene (Aza-BODIPY).[115,116] The structures of these materials are depicted in Fig. (1.10). These small molecules act as electron donors in organic solar cell devices.

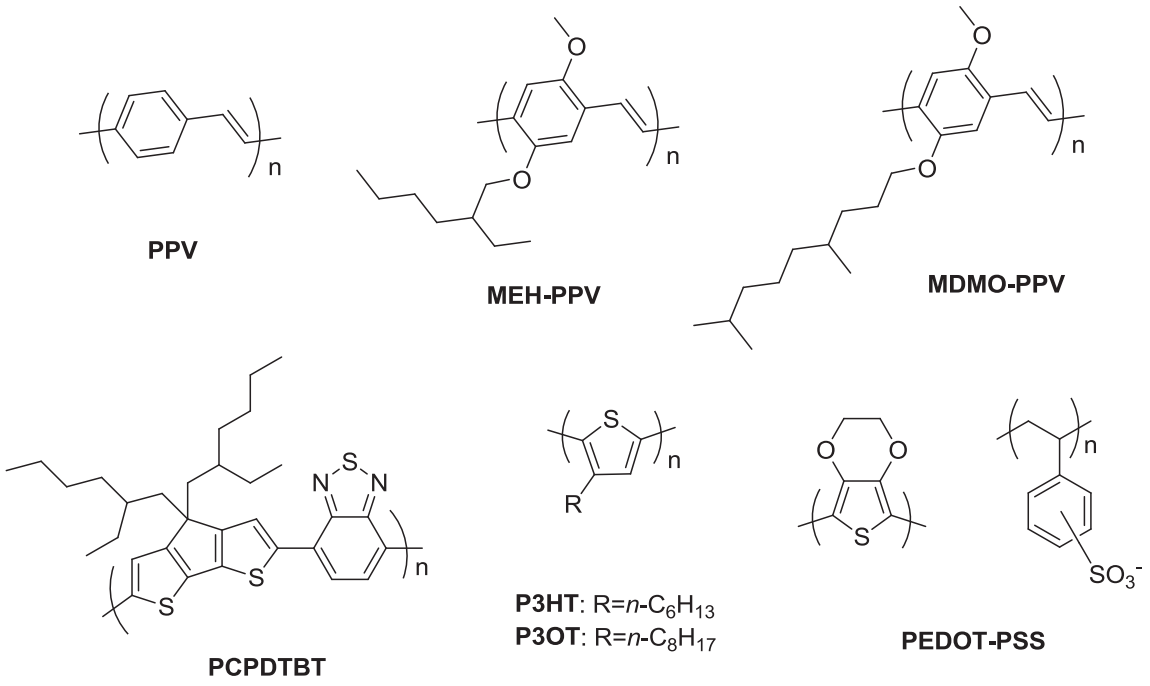

Figure 1.9 The chemical structures of the polymers (PPV, MEH-PPV, MDMO-PVV, PCPDTBT, P3HT, P3OT and PEDOT-PSS) that are used in organic solar cells.

Hole mobility, exciton diffusion length, thin-film morphology, band gap, and absorption coefficient are among the factors which affect the performances of solar cells. For the ideal donor, there are some obvious desirable properties such as absorbing as much light as possible and having high extinction coefficients.[117] Most organic molecules have narrow

ranges of absorption, which do not cover the entire solar spectrum. Broad absorption extending into the near-infrared region is highly desirable.

Small molecules, as distinct from macromolecules, do offer the following advantages:

- Small molecules have defined chemical structures and are much easier to purify than the typical polymer. The defined structure eliminates the most common problem with conjugated polymers, namely the variability in molecular weight, polydispersity and the structural regioregularity.
- The high absorption coefficients of these small molecules allow the use of lower thickness of the active layer, which benefits charge transport.
- Determining device performance and the relationships between the chemical structure and the electronic properties is more straightforward than with polymers.

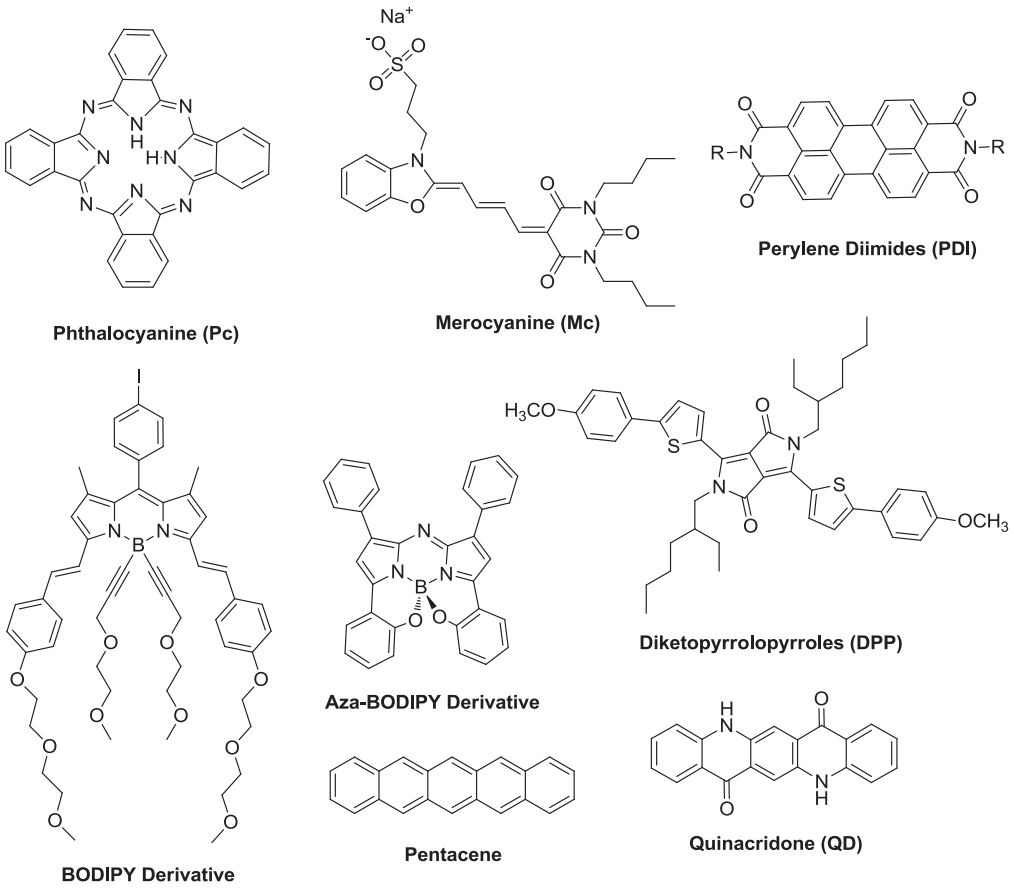

Figure 1.10 The chemical structures of small molecules commonly used as donors in organic solar cells

1.4.2 Acceptor Materials

The standard organic bulk-heterojunction solar cell incorporates fullerene derivatives in the active layer. $PC_{60}BM$ ([6,6]-phenyl-C_{61}-butyric acid methyl ester) (Fig. 1.11) is a derivative of the C_{60}-fullerene first synthesized in 1995,[118] which has been used in this work as the standard acceptor due to its availability and cheap price when compared with the newer $PC_{70}BM$ ([6,6]-phenyl-C_{71}-butyric acid methyl ester). The structures and properties of fullerene derivatives are discussed here.

The remarkable discovery of the carbon-60 fullerene (known as buckyball) was made by Kroto et al. over two decades ago.[119] The interaction of fullerene derivatives with light, and the unique electrochemical properties in which this fullerene can accept reversibly up to six electrons in solution,[120-122] make these compounds interesting for applications related to photochemical and photo-induced charge transfer properties. It has been demonstrated that the fullerene core is able to capture electrons from π-conjugated polymers and maintain charge-separated states.[123]

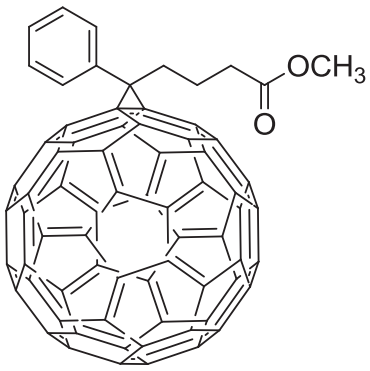

Figure 1.11 The structure of $PC_{60}BM$ ([6,6]-phenyl-C_{61}-butyric acid methyl ester)

Fullerene-based solar cells are fabricated in the usual way by sandwiching donor and acceptor materials between two electrodes (Fig. 1.12). One of the electrodes is a thin semi-transparent metal layer, often indium tin oxide (ITO), while the other layer is often aluminum. The layer of PEDOT-PSS is again quite usual.

The carbon-70 compound $PC_{70}BM$ has been demonstrated to give an improvement in light absorption and cell performance. Higher current densities have been obtained, as well as an overall efficiency of 3% in comparison to 2.5% for $PC_{60}BM$ in the same conditions.[124]

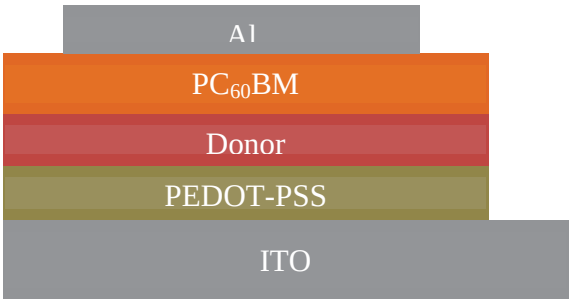

Figure 1.12 A basic bi-layer fullerene based heterojunction solar cell.

1.5 BF_2-Aza-dipyrromethenes (Aza-BODIPYs)

1.5.1 Chemical Structure of Aza-BODIPYs

Pyrrole is a heterocyclic aromatic compound and a very important conjugated building block for a variety of organic molecules and polymers. The most interesting and intensively investigated types of pyrrole compounds are boron difluoride (BF_2) chelated with dipyrromethene (called BODIPY), and boron difluoride(BF_2)-chelated aza-dipyrromethene dyes (called aza-BODIPY). During the past ten years, various experimental and theoretical studies have been carried out on aza-BODIPYs because of their long-wavelength absorptions and intense emissions.

The simplest of the aza-BODIPY family is difluoro-bora-1,3,5,7-tetraphenyl aza-dipyrromethene. The standard numbering systems of the BODIPY core and of the aza-BODIPY core are depicted in Fig. (1.13). The aza-BODIPY core consists of two pyrrole rings linked via a nitrogen atom to produce a fully conjugated system.

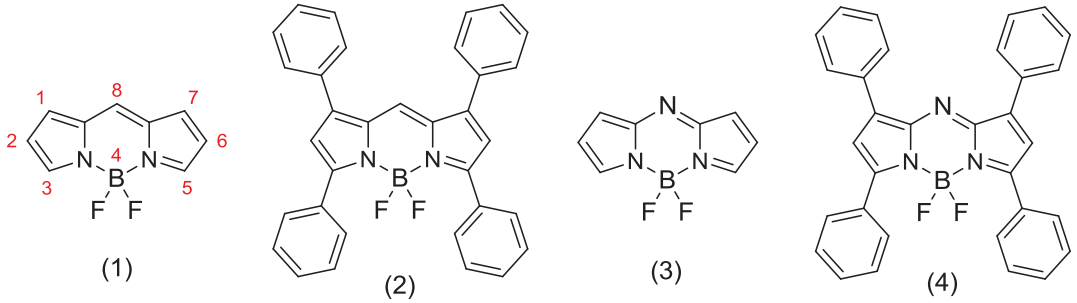

Figure 1.13 Structure of (1) BODIPY core showing IUPAC numbering (2) Difluoro-bora - 1,3,5,7-tetraphenyl dipyrromethene boron difluoride (3) aza-BODIPY core (4) 1,3,5,7-tetraphenyl aza-dipyrromethene boron difluoride .

The first synthesis of dipyrromethenes (DIPYs) was carried out in the 1930s.[125] The intense colors and semi-conducting properties of metal complexes of DIPYs were investigated later.[126] Boron difluoride (BF_2) chelated dipyrromethene (BODIPY) was synthesized for the first time in 1966.[126] Incorporation of BF_2 through the reaction of dipyrromethene with boron trifluoride etherate ($BF_3{\cdot}OEt_2$) led to a neutral BODIPY core.

The most important properties that have been shown by the rigid structure of the BODIPY core are the broad absorption bands with very intense fluorescence and high quantum yields, which later on became the unique characteristics of BODIPY compounds. The fully conjugated framework of the BODIPY core represents a conjugated system suitable for attachment of substituents in order to tune-up the fluorescence properties. The aza-BODIPY structure has been obtained by the substitution of the meso-carbon atom bridge (position 8) with a nitrogen atom, Fig. (1.13). The first aza-dipyrromethene (aza-DIPY) was reported in the 1940s,[127] but the BF_2 chelated aza-dipyrromethene (aza-BODIPY) was first synthesized by Boyer et al.[128] in 1993. Since then, the aza-BODIPYs have been studied less in comparison with BODIPY due to the difficulties associated with their preparations.

Substituted aza-BODIPYs with different aryl groups, as well as their syntheses, characterization and evaluation as donors for bulk heterojunction solar cells will be discussed in detail in the following chapters of this thesis. The general synthetic procedure and mechanisms of formation of aza-BODIPYs will be discussed in the next section. This

thesis also describes the synthesis of some BODIPY monomers (non aza-analogues) and a basic study of their optical properties.

1.5.2 Synthesis of Aza-BODIPYs

Symmetrically substituted aza-BODIPYs with aryl groups (on positions 1, 3, 5 and 7 of the dipyrrin core) can each be synthesized by a four step synthesis route (Fig. (1.14)). The first step involves the aldol condensation reaction of benzaldehyde and acetophenone to produce 1,3-diphenyl-2-propen-1-one (chalcone) (Fig. (1.14), compound (6)). The 1,3-diphenyl-4-nitrobutan-1-one (compound (7)) is obtained from the Michael addition of nitromethane to the compound (6), with diethylamine (DEA) as base. These two classical synthesis reactions very effectively provided the precursors to the aza-DIPY (compound (8)). The BF_2 chelated aza-dipyrromethenes (compound (9)) is readily produced by adding boron trifluoride etherate ($BF_3.OEt_2$) to aza-DIPY at room temperature. This synthesis approach allows the introduction of up to two different aryl substituents on positions 1, 3, 5 and 7 of the dipyrrin core. Aza-BODIPY compounds are interesting because their photophysical and electronic properties can be easily manipulated by increasing the π-conjugation along the aza-BODIPY molecule and by substituting them with electron-donating and electron-withdrawing groups. In Chapter 2 of this thesis, the chemical modification of aza-BODIPY compounds with a view to tuning-up their electronic properties and broadening their absorption into the near-infrared region is described.

The synthesis of symmetrically substituted aza-BODIPYs was described by O'Shea et al.[129] who also optimized the reaction conditions by introducing a new solvent and an alternative ammonium source. Ammonium acetate replaced ammonium formate, Fig. (1.14).

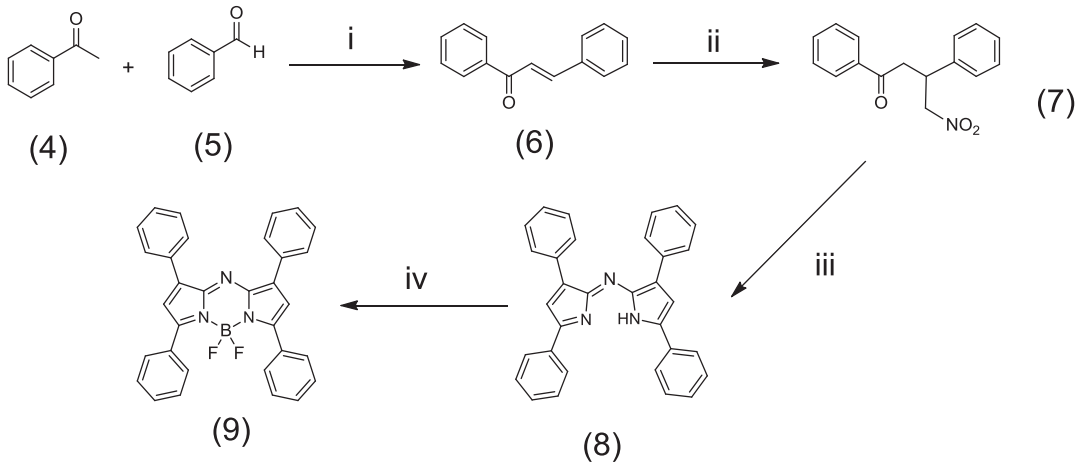

Figure 1.14 The synthesis of aza-BODIPY. Reagents and conditions: (i) KOH, EtOH, room temperature, 24h. (ii) CH_3NO_2, diethylamine, MeOH, reflux, 24h. (iii) NH_4CO_2H, EtOH, reflux, 24h. (iv) $BF_3.OEt_2$, *N*,*N*-diisopropylethylamine, CH_2Cl_2, room temperature, 24 h.[129]

The method of O'Shea et al.[129] involves the formation of Michael addition products from chalcones and nitromethane (or cyanide), which react with an ammonia source (ammonium acetate or ammonium formate) to produce the aza-DIPY core. Production of symmetrically substituted aza-BODIPYs is shown in Fig. (1.15). The proposed mechanism for the formation of the aza-DIPYs from the nitromethane adducts is depicted in Fig. (1.16). The cyclisation product (23) is formed by deprotonating (11), and eliminating HNO_2 from (19). The compound (17) can also be nitrosated to give the nitroso-pyrrole (22), which condenses with another pyrrole (23) to produce the aza-DIPY (25). Using alcohol solvents enhances the isolation and yields of aza-DIPY, and using ammonium acetate instead of formate in the dry-melt process doubles the yield.[130-132] The BF_2 chelated aza-dipyrromethenes (aza-BODIPYs) are synthesized by adding boron trifluoride etherate ($BF_3.OEt_2$) to the aza-DIPYs at room temperature. The precipitated product is then washed with ethanol and usually no further purification is required. Boyer et al.[128] performed this reaction for the first time in 1993.

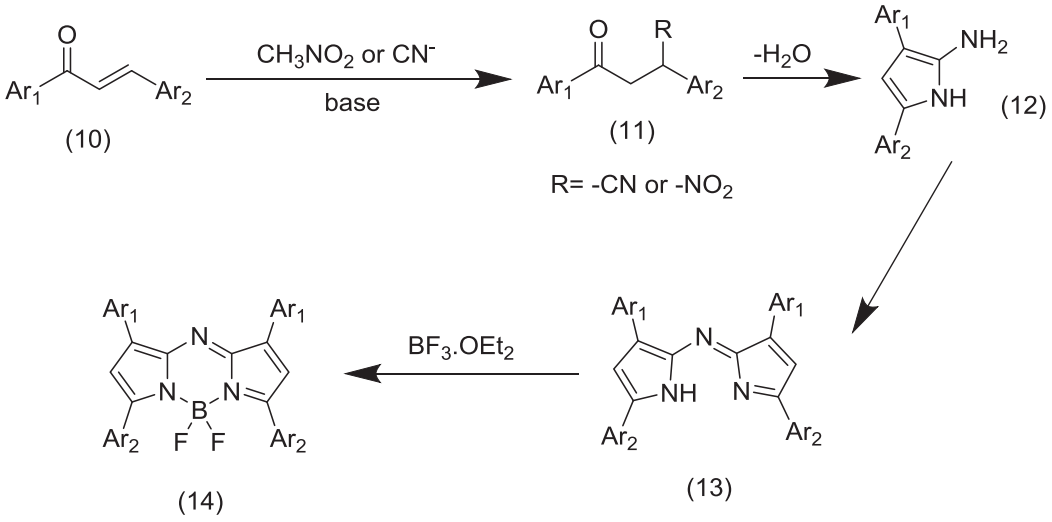

Figure 1.15 The formation of symmetrical aza-BODIPYs

For the syntheses of unsymmetrical substituted aza-BODIPY, 2,4-diarylpyrroles are converted into 5-nitroso derivatives, followed by a condensation reaction with a second molecule of pyrrole. The BF_2 chelated aza-dipyrromethenes (aza-BODIPYs) are synthesized by adding boron trifluoride etherate ($BF_3.OEt_2$) to the aza-DIPYs at room temperature, Fig. (1.17).[133]

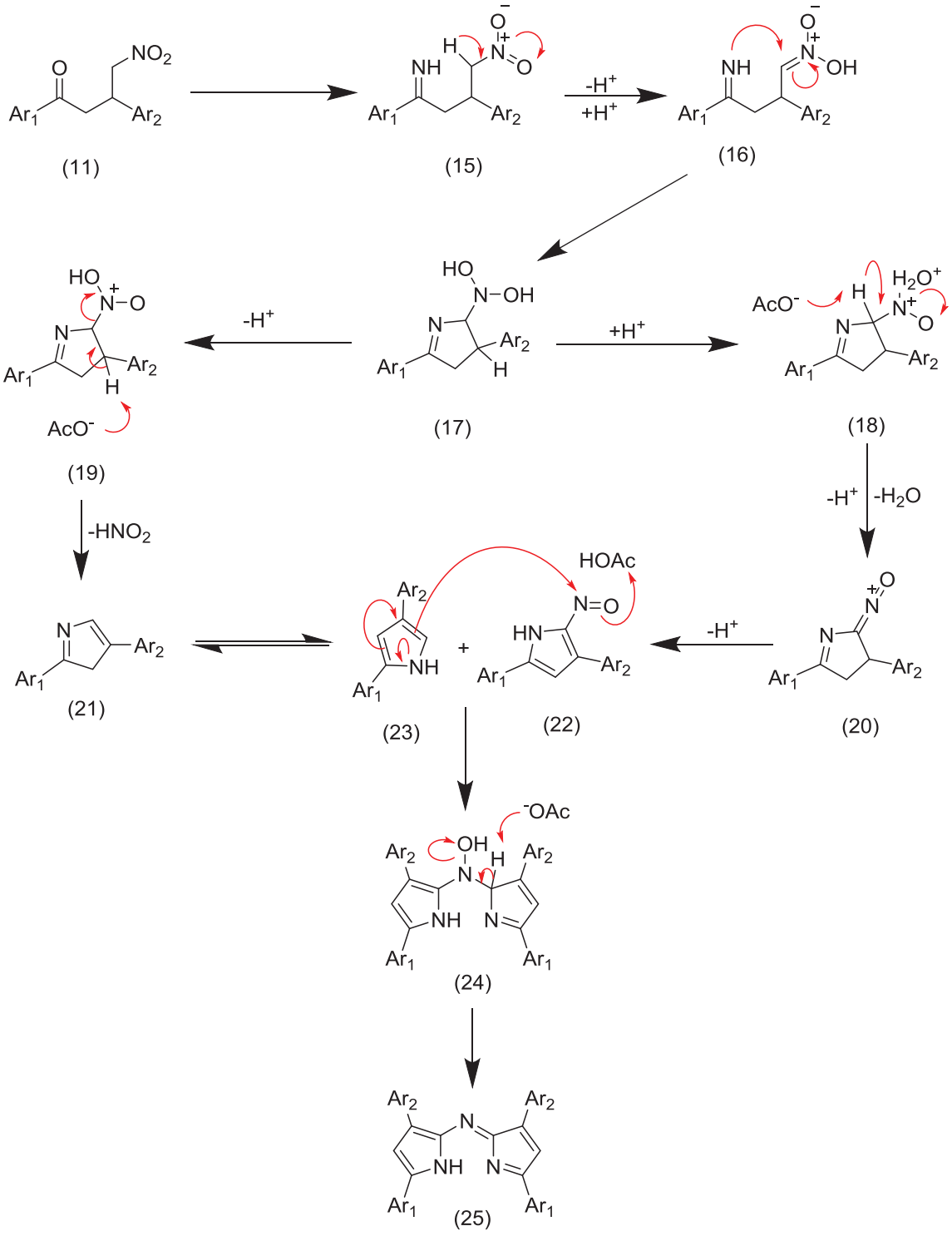

Figure 1.16 The proposed mechanism for the formation of aza-DIPYs from nitromethane adducts.[134]

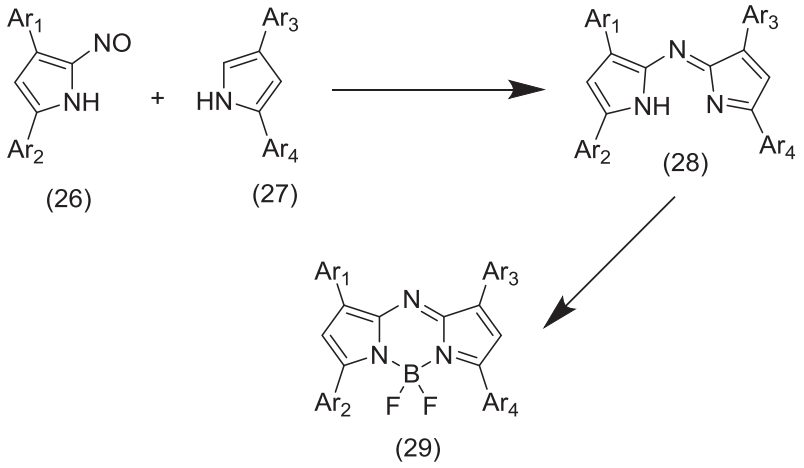

Figure 1.17 The general synthesis method of unsymmetrical aza-BODIPY.

Derivatives of the intermediate compound (aza-DIPY) can also be synthesised [135,136] by the addition of Grignard reagents (such as phenylmagnesium bromide (30)) to succinonitrile (31) or phthalodinitrile (32), see Fig. (1.18).

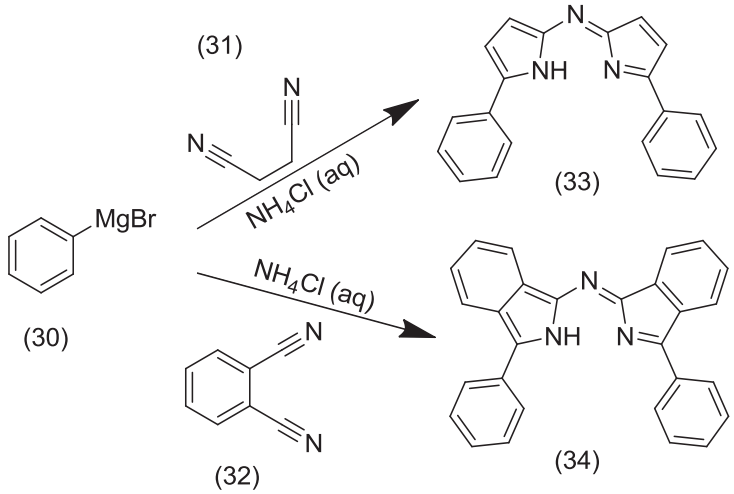

Figure 1.18 Synthesis of aza-dipyrromethenes (aza-DIPY) using Grignard reagents.

Finally, there is one other method which has been investigated for obtaining symmetrical and asymmetrical conformationally restricted aza-BODIPYs. The starting points of this method are pyrroles that can be produced from cyclized and restricted 2,4-diarylpyrroles.

The pyrrole is condensed with nitrosopyrrole, followed by complexation with boron trifluoride (Fig. (1.19)).

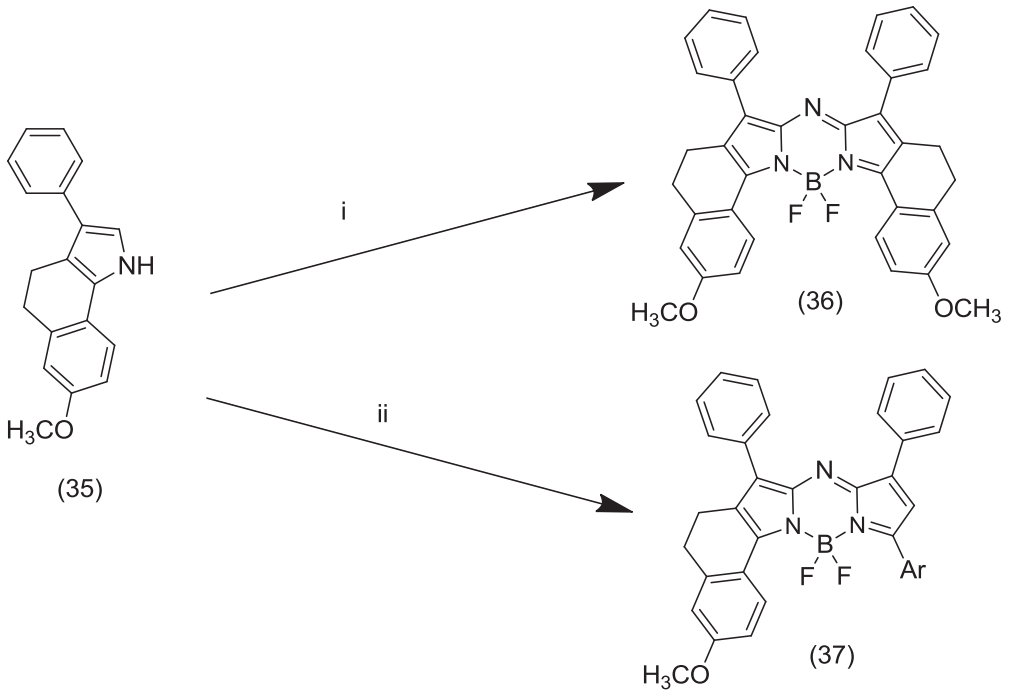

Figure 1.19 Synthesis of conformationally restricted aza-BODIPY. Reagents and conditions: (i) 1) HOAc, Ac_2O, $NaNO_2$ 2) Hunig's base $BF_3.OEt_2(CH_2Cl)_2$. (ii) 1) HOAc, $NaNO_2$ 2) aryl pyrrole, Ac_2O, HOAc 3) Hunig's base $BF_3.OEt_2(CH_2Cl)_2$.

1.5.3 Absorption and Emission Properties of Aza-BODIPYs

O'Shea and colleagues[129] have found that the UV absorption maxima of BF_2-chelated tetraaryl-aza-dipyrromethenes depend strongly on the substituents of the aryl groups (Fig. (1.20)). Electron-donating groups on 5-aryl-substituents cause a red shift in the absorption maxima and increase the extinction coefficients. Compounds (38), (39), (40), and (41) (Fig. (1.20)) fall in this category. Substituents with electron-donating groups at the 3-aryl position have less effect on the absorption maxima (compounds (42), (43), and (44) (Fig. (1.20)).

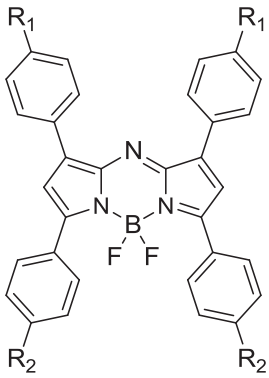

(38) R_1=R_2= H
λ_{max}= 650nm
ε= 79000 M^{-1} cm^{-1}
λ_{em}= 672nm

(39) R_1= H; R_2= OCH_3
λ_{max}= 688nm
ε= 85000 M^{-1} cm^{-1}
λ_{em}= 715nm

(40) R_1= OCH_3; R_2= H
λ_{max}= 664nm
ε= 78000 M^{-1} cm^{-1}
λ_{em}= 695nm

(41) R_1= Br; R_2= H
λ_{max}= 658nm
ε= 83000 M^{-1} cm^{-1}
λ_{em}= 680nm

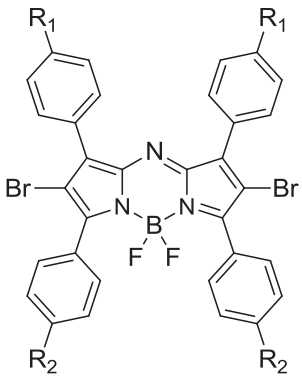

(42) R_1=R_2= H
λ_{max}= 650nm
ε= 79000 M^{-1} cm^{-1}
λ_{em}= 673nm

(43) R_1= H; R_2= OCH_3
λ_{max}= 679nm
ε= 75000 M^{-1} cm^{-1}
λ_{em}= 714nm

(44) R_1= OCH_3; R_2= H
λ_{max}= 653nm
ε= 80000 M^{-1} cm^{-1}
λ_{em}= 679nm

Figure 1.20 Spectroscopic properties of a series of BF_2-tetraaryl-aza-dipyrromethene in chloroform substituted with electron donating groups.

The unique red-shift in both UV-VIS absorption and fluorescence maxima upon mercuric-ion complexation of Aza-BODIPY derivatives have been of interest for chemosensors. For example compound (45) (Fig. (1.21)) is highly selective for mercuric ions, which can be chelated between the 2-pyridyl groups.[137]

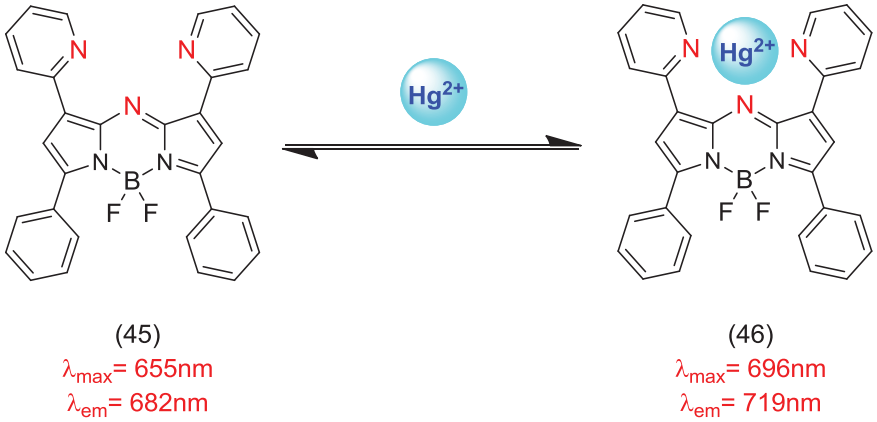

(45)
λ_{max}= 655nm
λ_{em}= 682nm

(46)
λ_{max}= 696nm
λ_{em}= 719nm

Figure 1.21 Spectroscopic properties of ion chelated aza-BODIPY.

The conformationally restricted aza-BODIPYs, Fig. (1.22), absorb in between 650 nm and 750 nm. Incorporating electron-donating groups at the 3-position of the aza-BODIPY core results in a slightly higher fluorescence quantum yield and small blue shift, while the extinction coefficient is not affected. Comparing the absorption spectra of these compounds with the normal aza-BODIPY (compound (4)), there is about a 50 nm shift in the absorption. The aza-BODIPYs containing two or one side carbocyclic rings have showed good chemical and photostability with intense fluorescence emission.[127,138]

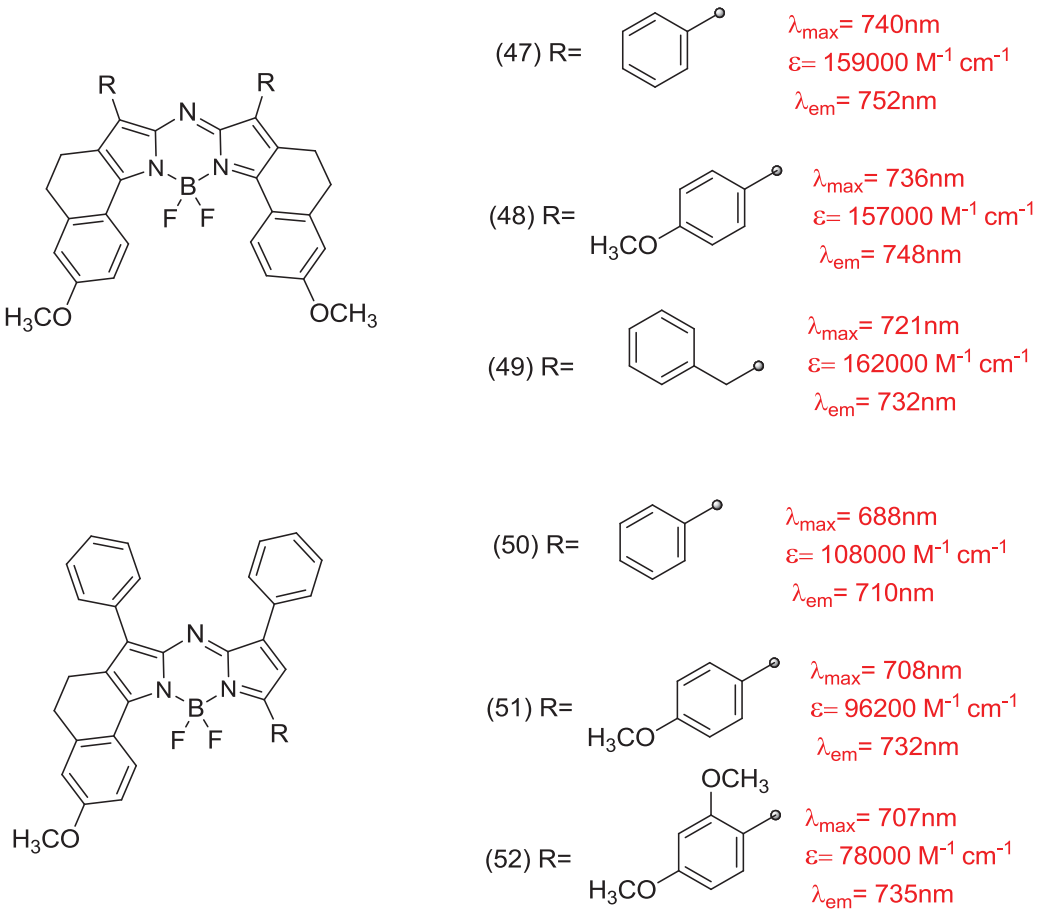

Figure 1.22 Spectroscopic properties of conformationally restricted aza-BODIPY (both R groups are the same in compounds (47), (48) and (49)). (∘) Represents the point of attachment of the R group to the aza-BODIPYs core).

1.5.4 Organic Solar Cells Based on Aza-BODIPYs

Aza-BODIPY compounds were investigated for use in organic solar cells[139-142] because of their intense absorption up to the near infra-red (NIR) region of the solar spectrum and the easy manipulation of their absorption and electronic properties by introduction of electron-donating and electron-deficient substituents on positions 1, 3, 5 and 7 of the dipyrrin core. The use of aza-BODIPYs in solar cells was reported by Mueller *et al* in 2012[139] who demonstrated the use of aza-BODIPYs as donor materials in heterojunction devices with $PC_{60}BM$ as an acceptor. Difluoro-bora-1,3,5,7-tetraphenyl aza-dipyrromethene (compound

(4), Fig. (1.23)) had a power conversion efficiency of 1.2% with enhanced V_{OC} (0.96V). A device with compound (54) showed a V_{OC} of 0.65 V with an efficiency of 1.1%. The loss in cell voltage compared to the previous device was due to the small energy gap of compound (54). A power conversion efficiency of 2.63% has been achieved using compound (56). [143] The energy offset between the highest occupied molecular orbital (HOMO) of the donor and the lowest unoccupied molecular orbital (LUMO) of the acceptor was the major factor which affected the solar cell performance (Fig. (1.24)). Compound (4) and (56) have the lower energy offsets in comparison with compounds (54) and (55).[144] These recent papers showed the great potential of the application of aza-BODIPY based molecules in organic solar cells.

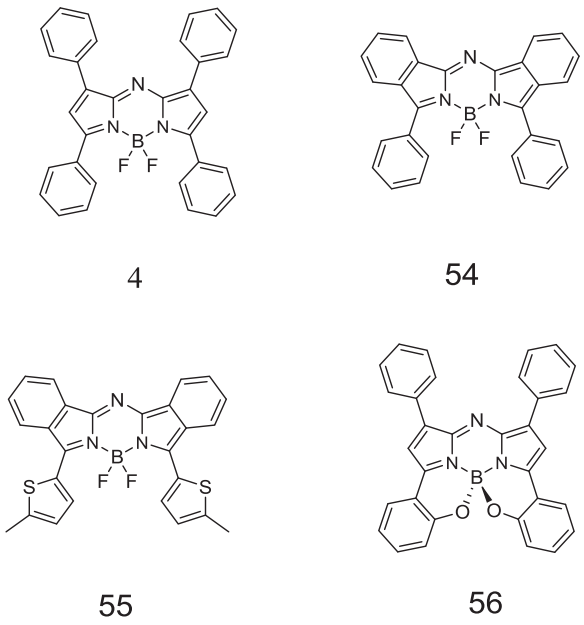

Figure 1.23 Structure of compound (4), (54), (55) and (56).

Several papers have addressed the energy levels of an ideal donor.[145-147] It has been proposed that the HOMO energy level must be below the air oxidation threshold (-5.27 eV)[147] in order to assure a high open circuit voltage (V_{OC}) in the solar cell device. The LUMO energy level of a donor must be located above the LUMO energy level of an acceptor (PCBM) and within 0.2-0.3 eV to ensure efficient electron transfer from the donor to the acceptor.[148,149]

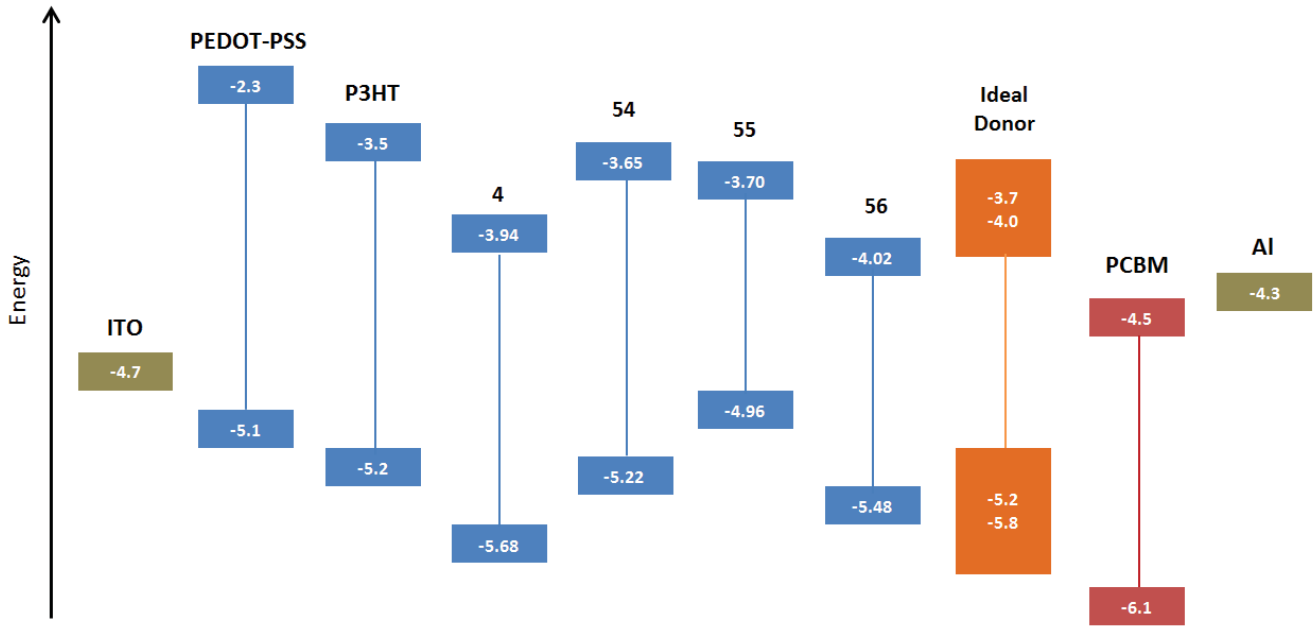

Figure 1.24 Energy levels (eV) for compounds (4), (54), (55), (56), PCBM and those of the ideal donor according to literature[145-147] (LUMO in the range -3.7 to -4.0 eV and HOMO in the range -5.2 to -5.8 eV).

The absorption maxima of the aza-BODIPY shift into the red spectral region by incorporating electron donating thiophene substituents into aza-BODIPY (Fig (1.25)).[150] It was found that the HOMO energies increased, while the LUMO energies remained more constant, which reduced the band gap, Fig. (1.26). It is obvious that the HOMO and LUMO energies of compound (60) are similar to that of compound (4), while the HOMO energies of compounds (57), (58) and (59) are significantly increased. Compound (59) showed the largest change in the HOMO energy in comparison with compound (4). Hence, compound (60) might be the best donor.[150]

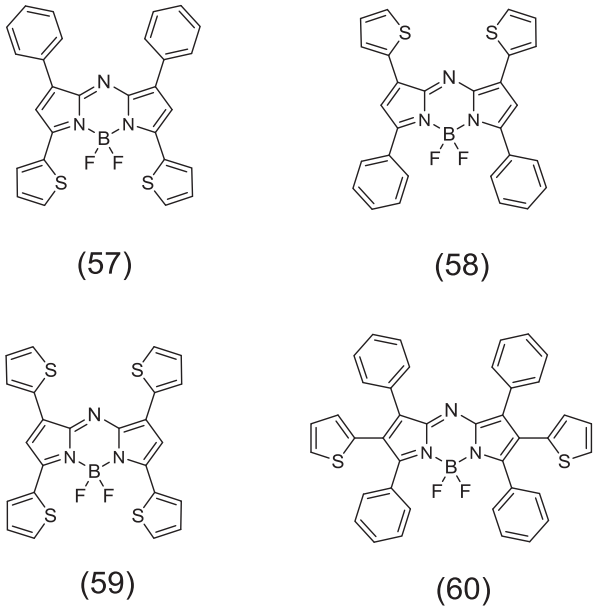

Figure 1.25 Structure of compounds (57), (58), (59) and (60).

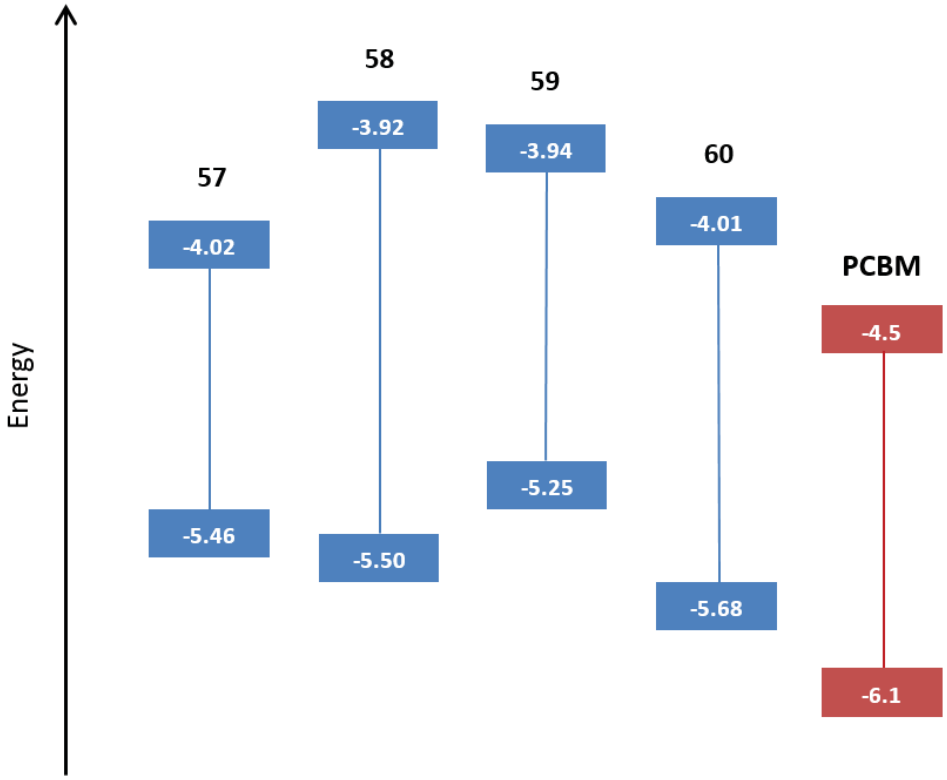

Figure 1.26 Energy levels (eV) for compounds (57), (58), (59), (60) and PCBM.

1.6 Fluorescence Spectroscopy

The emission of light from the excited states of substances is known as luminescence. Depending on the nature of the excited states, luminescence is divided into two categories: phosphorescence and fluorescence.[151] Phosphorescence is defined as the emission of light from triplet excited states. Lifetimes of phosphorescence are longer than those for fluorescence; millisecond to seconds with phosphorescence compared to in between nanoseconds to microseconds with fluorescence.[152,153]

Jablonski diagrams are regularly used to describe absorption and emission (Fig. (1.27)). Jablonski had many accomplishments in the field of fluorescence, one of them was introduction of the term “anisotropy” describing the polarized emission from solutions.[151]

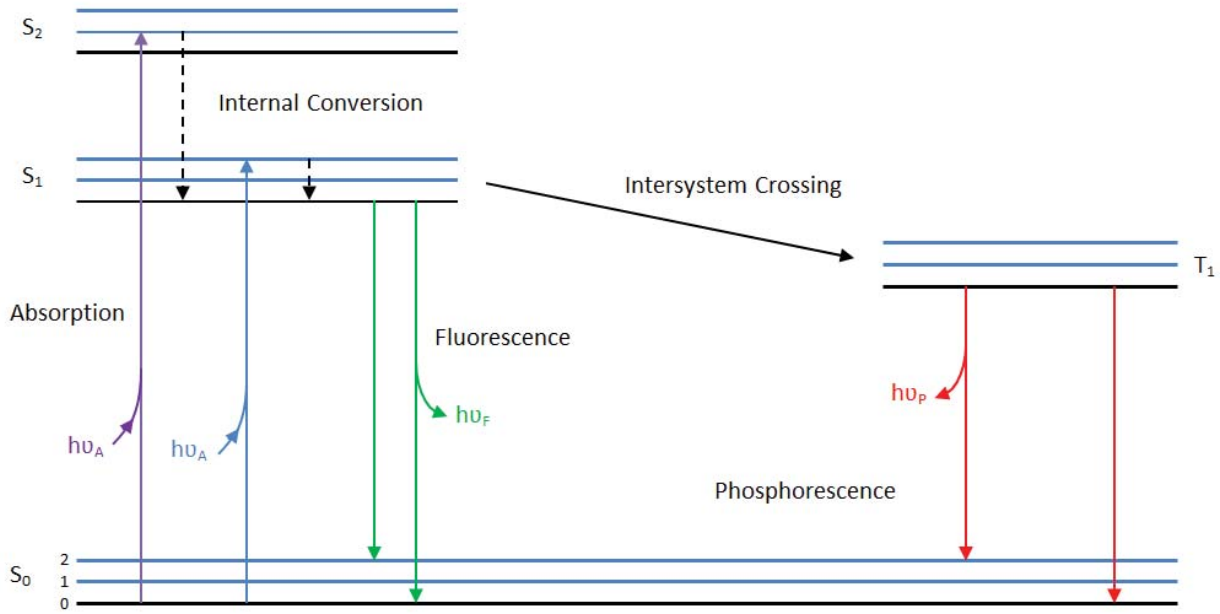

Figure 1.27 A Jablonski diagram

S_0, S_1, and S_2 represent the singlet ground, first, and second electronic states respectively. In each electronic state there are vibrational energy levels (0, 1, 2 depicted in Fig. (1.27)). The vertical lines represent transitions between states. These transitions occur in about 10^{-15} s, which is too short for significant displacement of nuclei. This is known as the Franck-Condon principle. Upon light absorption, the molecule is excited to a higher vibrational level of either S_1 or S_2, which relax rapidly to the lowest vibrational level of S_1. This process is called internal conversion. Emission from the lowest vibrational level at the S_1 is fluorescence. The emission spectrum is usually a mirror image of the absorption spectrum. This happens because electronic excitation does not alter the nuclear geometry. Intersystem crossing ($S_1 \rightarrow T_1$) occurs when the molecule in the S_1 state undergoes a spin conversion to the first triplet state (T_1). Phosphorescence is the emission that comes from the triplet T_1. The phosphorescence energy is lower than that of fluorescence. A molecule with heavy atoms in the structure facilitates intersystem crossing, which enhances the phosphorescence quantum yields.[151] One of the very interesting fluorescence phenomena is called "Stokes Shift", which was discovered at the University of Cambridge by Sir George G. Stokes in

1852.[119] This represents the difference between the maxima of the excitation and the emission.[154]

Fluorescence quenching occurs when the fluorescence intensities decrease either by dynamic quenching or static quenching.

Dynamic quenching occurs when the fluorophore in the excited state is deactivated in solution by a particular molecule called the quencher. The decrease in the intensity is described by *Stern-Volmer* equation (eq. 1.4). Upon quenching, the fluorophore is returned to the ground state without any alteration in the chemical structure. The sensitivity of the molecule to a quencher is described by the *Stern-Volmer* quenching constant (*K*).

$$\frac{I_0}{I} = 1 + \frac{K[\mathrm{Q}]}{K_0} \qquad \text{Eq. 1.4}$$

I_0 is the inherent fluorescence intensity, I is the quenched fluorescence intensity, K is the Stern-Volmer quenching constant, K_0 is the inherent internal decay constant, K/K_0 is the bimolecular quenching rate constant and [Q] is the quencher concentration. The fluorescence lifetime is described by the following equation:

$$\frac{\tau_0}{\tau} = \frac{I_0}{I} \qquad \text{Eq. 1.5}$$

τ_0 is the inherent lifetime and τ is the quenched lifetime. Hence, the lifetime shortens with addition of quencher. The life time is equal to

$$\tau = \frac{1}{(K_0 + K[Q])} \qquad \text{Eq. 1.6}$$

Static quenching occurs when the fluorophore and quencher form a non-fluorescent complex in the ground state. The association constant (K_{assoc}) between the fluorophore (F) and the quencher (Q) to form a complex is described by the following equation:

$$\frac{I_0}{I} = 1 + K_{assoc}[\mathrm{Q}] \qquad \text{Eq. 1.7}$$

The complex (F-Q) is non-fluorescent, therefore the unbound fluorophore (F) has a life time equal to (τ_0).

$$\frac{\tau_0}{\tau} = 1 \qquad \text{Eq. 1.8}$$

Static and dynamic quenching can be identified by lifetime measurements, which are usually carried out in a nanosecond range of time resolutions. Static quenching reduces the apparent concentration of the fluorophore, while dynamic quenching reduces the apparent fluorescent lifetime.[155] Sometimes, the effect of the quencher happens as a result of a combination of static and dynamic quenching (see Fig. (1.28) (c)), as described in the following modified equation:[156]

$$\frac{I_0}{I} = (1 + K[Q])(1 + K_{assoc}[Q]) = 1 + (K + K_{assoc})[Q] + KK_{assoc}[Q]$$

Temperature-effects can also determine the type of quenching. Dynamic quenching rates increase with higher temperature, while static quenching tends to be higher at lower temperatures because complex formation strength tends to be inversely proportional to temperature. Fig. (1.28) (a) and Fig. (1.28) (b) show these trend. When the quenching occurs, the quencher [Q] may interact with the fluorophore which can alter the fluorophore structure.[156] One method for examining this is the use of several quenchers with different properties. Quenching studies also determine the changes that alter the accessibility of the fluorophore to the quencher.[157]

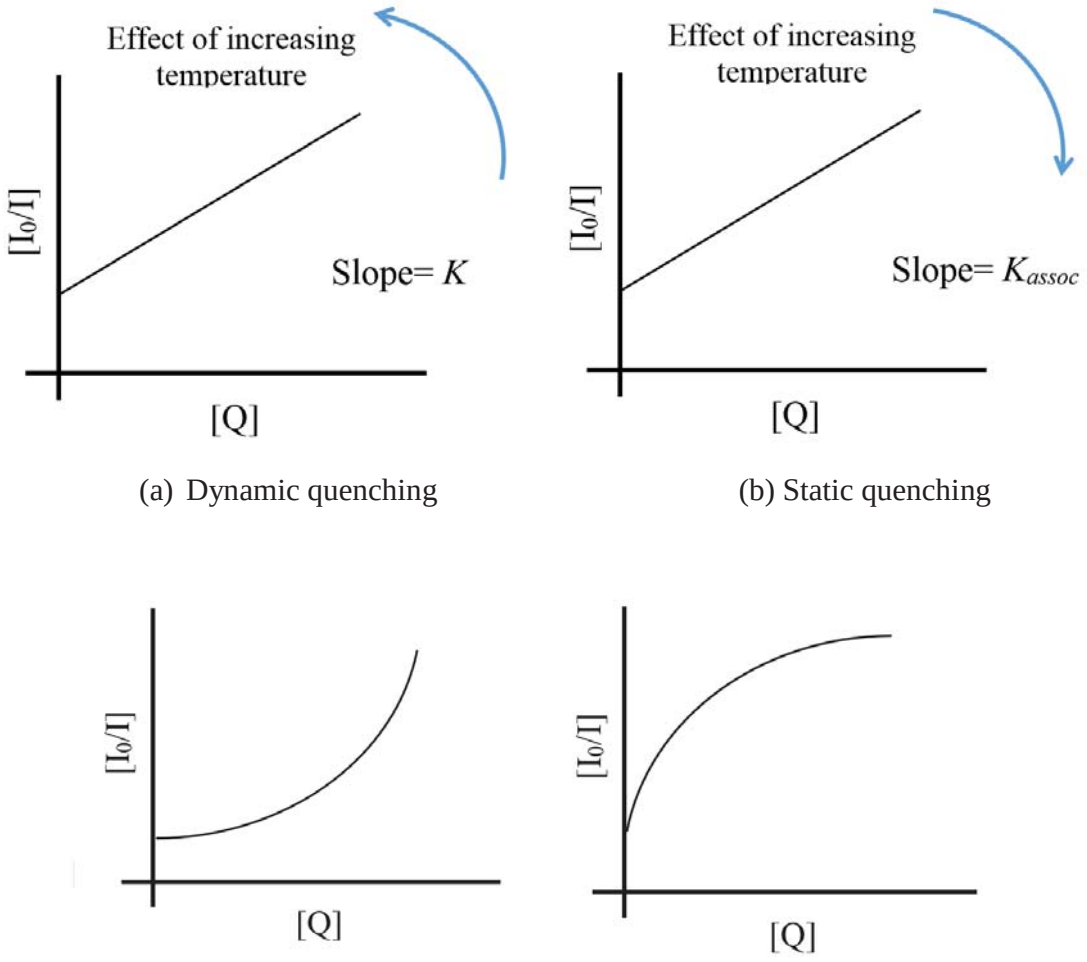

(a) Dynamic quenching (b) Static quenching

(c) Combined quenching

Figure 1.28 Comparison of dynamic and static quenching.

1.7 Time-Correlated Single-Photon Counting (TCSPC) Spectroscopy

Time-correlated single-photon counting (TCSPC) spectroscopy is a powerful analysis technique, which has been used to analyze the relaxation of molecules from an excited state to a lower energy state. TCSPC is commonly used for measurements of fluorescence lifetimes, photon migration, optical time-domain reflectometry, and time-of-flight. TCSPC has been in use since the 1970s.[158-160]

Fluorescence lifetime (τ) is a key characteristic which can be used to gain better understanding of the excited state properties of molecules,[161] to evaluate energy transfer efficiencies (through resonance energy transfer (FRET) experiments),[162-164] as an environmental probe (τ is often sensitive to the local environment)[165-170] and for fluorescent lifetime imaging microscopy (FLIM).[171-179]

The fluorescence lifetime is measured through TCSPC. Photons generated directly from the fluorescent decay (Fig. (1.29)) are counted and arrival times measured (typically picosecond (ps) or femtosecond (fs)). Laser light-sources with high mode-locked picosecond (ps) or femtosecond (fs) repetition-rates are used. A high-speed microchannel plate (MCP) is necessary for TCSPC.[180,181]

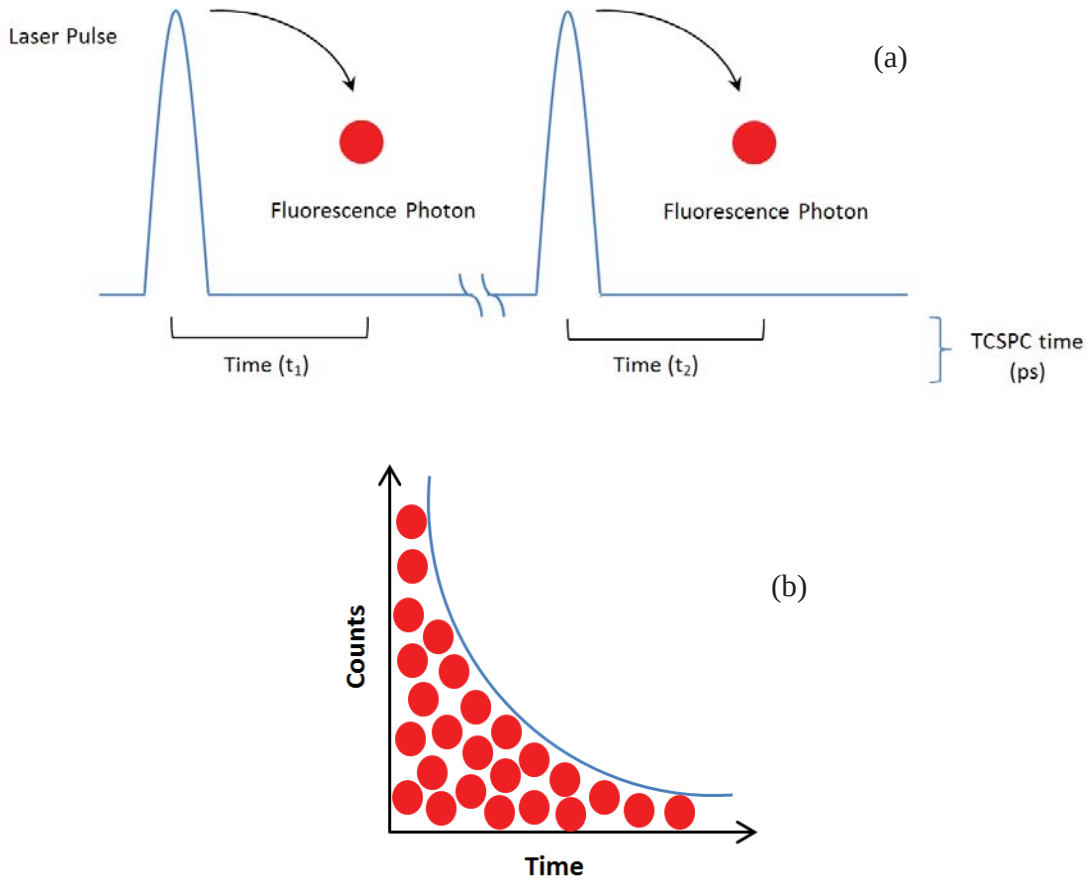

Figure 1.29 (a) TCSPC working principles and (b) the fluorescence lifetime histogram

1.8 Aims and Objectives:

The objective of this study was to make a significant contribution to the development and practical implementation of photovoltaic technology through the synthesis of novel photovoltaic (PV) materials. This study was an integral part of the MBIE project "High Efficiency Organic Photovoltaics (UOAX0911)" which is a broad-based programme including several Universities and industrial partners. The goal was to achieve high power conversion efficiencies (η). With current PV technology, much of the absorbed light is not converted to electricity, but dissipated as heat. The aim was to devise and explore a number of novel PV materials, and to pursue at least one of these through to device fabrication. The specific aims were design and synthesis of ruthenium complexes, which would be attached to silicon quantum dots (Si-QDs), of thiophene-containing polymers, which again would be attached to silicon quantum dots (Si-QDs), and of solution-processable small molecules.

Silicon quantum dots (Si-QDs) are nano-materials and their unique optoelectronic are well recognized. The aim was to produce new silicon quantum dots (Si-QDs) for solar cells applications through modification of their surfaces. Silicon quantum dots were to be made by Richard Tilley's group at Victoria University of Wellington (VUW). The aim at Massey University was to synthesise ruthenium complexes with free carboxylic acid groups and phosphonic acid on bipyridyl units, and to synthesise β'-substituted terthiophene monomers.

Aza-BODIPYs were chosen as the target solution-processable small molecules, following careful consideration of the prior work of O'Shea et. al.[182] Aza-BODIPYs have a unique set of photophysical characteristics. The study came to focus on the aza-BODIPYs, because these appeared to be the most promising materials. The aza-BODIPYs are solution-processable, and have the desirable property that they can be deposited from solution, rather like inks. The known aza-BODIPYs absorbed in the visible region of the solar spectrum (e.g. λ_{max}=650 nm for 1,3,5,7-tetraphenyl aza-dipyrromethene boron difluoride). The aim was to shift the absorption to near-infrared and tune the electronic properties of

new compounds by incorporation of electron-donating and electron- deficient groups onto the dipyrrin core structure.

The aim was to synthesise symmetrical aza-BODIPY compounds with up to two different aryl substituents (on positions 1, 3, 5 and 7) using the previously reported four-step route. The goal was design and synthesise a number of symmetrical aza-BODIPY including: terthiophene-BF_2-aza-dipyrromethene (87), methoxy-terthiophene-BF_2-aza-dipyrromethene (88), triphenylamine-BF_2-aza-dipyrromethene (100), thiophene-triphenylamine-BF_2-aza-dipyrromethene (106), benzothiadiazole-BF_2-aza-dipyrromethene (111), benzothiadiazole-thiophene-BF_2-aza-dipyrromethene (112), benzothiadiazole-triphenylamine-BF_2-aza-dipyrromethene (113), ethylenedioxythiophene-BF_2-aza-dipyrromethene (125), thiophene-phenothiazine-BF_2-aza-dipyrromethene (132), thiophene-methylpyrrole-BF_2-aza-dipyrromethene (139), thiophene-carbazole-BF_2-aza-dipyrromethene (145), fluorenone-BF_2-aza-dipyrromethene (150), and thiophene-fluorenone-BF_2-aza-dipyrromethene (151).

Characterization of the new aza-BODIPYs was to be carried out using the available techniques at the Institute of Fundamental Sciences: NMR spectroscopy, mass spectrometry, ultraviolet-visible (UV-VIS) absorption spectroscopy and fluorescence. The intention was to use time-dependent density functional theory (TD-DFT) calculations to provide a guide to the absorption energies for aza-BODIPYs. The intention was to exploit time-correlated single photon counting measurements (TCSPC) to explore donor-acceptor interactions by measuring fluorescence lifetime.

The final aim was to fabricate at Victoria University of Wellington (VUW) working organic photovoltaic (OPV) devices from the new aza-BODIPY compounds, using standard device fabrication conditions for making bulk heterojunction devices. The aim was to measure the external quantum efficiencies (EQEs) and current density-voltage (J-V) characteristics under standard test condition (STC) of Air Mass 1.5 spectrum using a xenon arc lamp as a solar simulator.

The dependence of external quantum efficiency (EQE) upon wavelength of incident light would be investigated. EQE depends on the absorption of incident light and the collection of resulted charges. When a photon is absorbed and generates an electron-hole pair, these charges must be separated and collected at the electrode. A high-efficiency material avoids charge recombination. The aim was to make these measurements of current density-voltage (J-V) characteristics and investigate of wavelength dependence for as many as possible of the novel materials, and thereby evaluate the materials for potential use in practical solar cells.

1.9 References

(1) Espinosa, N.; Hosel, M.; Angmo, D.; Krebs, F. C. *Energy & Environmental Science* **2012**, *5*, 5117.

(2) Knohl, A.; Veldkamp, E. *Nature* **2011**, *475*, 177.

(3) Aernouts, T., Katholieke Universiteit Leuven, 2006.

(4) Becquerel, A. E. *Comt*. *Rend*. *Acad*. *Sci*. **1839**, *9*, 561.

(5) Goetzberger, A.; Hoffmann, V. U.; Editors *Photovoltaic Solar Energy Generation*; Springer, 2005.

(6) Nijs, J. F.; Szlufcik, J.; Poortmans, J.; Sivoththaman, S.; Mertens, R. P. *Solar Energy Materials and Solar Cells* **2001**, *65*, 249.

(7) Aberle, A. G. *Thin Solid Films* **2009**, *517*, 4706.

(8) Bonnet, D. *Thin Solid Films* **2000**, *361–362*, 547.

(9) Raugei, M.; Bargigli, S.; Ulgiati, S. *Energy* **2007**, *32*, 1310.

(10) R.R. King, A. B., W. Hong, X.-Q. Liu, D. Bhusari, D. Larrabee, K.M. Edmondson, D.C. Law, C.M. Fetzer, S. Mesropian, N.H. Karam In *24th European Photovoltaic Solar Energy Conference* Hamburg, Germany, 2009, p 55.

(11) Fujishima, A.; Honda, K. *Nature (London)* **1972**, *238*, 37.

(12) Würfel, P. In *Physics of Solar Cells*; Wiley-VCH Verlag GmbH: 2007, p 155.

(13) McEvoy, A.; Markvart, T.; Castaner, L.; Editors *Practical Handbook of Photovoltaics: Fundamentals and Applications, Second Edition*; Elsevier Inc., 2012.

(14) Gratzel, M. *J*. *Photochem*. *Photobiol*., *C* **2003**, *4*, 145.

(15) Roncali, J. *Acc*. *Chem*. *Res*. **2009**, *42*, 1719.

(16) Snaith, H. J. *The Journal of Physical Chemistry Letters* **2013**, *4*, 3623.

(17) Kojima, A.; Teshima, K.; Shirai, Y.; Miyasaka, T. *J*. *Am*. *Chem*. *Soc*. **2009**, *131*, 6050.

(18) Qiu, J.; Qiu, Y.; Yan, K.; Zhong, M.; Mu, C.; Yan, H.; Yang, S. *Nanoscale* **2013**, *5*, 3245.

(19) Loi, M. A.; Hummelen, J. C. *Nat. Mater.* **2013**, *12*, 1087.

(20) Lee, M. M.; Teuscher, J.; Miyasaka, T.; Murakami, T. N.; Snaith, H. J. *Science (Washington, DC, U. S.)* **2012**, *338*, 643.

(21) Burschka, J.; Pellet, N.; Moon, S.-J.; Humphry-Baker, R.; Gao, P.; Nazeeruddin, M. K.; Graetzel, M. *Nature (London, U. K.)* **2013**, *499*, 316.

(22) Liu, M.; Johnston, M. B.; Snaith, H. J. *Nature (London, U. K.)* **2013**, *501*, 395.

(23) Weinberger, B. R.; Akhtar, M.; Gau, S. C. *Synthetic Metals* **1982**, *4*, 187.

(24) Glenis, S.; Tourillon, G.; Garnier, F. *Thin Solid Films* **1986**, *139*, 221.

(25) Kekuda, D.; Chu, C.-W. *AIP Conf. Proc.* **2011**, *1391*, 229.

(26) Pate, B. D.; Rogers, J. E.; Taylor, B. E.; Minch, B. A.; Deneault, J. R.; Smith, A. P.; Durstock, M. F.; American Chemical Society: 2007, p AEI.

(27) Wong, M. K.; Wong, K. Y. *Synth. Met.* **2013**, *170*, 1.

(28) Nelson, J.; Editor *The Physics of Solar Cells: Photons In, Electrons Out*; World Sci, 2003.

(29) Benanti, T.; Venkataraman, D. *Photosynth Res* **2006**, *87*, 73.

(30) Cohn, A. W.; Schimpf, A. M.; Gunthardt, C. E.; Gamelin, D. R. *Nano Lett.* **2013**, *13*, 1810.

(31) Kato, S.; Watanabe, Y.; Kurokawa, Y.; Yamada, A.; Ohta, Y.; Niwa, Y.; Hirota, M. *MRS Online Proc. Libr.* **2012**, *1512*, 1747.

(32) Nawaz, M.; Ahmad, A. *J. Semicond.* **2012**, *33*, 042001/1.

(33) Oh, J.; Yuan, H.-C.; Branz, H. M. *Nat. Nanotechnol.* **2012**, *7*, 743.

(34) Polly, S. J.; Bailey, C. G.; Bittner, Z. S.; Dai, Y.; Fernandez, E. G.; Hubbard, S. M. *Proc. SPIE* **2012**, *8256*, 825615/1.

(35) Richter, A.; Werner, F.; Cuevas, A.; Schmidt, J.; Glunz, S. W. *Energy Procedia* **2012**, *27*, 88.

(36) Shockley, W.; Queisser, H. J. *Journal of Applied Physics* **1961**, *32*, 510.

(37) Nef, J. U. *Annalen* **1894**, *280*, 263.

(38) Luque, A.; Hegedus, S.; Editors *Handbook of Photovoltaic Science and Engineering*, *Second Edition*; John Wiley & Sons Ltd., 2011.

(39) Petr, A.; Zhang, F.; Peisert, H.; Knupfer, M.; Dunsch, L. *Chem*. *Phys*. *Lett*. **2004**, *385*, 140.

(40) Al-Ibrahim, M.; Roth, H. K.; Zhokhavets, U.; Gobsch, G.; Sensfuss, S. *Sol*. *Energy Mater*. *Sol*. *Cells* **2005**, *85*, 13.

(41) Koster, L. J. A.; Mihailetchi, V. D.; Ramaker, R.; Blom, P. W. M. *Appl*. *Phys*. *Lett*. **2005**, *86*, 123509/1.

(42) Liu, J.; Shi, Y.; Yang, Y. *Adv*. *Funct*. *Mater*. **2001**, *11*, 420.

(43) Araújo, G. L.; Martí, A. *Solar Energy Materials and Solar Cells* **1994**, *33*, 213.

(44) Brabec, C. J.; Winder, C.; Sariciftci, N. S.; Hummelen, J. C.; Dhanabalan, A.; Van, H. P. A.; Janssen, R. A. J. *Adv*. *Funct*. *Mater*. **2002**, *12*, 709.

(45) Carsten, B.; Szarko, J. M.; Son, H. J.; Wang, W.; Lu, L.; He, F.; Rolczynski, B. S.; Lou, S. J.; Chen, L. X.; Yu, L. *Journal of the American Chemical Society* **2011**, *133*, 20468.

(46) Scharber, M. C.; Muehlbacher, D.; Koppe, M.; Denk, P.; Waldauf, C.; Heeger, A. J.; Brabec, C. J. *Adv*. *Mater*. *(Weinheim, Ger.)* **2006**, *18*, 789.

(47) Mihailetchi, V. D.; Xie, H.; de, B. B.; Popescu, L. M.; Hummelen, J. C.; Blom, P. W. M.; Koster, L. J. A. *Appl*. *Phys*. *Lett*. **2006**, *89*, 012107/1.

(48) Hoppe, H.; Arnold, N.; Sariciftci, N. S.; Meissner, D. *Sol*. *Energy Mater*. *Sol*. *Cells* **2003**, *80*, 105.

(49) Arias, A. C.; Granstrom, M.; Thomas, D. S.; Petritsch, K.; Friend, R. H. *Phys*. *Rev*. *B: Condens*. *Matter Mater*. *Phys*. **1999**, *60*, 1854.

(50) de, B. B. *Chemisch2Weekblad* **2001**, *97*, 26.

(51) Schroeder, R.; Feistritzer, G.; Graupner, W.; Meinhardt, G.; Berman, D.; Preishuber-Pfluegl, P.; Stelzer, F.; Faiman, D.; Leising, G. *Annu*. *Tech*. *Conf*. - *Soc*. *Plast*. *Eng*. **1999**, *57th*, 3844.

(52) Stubinger, T.; Brutting, W. *J*. *Appl*. *Phys*. **2001**, *90*, 3632.

(53) Chen, S. B.; Zhong, Z. Y. *Appl*. *Mech*. *Mater*. **2012**, *217-219*, 695.

(54) Chen, W. B.; Deng, M. Z.; Zou, H. J.; Li, C. Y.; Deng, L. F.; Lai, P. T.; Institute of Electrical and Electronics Engineers: 2010, p 447.

(55) Nguyen, N. D.; Chung, D. N.; Thao, T. T.; Hui, D. *J*. *Nanomater*. **2012**, 190290.

(56) Sarah, M. S. P.; Zahid, F. S. S.; Rusop, M. *Adv*. *Mater*. *Res*. *(Durnten-Zurich, Switz.)* **2012**, *576*, 773.

(57) Sarah, M. S. P.; Zahid, F. S. S.; Rusop, M. *Int*. *J*. *Photoenergy* **2012**, 872324.

(58) Schnegg, A.; Behrends, J.; Fehr, M.; Lips, K. *Phys*. *Chem*. *Chem*. *Phys*. **2012**, *14*, 14418.

(59) Dantanarayana, V.; Moule, A.; Faller, R.; 243rd ACS National Meeting & Exposition, San Diego, CA, United States: 2012, p 132.

(60) Hou, L.-t.; Wang, B.; Wang, E.-g. *Faguang Xuebao* **2012**, *33*, 322.

(61) Nevil, N.; Ling, Y.; Mierloo, S. V.; Kesters, J.; Piersimoni, F.; Adriaensens, P.; Lutsen, L.; Vanderzande, D.; Manca, J.; Maes, W.; Doorslaer, S. V.; Goovaerts, E. *Phys*. *Chem*. *Chem*. *Phys*. **2012**, *14*, 15774.

(62) Soldera, M.; Taretto, K.; Kirchartz, T. *Phys*. *Status Solidi A* **2012**, *209*, 207.

(63) Tan, F.; Qu, S.; Wu, J.; Liu, K.; Zhou, S.; Wang, Z. *Nanoscale Res*. *Lett*. **2011**, *6*, 298.

(64) Goh, C.; Scully, S. R.; McGehee, M. D. *J*. *Appl*. *Phys*. **2007**, *101*, 114503/1.

(65) Lee, Y.-J.; Lloyd, M. T.; Olson, D. C.; Grubbs, R. K.; Lu, P.; Davis, R. J.; Voigt, J. A.; Hsu, J. W. P. *J*. *Phys*. *Chem*. *C* **2009**, *113*, 15778.

(66) Li, Y.; Lu, P.; Jiang, M.; Dhakal, R.; Thapaliya, P.; Peng, Z.; Jha, B.; Yan, X. *J*. *Phys*. *Chem*. *C* **2012**, *116*, 25248.

(67) Moon, S.-J.; Baranoff, E.; Zakeeruddin, S. M.; Yeh, C.-Y.; Diau, E. W.-G.; Graetzel, M.; Sivula, K. *Chem*. *Commun*. *(Cambridge, U*. *K*.*)* **2011**, *47*, 8244.

(68) Rattanavoravipa, T.; Sagawa, T.; Yoshikawa, S. *Sol*. *Energy Mater*. *Sol*. *Cells* **2008**, *92*, 1445.

(69) Cortina, H.; Pineda, E.; Hu, H. *Sol*. *Energy* **2012**, *86*, 1004.

(70) Pineda, E.; Nicho, M. E.; Nair, P. K.; Hu, H. *Sol*. *Energy* **2012**, *86*, 1017.

(71) Wang, H.; He, D.; Wang, Y.; Liu, Z.; Wu, H.; Wang, J. *Phys*. *Status Solidi A* **2011**, *208*, 2339.

(72) Wang, H. T.; He, D. W.; Wang, Y. S.; Liu, Z. Y.; Wu, H. P.; Wang, J. G.; Zhao, Y. *Sci*. *China: Phys*., *Mech*. *Astron*. **2012**, *55*, 1356.

(73) Wang, J.; Wang, Y.; He, D.; Wu, H.; Wang, H.; Zhou, P.; Zhang, Y.; Fu, M. *Adv*. *Mater*. *Res*. *(Durnten-Zurich, Switz.)* **2012**, *396-398*, 2471.

(74) Barlier, V.; Bounor-Legare, V.; Boiteux, G.; Davenas, J.; Slazak, A.; Rybak, A.; Jung, J. *Synth*. *Met*. **2009**, *159*, 508.

(75) Lin, Y.-J.; Su, T.-H.; Lin, J.-C.; Su, Y.-C. *Synth*. *Met*. **2012**, *162*, 406.

(76) Albrecht, S.; Janietz, S.; Schindler, W.; Frisch, J.; Kurpiers, J.; Kniepert, J.; Inal, S.; Pingel, P.; Fostiropoulos, K.; Koch, N.; Neher, D. *J*. *Am*. *Chem*. *Soc*. **2012**, *134*, 14932.

(77) Chen, H.; Shi, Y.; Fu, W.; Qiu, W.; Wang, L.; Nan, Y.; Shi, M.; Li, H.; Zhejiang University, Peop. Rep. China . 2012, p 13pp.

(78) Distler, A.; Kutka, P.; Sauermann, T.; Egelhaaf, H.-J.; Guldi, D. M.; Di, N. D.; Meskers, S. C. J.; Janssen, R. A. J. *Chem*. *Mater*. **2012**, *24*, 4397.

(79) Imamura, S.; Palanisamy, K.; Kannappan, S.; Ochiai, S. *J*. *Korean Phys*. *Soc*. **2012**, *61*, 464.

(80) Kirchartz, T.; Agostinelli, T.; Campoy-Quiles, M.; Gong, W.; Nelson, J. *J*. *Phys*. *Chem*. *Lett*. **2012**, *3*, 3470.

(81) Wang, A. *Cailiao Yanjiu Xuebao* **2012**, *26*, 327.

(82) Wang, H.-Q.; Li, N.; Guldal, N. S.; Brabec, C. J. *Org*. *Electron*. **2012**, *13*, 3014.

(83) Abdel-Malik, T. G.; Elsayed, A. H. *Proc*. *SPIE-Int*. *Soc*. *Opt*. *Eng*. **2007**, *6656*, 66560H/1.

(84) Coffey, D. C.; Ferguson, A. J.; Kopidakis, N.; Rumbles, G. *ACS Nano* **2010**, *4*, 5437.

(85) Ji, R.; Tang, L.; Song, L.; Chen, X.; Ma, Y.; Wang, Y.; Kunming Institute of Physics, Peop. Rep. China . 2011, p 10pp.

(86) Klenkler, R. A.; Yuen, A. P.; Bamsey, N. M.; Xerox Corp., USA . 2012, p 18pp.

(87) Liu, Y.; Liu, A.; Liu, W.; Sang, Y.; Hu, Z.; Kang, D. *Appl*. *Surf*. *Sci*. **2010**, *257*, 2176.

(88) Wu, J.; Li, W.; Xi, X.; Wang, Z.; Ji, J.; Gu, X.; Li, G. *Bandaoti Jishu* **2011**, *36*, 505.

(89) Zheng, F.; Shen, Y.; Gu, F.; Zhang, J.; Zhang, J. *Proc*. *SPIE* **2008**, *6984*, 69843J/1.

(90) Lutsyk, P.; Misiewicz, J.; Podhorodecki, A.; Vertsimakha, Y. *Sol*. *Energy Mater*. *Sol*. *Cells* **2007**, *91*, 47.

(91) Reddy, V. S.; Karak, S.; Ray, S. K.; Dhar, A. *J*. *Phys*. *D: Appl*. *Phys*. **2009**, *42*, 145103/1.

(92) Schon, J. H.; Kloc, C.; Batlogg, B. *Synth*. *Met*. **2001**, *124*, 95.

(93) Schon, J. H.; Kloc, C.; Bucher, E.; Batlogg, B. *Nature (London)* **2000**, *403*, 408.

(94) Signerski, R.; Jarosz, G.; Godlewski, J. *Macromol*. *Symp*. **2004**, *212*, 357.

(95) Chamberlain, G. A. *J*. *Appl*. *Phys*. **1982**, *53*, 6262.

(96) Skotheim, T.; Yang, J. M.; Otvos, J.; Klein, M. P. *J*. *Chem*. *Phys*. **1982**, *77*, 6151.

(97) Chen, J.; Huang, F.; Zhang, J.; Zhu, Y.; Mo, Y.; Sun, J.; South China University of Technology, Peop. Rep. China; AU Optronics Suzhou Corp.; AU Optronics Corporation . 2012, p 30pp.

(98) Chen, M.; Fu, W.; Shi, M.; Hu, X.; Pan, J.; Ling, J.; Li, H.; Chen, H. *J*. *Mater*. *Chem*. *A* **2013**, *1*, 105.

(99) Choi, D. H.; Kim, G. H.; Ha, J. S.; Korea University, Research and Business Foundation, S. Korea . 2012, p 14pp.

(100) Lee, J. W.; Choi, Y. S.; Jo, W. H. *Org*. *Electron*. **2012**, *13*, 3060.

(101) Mustonen, T.; Chebotareva, N.; BASF SE, Germany; BASF China Company Limited . 2012, p 126pp.

(102) Yuan, J.; Huang, X.; Zhang, F.; Lu, J.; Zhai, Z.; Di, C.; Jiang, Z.; Ma, W. *J. Mater. Chem.* **2012**, *22*, 22734.

(103) Kamm, V.; Howard, I. A.; Li, C.; Muellen, K.; Laquai, F.; ACS, Pacifichem 2010, International Chemical Congress of Pacific Basin Societies, Honolulu, HI, United States: 2010, p 674.

(104) Kotowski, D.; Kozma, E.; Catellani, M.; Luzzati, S. *MRS Online Proc. Libr.* **2011**, *1390*, No pp. given.

(105) Li, C.; Wonneberger, H. *Adv. Mater. (Weinheim, Ger.)* **2012**, *24*, 613.

(106) Shi, M.-m.; Hao, F.; Zuo, L.-j.; Hu, X.-l.; Fu, W.-f.; Chen, H.-z. *Gongneng Cailiao* **2012**, *43*, 1122.

(107) Hiramoto, M.; Nakamura, H.; Shiojiri, T.; Yokoyama, M. *Kobunshi Ronbunshu* **1990**, *47*, 915.

(108) Minami, N.; Yokoyama, Y. *Kenkyu Hokoku - Sen'i Kobunshi Zairyo Kenkyusho* **1992**, *171*, 7.

(109) Yoshikawa, M.; Suzuki, T.; Ricoh Co., Ltd., Japan . 1991, p 7 pp.

(110) Bura, T.; Leclerc, N.; Fall, S.; Leveque, P.; Heiser, T.; Retailleau, P.; Rihn, S.; Mirloup, A.; Ziessel, R. *J. Am. Chem. Soc.* **2012**, *134*, 17404.

(111) Hattori, S.; Ohkubo, K.; Urano, Y.; Sunahara, H.; Nagano, T.; Wada, Y.; Tkachenko, N. V.; Lemmetyinen, H.; Fukuzumi, S. *J. Phys. Chem. B* **2005**, *109*, 19042.

(112) Hattori, S.; Ohkubo, K.; Urano, Y.; Sunahara, H.; Nagano, T.; Wada, Y.; Tkachenko, N. V.; Lemmetyinen, H.; Fukuzumi, S. *J. Phys. Chem. B* **2005**, *109*, 15368.

(113) Lin, H.-Y.; Huang, W.-C.; Chen, Y.-C.; Chou, H.-H.; Hsu, C.-Y.; Lin, J. T.; Lin, H.-W. *Chem. Commun. (Cambridge, U. K.)* **2012**, *48*, 8913.

(114) Suzuki, S.; Kozaki, M.; Nozaki, K.; Okada, K. *J. Photochem. Photobiol., C* **2011**, *12*, 269.

(115) Flavin, K.; Lawrence, K.; Bartelmess, J.; Tasior, M.; Navio, C.; Bittencourt, C.; O'Shea, D. F.; Guldi, D. M.; Giordani, S. *ACS Nano* **2011**, *5*, 1198.

(116) Leblebici, S. Y.; Catane, L.; Barclay, D. E.; Olson, T.; Chen, T. L.; Ma, B. *ACS Appl. Mater. Interfaces* **2011**, *3*, 4469.

(117) Lin, Y.; Li, Y.; Zhan, X. *Chem. Soc. Rev.* **2012**, *41*, 4245.

(118) Hummelen, J. C.; Knight, B. W.; LePeq, F.; Wudl, F.; Yao, J.; Wilkins, C. L. *The Journal of Organic Chemistry* **1995**, *60*, 532.

(119) Stokes, G. G. *Philosophical Transactions of the Royal Society of London* **1852**, *142*, 463.

(120) Guldi, D. M. *Chem. Commun. (Cambridge)* **2000**, 321.

(121) Prato, M. *J. Mater. Chem.* **1997**, *7*, 1097.

(122) Diederich, F.; Gomez-Lopez, M. *Chem. Soc. Rev.* **1999**, *28*, 263.

(123) Akasaka, T. *Angew. Chem., Int. Ed.* **2008**, *47*, 633.

(124) Wienk, M. M.; Kroon, J. M.; Verhees, W. J. H.; Knol, J.; Hummelen, J. C.; van, H. P. A.; Janssen, R. A. J. *Angew. Chem., Int. Ed.* **2003**, *42*, 3371.

(125) Tschesche, R. *Angewandte Chemie* **1938**, *51*, 27.

(126) Scheibe, G.; Daltrozzo, E. *Adv. Heterocycl. Chem.* **1966**, *7*, 153.

(127) Loudet, A.; Burgess, K. *Chem. Rev. (Washington, DC, U. S.)* **2007**, *107*, 4891.

(128) Boyer, J. H.; Haag, A. M.; Sathyamoorthi, G.; Soong, M. L.; Thangaraj, K.; Pavlopoulos, T. G. *Heteroat. Chem.* **1993**, *4*, 39.

(129) Gorman, A.; Killoran, J.; O'Shea, C.; Kenna, T.; Gallagher, W. M.; O'Shea, D. F. *J. Am. Chem. Soc.* **2004**, *126*, 10619.

(130) Rogers, M. A. T. *J. Chem. Soc.* **1943**, 590.

(131) Knott, E. B. *J. Chem. Soc.* **1947**, 1196.

(132) Davies, W. H.; Rogers, M. A. T. *J. Chem. Soc.* **1944**, 126.

(133) Hall, M. J.; McDonnell, S. O.; Killoran, J.; O'Shea, D. F. *J. Org. Chem.* **2005**, *70*, 5571.

(134) Loudet, A.; Burgess, K. *Chemical Reviews* **2007**, *107*, 4891.

(135) Bird, C. W.; Jiang, L. *Tetrahedron Lett*. **1992**, *33*, 7253.

(136) Bredereck, H.; Vollmann, H. W. *Chem*. *Ber*. **1972**, 2271.

(137) Coskun, A.; Yilmaz, M. D.; Akkaya, E. U. *Org*. *Lett*. **2007**, *9*, 607.

(138) Zhao, W.; Carreira, E. M. *Angew*. *Chem*., *Int*. *Ed*. **2005**, *44*, 1677.

(139) Mueller, T.; Gresser, R.; Leo, K.; Riede, M. *Solar Energy Materials and Solar Cells* **2012**, *99*, 176.

(140) Rousseau, T.; Cravino, A.; Bura, T.; Ulrich, G.; Ziessel, R.; Roncali, J. *Chem*. *Commun*. *(Cambridge*, *U*. *K*.*)* **2009**, 1673.

(141) Min, J.; Ameri, T.; Gresser, R.; Lorenz-Rothe, M.; Baran, D.; Troeger, A.; Sgobba, V.; Leo, K.; Riede, M.; Guldi, D. M.; Brabec, C. J. *ACS Appl*. *Mater*. *Interfaces* **2013**, *5*, 5609.

(142) Mueller, T.; Gresser, R.; Leo, K.; Riede, M. *Sol*. *Energy Mater*. *Sol*. *Cells* **2012**, *99*, 176.

(143) Leblebici, S. Y.; Catane, L.; Barclay, D. E.; Olson, T.; Chen, T. L.; Ma, B. *ACS Applied Materials & Interfaces* **2011**, *3*, 4469.

(144) Min, J.; Ameri, T.; Gresser, R.; Lorenz-Rothe, M.; Baran, D.; Troeger, A.; Sgobba, V.; Leo, K.; Riede, M.; Guldi, D. M.; Brabec, C. J. *ACS Applied Materials & Interfaces* **2013**, *5*, 5609.

(145) Koster, L. J. A.; Mihailetchi, V. D.; Blom, P. W. M. *Applied Physics Letters* **2006**, *88*, 093511.

(146) Scharber, M. C.; Mühlbacher, D.; Koppe, M.; Denk, P.; Waldauf, C.; Heeger, A. J.; Brabec, C. J. *Advanced Materials* **2006**, *18*, 789.

(147) de Leeuw, D. M.; Simenon, M. M. J.; Brown, A. R.; Einerhand, R. E. F. *Synthetic Metals* **1997**, *87*, 53.

(148) Choulis, S. A.; Nelson, J.; Kim, Y.; Poplavskyy, D.; Kreouzis, T.; Durrant, J. R.; Bradley, D. D. C. *Applied Physics Letters* **2003**, *83*, 3812.

(149) Blouin, N.; Michaud, A.; Gendron, D.; Wakim, S.; Blair, E.; Neagu-Plesu, R.; Belletête, M.; Durocher, G.; Tao, Y.; Leclerc, M. *Journal of the American Chemical Society* **2007**, *130*, 732.

(150) Gresser, R.; Hartmann, H.; Wrackmeyer, M.; Leo, K.; Riede, M. *Tetrahedron* **2011**, *67*, 7148.

(151) Albrecht, C. *Anal*. *Bioanal*. *Chem*. **2008**, *390*, 1223.

(152) Itoh, T. *Chem*. *Rev*. *(Washington, DC, U*. *S.)* **2012**, *112*, 4541.

(153) Ye, J.; Zheng, C.-J.; Ou, X.-M.; Zhang, X.-H.; Fung, M.-K.; Lee, C.-S. *Adv*. *Mater*. *(Weinheim, Ger.)* **2012**, *24*, 3410.

(154) Rost, F. W. D. *Fluorescence Microscopy*; Cambridge University Press, 1992; Vol. One.

(155) Lakowicz, J. R.; Weber, G. *Biochemistry* **1973**, *12*, 4161.

(156) Lakowicz, J. *Principles of Fluorescence Spectroscopy*; Kluwer Academic/Plenum Publishers: New York, Boston, Dordrecht, London, Moscow, 1999.

(157) Johnson, D. A.; Yguerabide, J. *Biophysical Journal* **1985**, *48*, 949.

(158) Wild, U. P.; Holzwarth, A. R.; Good, H. P. *Rev*. *Sci*. *Instrum*. **1977**, *48*, 1621.

(159) Lytle, F. E.; Kelsey, M. S. *Anal*. *Chem*. **1974**, *46*, 855.

(160) Visser, A. J. W. G.; Van, H. A. *J*. *Biochem*. *Biophys*. *Methods* **1979**, *1*, 195.

(161) Nagy, A. M.; Talbot, F. O.; Czar, M. F.; Jockusch, R. A. *Journal of Photochemistry and Photobiology A: Chemistry* **2012**, *244*, 47.

(162) Nakada, S.; Kimura, N.; Mitsui Engineering & Shipbuilding Co., Ltd., Japan . 2009, p 72pp.

(163) Rusanov, A. L.; Ivashina, T. V.; Vinokurov, L. M.; Fiks, I. I.; Orlova, A. G.; Turchin, I. V.; Meerovich, I. G.; Zherdeva, V. V.; Savitsky, A. P. *J*. *Biophotonics* **2010**, *3*, 774.

(164) Zhong, W. *Anal*. *Bioanal*. *Chem*. **2009**, *394*, 47.

(165) Achilefu, S.; Berezin, M.; Akers, W.; Lee, H.; Bai, M.; Bloch, S.; Zhang, Z.; Ye, Y.; Nothdurft, R.; Culver, J.; Almutairi, A.; Frechet, J. M. J.; 236th ACS National Meeting, Philadelphia, PA, United States: 2008, p 272.

(166) Elgass, K.; Caesar, K.; Schleifenbaum, F.; Meixner, A. J.; Harter, K.; Farkas, D. L.; Nicolau, D. V.; Leif, R. C. *Proc*. *SPIE* **2010**, *7568*, 756804/1.

(167) Fager, D. R.; Schuster, K. C.; Burden, D. L.; Walhout, P. K.; American Chemical Society: 2010, p PHYS.

(168) Pliss, A.; Zhao, L.; Ohulchanskyy, T. Y.; Qu, J.; Prasad, P. N. *ACS Chem*. *Biol*. **2012**, *7*, 1385.

(169) Vallee, R. A. L.; Baruah, M.; Hofkens, J.; De, S. F. C.; Boens, N.; Van, d. A. M.; Beljonne, D. *J*. *Chem*. *Phys*. **2007**, *126*, 184902/1.

(170) Yoshikawa, Y.; Fujitsuka, M.; Watanabe, A.; Ito, O.; Sato, E.; Kokubun, H. *Heterocycles* **2003**, *59*, 759.

(171) Esposito, A.; Wouters, F. S. *Curr*. *Protoc*. *Cell Biol*. **2004**, *Chapter 4*, Unit 4.14.

(172) Godavarty, A.; Sevick-Muraca, E. M.; Eppstein, M. J. *Med Phys* **2005**, *32*, 992.

(173) Herl, L.; Lleo, A.; Thomas, A. V.; Nyborg, A. C.; Jansen, K.; Golde, T. E.; Hyman, B. T.; Berezovska, O. *Biochem*. *Biophys*. *Res*. *Commun*. **2006**, *340*, 668.

(174) Kahn, E.; Lizard, G.; Dumas, D.; Frouin, F.; Menetrier, F.; Stoltz, J.-F.; Todd-Pokropek, A. *Anal*. *Quant*. *Cytol*. *Histol*. **2004**, *26*, 233.

(175) Pena, E. J.; Robles, L. G.; Zanek, M. C.; Borniego, M. B.; Reyes, C. A.; Heinlein, M.; Garcia, M. L. *Virus Res*. **2012**, *170*, 34.

(176) Provenzano, P. P.; Eliceiri, K. W.; Keely, P. J. *Clin*. *Exp*. *Metastasis* **2009**, *26*, 357.

(177) Uemura, K.; Farner, K. C.; Nasser-Ghodsi, N.; Jones, P.; Berezovska, O. *Mol*. *Neurodegener*. **2011**, *6*, 15.

(178) Xiong, J.-P.; Mahalingham, B.; Alonso, J. L.; Borrelli, L. A.; Rui, X.; Anand, S.; Hyman, B. T.; Rysiok, T.; Muller-Pompalla, D.; Goodman, S. L.; Arnaout, M. A. *J*. *Cell Biol*. **2009**, *186*, 589.

(179) Yasuda, R. *Cold Spring Harb*. *Protoc*. **2012**, *2012*.

(180) O'Connor, D. V.; Ware, W. R.; Andre, J. C. *J*. *Phys*. *Chem*. **1979**, *83*, 1333.

(181) Phillips, D.; Drake, R. C.; O'Connor, D. V.; Christensen, R. L. *Anal*. *Instrum*. *(N*. *Y*.*)* **1985**, *14*, 267.

(182) Gorman, A.; Killoran, J.; O'Shea, C.; Kenna, T.; Gallagher, W. M.; O'Shea, D. F. *Journal of the American Chemical Society* **2004**, *126*, 10619.

Chapter 2

Syntheses of Aza-BODIPYs and other Small Molecules

Chapter 2

2.1 Introduction

The experimental techniques and methods which have been employed to synthesize and characterize the various novel photovoltaic (PV) materials are described in this Chapter. The syntheses of *β'*-substituted terthiophene monomers and ruthenium complexes, to which it was intended to attach the silicon quantum dots (Si-QDs), are discussed in Sections (2.33) and (2.34) respectively. The syntheses of silicon quantum dots and their surface modification are discussed in Section (2.35). The syntheses of the promising solution-processable aza-BODIPYs are discussed more fully in Sections (2.4) to (2.22). The details of the attempted syntheses of other aza-BODIPYs are given in Sections (2.23) to (2.32).

The effect of substitution on the formation of aza-BODIPYs and the expected effects on the electronic energy levels are discussed in Section (2.2). Shifts to significantly longer wavelengths were sought in both absorption and emission spectra, through adding substituents and creating additional conjugation. Among substituents investigated were triphenylamine (TPA), terthiophene (TT), benzothiadiazole (BTZ), ethylenedioxythiophene (EDOT), thiophene, phenothiazine (PTZ), methylpyrrole (MPy), carbazole (CB), and fluorenone (FN) (Fig. 2.1). The mechanism of the four-step route used to synthesise aza-BODIPYs is examined in this Chapter (Section (2.3)). ^{1}H NMR and mass spectrometry are discussed in Section (2.37), while detailed results are listed in Section (2.39).

Because of the large number of aza-BODIPYs and their unwieldy names, a rule has been adopted which considers only the groups of interest at positions 1, 3, 5, and 7. Fig. (2.1) (a) shows the IUPAC numbering of the BF_2-aza-dipyrromethene core (aza-BODIPY); Fig. (2.1) (b)-(j) give the structures of the substituent groups. The aza-dipyrromethene core (without BF_2 substituents) will be referred to as aza-DIPY. The new compounds were numbered according to the chronological order in which they were synthesised.

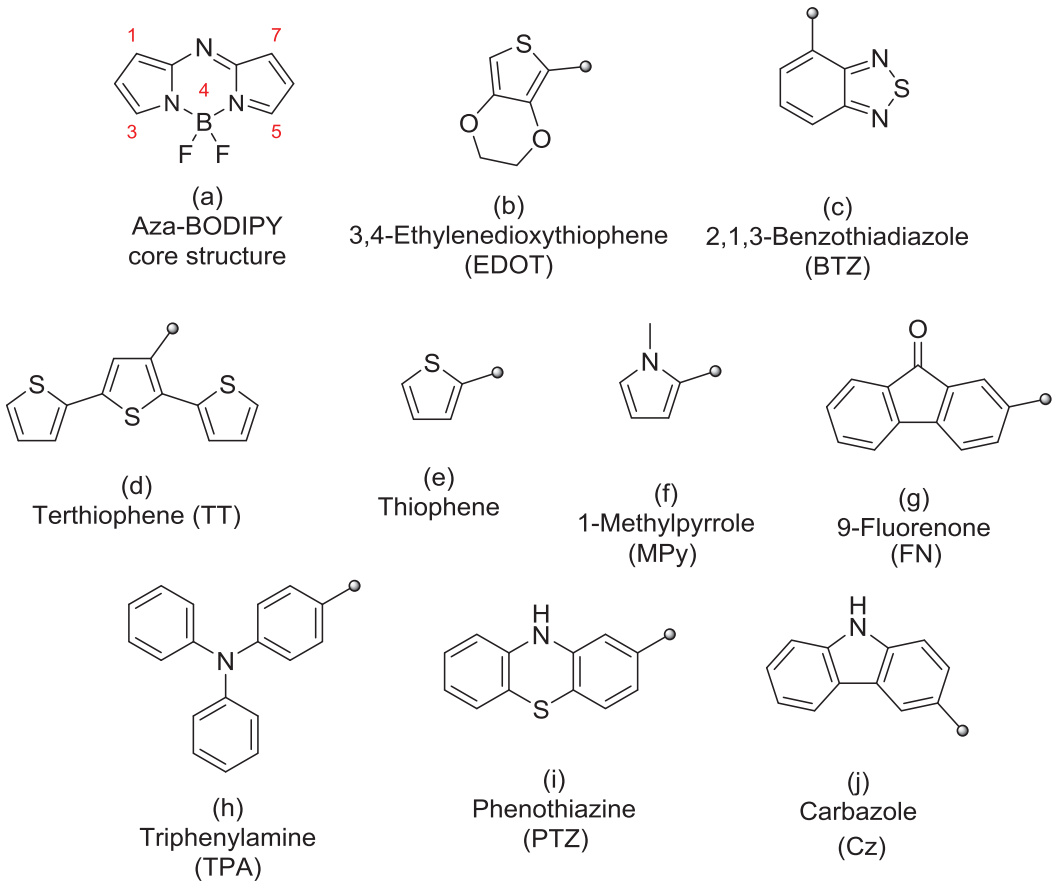

Figure 2.1 (a) IUPAC numbering of the aza-BODIPY core; (b)-(j) the key building-blocks of the target aza-BODIPYs. (∘) represents the point of attachment of a group to the aza-BODIPY core)

2.2 Yields and Structure–Property Relationships of the Aza-BODIPYs

The aim was to substitute the aza-BODIPY π-conjugated core symmetrically (on positions 1, 3, 5 and 7), using a previously reported four-step route (Fig. 2.2),[1-3] which allowed the introduction of up to two different aryl substituents (i.e. both positions 1 and 7 are substituted equally with an aryl group; positions 3 and 5 substituted equally with a different aryl group). The successfully synthesised aza-BODIPYs were terthiophene-BF_2-aza-dipyrromethene (87), methoxy-terthiophene-BF_2-aza-dipyrromethene (88), triphenylamine-BF_2-aza-dipyrromethene (100), thiophene-triphenylamine-BF_2-aza-dipyrromethene (106), benzothiadiazole-BF_2-aza-dipyrromethene (111), benzothiadiazole-thiophene-BF_2-aza-dipyrromethene (112), benzothiadiazole-triphenylamine-BF_2-aza-dipyrromethene (113), ethylenedioxythiophene-BF_2-aza-dipyrromethene (125), thiophene-phenothiazine-BF_2-aza-dipyrromethene (132), thiophene-methylpyrrole-BF_2-aza-dipyrromethene (139), thiophene-carbazole-BF_2-aza-dipyrromethene (145), fluorenone-BF_2-aza-dipyrromethene (150), and thiophene-fluorenone-BF_2-aza-dipyrromethene (151) (Fig. 2.3).

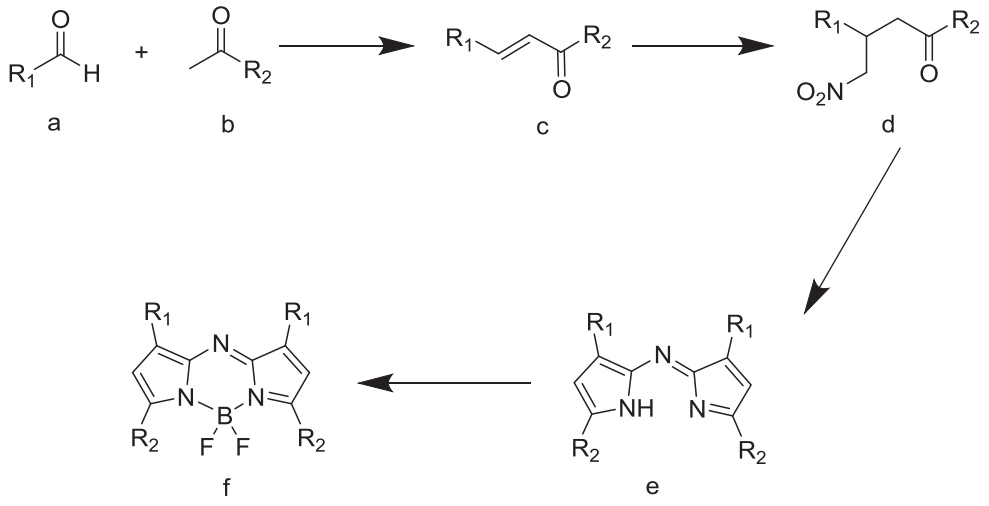

Figure 2.2 The synthesis of aza-BODIPYs.

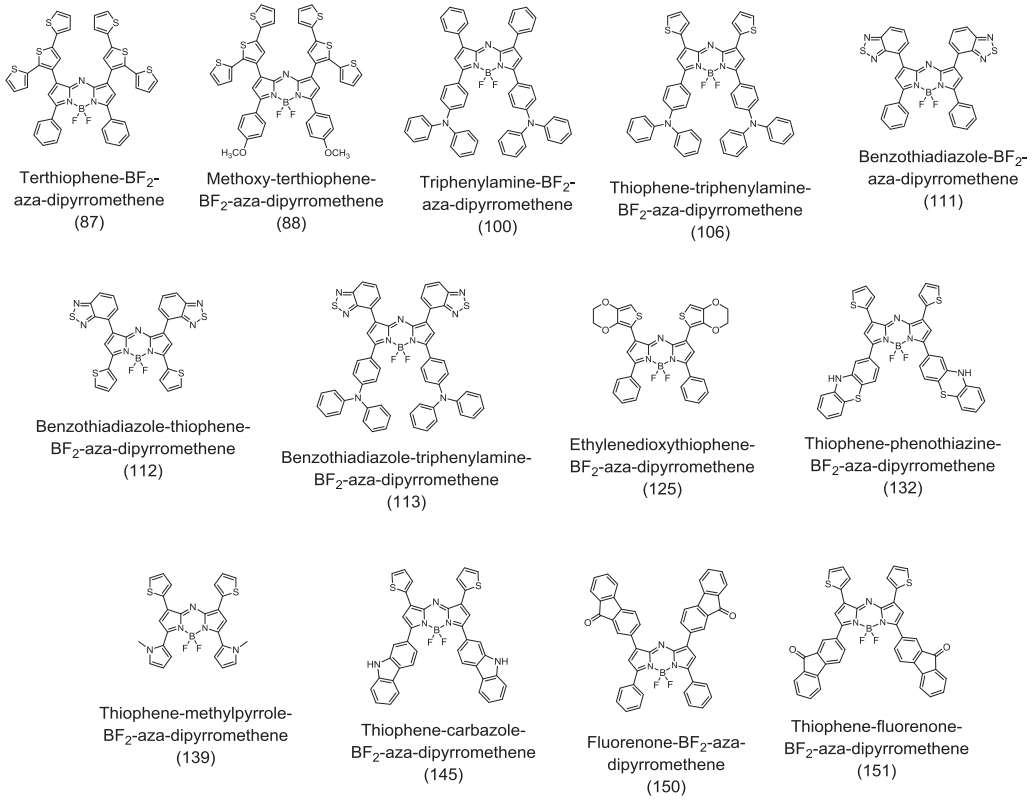

Figure 2.3 The new successfully synthesised aza-BODIPYs (aza-BODIPYs were numbered chronologically as they were synthesised).

Table (2.1) shows the yields for compounds (c), (d), (e) and (f) (see Fig. (2.2)) in comparison with the standard aza-BODIPY (compound (4)). Rows (1) and (2) (Table 2.1) are literature yields,[4-8] while rows (3) to (15) are the experimental yields for the novel aza-BODIPYs synthesised in this study (Sections (2.2) to (2.32)).

Replacement of the phenyl R_1 group of the standard aza-BODIPY compound (entry 1) with thiophene to give compound (58) gave somewhat similar yields[2,6-9] for step (c), step (d) and step (f), but step (e) at 6% is lower for the latter (see Table (2.1)). Replacement however with terthiophene (compound (87)), BTZ (compound (111)), EDOT (compound (125)) or fluorenone (compound (150)) resulted in a reduction in the yields of intermediates (c) to 70%, 60%, 60% and 28% respectively (Table (2.1)). These lower yields might have been due to steric factors, as well as electronic effects. Intermediate (e) was also produced in low yield in this set and indeed for all of the compounds. Given that the R_2 (phenyl) group was the same (entry 1 and compounds (58), (87) and (125)) the derived nucleophile was the same for reaction (c) and this interacted with the variously positively charged aldehydic carbon moieties containing the R_1 groups which were electron donating or accepting. The formation of intermediate (e) required the correct orientation of two differently substituted pyrrole molecules and the steric bulk of the R_1 and R_2 groups would quite likely have been one factor that determined the yields.

Table 2.1: Substitution effects on the formation of the novel aza-BODIPYs. Rows (1) and (2) are literature yields,[4-8] while rows (3) to (15) are the experimental yields for the novel aza-BODIPYs obtained experimentally (Sections (2.2) to (2.32)).

	Compound	R_1 Group	R_2 Group	% yield of intermediate (c)[i]	% yield of intermediate (d)[ii]	% yield of aza-DIPY (e)[iii]	% yield of aza-BODIPY (f)[iv]
1	Compound (4)[4,5]	Phenyl	Phenyl	84	85	33	86
2	Compound (58)[6-8]	Thiophene	Phenyl	87	80	6	68
3	Compound (87)	Terthiophene	Phenyl	70	75	14	75
4	Compound (88)	Terthiophene	Methoxyphenyl	69	80	19	77
5	Compound (100)	Phenyl	TPA	65	70	10-16*	18
6	Compound (106)	Thiophene	TPA	80	65	18	20
7	Compound (111)	BTZ	Phenyl	60	70	8	50
8	Compound (112)	BTZ	Thiophene	40	50	10	40
9	Compound (113)	BTZ	TPA	40	45	7	35
10	Compound (125)	EDOT	Phenyl	60	50	10	50
11	Compound (132)	Thiophene	Phenothiazine	54	45	9	20
12	Compound (139)	Thiophene	N-methyl pyrrole	40	40	10	60
13	Compound (145)	Thiophene	Carbazole	46	60	10	35
14	Compound (150)	Fluorenone	Phenyl	28	56	5	31
15	Compound (151)	Thiophene	Fluorenone	46	60	15	65

(i) KOH, EtOH/H_2O. (ii) CH_3NO_2, DEA, MeOH, reflux, 24h. (iii) NH_4OAc/EtOH, reflux, 24h. (iv) $BF_3.OEt_2$, DIEA, CH_2Cl_2, rt, 24h.* Using NH_4HCO_2 instead of NH_4OAc.

In a second set of compounds, the R_2 phenyl group of compound (58) was replaced with electron-donating groups N-methyl pyrrole and carbazole and electron-accepting groups fluorenone and phenothiazine, to give compounds (132), (139), (145), and (151) respectively. The result was a reduction in the yields of intermediates (c) to 54%, 40%, 46% and 46% respectively (Table (2.1)). With this second set the nature of the derived nucleophile containing the R_2 group changed, but the moiety containing the R_1 group and the positively charged aldehydic carbon atom was the same for the intermediate (c) reaction.

In a third set of compounds (100), (106) and (113), R_2 (TPA) was constant, hence the derived nucleophile was constant and R_1 was varied from phenyl to thiophene to BTZ with yields for intermediate (c) being 65%, 80%, and 40% respectively. Despite the fact that TPA is a highly electron-donating group, the yields were still moderate. Whether the R_2 group changed as in the second set of compounds above or remained constant (as e.g. with TPA) as in the third set of compounds, the yields for intermediates (c) were not vastly different.

Ammonium formate was tested as an alternative to ammonium acetate in the syntheses of intermediate (e) under the same conditions. A slight improvement in the yield (to 10-16%) was observed for the synthesis of compound (100) (Table (2.1)), and no improvements in the yield were observed for the remaining compounds. Optimized synthetic procedures have already been reported in the literature[3,6,9-11] with various reaction conditions, such as using an alternative ammonium source, trying a number of alcoholic solvents or a solvent-less reaction with excess of ammonium formate.

Phenothiazine-based aza-BODIPY derivatives proved to be difficult to make (compounds (182) and (183) in Sections (2.28) and (2.29) respectively), because the phenothiazine could be readily oxidized in the presence of sunlight and moisture.

The combination of electron-donating and withdrawing groups (Fig. 2.1) with aza-BODIPY conjugated core was expected to enhance intramolecular charge transfer (ICT), shift the absorption towards the IR region and tune the band gap. Li[12] has emphasised the requirements in the molecular design of high-efficiency OPV materials. The key requirements for donor materials were broad absorption, narrower energy band gap and suitable highest occupied molecular orbital (HOMO) and lowest unoccupied molecular orbital (LUMO) (see Fig. 1.24 for ideal energy levels).[12] The HOMO level depended on the donor groups and these levels increased in energy, while the LUMO level was related to the acceptor groups and these decreased in energy.[12] This same strategy has been adopted in this study.

Substituents investigated (Fig. 2.1) were chosen due to their previously reported effects on the energy levels. For example, it was found[6] that the introduction of thiophene into the aza-BODIPY core tuned the energy levels, e.g. the HOMO energies for compounds (57), (58) and (59) were significantly higher in comparison with the standard aza-BODIPY (compound (4)) (Fig. (1.25), Chapter 1). Substituents incorporated on the new aza-BODIPYs were expected to affect the energies of the highest occupied molecular orbital (HOMO) and lowest unoccupied molecular orbital (LUMO). The intent was to position the energy levels at the proposed ideal levels (refer to Fig. (1.24) in Chapter 1) in order to achieve efficient electron transfer between the aza-BODIPY and an acceptor ($PC_{60}BM$).

3,4-Ethylenedioxythiophene (EDOT) has been reported[13] to have a bandgap in the desirable range of 1.6-1.7 eV. It has also been reported recently that PCDTBT (polycarbazole-benzothiadiazole derivative) has a desirable low HOMO energy level and a high open circuit voltage (V_{OC}).[14] The design and syntheses of new donors with an ideal LUMO energy level in between 3.7 and 4.0 eV and a band gap between 1.5 and 1.8 eV was seen as being crucial. The ideal energy levels of a donor (to be used with $PC_{60}BM$) have been calculated by Scharber et al.[15] These ideal energy levels minimized the energy loss and maximize the cell voltage in an organic solar device.[15] Devices based on triphenylamine derivatives (TTPA as depicted in Fig. (2.4)) as electron donors and $PC_{60}BM$ as an electron acceptor showed good performance, exhibiting fill factors of 0.62–0.71 and power conversion efficiencies of 1.5%–1.7% under AM1.5 G illumination at 100 mW cm^{-2}. π-

conjugated molecules containing the fluorenone building block coupled to differently functionalized electron-donating thiophenes or thienylene–vinylene oligomers have been investigated previously.[16] It was found that these molecules have the appropriate positions of their HOMO and LUMO levels, which made possible their use in bulk heterojunction photovoltaic cells with PCBM as an electron acceptor component.[16]

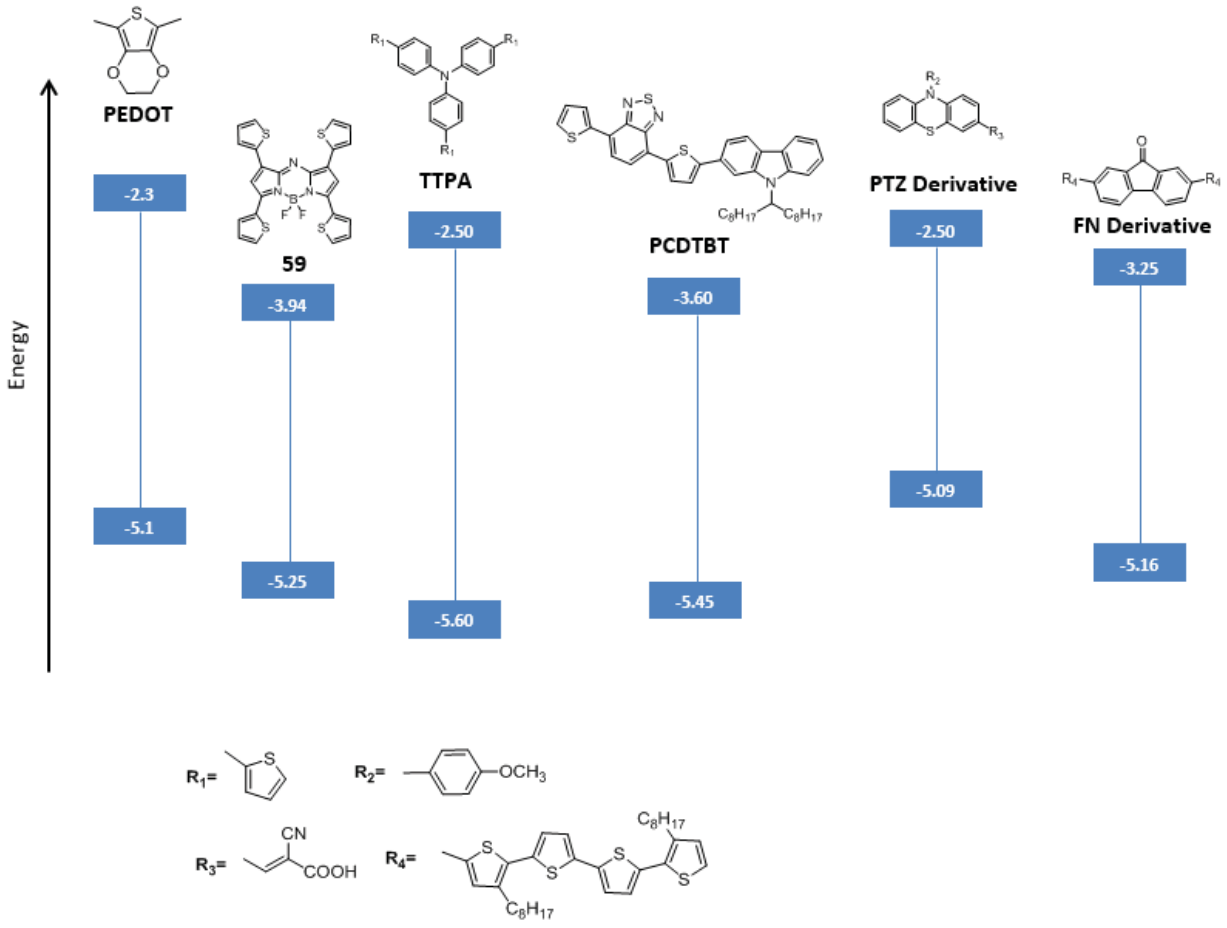

Figure 2.4 Energy levels for selected derivatives of PEDOT, aza-BODIPY (59), TTPA, PCDTBT, PTZ, and FN.[6,13-16]

2.3 Mechanism of Syntheses of the Aza-BODIPYs

The first step in the syntheses of aza-BODIPYs involves the production of chalcone via the aldol condensation between an aldehyde and a ketone in the presence of a base. Fig. (2.5) illustrates the mechanism of aldol condensation. Compound (64) was made from the ketone (63), using a base such as KOH. Then (64) attacks the carbonyl group of the aldehyde (65) to produce the intermediate compound (66). Compound (66) is protonated by the water molecule, released in the previous steps to give the product (67). The chalcone (68) is produced by elimination of the hydroxyl group (OH) from (67) with water as a leaving group.

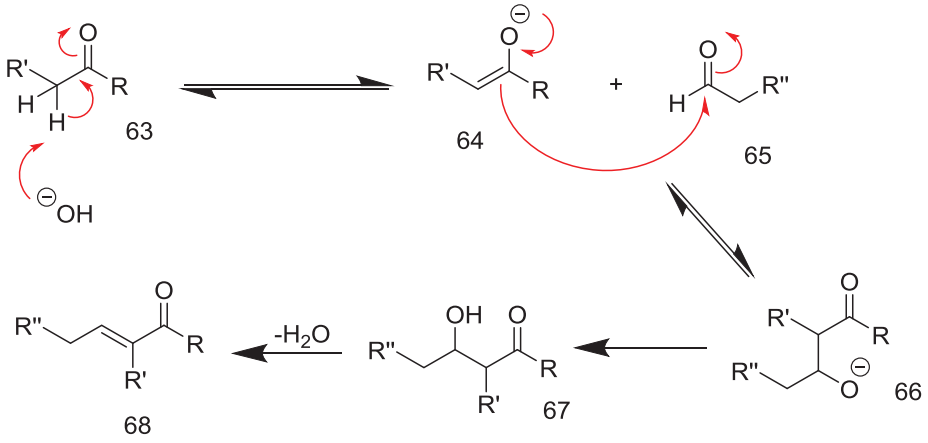

Figure 2.5 The reaction mechanism of chalcone's synthesis.

The next step in the mechanism is a nitration mechanism which occurs via a Michael-addition reaction of nitromethane to the chalcone, producing nitro-ketone (75), as shown in Fig. (2.6). These two classic reactions very effectively provided the precursors to the aza-DIPY (compound (86)). Diethylamine (DEA) has been used as a weak base to deprotonate nitromethane to produce (70). This was followed by the attack of (70) on chalcone (71) to produce nitro-ketone (75). Compound (78) can also be nitrosated to give the nitroso-pyrrole (84), which condenses with another pyrrole (81) to produce the aza-DIPY (compound (86)). The last part of the mechanism has also been discussed in Chapter 1 (Section (1.5.2)). Full details of the synthetic procedures for all of the following compounds are given in the Experimental section.

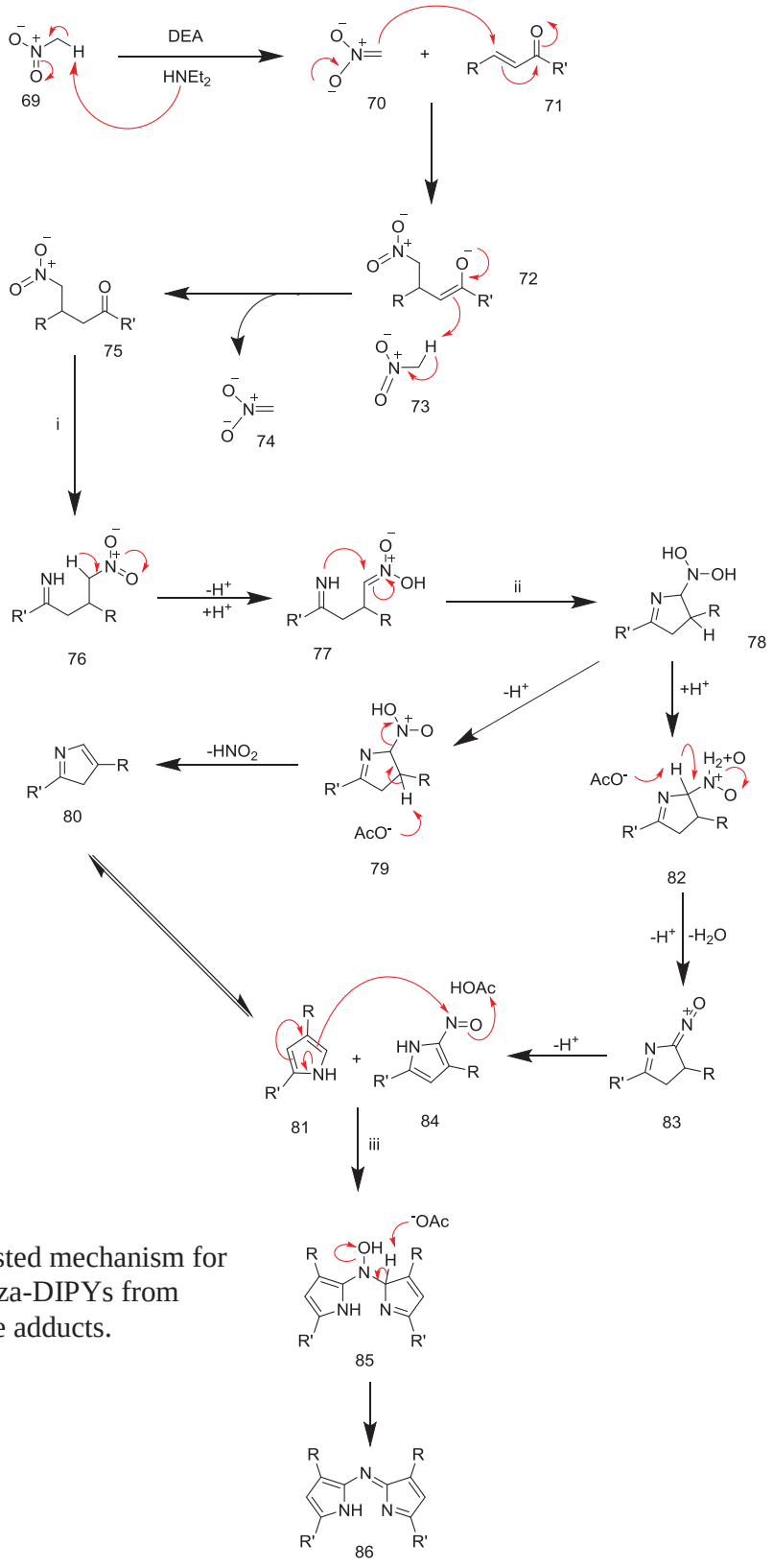

Figure 2.6 The suggested mechanism for the formation of aza-DIPYs from nitromethane adducts.

2.4 Synthesis of Terthiophene- BF_2-Aza-Dipyrromethene (TT-aza-BODIPYs).

Incorporating thiophene substituents on BODIPY (non-aza-analogue) has been shown to create long wavelength absorption and emission.[17-21] Some of the (non-aza) thiophene-substituted BODIPY compounds have in fact been used as light collectors. [22] Therefore, application of this strategy to aza-BODIPY might lead to a new class of aza-BODIPY compounds with spectacular optical properties.

The first series of aza-BODIPY derivatives was designed in a way that the two phenyl groups at position 1 and 7 in the aza-BODIPY core were replaced with strong electron-donating groups such as terthiophene. In order to improve the solubility and/or shift the absorption maxima of aza-BODIPY compounds, the aim was to introduce electron donating and withdrawing groups into the phenyl groups (at positions 3 and 5). These targets were named as TT-aza-BODIPY1, TT-aza-BODIPY2, TT-aza-BODIPY3, and TT-aza-BODIPY4, as depicted in Fig. (2.7). The synthesis procedures for TT-aza-BODIPY1 and TT-aza-BODIPY2 are discussed in Sections (2.5) and (2.6) respectively, while the attempted syntheses of TT-aza-BODIPY3, and TT-aza-BODIPY4 are discussed in Section (2.24). Due to the difficulties with solubility for TT-aza-BODIPY3 and TT-aza-BODIPY4, purification and characterization was not possible.

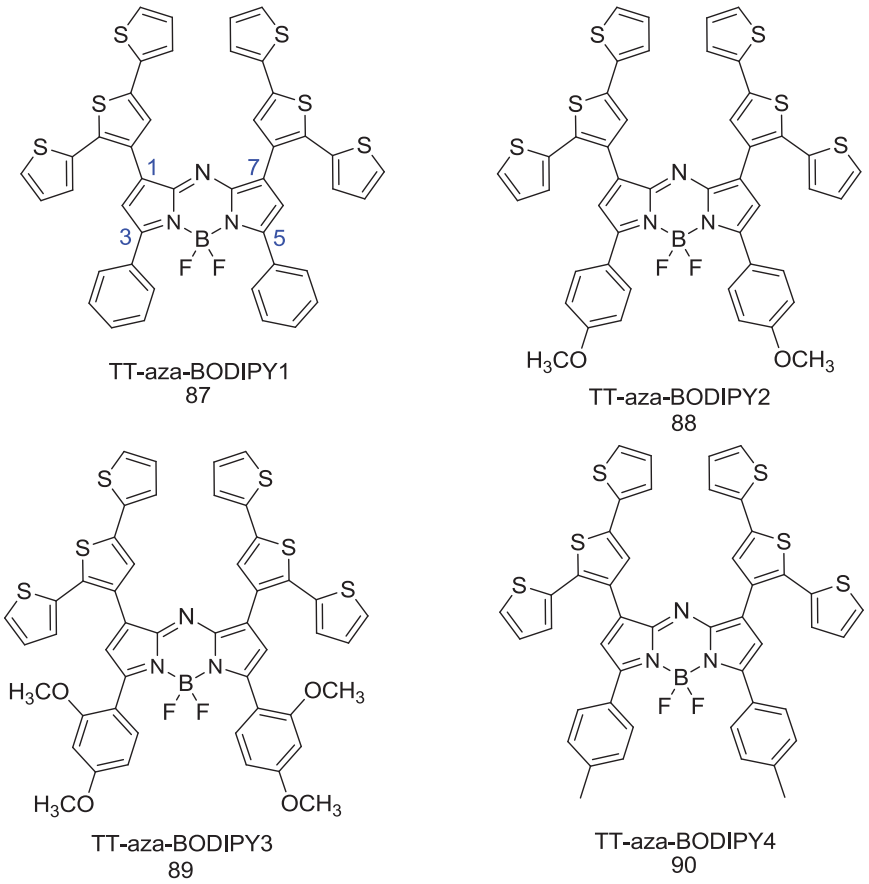

Figure 2.7 The target molecular structures of terthiophene-substituted BF_2-aza-dipyrromethenes (TT-aza-BODIPYs)

2.5 Synthesis of BF_2-terthiophene-aza-dipyrromethene (TT-aza-BODIPY1)

2.5.1 Synthesis of Intermediate Compounds (93) and (94)

The key building-block 3'-formylterthiophene (91) (Fig. 2.8) was prepared using a standard procedure.[23] The intermediate compounds (93) and (94) (Fig. 2.8) were prepared using a modified procedure of the method of O'Shea *et al.*[9] This method employs an aldol condensation of acetophenone (92) with 3'-formylterthiophene (91) to produce the required terthiophene-substituted chalcone (93) in very good yield (70%). This was followed by a Michael-addition reaction of terthiophene substituted chalcone (93). Intermediate compound (94) is readily produced by a base-mediated Michael-addition of nitromethane to (93). The reaction gave a good yield (75%) of 4-nitro-3-(3'-terthiophene)-1-phenyl-

butanone (94) after the aqueous work-up, which was followed by a re-crystallization from ethanol. ^{1}H NMR and mass spectra were used to confirm the structures and the molecular weights of all of these products.

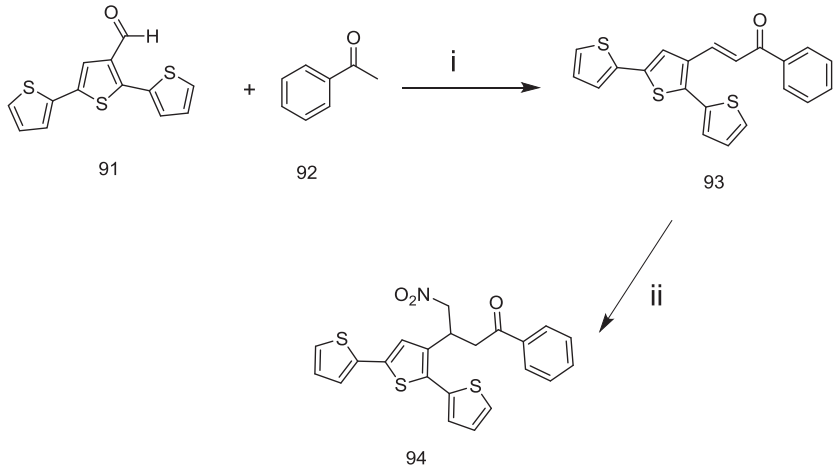

Figure 2.8 Synthesis of intermediate compounds (93) and (94). Reagents and conditions: (i) KOH, EtOH/H_2O. (ii) CH_3NO_2, DEA, MeOH, reflux, 24h.

2.5.2 Synthesis of Terthiophene-dipyrromethene (TT-aza-DIPY1)

The important and crucial step is the formation of terthiophene-substituted dipyrromethene (TT-aza-DIPY), as depicted in Fig. (2.9). This was achieved via the reaction of 4-nitro-3-(3'-terthiophene)-1-phenyl-butanone (94) with ammonium acetate to produce the appropriate pyrroles and nitroso-pyrroles, followed by a subsequent condensation of both intermediates to form TT-aza-DIPY (95). After washing with ethanol, TT-aza-DIPY was obtained in a yield of 14%. The TT-aza-DIPY was used in the next reaction without any further purification due to its poor solubility. ^{1}H NMR and mass spectra were consistent with the proposed structure and molecular weight of the product (TT-aza-DIPY).

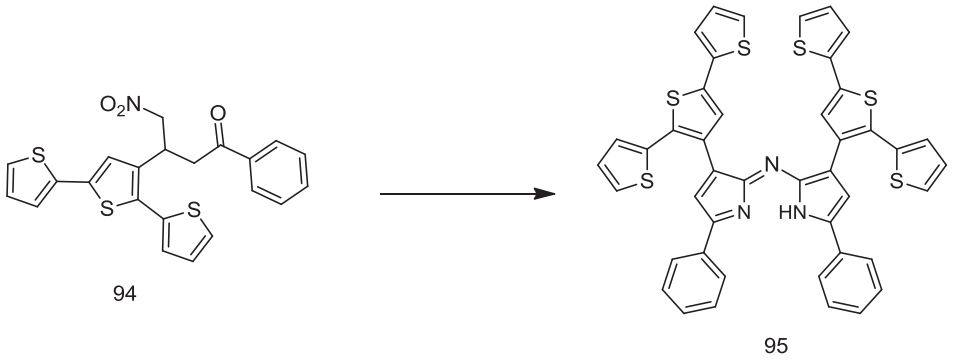

Figure 2.9 Synthesis of terthiophene-dipyrromethene (TT-aza-DIPY1) (95). Reagents and conditions: NH_4OAc/EtOH, reflux, 24h.

2.5.3 Synthesis of BF_2-terthiophene-aza-dipyrromethene (TT-aza-BODIPY1) (87)

The final desired product terthiophene-substituted BF_2-aza-dipyrromethene (TT-aza-BODIPY1) was prepared by reaction of TT-aza-DIPY1 (95) with the boron trifluoride etherate ($BF_3.OEt_2$) under mild conditions. The final product (TT-aza-BODIPY1) (87) with chelated boron offered more stability and was produced in good yield 75%. Fig. (2.10) illustrates the formation of TT-aza-BODIPY1. ^{1}H NMR spectrum confirmed the structure of compound (87). The mass spectrum confirmed the molecular weight as that of the expected product TT-aza-BODIPY1.

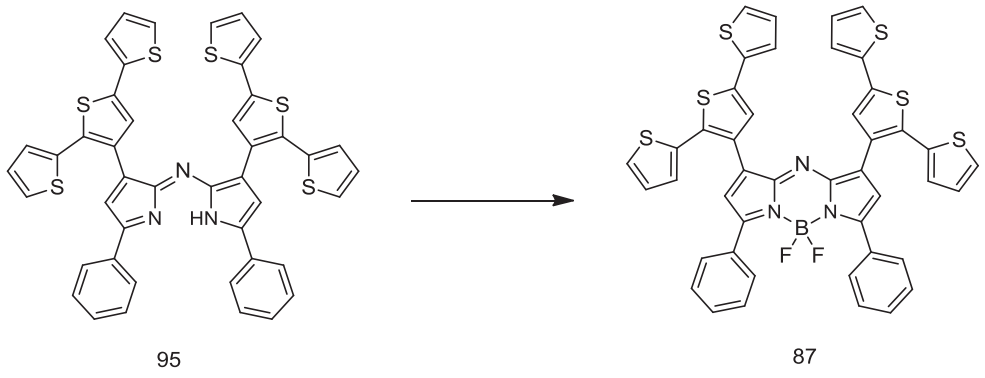

Figure 2.10 Synthesis of BF_2-terthiophene-aza-dipyrromethene (TT-aza-BODIPY1) (87). Reagents and conditions: $BF_3.OEt_2$, DIEA, CH_2Cl_2, rt, 24h.

2.6 Synthesis of Methoxy-terthiophene BF_2-aza-dipyrromethene (TT-aza-BODIPY2) (101)

2.6.1 Synthesis of Intermediate Compounds (98) and (99)

The same key building block 3'-formylterthiophene (91) was used here. 4'-methoxyacetophenone (96) was reacted with 3'-formylterthiophene (91) via an aldol condensation to make the intermediate compound (97) (1-(4'-methoxy)phenyl-3-(3"-terthiophene)prop-2-en-1-one). Compound (98) has been made in excellent yield comparing well with intermediate (93) in Section (2.5.1). The presence of the methoxy group in the ketone has led to a high yield of the product (98). The Michael addition reaction has been carried out for the intermediate (97) in order to make the intermediate (98) (4-nitro-3-(3'-terthiophene)-1-(4"-methoxy)phenyl-butanone. The yield of compound (98) is still higher than its parent compound (94) (which was mentioned in Section (2.5.1)). The same procedure from Section (2.5.1) was used here. Compound (98) was recrystallized from ethanol, Fig. (2.11). ^{1}H NMR and mass spectra were also used to confirm the structures and the molecular weights of these products.

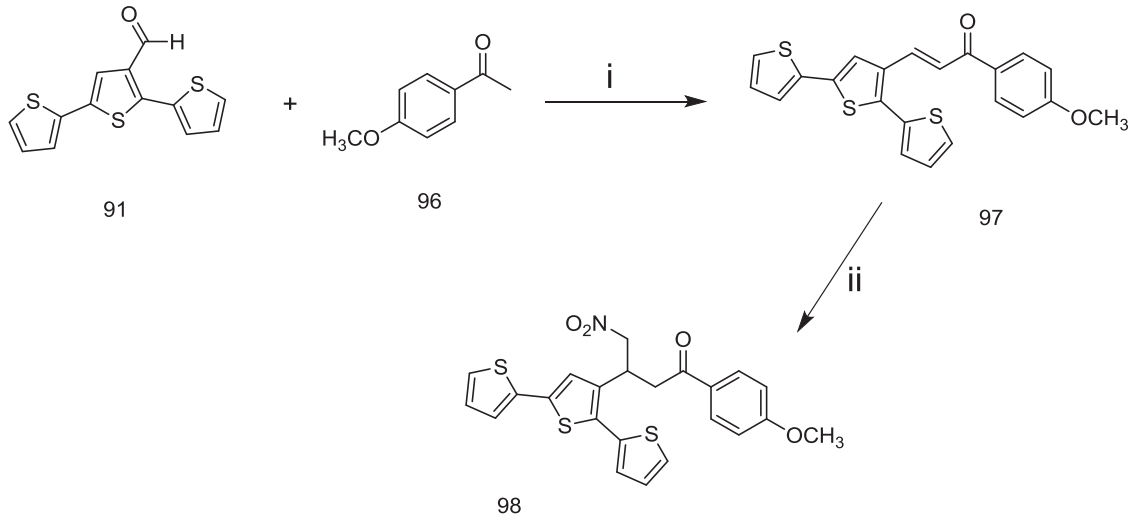

Figure 2.11 Synthesis of intermediate compounds (97) and (98). Reagents and conditions: (i) KOH, EtOH/H_2O. (ii) CH_3NO_2, DEA, MeOH, reflux, 24h.

2.6.2 Synthesis of Methoxy-terthiophene-dipyrromethene (TT-aza-DIPY2) (99)

The formation of methoxy-terthiophene-substituted aza-dipyrromethene (TT-aza-DIPY2), as depicted in Fig. (2.12), was straight forward. 4-nitro-3-(3'-terthiophene)-1-(4"-methoxyphenyl)-butanone (98) reacted with ammonium acetate, and the product was washed with ethanol producing the TT-aza-DIPY2 in a yield of 19%. The TT-aza-DIPY2 was used in the next reaction without any further purification. ^{1}H NMR and mass spectra have been obtained for the purified compound, confirming the structure and molecular weight of the product (TT-aza-DIPY2) (99).

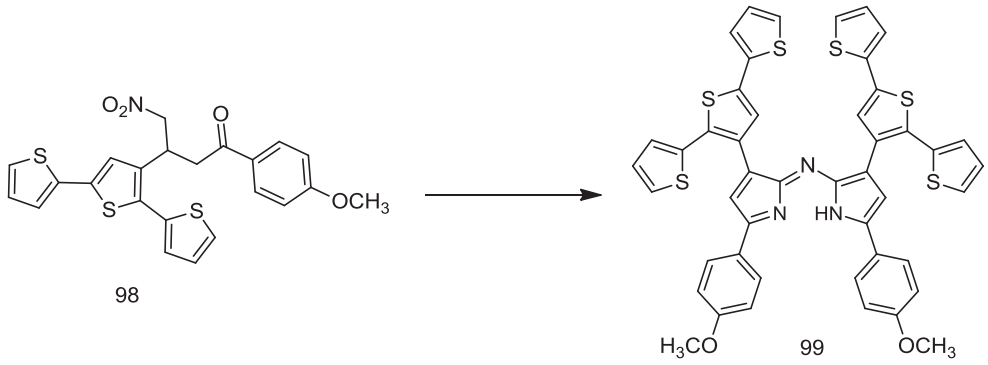

Figure 2.12 Synthesis of methoxy-terthiophene-substituted aza-dipyrromethene (TT-aza-DIPY2) (99). Reagents and conditions: NH_4OAc/EtOH, reflux, 24h.

2.6.3 Synthesis of Methoxy-terthiophene BF_2-aza-dipyrromethene (TT-aza-BODIPY2)

Methoxy-terthiophene-substituted BF_2-aza-dipyrromethene (TT-aza-BODIPY2) (88) was prepared by reaction of TT-aza-DIPY2 (99) with the boron trifluoride etherate ($BF_3.OEt_2$) under the same mild conditions as used before. TT-aza-BODIPY2 has greater stability compared with TT-aza-DIPY2, due to the chelated boron atom. The yield of TT-aza-BODIPY2 was about 77%. Fig. (2.13) illustrates the synthesis of TT-aza-BODIPY2. ^{1}H

NMR spectra and mass spectra were in good agreement with the structure of the product TT-aza-BODIPY2. Details of the characterization are given in the experimental section of this thesis.

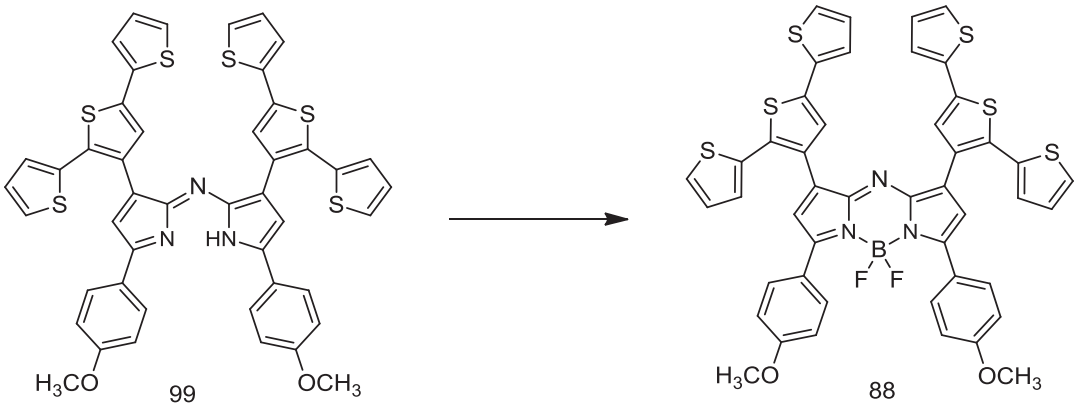

Figure 2.13 Synthesis of methoxy-terthiophene-substituted BF_2-aza-dipyrromethene (TT-aza-BODIPY2) (88). Reagents and conditions: $BF_3.OEt_2$, DIEA, CH_2Cl_2, rt, 24h.

2.7 Synthesis of Triphenylamine-Substituted BF_2-Aza-Dipyrromethene (TPA-aza-BODIPY)

Triphenylamine (TPA) derivatives represent a very interesting platform for building a donor molecule. TPA has been intensively investigated as a donor material with internal charge transfer for hetero-junction solar cells [24-26] and dye-sensitized solar cells (DSSC). [27,28] The new design to be investigated has incorporated TPA in position 3 and 5 of the aza-BODIPY core, Fig. (2.14). The synthetic route of TPA-aza-BODIPY will be investigated in the next sections. The targeted TPA-aza-BODIPY achieved a remarkable shift in the absorption and emission properties, which will be discussed intensively in Chapter Three of this thesis.

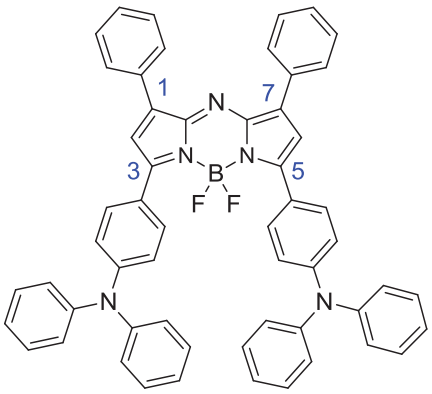

TPA-aza-BODIPY
100

Figure 2.14 The target molecular structure of triphenylamine-substituted BF_2-aza-dipyrromethene (TPA-aza-BODIPY) (100).

2.7.1 Synthesis of Intermediate Compounds (103) and (104)

The building block 4-diphenylaminoacetophenone (101), Fig. (2.15) was prepared using a standard procedure from the literature.[29] The intermediate compound (103) was synthesized by the reaction of benzaldehyde (102) with 4-diphenylaminoacetophenone (101) using KOH as the base. Column chromatography was used to purify the product over a silica gel column to produce the intermediate compound (103). The next step involved a base-mediated Michael-addition of the nitromethane to compound (103) to produce the nitro-adduct intermediate compound (104) in a good yield (70%) after recrystallization (Fig. (2.15)). The characterization for both intermediate compounds was by ^{1}H NMR and mass spectrometry.

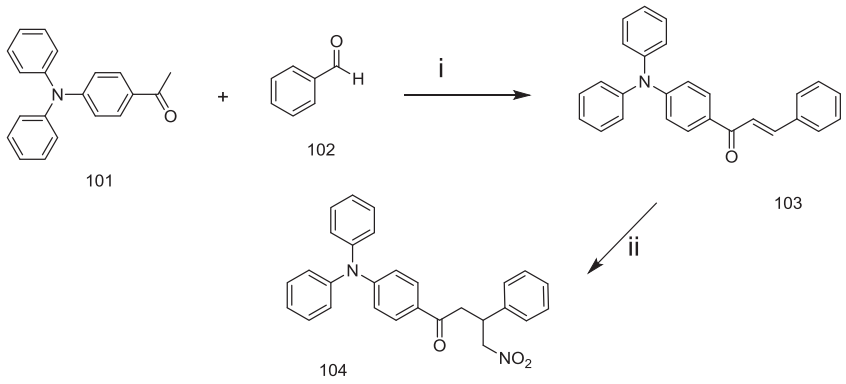

Figure 2.15 Synthesis of intermediate compounds (103) and (104). Reagents and conditions: (i) KOH, EtOH/H_2O. (ii) CH_3NO_2, DEA, MeOH, reflux, 24h.

2.7.2 Synthesis of Triphenylamine-Substituted Aza-dipyrromethene (TPA-aza-DIPY) (105)

The difficulties of intermediate compound (104) with solubility led to some limitations in the synthesis of TPA-aza-DIPY. This crucial step was achieved by trying different alcohol solvents, as well as trying ammonium acetate and ammonium formate. The yield was in between 10% to 16% using methanol, ethanol and *n*-butanol. The product triphenylamine-substituted aza-dipyrromethene (105) (TPA-aza-DIPY) was purified by passing through an alumina column. Fig. (2.16) illustrates the formation of TPA-aza-DIPY. The product TPA-aza-DIPY was characterized using ^{1}H NMR and mass spectrometry.

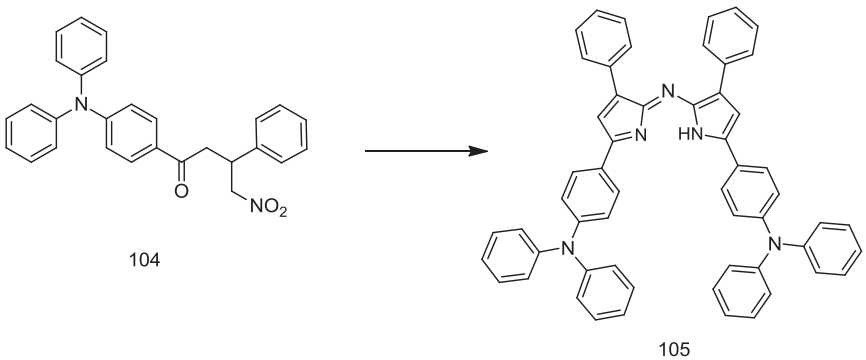

Figure 2.16 Synthesis of triphenylamine-substituted aza-dipyrromethene (TPA-aza-DIPY) (105). Reagents and conditions: NH_4HCO_2/*n*-BuOH, reflux, 24h.

2.7.3 Synthesis of Triphenylamine-Substituted BF_2-aza-dipyrromethene (TPA-aza-BODIPY)

The final step was more straight forward than the one before. The desired TPA-aza-BODIPY was prepared in 18% yield by the reaction of TPA-aza-DIPY with the boron trifluoride etherate ($BF_3.OEt_2$) under mild conditions. The TPA-aza-BODIPY seemed to be more stable and soluble in organic solvents such as chloroform, DCM, and ethyl acetate. Fig. (2.17) illustrates the synthesis of TPA-aza-BODIPY 100. The structure of TPA-aza-BODIPY has been confirmed by ^1H NMR and mass spectrometry.

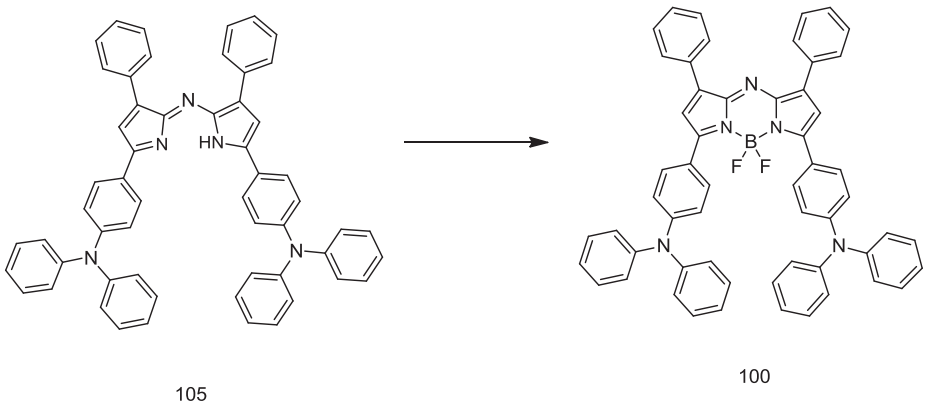

Figure 2.17 The synthesis of triphenylamine-substituted BF_2-aza-dipyrromethene (TPA-aza-BODIPY) (100). Reagents and conditions: $BF_3.OEt_2$, DIEA, CH_2Cl_2, rt, 24h.

2.8 Synthesis of Thiophene-Triphenylamine-Substituted BF_2-Aza-dipyrromethene (T-TPA-aza-BODIPY)

A donor molecule containing both thiophene and triphenylamine (TPA) units represents another interesting platform and these units have been intensively used in solar cells. [30-35] The new target design was an aza-BODIPY compound incorporating thiophene in positions 1 and 7 and TPA in positions 3 and 5 (Fig. (2.18)). The synthetic route of the thiophene-triphenylamine-substituted BF_2-aza-dipyrromethene (T-TPA-aza-BODIPY) will be investigated in later sections.

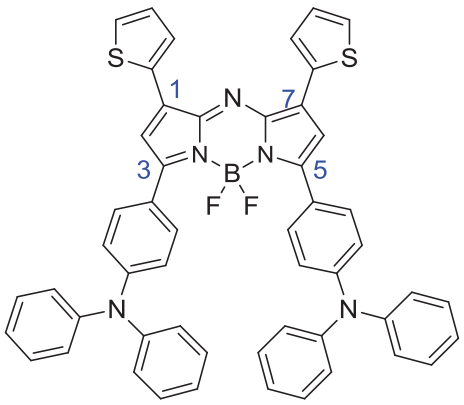

T-TPA-aza-BODIPY
106

Figure 2.18 The target molecular structure of thiophene-triphenylamine-substituted BF_2-aza-dipyrromethene (T-TPA-aza-BODIPY) (106).

2.8.1 Synthesis of Intermediate Compounds (108) and (109)

2-Thiophenecarboxaldehyde (107) and 4-diphenylaminoacetophenone (101) (Fig. (2.19)) were prepared using known procedures from the literature.[36,37] Compound (108) was synthesized by the aldol condensation of 2-thiophenecarboxaldehyde and 4-diphenylaminoacetophenone. Following re-crystallization, the yield of (108) was 80%. The Michael-addition reaction of compound (108) with nitromethane was carried out (Fig. (2.19)), followed by column chromatography using a silica gel column; the intermediate compound (109) was produced in 65% yield. Both intermediate compounds (108) and (109) were characterized using ^{1}H NMR and mass spectrometry.

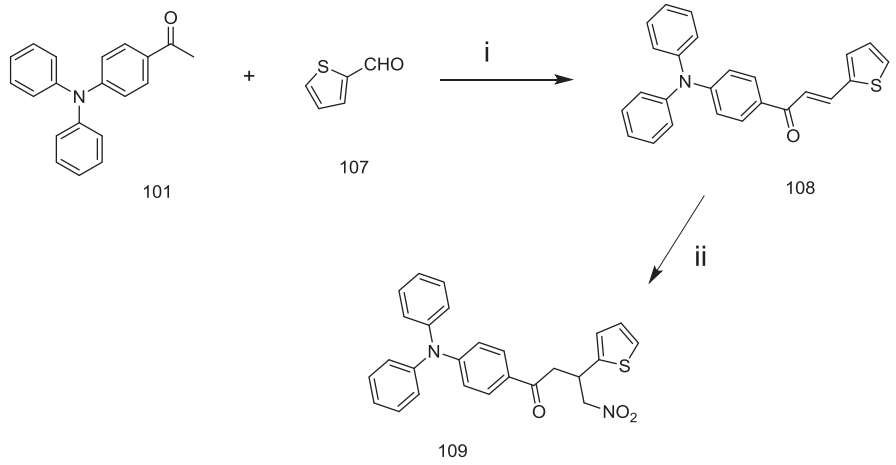

Figure 2.19 Synthesis of intermediate compounds (108) and (109). Reagents and conditions: (i) KOH, EtOH/H_2O. (ii) CH_3NO_2, DEA, MeOH, reflux, 24h.

2.8.2 Synthesis of Thiophene-Triphenylamine- Substituted Aza-dipyrromethene (T-TPA-aza-DIPY) (110)

Intermediate compound (109) was used in the following reaction without any further purification. The addition of ammonium acetate to compound (109) in n-butanol under reflux, followed by column chromatography produced the thiophene-triphenylamine-substituted aza-dipyrromethene (T-TPA-aza-DIPY) (Fig. (2.20)). The product TPA-aza-DIPY was characterized using ^{1}H NMR and mass spectrometry.

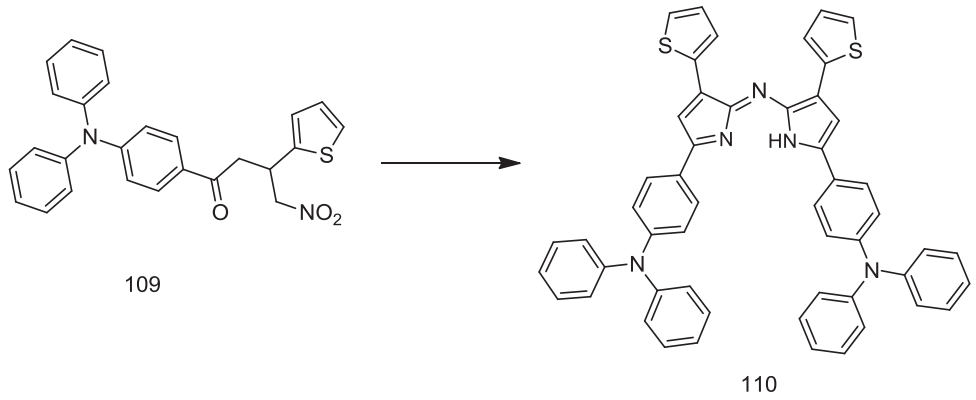

Figure 2.20 The synthesis of thiophene-triphenylamine-substituted aza-dipyrromethene (T-TPA-aza-DIPY) (110). Reagents and conditions: NH_4OAc/*n*-BuOH, reflux, 24h.

2.8.3 Synthesis of Thiophene-Triphenylamine- Substituted BF_2-Aza-dipyrromethene (T-TPA-aza-BODIPY)

The desired T-TPA-aza-BODIPY was prepared in 20% yield by the reaction of T-TPA-aza-DIPY with boron trifluoride etherate ($BF_3.OEt_2$) under mild conditions. The T-TPA-aza-BODIPY was soluble in organic solvents such as chloroform, DCM, and ethyl acetate. Fig. (2.21) illustrates the synthesis. The structure and molecular weight of T-TPA-aza-BODIPY were confirmed by ^1H NMR, ^{13}C NMR, and mass spectrometry.

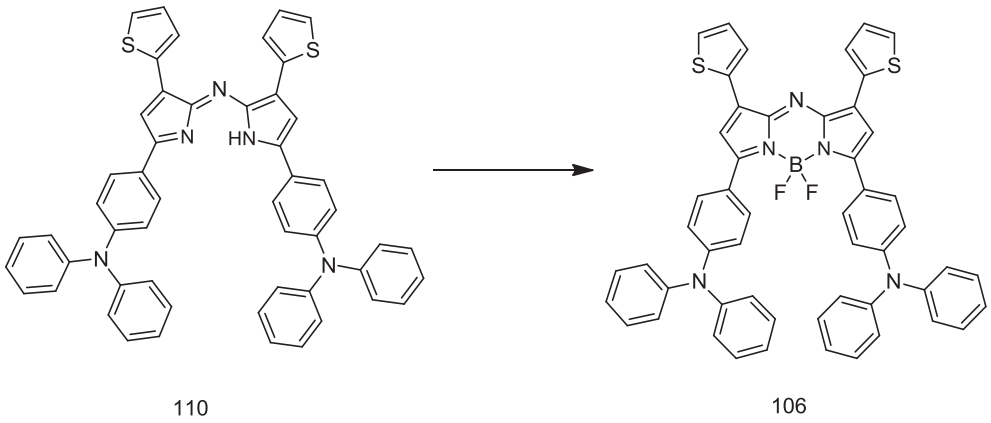

Figure 2.21 Synthesis of thiophene-triphenylamine-substituted BF_2-aza-dipyrromethene (T-TPA-aza-BODIPY) 106. Reagents and conditions: $BF_3.OEt_2$, DIEA, CH_2Cl_2, rt, 24h.

2.9 Synthesis of Benzothiadiazole-Thiophene-Terthiophene-Substituted BF_2-Aza-dipyrromethenes (BTZ-T-TT-aza-BODIPYs)

Solar cells based on benzothiadiazole derivatives copolymers have been recently investigated.[38-40] Some of these efforts have been focused on achieving low band-gap polymers through introducing benzothiadiazole derivatives into the polymer backbone. [41-43] A new class of BF_2-aza-dipyrromethene compounds based on benzothiadiazole derivatives was designed in this study in order to alter the absorption properties of BF_2-aza-dipyrromethene. Fig. (2.22) shows the target compounds based on benzothiadiazole (BTZ), triphenylamine (TPA), and thiophene aza-BODIPYs. These new compounds did bring very interesting absorptions properties, with the absorption wave lengths being shifted towards

the near-infrared (IR) region. The photo-physical properties of these new dyes will be discussed in Chapter 3. The synthetic route of benzothiadiazole-substituted BF_2-aza-dipyrromethene (BTZ-aza-BODIPY) is discussed in the following sections; the synthetic routes of benzothiadiazole-triphenylamine-substituted BF_2-aza-dipyrromethene (BTZ-TPA-aza-BODIPY) and the thiophene-triphenylamine-substituted BF_2-aza-dipyrromethene (T-TPA-aza-BODIPY) are discussed in Sections (2.12) and (2.8) respectively.

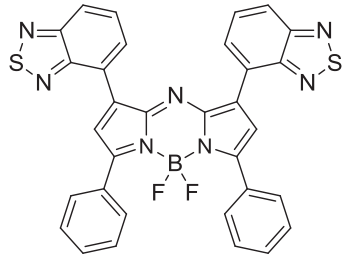

BTZ-aza-BODIPY
111

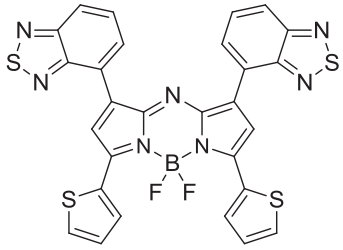

BTZ-T-aza-BODIPY
112

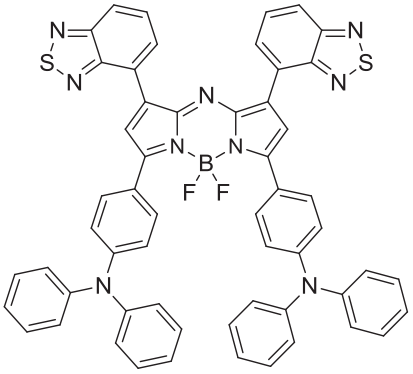

BTZ-TPA-aza-BODIPY
113

Figure 2.22 The target structures of BTZ-aza-BODIPY, BTZ-T-aza-BODIPY and BTZ-TPA-aza-BODIPY

2.10 Synthesis of Benzothiadiazole-Substituted BF_2-Aza-dipyrromethene (BTZ-aza-BODIPY) (117)

2.10.1 Synthesis of Intermediate Compounds (115) and (116)

The starting material 2,1,3-benzothiadiazole-4-carbaldehyde (114) (Fig. (2.23)) was synthesized by use of a standard literature procedure.[44] The reaction was carried under argon gas and extra care was taken with handling the material (114), because it was extremely sensitive to the atmosphere. The intermediate compound (115) was prepared by a reaction of 2,1,3-benzothiadiazole-4-carbaldehyde (114) with acetophenone (92) in the presence of a base (KOH) under argon gas. The yield of the intermediate compound (115) was 60%. The product was re-crystallized from ethanol, and used as was for the next reaction. The addition of nitromethane into intermediate compound (115) under reflux resulted in a yellow product (intermediate compound (116), which was dried and recrystallized to give a yield of 70%. All reactions were carried out under argon inert gas. Intermediate compounds (115) and (116) were fully characterized and the synthetic route is depicted in Fig. (2.23).

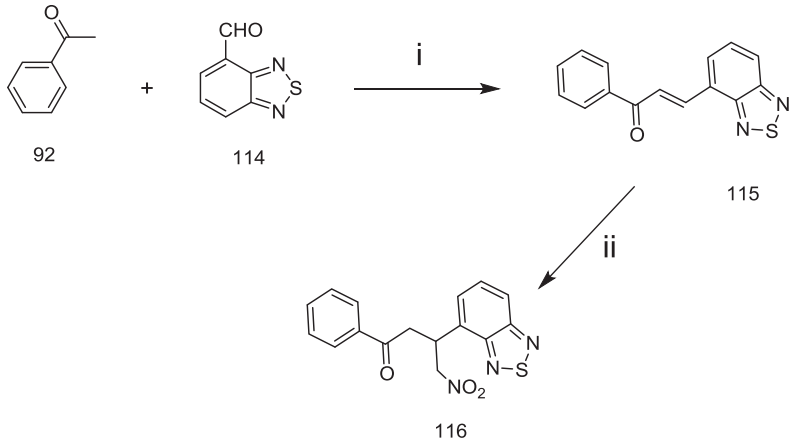

Figure 2.23 Synthesis of intermediate compounds (115) and (116). Reagents and conditions: (i) KOH, $EtOH/H_2O$. (ii) CH_3NO_2, DEA, MeOH, reflux, 24h.

2.10.2 Synthesis of Benzothiadiazole-Substituted Aza-dipyrromethene (BTZ-aza-DIPY)

Due to the sensitive nature of the intermediate compound (116), extra care was taken during this crucial step of the synthesis. Argon gas was used during the reaction of intermediate compound (116) with ammonium acetate in n-butanol as a solvent to produce the BTZ-aza-DIPY compound (117) (Fig. (2.24)). The low yield (≈ 8%) and the low solubility of this compound made the purification process more difficult. After drying the crude mixture under argon and passing through an alumina column, followed by recrystallization from ethanol, a precipitate was obtained. The structure of BTZ-aza-DIPY was confirmed by ^{1}H NMR and mass spectrometry.

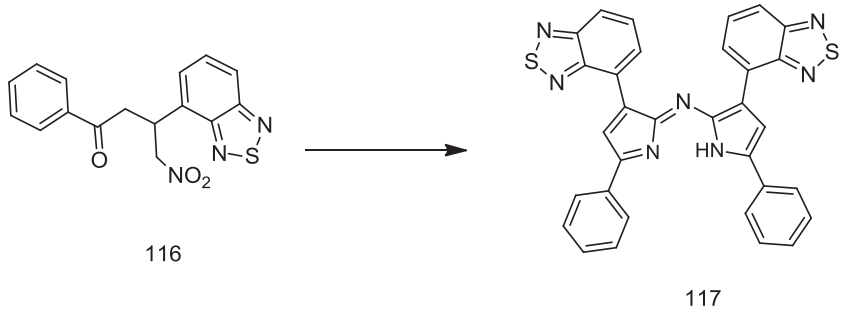

116 117

Figure 2.24 The synthesis of benzothiadiazole-substituted aza-dipyrromethene (BTZ-aza-DIPY) (117). Reagents and conditions: NH_4OAc/*n*-BuOH, reflux, 24h.

2.10.3 Synthesis of Benzothiadiazole-Substituted BF_2-Aza-dipyrromethene (BTZ-aza-BODIPY) (111)

BTZ-aza-DIPY was used for the following reaction without any further purification. Boron trifluoride etherate ($BF_3.OEt_2$) was added to BTZ-aza-DIPY under room temperature and argon gas. The final product BTZ-aza-BODIPY precipitated from the reaction mixture over time, and was purified using a column chromatography and then re-crystallized from ethanol to give a yield of 50%. Fig. (2.25) shows the reaction. ^{1}H NMR and mass spectra confirmed the molecular structure of BTZ-aza-BODIPY.

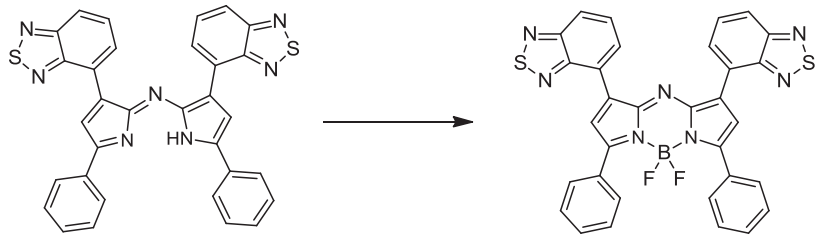

117 111

Figure 2.25 The synthesis of benzothiadiazole-substituted BF_2-aza-dipyrromethene (BTZ-aza-BODIPY) (111). Reagents and conditions: $BF_3.OEt_2$, DIEA, CH_2Cl_2, rt, 24h.

2.11 Synthesis of Benzothiadiazole-Thiophene-Substituted BF_2-Aza-dipyrromethene (BTZ-T-aza-BODIPY) (121)

2.11.1 Synthesis of Intermediate Compounds (119) and (120)

The key building-block 2-acetylthiophene was prepared using a standard procedure.[45] The intermediate compounds (119) and (120) were prepared using a modified procedure of the method of O'Shea *et al*.[9] The aldol condensation of 2-acetylthiophene with 2,1,3-benzothiadiazole-4-carbaldehyde gave compound (119) in moderate yield (40%). A base-mediated Michael-addition of nitro methane to compound (119) gave a moderate yield (50%) of compound (120) after the aqueous work-up, which was followed by a recrystallization using ethanol (Fig. (2.26)). These compounds were characterized using ^1H NMR and mass spectrometry.

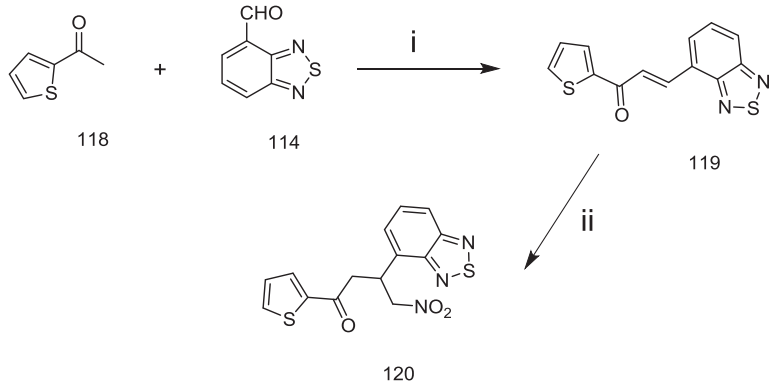

118 114 119 120

Figure 2.26 Synthesis of intermediate compounds (119) and (120). Reagents and conditions: (i) KOH, $EtOH/H_2O$. (ii) CH_3NO_2, DEA, MeOH, reflux, 24h.

2.11.2 Synthesis of Benzothiadiazole-Thiophene-Substituted Aza-dipyrromethene (BTZ-T-aza-DIPY)

A procedure similar to that in Section (2.10.2) was used here. The formation of benzothiadiazole-thiophene-substituted aza-dipyrromethene (BTZ-T-aza-DIPY) (121) was achieved by adding ammonium acetate to compound (120) (Fig. (2.27)). A yield of 10% was obtained for BTZ-T-aza-DIPY (121) after purification by column chromatography using an alumina column. There were issues with solubility for (121). The structure of this compound was confirmed by ^{1}H NMR and mass spectrometry.

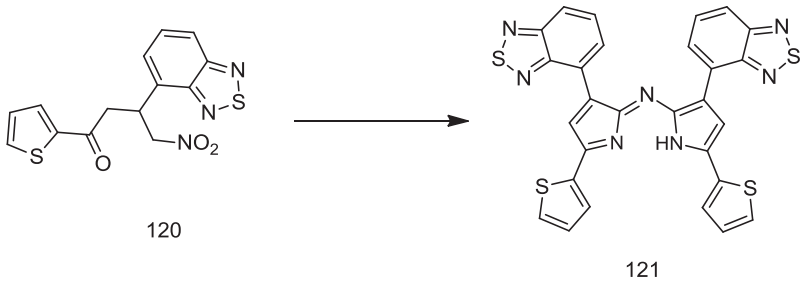

Figure 2.27 Synthesis of benzothiadiazole-thiophene-substituted aza-dipyrromethene (BTZ-T-aza-DIPY) (121). Reagents and conditions: NH_4OAc/EtOH, reflux, 24h.

2.11.3 Synthesis of Benzothiadiazole-Thiophene-Substituted BF_2-Aza-dipyrromethene (BTZ-T-aza-BODIPY) (112)

A similar procedure to that described in Section (2.10.3) was used to prepare BTZ-T-aza-BODIPY 112. Boron trifluoride etherate ($BF_3.OEt_2$) was added to BTZ-aza-DIPY at room temperature (Fig. (2.28)). BTZ-T-aza-BODIPY precipitated from the reaction mixture over time. This product was purified by column chromatography and then recrystallized from ethanol to give a yield of 40% of BTZ-T-aza-BODIPY. ^{1}H NMR, ^{13}C NMR, mass spectrometry and elemental analysis were carried out for the final product.

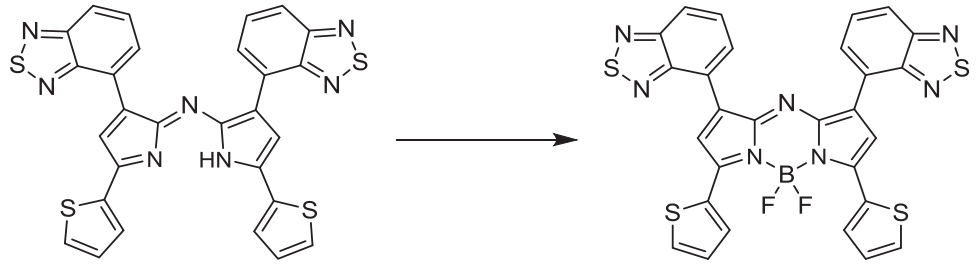

121 112

Figure 2.28 Synthesis of benzothiadiazole-thiophene-substituted BF_2-aza-dipyrromethene (BTZ-T-aza-BODIPY) (112). Reagents and conditions: $BF_3.OEt_2$, DIEA, CH_2Cl_2, rt, 24h.

2.12 Synthesis of Benzothiadiazole-Triphenylamine-Substituted BF_2-Aza-dipyrromethene (BTZ-TPA-aza-BODIPY) (113)

Combining both benzothiadiazole (BTZ) and triphenylamine (TPA) into an aza-BODIPY core structure was challenging because of the air sensitivity of benzothiadiazole derivatives and the low solubility for intermediate compounds (122), (123) and (124) (Fig. 2.29 and Fig. 2.30). The final target (113) was stable and showed absorption at longer wavelengths in the near-IR region. It was clear that the solution processable property of a small molecule had been retained. Optical properties of this compound are discussed in Chapter 3. The synthetic route for benzothiadiazole-triphenylamine-substituted BF_2-aza-dipyrromethene (BTZ-TPA-aza-BODIPY) (113) is discussed in the following sections.

2.12.1 Synthesis of Intermediate Compounds (122) and (123)

2,1,3-Benzothiadiazole-4-carbaldehyde (114) and 4-diphenylaminoacetophenone (101) were used as starting materials for the synthesis of the intermediate compound (122). The reaction conditions described in Section (2.8.1) were applied here. The compound (122) was formed in moderate yield (40%) after recrystallization with ethanol. The nitromethane adduct (123) was prepared via the reaction of nitromethane with (122). A yellow product (123) was separated in a yield of (45%) by column chromatography using an alumina column. All reactions were carried out under argon. Both compounds (122) and (123) were

fully characterized using ^{1}H NMR and mass spectrometry. The reaction routes for both compounds (122) and (123) are depicted in Fig. (2.29).

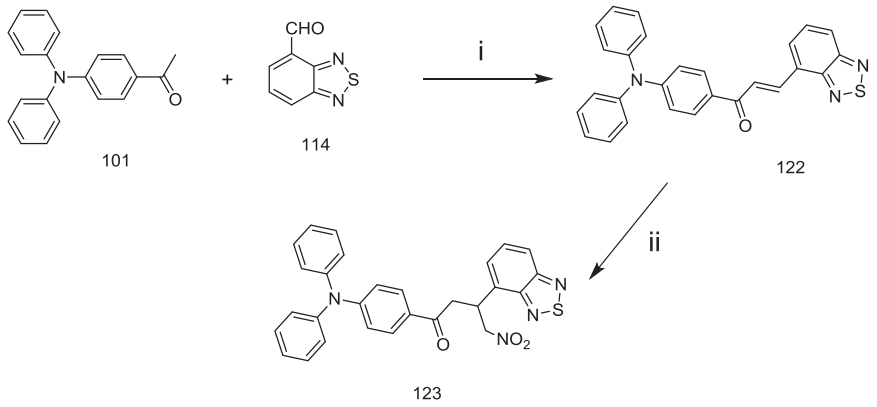

Figure 2.29 Synthesis of intermediate compounds (122) and (123). Reagents and conditions: (i) KOH, EtOH/H_2O. (ii) CH_3NO_2, DEA, MeOH, reflux, 24h.

2.12.2 Synthesis of Benzothiadiazole-Triphenylamine-Substituted Aza-dipyrromethene (BTZ-TPA-aza-DIPY) (124)

This is the most important step in the aza-BODIPY synthesis. This step includes the formation of benzothiadiazole-triphenylamine-substituted aza-dipyrromethene (BTZ-TPA-aza-DIPY) (124), as depicted in Fig. (2.30). The intermediate compound (123) was reacted with ammonium acetate to produce the appropriate pyrroles and nitroso-pyrroles (mechanism shown in Section (2.3)). This was followed by a condensation of both intermediates under argon to form BTZ-TPA-aza-DIPY. The product was washed with ethanol to produce BTZ-TPA-aza-DIPY in a yield of 7%. The TT-aza-DIPY was used in the next reaction without any further purification, because of the low solubility resulting from the highly conjugated system of BTZ-TPA-aza-DIPY (124). ^{1}H NMR and mass spectra confirmed the identity of the product.

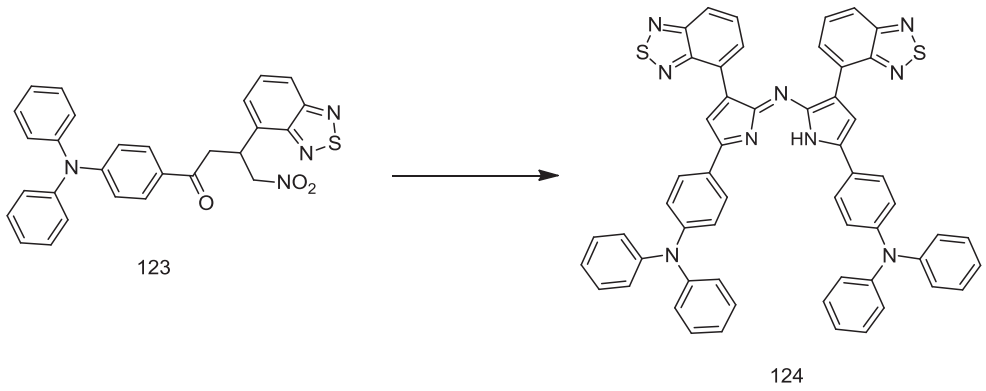

Figure 2.30 The synthesis of benzothiadiazole-triphenylamine-substituted aza-dipyrromethene (BTZ-aza-DIPY) (124). Reagents and conditions: NH_4OAc/EtOH, reflux, 24h.

2.12.3 Synthesis of Benzothiadiazole-Triphenylamine-Substituted BF_2-Aza-dipyrromethene (BTZ-TPA-aza-BODIPY) (113)

Boron trifluoride etherate ($BF_3.OEt_2$) was reacted with BTZ-TPA-aza-DIPY under mild conditions (Fig. (2.31)). The reaction was carried out under argon. The final product BTZ-TPA-aza-BODIPY was obtained over time as a blue-green precipitate from the reaction mixture. The product BTZ-TPA-aza-BODIPY was purified using column chromatography, followed by recrystallization from ethanol and the yield was 35%. ^{1}H NMR, ^{13}C NMR, and mass spectra confirmed the structure of BTZ-TPA-aza-BODIPY. This product showed exceptional absorption and emission properties, in that the wavelength was shifted into the near-infrared region by about 250 nm compared to the tetraphenyl-aza-BODIPY.

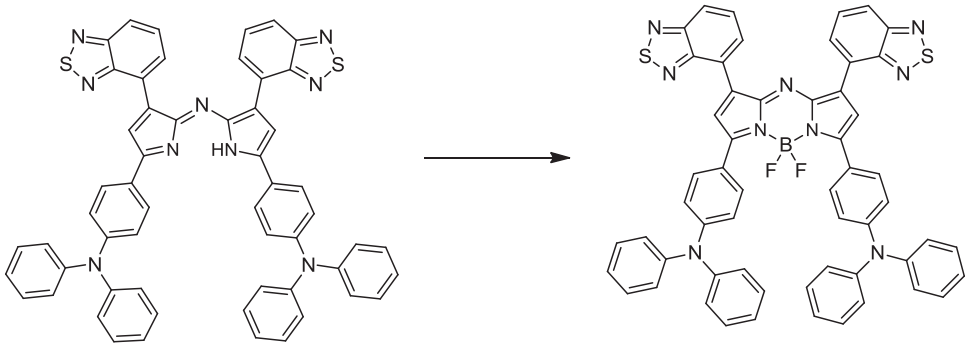

Figure 2.31 The synthesis of benzothiadiazole-triphenylamine-substituted BF_2-aza-dipyrromethene (BTZ-TPA-aza-BODIPY) (113). Reagents and conditions: $BF_3.OEt_2$, DIEA, CH_2Cl_2, rt, 24h.

2.13 Synthesis of Ethylenedioxythiophene-Triphenylamine-Substituted BF_2-Aza-dipyrromethene (EDOT-TPA-aza-BODIPYs)

A well-known building-block with very interesting strong electron-donor properties, non-covalent sulfur-oxygen interactions and self-organisation ability is 3,4-ethylenedioxythiophene (EDOT).[46-48] EDOT has been intensively investigated as a hole-transport material.[49-54] Aza-BODIPYs with donor molecule (EDOT) have been synthesized and their preliminary evaluation as a donor material in OPV cells is discussed in Chapter 3 and 4. The structures of the target EDOT based aza-BODIPY compounds are depicted in Fig. (2.32). The synthesis of EDOT-aza-BODIPY is discussed in the next sections, while the attempted synthesis of EDOT-TPA-aza-BODIPY is discussed in Section (2.25).

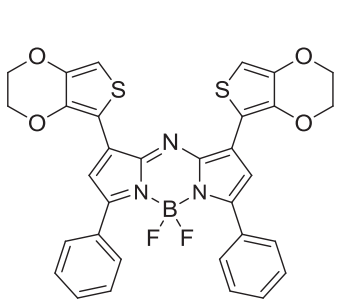

EDOT-aza-BODIPY

125

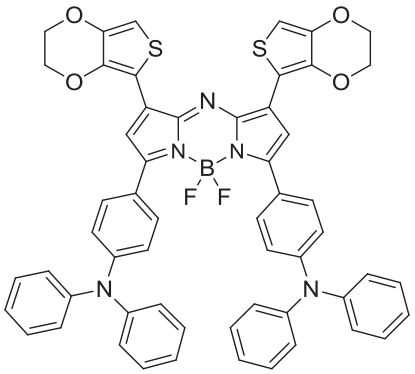

EDOT-TPA-aza-BODIPY

126

Figure 2.32 The target chemical structures of ethylenedioxythiophene-substituted BF_2-aza-dipyrromethene (EDOT-aza-BODIPYs) are shown.

2.14 Synthesis of Ethylenedioxythiophene-Substituted BF_2-Aza-dipyrromethene (EDOT-aza-BODIPYs) (125)

2.14.1 Synthesis of Intermediate Compounds (128) and (129)

The key building-block 3,4–ethylenedioxythiophene-2-carbaldehyde was prepared using a known procedure.[55] Aldol condensation of 3,4–ethylenedioxythiophene-2-carbaldehyde with acetophenone gave the intermediate compound (128) in good yield (60%), which was readily converted by a base-mediated Michael-addition to compound (129) (in 50% yield). Finally, the compound was purified by column chromatography using a silica gel column. Both compounds (128) and (129) were characterized. Fig. (2.33) shows the reaction pathway.

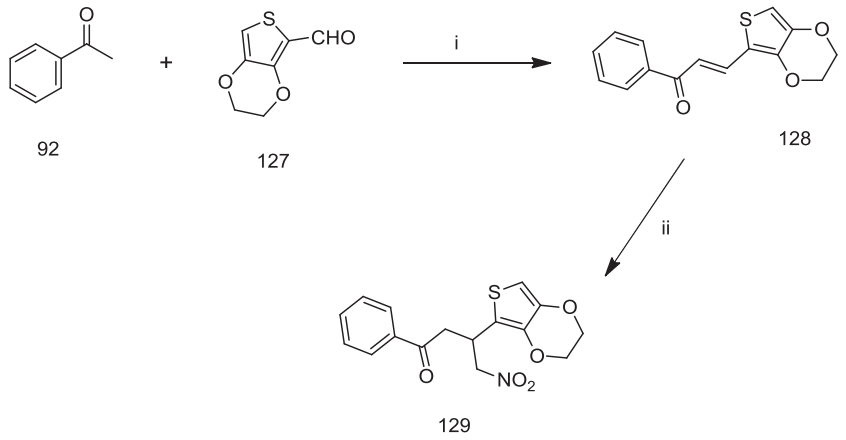

Figure 2.33 Synthesis of intermediate compounds (128) and (129). Reagents and conditions: (i) KOH, EtOH/H_2O. (ii) CH_3NO_2, DEA, MeOH, reflux, 24h.

2.14.2 Synthesis of Ethylenedioxythiophene-Substituted Aza-dipyrromethene (EDOT-aza-DIPY) (130)

This step involves the reaction of compound (129) with ammonium formate to give ethylenedioxythiophene-substituted aza-dipyrromethene (EDOT-aza-DIPY), as depicted in Fig. (2.34). The product was washed with ethanol to produce the EDOT-aza-DIPY in low yield (10%). The product was fully characterized using ^{1}H NMR and mass spectrometry.

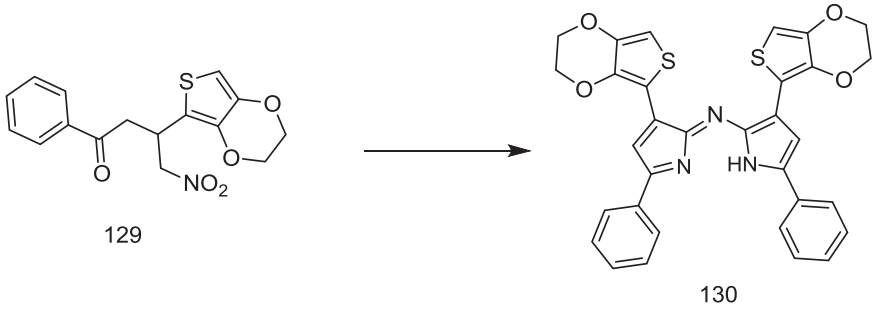

Figure 2.34 The synthesis of ethylenedioxythiophene-substituted aza-dipyrromethene (EDOT-aza-DIPY) (130). Reagents and conditions: NH_4HCO_2/EtOH, reflux, 24h.

2.14.3 Synthesis of Ethylenedioxythiophene-Substituted BF_2-Aza-dipyrromethene (EDOT-aza-BODIPY) (125)

The final desired product ethylenedioxythiophene-substituted BF_2-aza-dipyrromethene (EDOT-aza-BODIPY) (125) was prepared by a standard reaction of (130) with boron trifluoride etherate ($BF_3.OEt_2$) under mild conditions (Fig. (2.35)). Silica gel column and then recrystallization were carried out for the product. The final product EDOT-aza-BODIPY was obtained in a moderate yield (50%). Characterizations were carried out and confirmed the EDOT-aza-BODIPY structure.

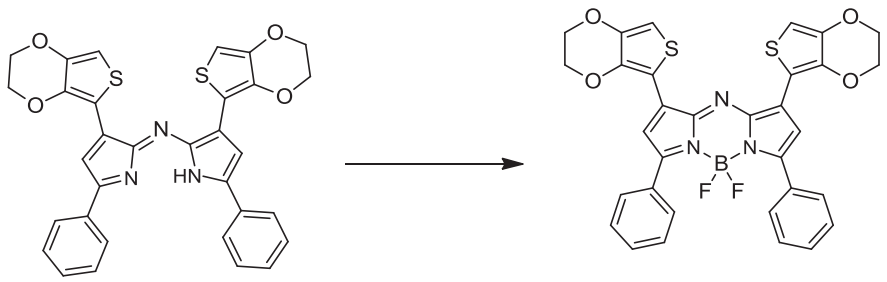

130 125

Figure 2.35 The synthesis of ethylenedioxythiophene-substituted BF_2-aza-dipyrromethene (EDOT-aza-BODIPY) (125). Reagents and conditions: $BF_3.OEt_2$, DIEA, CH_2Cl_2, rt, 24h.

2.15 Synthesis of Thiophene-Phenothiazine-Fluorenone Substituted BF_2-Aza-dipyrromethenes (T-FN-PTZ-aza-BODIPYs)

The new design of aza-BODIPYs was extended to other types of structures, including phenothiazine, thiophene, and fluorenone. These targets are depicted in Fig. (2.36). Only one of these targets was prepared successfully and isolated (thiophene-phenothiazine-substituted BF_2-aza-dipyrromethene (T-PTZ-aza-BODIPY) (132). Phenothiazine-substituted BF_2-aza-dipyrromethene (PTZ-aza-BODIPY) (131) and fluorenone-phenothiazine-substituted BF_2-aza-dipyrromethene (FN-PTZ-aza-BODIPY) (133) were not obtained due to the solubility difficulties which affected the purification and characterization of the intermediate compounds (182) and (183) (Fig. 2.62 and Fig. 2.63). The synthesis detail of T-PTZ-aza-BODIPY is discussed in the next section; the attempted

syntheses of PTZ-aza-BODIPY (131) and FN-PTZ-aza-BODIPY (133) are discussed in Sections (2.28) and (2.29) respectively.

The structure of thiophene-phenothiazine-substituted BF_2-aza-dipyrromethene (T-PTZ-aza-BODIPY) (132), (Fig. (2.36)), shows unique features different from those of a typical tetra-aryl-aza-BODIPY. In this study, a phenothiazine-based aza-BODIPY was synthesized, and its optical properties were investigated. The nature of the phenothiazine moiety as an electron-rich molecule constitutes an excellent relay for electron migration from the donor to the aza-BODIPY core. Modeling suggests that the arrangements of the two phenyl groups of phenothiazine are nearly co-planar, so that the pi-delocalization is extended over the entire molecule. The thiophene groups in the aza-BODIPY structure extend the range of pi-electron delocalization, which leads to an increase in the molar absorptivity of the materials and a red-shift of the absorption wavelength.

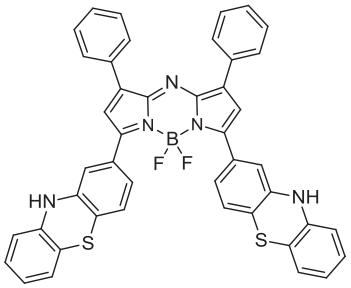

PTZ-aza-BODIPY

131

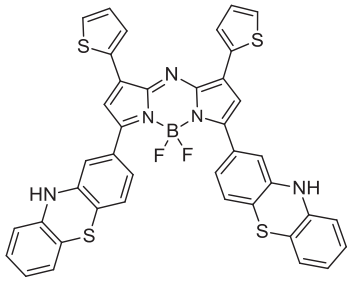

T-PTZ-aza-BODIPY

132

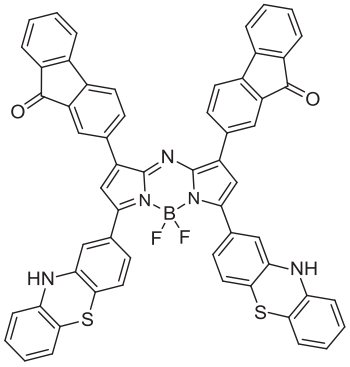

FN-PTZ-aza-BODIPY

133

Figure 2.36 The target structures of thiophene-phenothiazine-fluorenone substituted BF_2-aza-dipyrromethenes (T-FN-PTZ-aza-BODIPYs)

2.16 Synthesis of Thiophene-Phenothiazine-Substituted BF_2-Aza-dipyrromethenes (T-FN-PTZ-aza-BODIPYs)

2.16.1 Synthesis of Intermediate Compounds (135) and (136)

The key building block 2-acetylphenothiazine (134) was prepared using a standard procedure.[56] Employing the same methods as used in the previous aldol condensation reactions, the reaction gave compound (135) after recrystallization, and with a moderate yield (54%). Compound (135) was carried on for the next reaction with nitromethane to produce compound (136). This was followed by purification with column chromatography to give a yield of 45% for compound (136). Fig. (2.37). ^{1}H NMR spectra and mass spectra were used to confirm the structure and the molecular weight of these products.

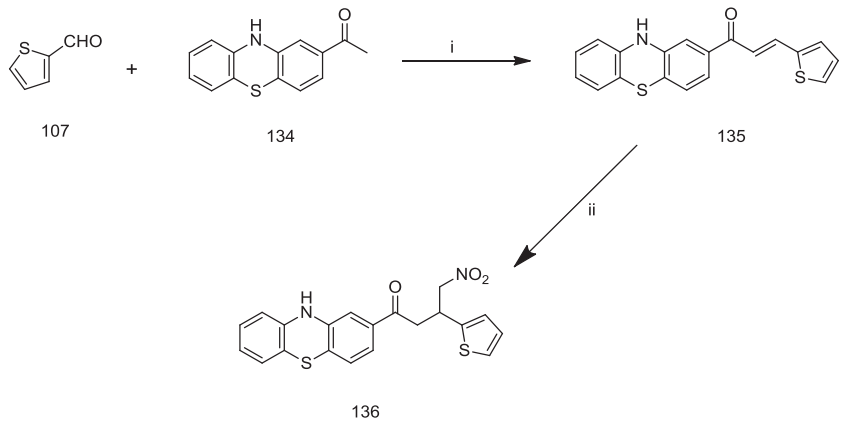

Figure 2.37 Synthesis of intermediate compounds (135) and (136). Reagents and conditions: (i) KOH, EtOH/H_2O. (ii) CH_3NO_2, DEA, MeOH, reflux, 24h.

2.16.2 Synthesis of Thiophene-Phenothiazine-Substituted Aza-dipyrromethene (T-PTZ-aza-DIPY) (137)

The appropriate pyrroles and nitroso-pyrroles of thiophene-phenothiazine derivatives were produced by the reaction of compound (136) with ammonium acetate, which was followed by a subsequent condensation of intermediates to form T-PTZ-aza-DIPY (137) (Fig. (2.38)), and after washing with ethanol gave a yield 9% of the product T-PTZ-aza-DIPY. Further purification was carried out using an alumina chromatography column. This step

was very important and resulted in the product T-PTZ-aza-DIPY. In order to synthesize a more stable form of aza-BODIPY, BF_2 was introduced into the structure of T-PTZ-aza-DIPY as described in the next section. ^{1}H NMR and mass spectrometry were used to confirm the structure of T-PTZ-aza-DIPY.

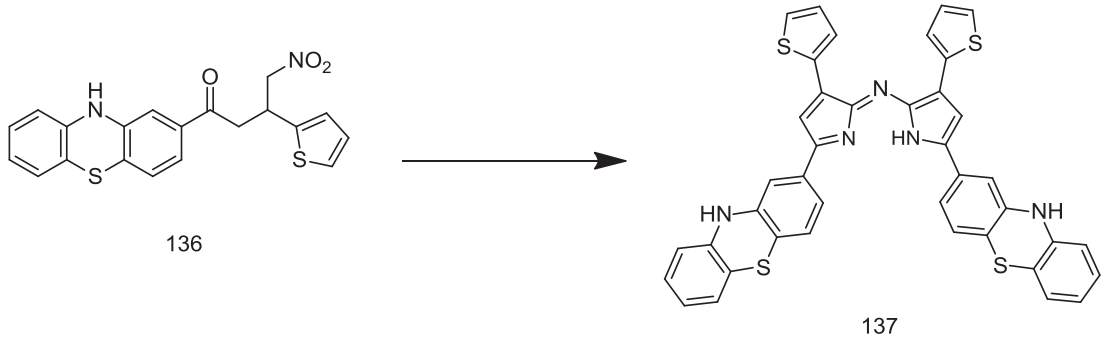

Figure 2.38 The synthesis of thiophene-phenothiazine-substituted aza-dipyrromethene (T-PTZ-aza-DIPY) (137). Reagents and conditions: NH_4OAc/EtOH, reflux, 24h.

2.16.3 Synthesis of Thiophene-Phenothiazine-Substituted BF_2-Aza-dipyrromethene (T-PTZ-aza-BODIPY) (132)

The BF_2-chelated aza-BODIPY derivative (132) was synthesized by the reaction under mild conditions of T-PTZ-aza-DIPY 137 with boron trifluoride etherate ($BF_3.OEt_2$) (Fig. (2.39)). This more stable form was produced in 20% yield. The final product was purified using an alumina column, followed by recrystallization to produce dark-blue crystals of T-PTZ-aza-BODIPY. The product T-PTZ-aza-BODIPY was soluble in most organic solvents, for example chloroform and DCM, but was less soluble in non-polar solvents such as hexane. Mass spectrometry, ^{1}H NMR and ^{13}C NMR spectra were used to confirm the structure of the product T-PTZ-aza-BODIPY (132).

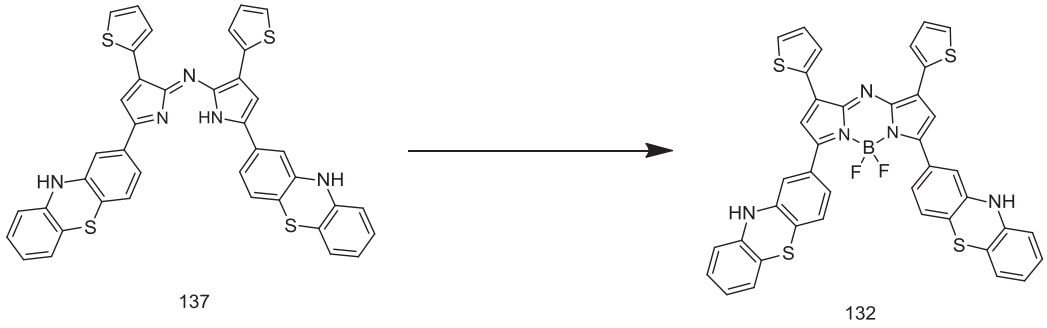

Figure 2.39 Synthesis of thiophene-phenothiazine-substituted BF_2-aza-dipyrromethene (T-PTZ-aza-BODIPY) (132). Reagents and conditions: $BF_3.OEt_2$, DIEA, CH_2Cl_2, rt, 24h.

2.17 Synthesis of Thiophene-Fluorenone-MethylPyrrole-Substituted BF_2-Aza-dipyrromethenes (T-FN-MPy-aza-BODIPYs)

It is known that a small change in π-conjugation in organic dyes causes a significant change in photovoltaic parameters.[57] It is noteworthy that donor molecules based on aryl amine in DSSCs have given efficient charge separation in solar cells.[58] Pyrrole derivatives also have interesting donor properties, and pyrrole derivatives have been incorporated into many donor molecular structures such as charge transfer complexes [59-62] and solution-processable donors in bulk heterojunction solar cells.[60,63,64] Compounds that have substituents such as N-methyl pyrrole, thiophene and fluorenone on the aza-BODIPY core structure have been investigated in this study. This investigation was of interest because methyl pyrrole is electron rich with a low delocalization energy, which makes it an appropriate donor for incorporation into the aza-BODIPY structure. Three structures of aza-BODIPYs based on methyl pyrrole have been investigated. These are methylpyrrole-substituted BF_2 aza-dipyrromethene (MPy-aza-BODIPY), thiophene-methylpyrrole-substituted BF_2 aza-dipyrromethene (T-MPy-aza-BODIPY), and fluorenone-methylpyrrole-substituted BF_2 aza-dipyrromethene (FN-MPy-aza-BODIPY) (Fig. (2.40)). The synthesis of T-MPy-aza-BODIPY is described in the following sections, while the attempted syntheses of MPy-aza-BODIPY and FN-MPy-aza-BODIPY are discussed in Sections (2.30) and (2.31) respectively. The optical and photovoltaic properties of (139) are discussed in Chapter 3 and 4 respectively. The target MPy-aza-BODIPY incorporates N-methyl pyrrole groups in

position 3 and 5 of aza-BODIPY. T-MPy-aza-BODIPY (139) incorporates thiophene groups in position 1 and 7 as well as N-methyl pyrrole in position 3 and 5; FN-MPy-aza-BODIPY (140) incorporates fluorenone groups in position 1 and 7 as well as N-methyl pyrrole groups in position 3 and 5 (Fig. (2.40)).

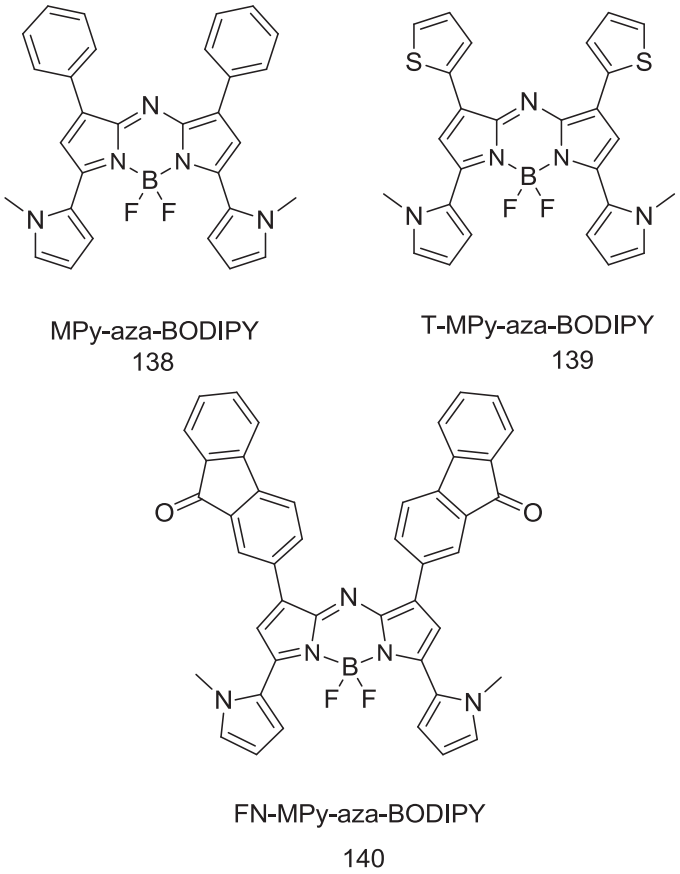

Figure 2.40 The target structures of methylpyrrole-substituted BF_2-aza-dipyrromethene (MPy-aza-BODIPY), thiophene-methylpyrrole-substituted BF_2-aza-dipyrromethene (T-MPy-aza-BODIPY), and fluorenone-methylpyrrole-substituted BF_2-aza-dipyrromethene (FN-MPy-aza-BODIPY).

2.18 Synthesis of Thiophene-MethylPyrrole-Substituted BF_2-Aza-dipyrromethene (T-MPy-aza-BODIPY) (139)

2.18.1 Synthesis of Intermediate Compounds (142) and (143)

2-Acetyl-1-methylpyrrole and 2-thiophenecarboxaldehyde were used as building blocks for the synthesis of compound (142). These building blocks were prepared using standard procedures.[36,65] Compound (142) was prepared using a modified procedure of the method of O'Shea *et al*.[9] This procedure involved reaction of 2-acetyl-1-methylpyrrole with 2-thiophenecarboxaldehyde in the presence of a base, producing the required compound (142) in moderate yield (40%) after crystallization from ethanol. Compound (142) was reacted with nitromethane to produce the nitromethane-adduct compound (143) (Fig. (2.41)). A base-mediated Michael-addition of nitromethane to (142) gave compound (143) in 40% yields. The compounds were characterized by ^{1}H NMR and mass spectrometry.

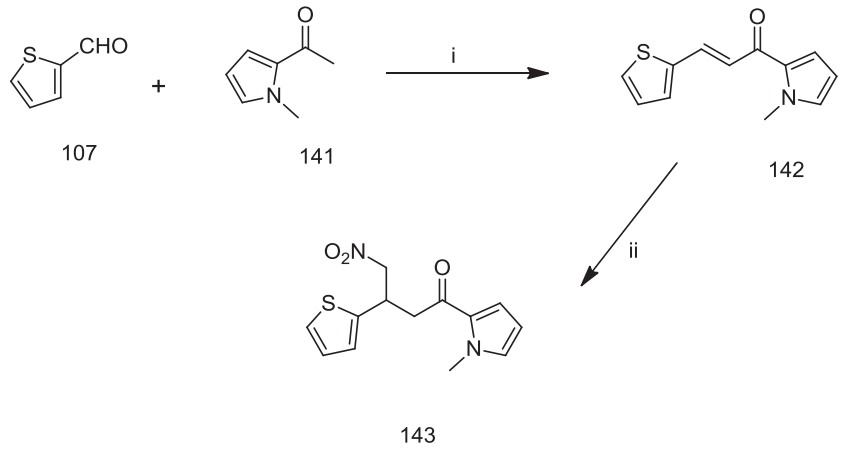

Figure 2.41 Synthesis of intermediate compounds (142) and (143). Reagents and conditions: (i) KOH, EtOH/H_2O. (ii) CH_3NO_2, DEA, MeOH, reflux, 24h.

2.18.2 Synthesis of Thiophene-MethylPyrrole-Substituted Aza-dipyrromethene (T-MPy-aza-DIPY) (144)

Intermediate compound (143) was reacted with ammonium acetate to produced thiophene-methylpyrrole-substituted aza-dipyrromethene (T-MPy-aza-DIPY) (144) in 10% yield (Fig. (2.42)). The product was purified using an alumina column, and then characterized using ^{1}H NMR and mass spectrometry.

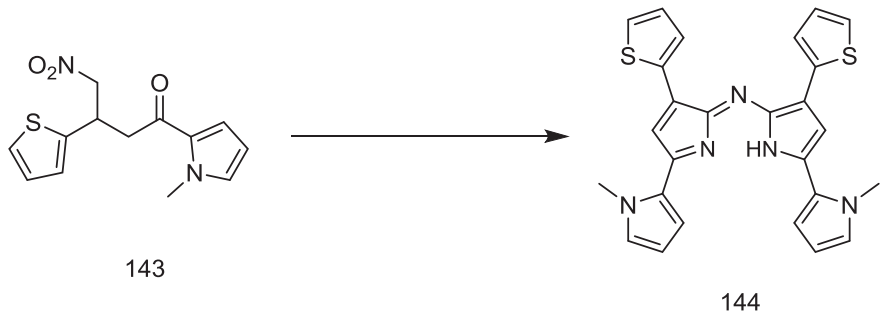

Figure 2.42 The synthesis of thiophene-methylpyrrole-substituted aza-dipyrromethene (T-MPy-aza-DIPY) (144). Reagents and conditions: NH_4OAc/EtOH, reflux, 24h.

2.18.3 Synthesis of Thiophene-MethylPyrrole-Substituted BF_2-Aza-dipyrromethene (T-MPy-aza-BODIPY) (139)

The final desired thiophene-methylpyrrole-substituted BF_2-aza-dipyrromethene (T-MPy-aza-BODIPY) (139) was prepared by reaction of T-MPy-aza-DIPY (144) with the boron trifluoride etherate ($BF_3.OEt_2$) under mild conditions. T-MPy-aza-BODIPY has greater stability than T-MPy-aza-DIPY and has been produced in a good yield of 60%. Fig. (2.43) illustrates the synthesis of T-MPy-aza-DIPY. ^{1}H NMR and mass spectra were used to confirm the structure of the product T-MPy-aza-BODIPY (139).

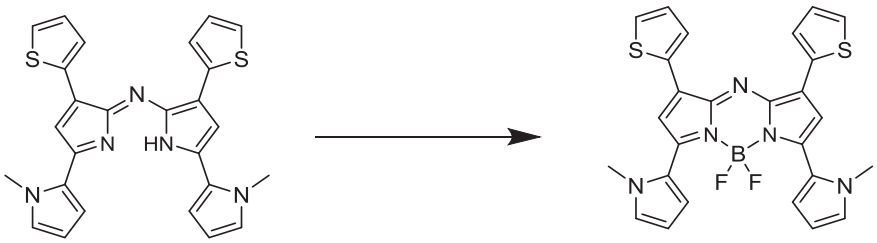

144 139

Figure 2.43 The synthesis of thiophene-methylpyrrole-substituted BF_2-aza-dipyrromethene (T-MPy-aza-BODIPY) (139). Reagents and conditions: $BF_3.OEt_2$, DIEA, CH_2Cl_2, rt, 24h.

2.19 Synthesis of Thiophene-Carbazole-Substituted BF_2-Aza-dipyrromethene (T-Cz-aza-BODIPY) (145)

An aza-BODIPY with electron-donating groups (carbazole and thiophene) was designed and synthesized, as depicted in Fig. (2.44). Carbazole has a similar oxidation potential to pyrrole, and has been used as an electron donor. High efficiencies have been achieved in OPV cells. [66-69] The carbazole unit is fully aromatic, which provides better chemical and environmental stability. Thiophene-carbazole-substituted BF_2-aza-dipyrromethene (T-Cz-aza-BODIPY) (145) with carbazole bonded to positions 3 and 5 of aza-BODIPY core and thiophene bonded to 1 and 7 positions of the same aza-BODIPY core has been synthesized (Fig. (2.44)).

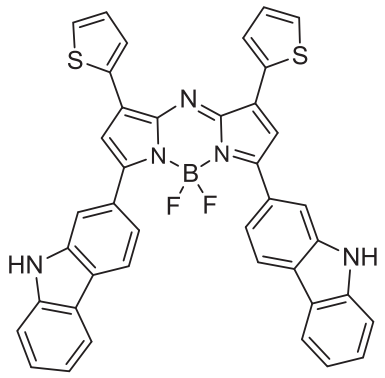

(145)

Figure 2.44 The structure of the target thiophene-carbazole-substituted BF_2-aza-dipyrromethene (T-Cz-aza-BODIPY) (145).

2.19.1 Synthesis of Intermediate Compounds (147) and (148)

The key building-blocks 2-acetylcarbazole and 2-thiophenecarboxaldehyde were prepared using standard procedures. An aldol condensation of 2-acetylcarbazole with 2-thiophenecarboxaldehyde gave the intermediate compound (147). A 46% yield of compound (147) was obtained after purification. This was followed by a base mediated Michael-addition reaction of nitromethane to compound (147) gives 148. A good yield (60%) of 4-nitro-3-(3'-terthiophene)-1-phenyl-butanone (148) was obtained after the aqueous work-up (Fig. (2.45)). ^{1}H NMR spectra and mass spectrometry were used to confirm the structures of these products.

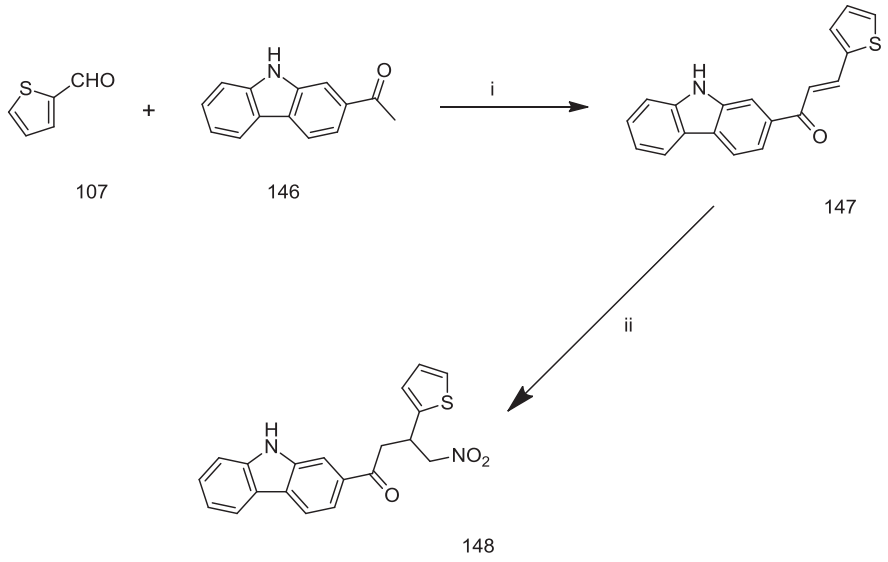

Figure 2.45 Synthesis of intermediate compounds (147) and (148). Reagents and conditions: (i) KOH, EtOH/H_2O. (ii) CH_3NO_2, DEA, MeOH, reflux, 24h.

2.19.2 Synthesis of Thiophene-Carbazole-Substituted Aza-dipyrromethene (T-Cz-aza-DIPY) (149)

The same procedure as in Section (2.16.2) was employed for the crucial step of the formation of thiophene-carbazole-substituted aza-dipyrromethene (T-Cz-aza-DIPY) (149) (Fig. (2.46)). The reaction of 4-nitro-3-(3'-terthiophene)-1-phenyl-butanone (148) with ammonium acetate formed the appropriate intermediate pyrroles and nitroso-pyrroles,

which was followed by a condensation of two intermediates to form T-Cz-aza-DIPY (149). The product was recrystallized with ethanol producing T-Cz-aza-DIPY in a yield of 10%. Full characterization using ^{1}H NMR and mass spectrometry has been carried out to confirm the structure of the product.

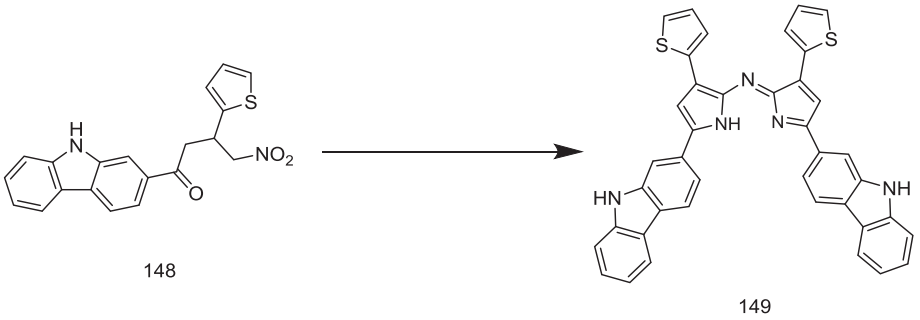

Figure 2.46 The synthesis of the thiophene-carbazole-substituted aza-dipyrromethene (T-Cz-aza-DIPY). Reagents and conditions: NH_4OAc/EtOH, reflux, 24h.

2.19.3 Synthesis of Thiophene-Carbazole-Substituted BF_2-Aza-dipyrromethene (T-Cz-aza-BODIPY) (145)

The final desired product thiophene-carbazole-substituted BF_2-aza-dipyrromethene (T-Cz-aza-BODIPY) 145 was synthesized by the reaction of T-Cz-aza-DIPY with boron trifluoride etherate ($BF_3.OEt_2$) under mild conditions (Fig. (2.47)). The final product was purified using alumina column chromatography, and then recrystallized to give T-Cz-aza-BODIPY as blue crystals in 35% yield. Characterization was carried out using ^{1}H NMR, mass spectrometry and elemental analysis.

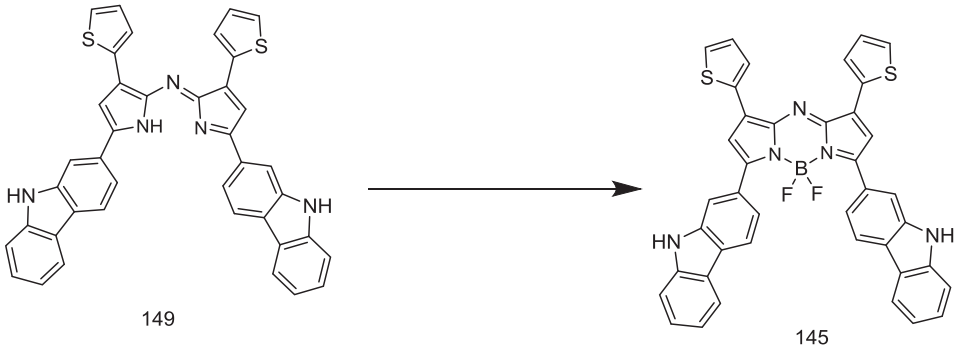

Figure 2.47 The synthesis of thiophene-carbazole-substituted BF_2-aza-dipyrromethene (T-Cz-aza-BODIPY) (145). Reagents and conditions: $BF_3.OEt_2$, DIEA, CH_2Cl_2, rt, 24h.

2.20 Synthesis of Fluorenone-Thiophene-Terthiophene-Triphenylamine-Phenothiazine-Methylpyrrole- Substituted BF_2-Aza-dipyrromethene (FN-T-TT-TPA-PTZ-MPy-aza-BODIPYs)

π-conjugated molecules containing fluorenone units have been used in photovoltaic applications. These compounds exhibit extended absorption bands in the visible part of the spectrum.[70-74] The design and synthesis of a new series of small aza-BODIPY molecules containing fluorenone units have been investigated. The incorporation of a weakly electron-withdrawing fluorenone moiety in the aza-BODIPY structure was expected to broaden the dyes' absorption spectra, so that in comparison with the tetraphenyl-aza-BODIPY a broader range of sunlight wavelengths would be accessible. The optical and photovoltaic properties of fluorenone-based aza-BODIPY are discussed in Chapter 3 and 4. This new series of aza-BODIPY derivatives included fluorenone, thiophene, triphenylamine, terthiophene, phenothiazine and methylpyrrole units on the aza-BODIPY structure, as shown in Fig. (2.48). The first target, namely fluorenone-substituted BF_2-aza-dipyrromethene (FN-aza-BODIPY) (150), incorporates fluorenone at positions 1 and 7 of the aza-BODIPY structure, while position 3 and 5 have phenyl groups. The second target, namely thiophene-fluorenone-substituted BF_2-aza-dipyrromethene (T-FN-aza-BODIPY) (151) incorporates fluorenone units at positions 3 and 5, and thiophene at positions 1 and 7. The third target, namely fluorenone-triphenylamine-substituted BF_2-aza-dipyrromethene (FN-TPA-aza-BODIPY) (153) having triphenylamine groups at positions 3 and 5, while positions 1 and 7 contain fluorenone units. Target five, namely terthiophene-fluorenone-substituted BF_2-aza-dipyrromethene (TT-FN-aza-BODIPY) (152), incorporates terthiophene at positions 1 and 7, while fluorenone units are located at positions 3 and 5. Target 6, namely fluorenone-phenothiazine-substituted BF_2-aza-dipyrromethene (FN-PTZ-aza-BODIPY) (154) consist of fluorenone units at positions 1 and 7, as well as phenothiazine groups at positions 3 and 5. The last target in this series, namely fluorenone-methylpyrrole-substituted BF_2-aza-dipyrromethene (FN-MPy-aza-BODIPY) (155), consists of fluorenone units at positions 1 and 7, as well as methylpyrrole groups at positions 3 and 5. The synthetic details of FN-aza-BODIPY and T-FN-aza-BODIPY are discussed in Sections (2.21) and (2.22) respectively. Due to the solubility difficulties, purification and characterization of the other

four compounds was not possible. The attempted syntheses of FN-TPA-aza-BODIPY (133), TT-FN-aza-BODIPY (152), FN-PTZ-aza-BODIPY (154), and FN-MPy-aza-BODIPY (155) are discussed in Sections 2.26, 2.27, 2.29, and 2.31 respectively.

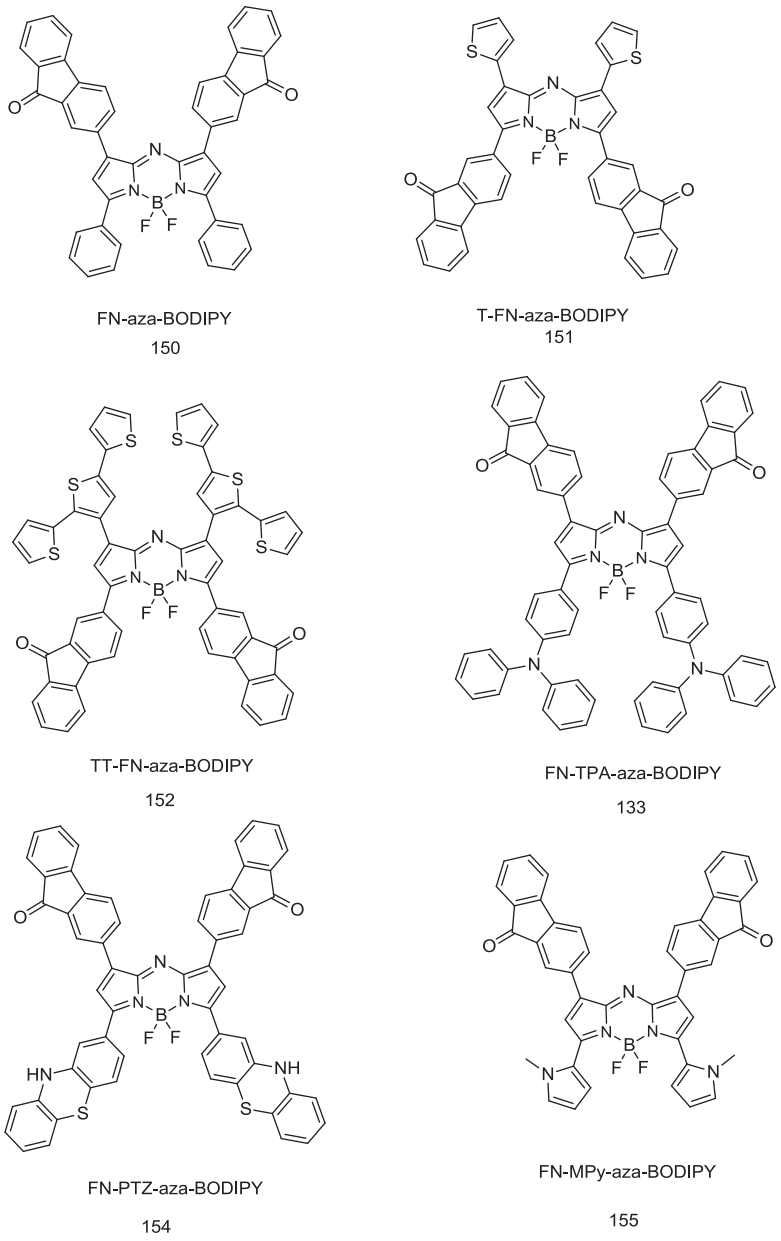

Figure 2.48 The target structures of fluorenone-based aza-BODIPYs.

2.21 Synthesis of Fluorenone-Substituted BF_2-Aza-dipyrromethene (FN-aza-BODIPY) (150)

2.21.1 Synthesis of Intermediate Compounds (157) and (158)

The key building-block 9-oxofluorene-2-carboxaldehyde was prepared via standard procedures.[75] The intermediate compounds (157) and (158) were prepared using a modified procedure of the method of O'Shea *et al* [9] (Fig. (2.49)). This procedure involved an aldol condensation of 9-oxofluorene-2-carboxaldehyde with acetophenone producing the required compound (157) in 28% yield. This was followed by a Michael-addition reaction of compound (157) with nitromethane to produce compound (158). The reaction gave a good yield (56%) after the aqueous work-up and the recrystallization. ^{1}H NMR and mass spectrometry were used to confirm the structures of both compounds.

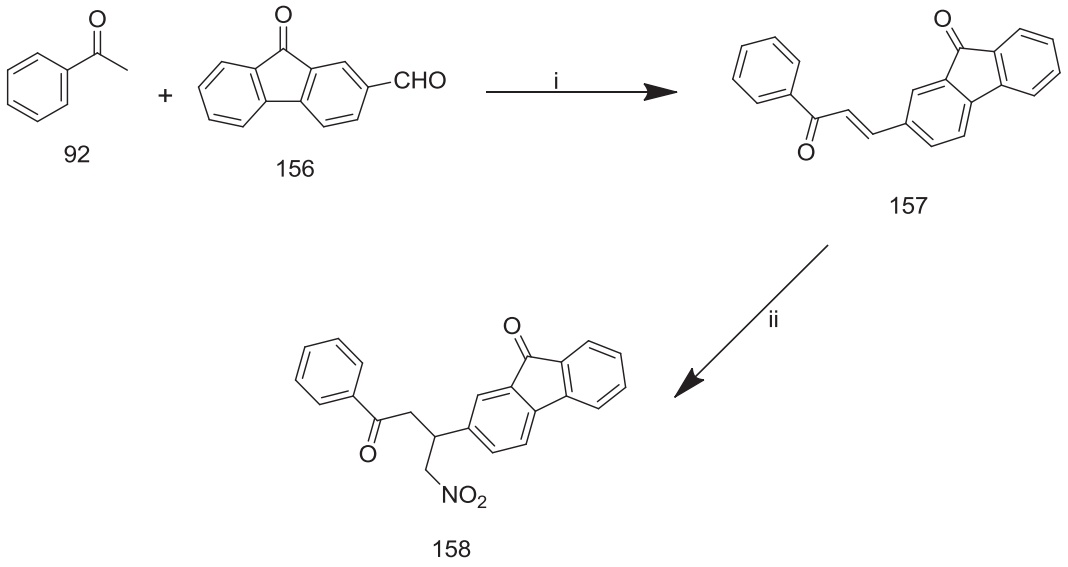

Figure 2.49 Synthesis of intermediate compounds (157) and (158). Reagents and conditions: (i) KOH, EtOH/H_2O. (ii) CH_3NO_2, DEA, MeOH, reflux, 24h.

2.21.2 Synthesis of Fluorenone-Substituted Aza-dipyrromethene (FN-aza-DIPY) (159)

This important synthesis of fluorenone-substituted aza-dipyrromethene (FN-aza-DIPY) (159) was achieved using the same procedure as in Section (2.7.2) (Fig. (2.50)). The FN-aza-DIPY was obtained in a yield of 5%, and was used in the next reaction without any further purification. ^{1}H NMR and mass spectrometry confirmed the chemical structure of the product (FN-aza-DIPY).

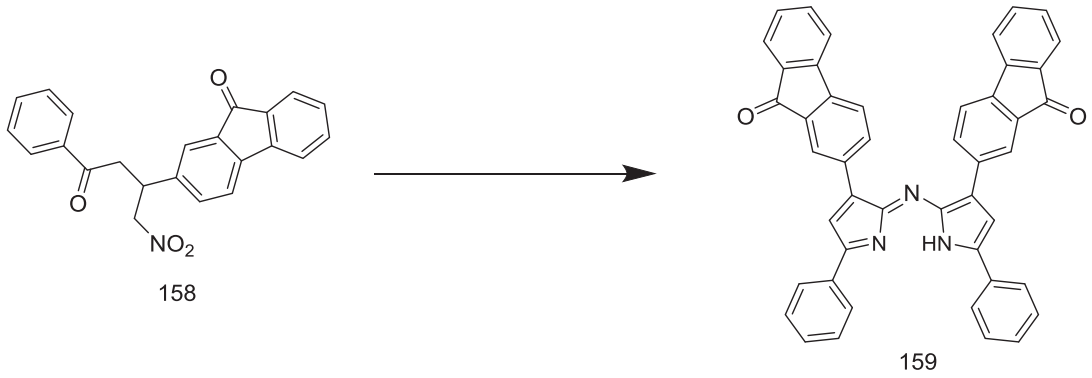

Figure 2.50 The synthesis of fluorenone-substituted aza-dipyrromethene (FN-aza-DIPY) (159). Reagents and conditions: NH_4OAc/EtOH, reflux, 24h.

2.21.3 Synthesis of Fluorenone-Substituted BF_2-Aza-dipyrromethene (FN-aza-BODIPY) (150)

The final product fluorenone-substituted BF_2-aza-dipyrromethene (FN-aza-BODIPY) (150) was prepared by reaction of FN-aza-DIPY (159) with boron trifluoride etherate ($BF_3.OEt_2$) under mild conditions (Fig. (2.51)). A yield of 31% was obtained for the product FN-aza-BODIPY after purification using an alumina column. ^{1}H NMR and mass spectrometry were used to confirm the structure of the product FN-aza-BODIPY.

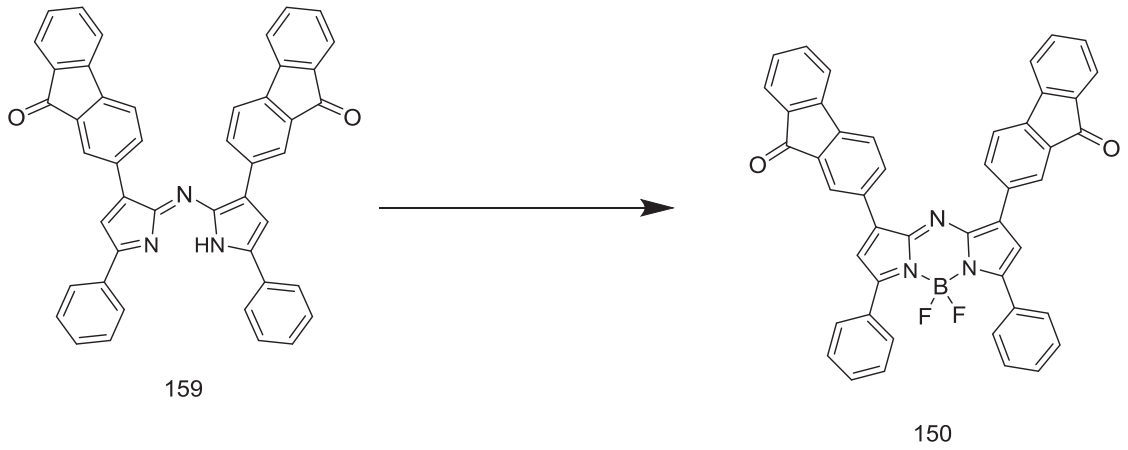

Figure 2.51 The synthesis of fluorenone-substituted BF_2-aza-dipyrromethene (FN-aza-BODIPY) (150). Reagents and conditions: $BF_3.OEt_2$, DIEA, CH_2Cl_2, rt, 24h.

2.22 Synthesis of Thiophene-Fluorenone-Substituted BF_2-Aza-dipyrromethene (T-FN-aza-BODIPY) (151)

Incorporation of thiophene substituents on the fluorenone-based aza-BODIPY structure was expected to show improvements in the yield and in the absorption properties, in comparison with FN-aza-BODIPY. Details of the optical properties of these compounds are discussed in Chapter 3. The synthetic route of the thiophene-fluorenone-substituted BF_2-aza-dipyrromethene (T-FN-aza-BODIPY) (151) is discussed in the following sections.

2.22.1 Synthesis of Intermediate Compounds (160) and (161)

The same key building-block 9-oxofluorene-2-carboxaldehyde has been used here to react with 2-thiophenecarboxaldehyde via aldol condensation to produce compound (160) in 46% yield. This compound was used in the next reaction with nitromethane to produce the nitro-adduct compound (161), and then was recrystallized to give a 60% yield (Fig. (2.52)). Both compounds (160) and (161) were characterized and their structures confirmed.

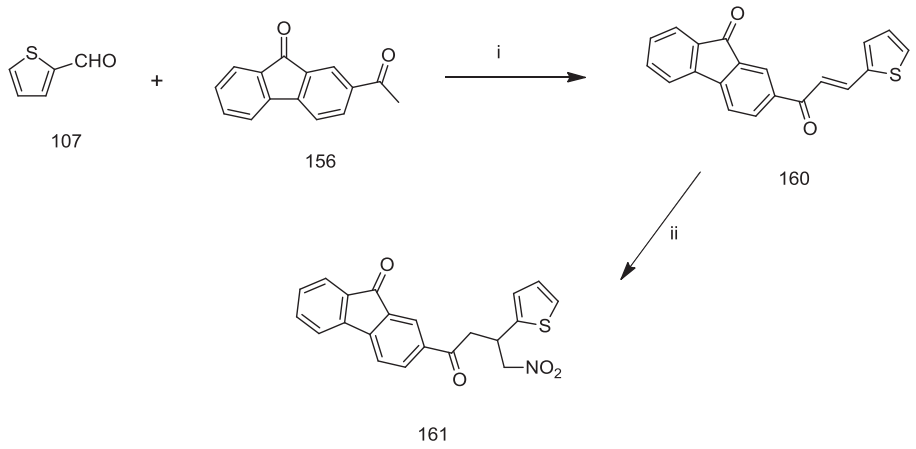

Figure 2.52 Synthesis of intermediate compounds (160) and (161). Reagents and conditions: (i) KOH, EtOH/H_2O. (ii) CH_3NO_2, DEA, MeOH, reflux, 24h.

2.22.2 Synthesis of Thiophene-Fluorenone-Substituted Aza-dipyrromethene (T-FN-aza-DIPY) (162)

The formation of thiophene-fluorenone-substituted aza-dipyrromethene (T-FN-aza-DIPY) (162) (Fig. 2.53) was achieved by the reaction of compound (161) with ammonium formate to produce the appropriate pyrroles and nitroso-pyrroles, and a subsequent condensation of both intermediates to form T-FN-aza-DIPY in 15% yield after purification with an alumina column (Fig. (2.53)). The structure of T-FN-aza-DIPY was confirmed by ^{1}H NMR and mass spectrometry.

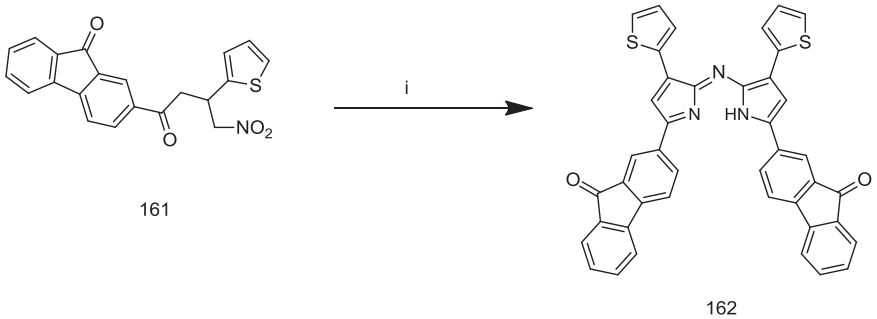

Figure 2.53 The synthesis of thiophene-fluorenone-substituted aza-dipyrromethene (T-FN-aza-DIPY) (162). Reagents and conditions: NH_4HCO_2/EtOH, reflux, 24h.

2.22.3 Synthesis of Thiophene-Fluorenone-Substituted BF_2-Aza-dipyrromethene (T-FN-aza-BODIPY) (151)

This final step in the synthesis of thiophene-fluorenone-substituted BF_2-aza-dipyrromethene (T-FN-aza-BODIPY) (151) proved to be straightforward via the reaction of T-FN-aza-DIPY (162) with boron trifluoride etherate ($BF_3.OEt_2$) under standard conditions (Fig. (2.54)). The final product T-FN-aza-BODIPY (151) was purified using column chromatography, followed by recrystallization to produce a 65% yield. ^1H NMR spectrum confirmed the structure, but ^{13}C NMR and mass spectra were not reliable.

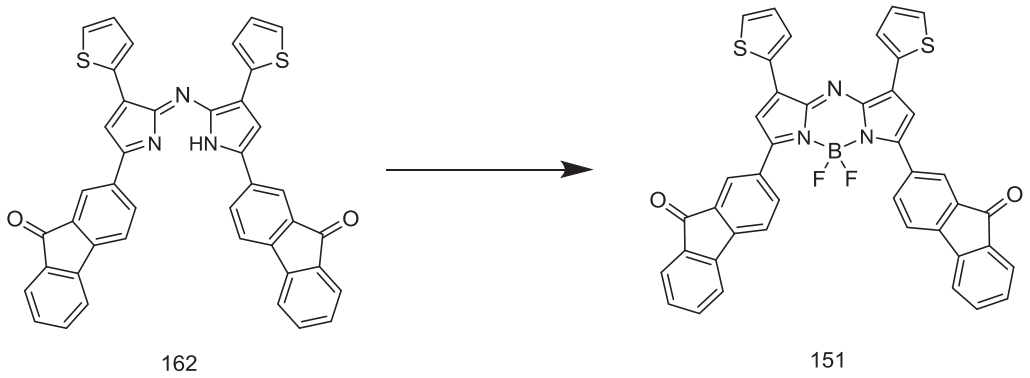

162 151

Figure 2.54 Synthesis of thiophene-fluorenone-substituted BF_2-aza-dipyrromethene (T-FN-aza-BODIPY) (151). Reagents and conditions: $BF_3.OEt_2$, DIEA, CH_2Cl_2, rt, 24h.

2.23 Attempted Synthesis of Other BF_2-Aza-dipyrromethenes (Aza-BODIPYs)

Although the design strategy provided for the insertion of a good number of different substituents into the aza-BODIPY core, not all of the planned targets were successfully synthesized. Several common factors affected adversely the syntheses of those targets, including lack of solubility, sensitivity of intermediate compounds to oxygen, as well as separation and purification difficulties. Some of these synthetic efforts have led to final aza-BODIPY compounds as indicated by their mass spectra, but obtaining ^{1}H NMR spectra was not possible due to the existence of impurities and purification difficulties. Other reactions did not lead to any products, as the crucial step of the aza-BODIPY synthesis, i.e. obtaining aza-DIPYs, was not successful. Two types of ammonium sources and four different alcohol solvents were used in the crucial step, but with same targets none of them worked. The structures of these aza-BODIPYs for which the syntheses were unproductive are shown in Fig. (2.55). The next few sections will discuss the synthetic attempts.

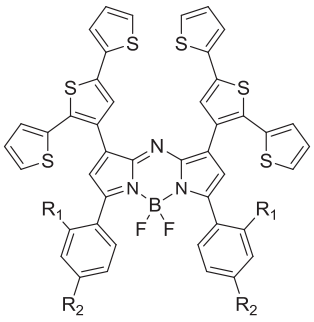

R_1=R_2= OCH_3 TT-aza-BODIPY3 89
R_1=H, R_2=CH_3 TT-aza-BODIPY4 90

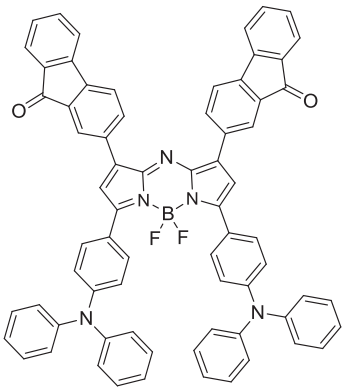

FN-TPA-aza-BODIPY
153

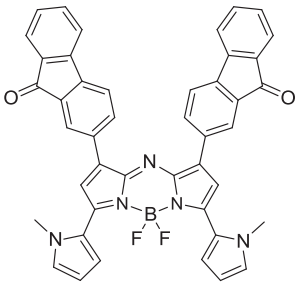

FN-MPy-aza-BODIPY
140

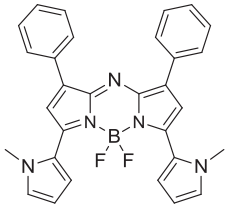

MPy-aza-BODIPY
138

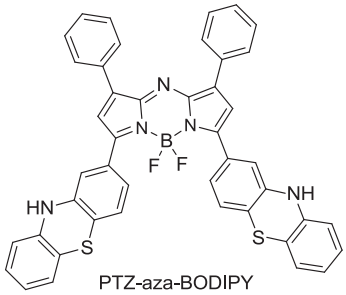

PTZ-aza-BODIPY
131

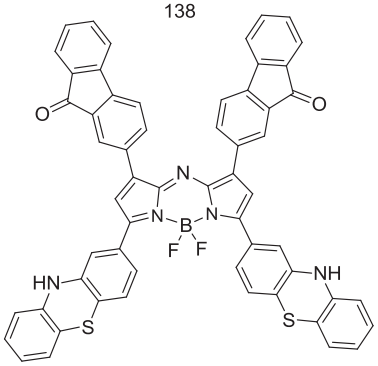

FN-PTZ-aza-BODIPY
133

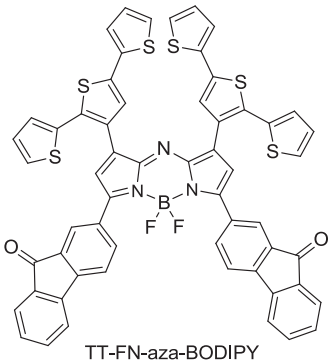

TT-FN-aza-BODIPY
152

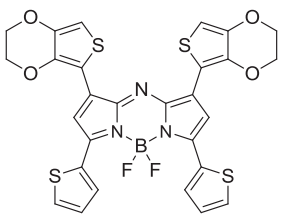

EDOT-T-aza-BODIPY
163

Figure 2.55 Structures of some proposed BF_2-aza-dipyrromethenes (aza-BODIPYs) which were *not* synthesized successfully.

2.24 Attempted Synthesis of Terthiophene-Substituted BF_2-Aza-dipyrromethene (TT-aza-BODIPYs)

Incorporation of thiophene substituents on an aza-BODIPY core gave compounds which showed interesting properties such as long wavelengths for absorption and emission. New terthiophene-substituted BF_2-aza-dipyrromethenes (TT-aza-BODIPYs) with electron donating and withdrawing groups in the phenyl rings (at positions 3 and 5) were conceived. Attempts to synthesize TT-aza-BODIPY3 (89) and TT-aza-BODIPY4 (90) (see Fig. (2.55)) are discussed in this section.

The target TT-aza-BODIPY3 (89) was designed with two methoxy groups at the ortho and para positions in each of the phenyl groups attached to the aza-BODIPY core. The key building block 3'-formylterthiophene (91) was reacted with 2',4'-dimethoxyacetophenone in the presence of KOH. Compound (165) (see Fig. (2.56)) was purified and isolated in 50% yield. Compound (166) (see Fig. (2.56)) was readily produced by a base-mediated Michael-addition of nitromethane to compound (165). The reaction gave a moderate yield of 57% of compound (166). The products (165) and (166) were characterized via ^{1}H NMR and mass spectrometry.

The important step was the reaction of compound (166) with an ammonium source to produce the desired aza-dipyrromethene (TT-aza-DIPY3) (167), as depicted in Fig. (2.56). The mass spectrum indicated the possible presence of TT-aza-DIPY, but obtaining a ^{1}H NMR spectrum was not possible for the reaction product which was a crude mixture and not very soluble. Several purification techniques were used to try and purify this product with no success. No further characterization was attempted.

The target TT-aza-BODIPY4 (90) (Fig. (2.55)) was designed with methyl groups at the para positions in the phenyl substituents attached on the aza-BODIPY core. The key building block 3'-formylterthiophene (91) (see Fig. (2.57)) was reacted with 4'-methylacetophenone under standard conditions. Compound (169) was formed, and then purified and isolated in 48% yield. Compound (170) was readily produced by a base-mediated Michael-addition of nitromethane to compound (169). The reaction gave a moderate yield of 40% of 4-nitro-3-(3'-terthiophene)-1-phenyl-butanone (170), as depicted

in Fig. (2.57). The products (169) and (170) were characterized via ^1H NMR and mass spectrometry. Two ammonium sources were tested in the attempted synthesis of TT-aza-DIPY4 (171). This reaction was monitored by thin layer chromatography (TLC) and mass spectrometry. The starting materials persisted without any observed reaction for the various reaction combinations that were investigated. The mass spectrum of the crude mixture did not show any peaks related to the proposed product TT-aza-DIPY4. Fig. (2.57) shows the route of the attempted synthesis of TT-aza-DIPY4 (171).

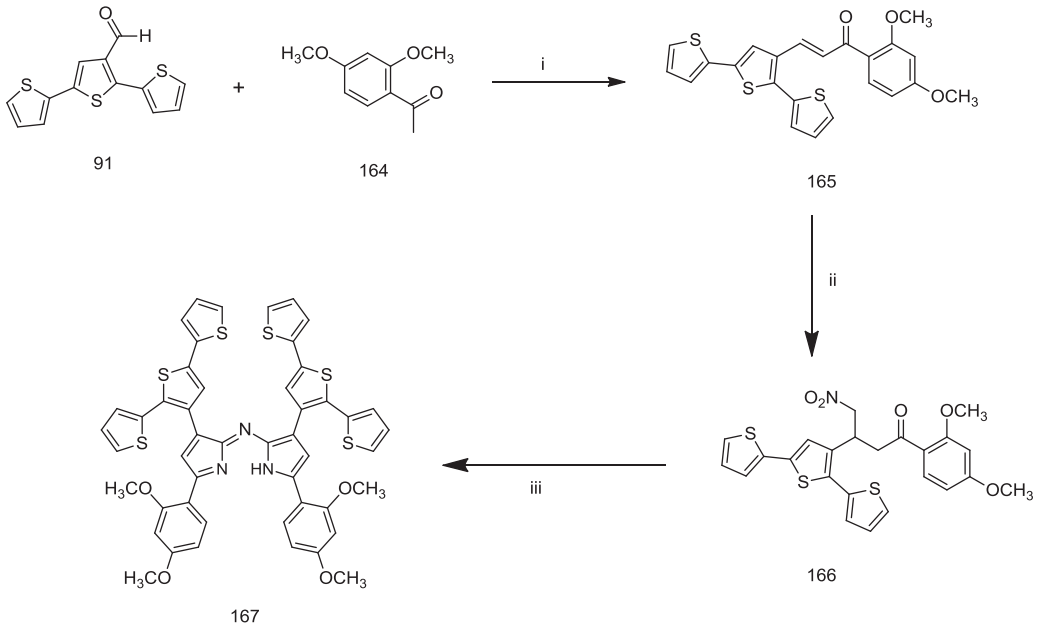

Figure 2.56 Synthesis of intermediate compounds (165), (166), and (167) (TT-aza-DIPY3). Reagents and conditions: (i) KOH, EtOH/H_2O. (ii) CH_3NO_2, DEA, MeOH, reflux, 24h.(iii) NH_4OAc/EtOH, reflux, 24h.

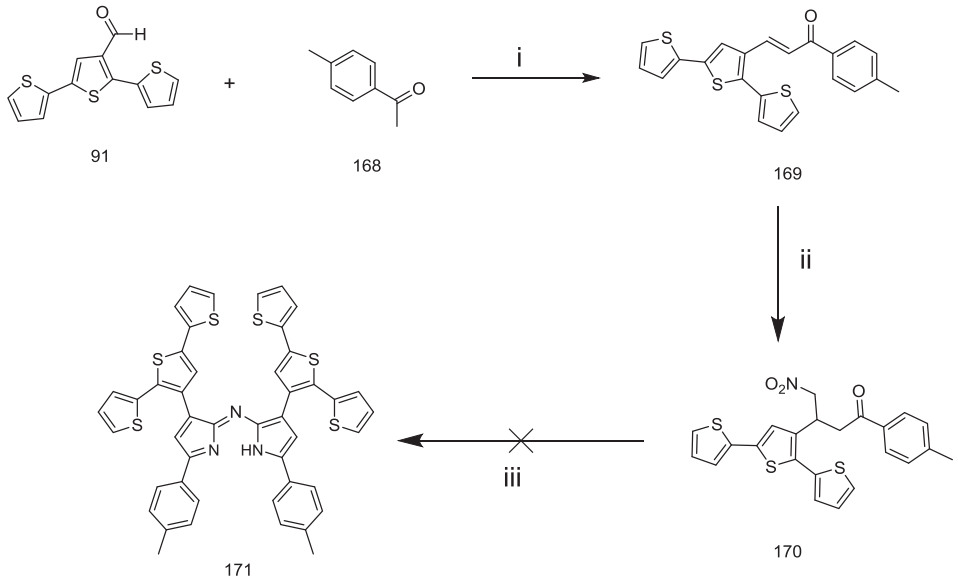

Figure 2.57 The attempted synthesis of TT-aza-DIPY4 (171). Reagents and conditions: (i) KOH, EtOH/H_2O. (ii) CH_3NO_2, DEA, MeOH, reflux, 24h.(iii) NH_4OAc/EtOH, reflux, 24h.

2.25 Attempted Synthesis of Ethylenedioxythiophene-Triphenylamine-Substituted BF_2-Aza-dipyrromethene (EDOT-TPA-aza-BODIPY)

2.25.1 Synthesis of Intermediate Compounds (172) and (173)

The EDOT-TPA-aza-BODIPY (126) (Fig. (2.32)) target was designed with ethylenedioxythiophene (EDOT) groups at position 1 and 7, and triphenylamine (TPA) groups at positions 3 and 5. The intermediate compound (172) (Fig. 2.58) was prepared in a moderate yield (45%) by the reaction of 3,4–ethylenedioxythiophene-2-carbaldehyde (127) with 4-diphenylaminoacetophenone (101) in the presence of a base (KOH). This was recrystallized from ethanol. A nitromethane adduct product was readily produced by a base-mediated Michael-addition of nitromethane to compound (172). After the aqueous work-up, followed by a recrystallization from ethanol, the product (173) was obtained in a 35% yield. Fig. (2.58) illustrates the synthesis pathway. ^{1}H NMR and mass spectrometry were used to confirm the structures of both compounds.

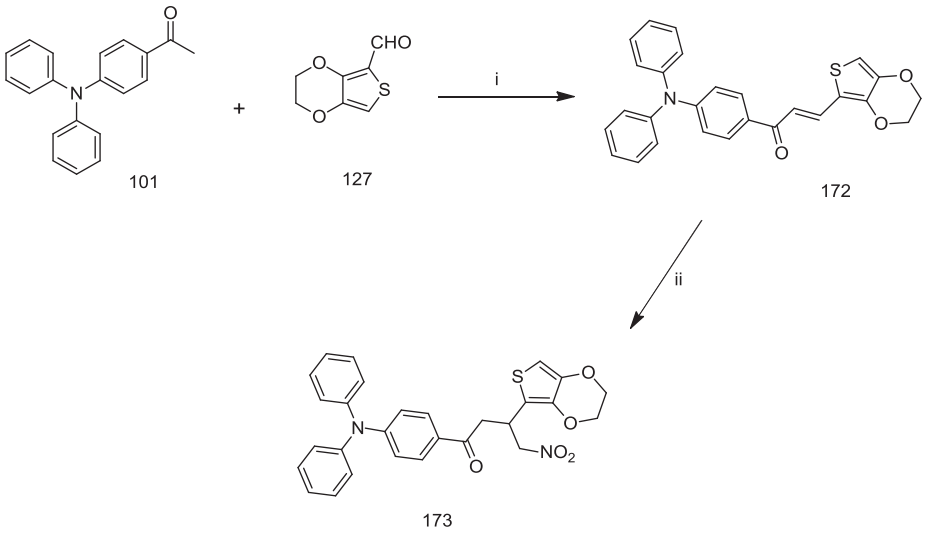

Figure 2.58 Synthesis of intermediate compounds (172) and (173). Reagents and conditions: (i) KOH, EtOH/H_2O. (ii) CH_3NO_2, DEA, MeOH, reflux, 24h.

The crucial step in the synthesis of EDOT-TPA-aza-BODIPY would be the formation of ethylenedioxythiophene-triphenylamine-substituted aza-dipyrromethene (EDOT-TPA-aza-DIPY) (174), as depicted in Fig. (2.59). Two ammonium sources were tried in this reaction. This reaction was monitored by TLC to detect changes in retardation factor (R_f) or color. In the reaction of compound (173) with ammonium acetate, the starting materials remained unchanged without observed reaction. The mass spectrum of the crude mixture showed no peaks for the desired product EDOT-TPA-aza-DIPY (174). Upon using ammonium formate instead of ammonium acetate, TLC studies indicated changes in color, while mass spectra suggested the presence of the desired product (EDOT-TPA-aza-DIPY). Several purification techniques were attempted to isolate and purify the product EDOT-TPA-aza-DIPY without success with any of them. The highly conjugated π-system of EDOT-TPA-aza-DIPY makes this compound very insoluble and purification was not possible. Apart from ^{1}H NMR and mass spectrometry, no further characterizations were carried out for EDOT-TPA-aza-DIPY.

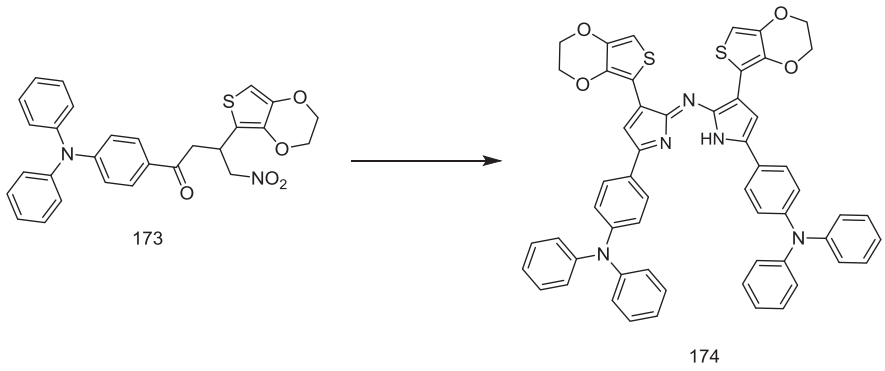

Figure 2.59 The synthesis of ethylenedioxythiophene-triphenylamine-substituted aza-dipyrromethene (EDOT-TPA-aza-DIPY) (174). Reagents and conditions: NH_4HCO_2/EtOH, reflux, 24h.

2.26 Attempted Synthesis of Fluorenone-Triphenylamine-Substituted BF_2-Aza-dipyrromethene (FN-TPA-aza-BODIPY) (177)

The targeted fluorenone-triphenylamine-substituted BF_2-aza-dipyrromethene (FN-TPA-aza-BODIPY) (153) had fluorenone units at positions 1 and 7, and triphenylamine units at positions 3 and 5. The intended synthetic route of the precursor FN-TPA-aza-DIPY is shown in Fig. (2.60). The first compound in this intended route was compound (175), which was prepared by the aldol condensation reaction of 9-oxofluorene-2-carboxaldehyde with 4-diphenylaminoacetophenone. This was followed by recrystallization to produce compound (175) in 35% yield. The product (176) was synthesized by the reaction of compound (175) with nitromethane and this was followed by an aqueous work-up and recrystallization. Product (176) was obtained in a 38% yield. Both products (175) and (176) were characterized via ^1H NMR and mass spectrometry. Attempted syntheses of fluorenone-triphenylamine-substituted aza-dipyrromethene (FN-TPA-aza-DIPY) (177) was carried out by reacting compound (176) with ammonium acetate or ammonium formate under various reaction conditions, but the starting materials remained unchanged with no observed reaction. The reactions were followed up by TLC and mass spectrometry.

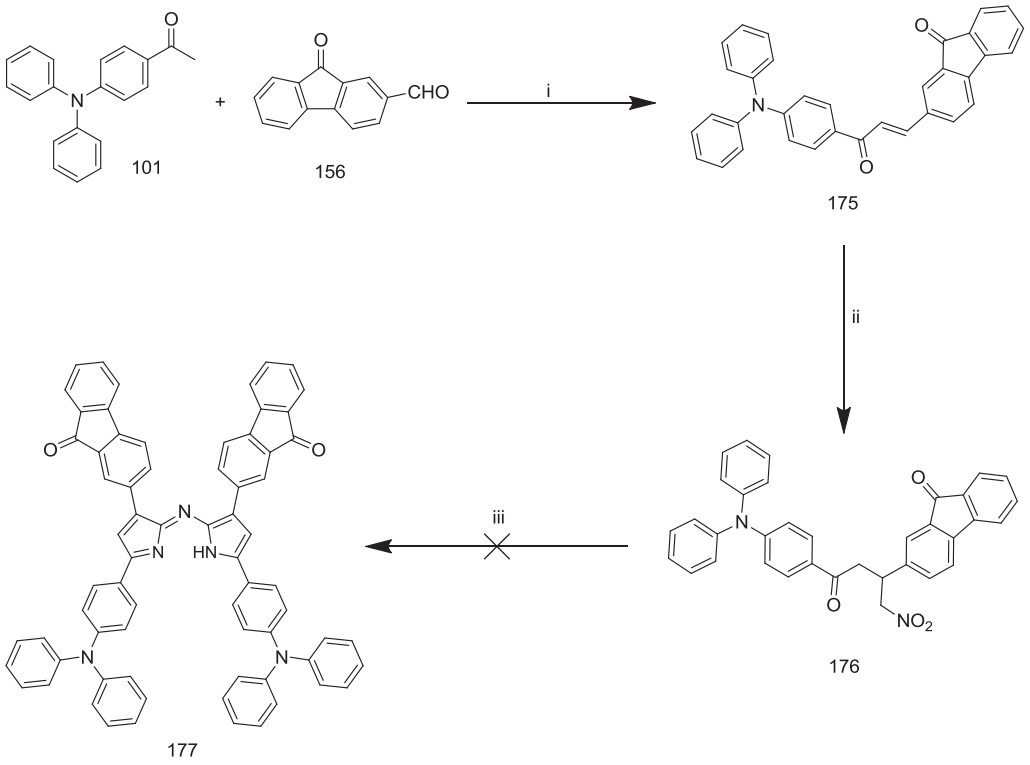

Figure 2.60 Attempted synthesis of fluorenone-triphenylamine-substituted aza-dipyrromethene (FN-TPA-aza-DIPY) (177). Reagents and conditions: (i) KOH, EtOH/H_2O. (ii) CH_3NO_2, DEA, MeOH, reflux, 24h.(iii) NH_4HCO_2/EtOH, reflux, 24h.

2.27 Attempted Synthesis of Terthiophene-Fluorenone-Substituted BF_2-Aza-dipyrromethene (TT-FN-aza-BODIPY).

In the light of the interesting absorption and emission properties of the terthiophene-based aza-BODIPYs (Sections (2.5) and (2.6)) as well as the effective platform fluorenone-based aza-BODIPYs (Sections (2.21) and (2.22)), a mixed terthiophene-fluoreneone based aza-BODIPY was designed. Terthiophene and fluorenone units were placed at positions 1 and 7 and 3 and 5 respectively on an aza-BODIPY core ((152) in Fig. (2.55)). The synthesis of the first intermediate compound (178) was a straightforward step via using the same aldol condensation procedure mentioned previously. Purification was carried out by recrystallization to give a yield of 47%. The second intermediate compound (179) was synthesized by the reaction of compound (178) with nitromethane; this was followed by

purification by column chromatography to give a yield of 40%. Fig (2.61) shows the synthetic routes for the intermediate compounds (178) and (179).

Both compounds (178) and (179) had limited solubilities in alcohol solvents. The important step would be the synthesis of the terthiophene-fluorenone-substituted aza-dipyrromethene (TT-FN-aza-DIPY (180)). Two solvents and two ammonium sources were tested. The first two reactions were carried out using ethanol as solvent with either ammonium acetate (reaction no. 1) or ammonium formate (reaction no. 2). The last two reactions were also carried out using n-butanol as solvent with either ammonium acetate (reaction no. 3) or ammonium formate (reaction no. 4). For reactions 1 and 2, the starting materials persisted without the observed product appearing. The mass spectrum of the crude mixture of reaction 3 and 4 suggested the presence of TT-FN-aza-DIPY. ^{1}H NMR characterization was not possible because of isolation and separation difficulties related to solubility issues. No further characterization has been done for compound (180).

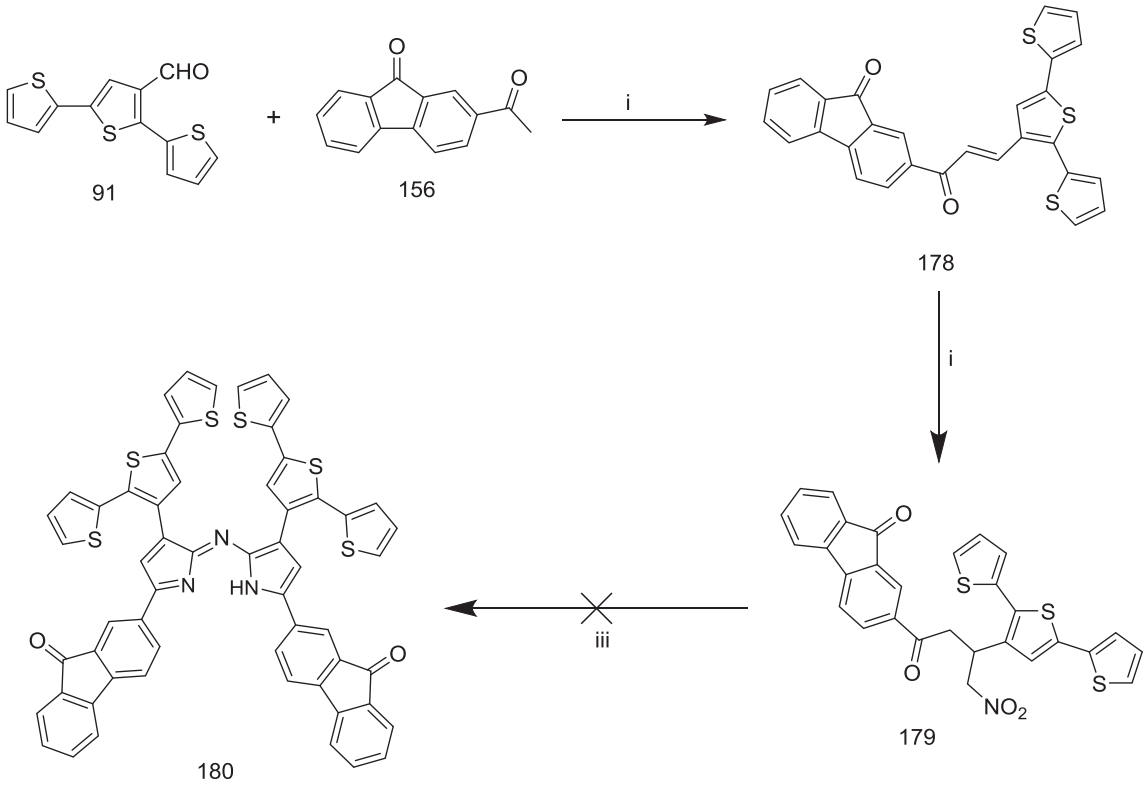

Figure 2.61 Synthesis of intermediate compound (178) and (179). Reagents and conditions: (i) KOH, EtOH/H_2O. (ii) CH_3NO_2, DEA, MeOH, reflux, 24h.(iii) NH_4HCO_2/*n*-BuOH, reflux, 24h.

2.28 Attempted Synthesis of Phenothiazine-Substituted BF_2-Aza-dipyrromethene (PTZ-aza-BODIPY)

The phenothiazine-based aza-BODIPY (131) (Fig. 2.55) incorporated phenothiazine units in positions 3 and 5, and phenyl groups at positions 1 and 7. The attempted synthesis of this target phenothiazine-substituted BF_2-aza-dipyrromethene (PTZ-aza-BODIPY) is discussed here. The reason behind wishing to incorporate phenothiazine units was their nature as electron-rich molecules, which should provide an excellent relay for the electron migration from the donor to the aza-BODIPY core. The orientation of the two phenyl groups of phenothiazine is nearly co-planar with the aza-BODIPY core, therefore the π-delocalization should be extended over the entire molecule. Compound (181) was synthesized by the reaction of 2-acetylphenothiazine with acetaldehyde. The product was isolated and purified to give a 35% yield. This product (181) was reacted with nitromethane via a base-mediated Michael-addition reaction. The starting materials persisted; no reaction was observed. TLC and mass spectrometry were used to monitor this reaction. Fig. (2.62) shows the intended synthetic route.

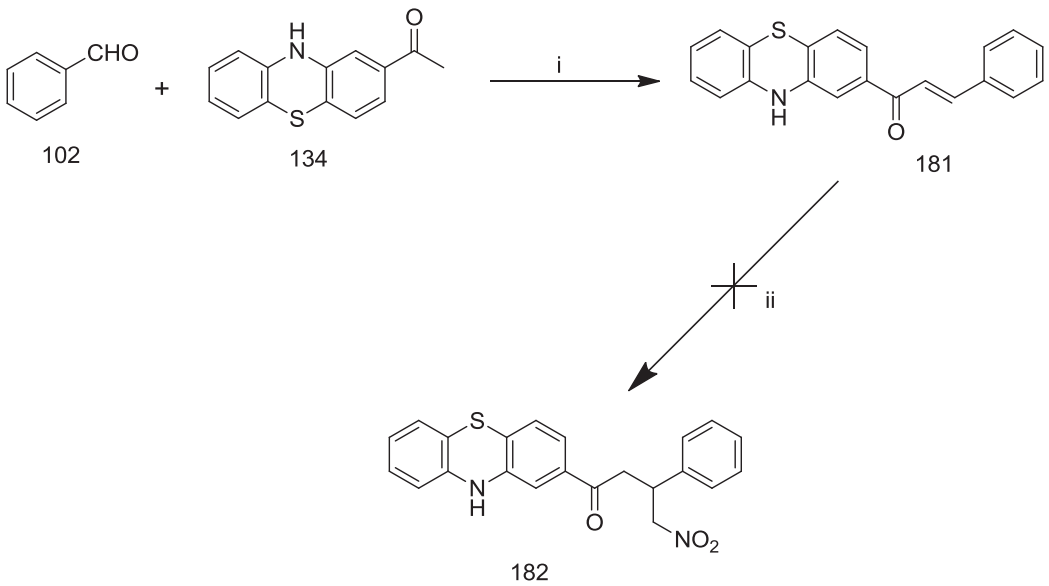

Figure 2.62 Synthesis of intermediate compounds (181) and (182). Reagents and conditions: (i) KOH, EtOH/H_2O. (ii) CH_3NO_2, DEA, MeOH, reflux, 24h.

2.29 Attempted Synthesis of Fluorenone-Phenothiazine-Substituted BF_2-Aza-dipyrromethene (FN-PTZ-aza-BODIPY)

The use of phenothiazine units to promote the electron-donating ability of a molecule, as well as the π-conjugated fluorenone units that exhibited an extended absorption band in the visible part of the spectrum, prompted the design of a new aza-BODIPY based on fluorenone and phenothiazine units. The target fluorenone-phenothiazine-substituted BF_2-aza-dipyrromethene (FN-PTZ-aza-BODIPY) (133) (Fig. 2.55) has fluorenone units at position 1 and 7, and phenothiazine units located at positions 3 and 5. The reaction of 2-acetylphenothiazine (134) with 9-oxofluorene-2-carboxaldehyde (156) was carried out using the standard aldol condensation procedure mentioned previously. Mass spectrometry was used along with TLC to follow the reaction. The starting materials persisted without any observed reaction. The target structure and the intended synthetic route are shown in Fig. (2.63).

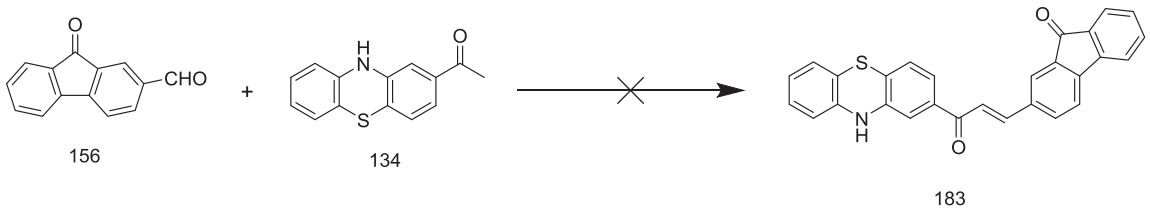

Figure 2.63 The attempted synthesis of compound (183). Reagents and conditions: KOH, EtOH/H_2O.

2.30 Attempted Synthesis of Methylpyrrole-Substituted BF_2-Aza-dipyrromethene (MPy-aza-BODIPY)

Pyrrole derivatives are well known for their interesting properties as donor molecules in charge transfer complexes (CT). The synthesis of a new aza-BODPY based on thiophene and methylpyrrole units was discussed in Section (2.18). A synthesis of methylpyrrole-based aza-BODIPY was attempted. Methylpyrrole units were to be incorporated in positions 3 and 5, while positions 1 and 7 were to be occupied by phenyl groups to give compound (138) (Fig. 2.55). The synthesis of the intermediate compound (184) was successful via the standard condensation reaction of acetaldehyde (102) with 2-acetyl-1-

methylpyrrole (141) in the presence of a base (KOH). The product (184) was purified by recrystallization to give a yield of 40%. Characterizations were carried out via ^1H NMR and mass spectrometry to confirm the structure of compound (184). The addition reaction of compound (184) to nitromethane was performed under standard conditions. The reactions were monitored by TLC and mass spectrometry. It was found that the starting materials persisted; no reaction was observed. Fig. (2.64) shows the attempted synthetic route.

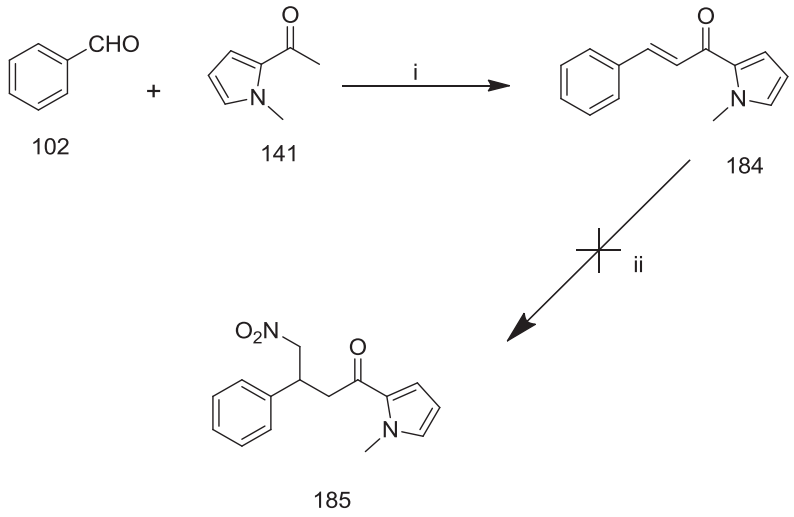

102 141 184 185

Figure 2.64 Synthesis of intermediate compound (184) and the attempted synthesis of compound (185). Reagents and conditions: (i) KOH, $EtOH/H_2O$. (ii) CH_3NO_2, DEA, MeOH, reflux, 24h.

2.31 Attempted Synthesis of Fluorenone-Methylpyrrole-Substituted BF_2-Aza-dipyrromethene (FN-MPy-aza-BODIPY)

As mentioned previously, fluorenone and methylpyrrole units are interesting platforms for the synthesis of donor molecules for bulk heterojunction solar cells. The design of the fluorenone-methylpyrrole-substituted BF_2-aza-dipyrromethene (FN-MPy-aza-BODIPY) (140) (Fig. 2.55) involved fluorenone units at positions 1 and 7, as well as methylpyrrole units at positions 3 and 5. The aldol condensation of 9-oxofluorenone-2-carboxaldehyde (156) with 2-acetyl-1-methylpyrrole (144) was carried out under standard conditions. The reaction was monitored by TLC and mass spectrometry. Both starting materials persisted

without any indication of a product. Fig. (2.65) shows the attempted synthesis of compound (186).

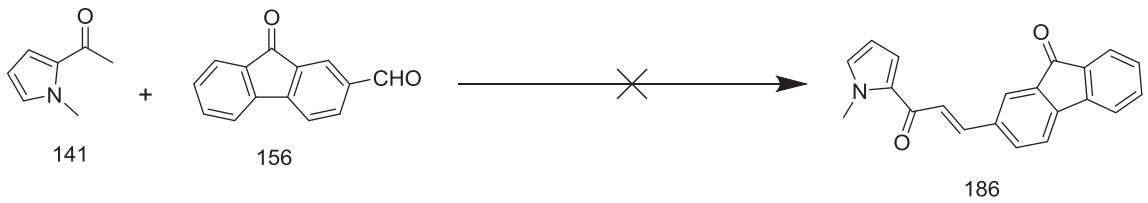

141 156 186

Figure 2.65 The attempted synthesis of compound (186). Reagents and conditions: KOH, EtOH/H_2O.

2.32 Attempted Synthesis of Ethylenedioxythiophene-Thiophene-Substituted BF_2-Aza-dipyrromethene (EDOT-T-aza-BODIPY)

Interesting strong electron-donor properties, as well as a self-organizational ability have been found in 3,4-ethylenedioxythiophene (EDOT). Incorporation of these units (EDOT) in a aza-BODIPY structure (as described in Section (2.13)) could potentially show promising donor materials based on EDOT-aza-BODIPY. A new design of aza-BODIPY 163 incorporated EDOT units at positions 1 and 7, while positions 3 and 5 were occupied by thiophene molecules. Thiophene derivatives are well known for their electron donor properties and most of the aza-BODIPYs in this Chapter which have incorporated them have shown absorption at longer wavelengths. The first step towards the target EDOT-T-aza-BODIPY (163) was the synthesis of compound (187) via the aldol condensation of 3,4-ethylenedioxythiophene-2-carbaldehyde with 2-acetylthiophene in the presence of potassium hydroxide. The product (187) was successfully isolated and purified in 15% yield. A base-mediated reaction of compound (187) with nitromethane was carried out to produce compound (188) in 9% yield. Compound (188) was purified using column chromatography via alumina. All reactions were carried out under a controlled atmosphere of argon gas. Attempts to synthesise compound (189) were carried out in either ethanol or n-butanol solvents by using ammonium acetate or ammonium formate as an ammonium source. These reactions were performed with extra care due to the air-sensitive nature of the intermediate compounds. For all of the attempted syntheses, the starting materials persisted

with no observed reaction. Mass spectrometry and TLC were used to monitor the reaction. Compounds (187) and (188) were characterized using ^1H NMR and mass spectrometry. Fig. (2.66) shows the synthetic route attempted for EDOT-T-aza-DIPY (189).

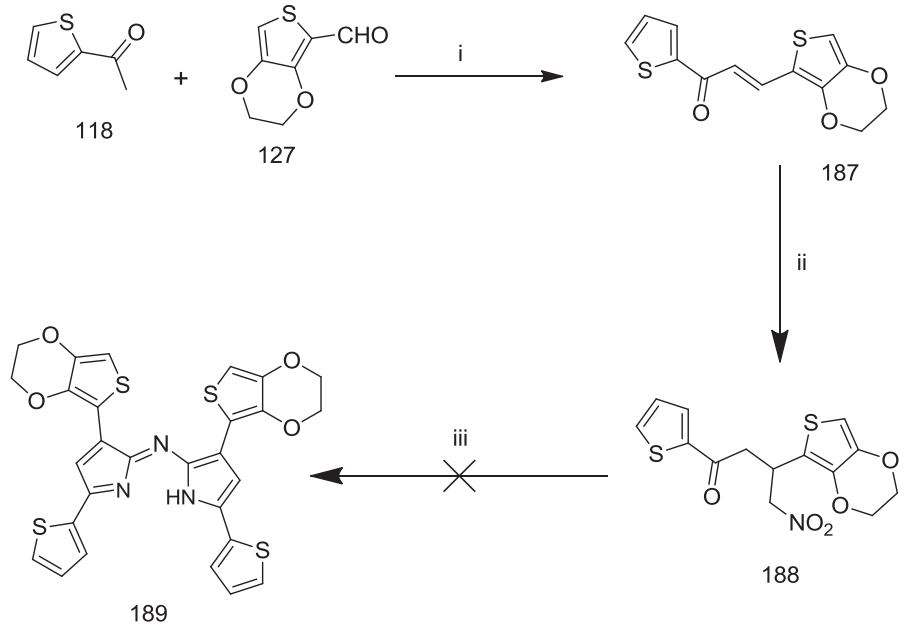

Figure 2.66 Synthesis of intermediate compound (187) and the attempted synthesis of compound (189). Reagents and conditions: (i) KOH, EtOH/H_2O. (ii) CH_3NO_2, DEA, MeOH, reflux, 24h. (iii) NH_4HCO_2/*n*-BuOH, reflux, 24h.

2.33 Synthesis of *β'*-Substituted Terthiophene Monomers

In this section, the syntheses of four new *β'*-substituted terthiophene monomers (TT1, TT2, TT3, and TT4) are described briefly. The structures of these terthiophene monomers are shown in Fig. (2.67). These new functionalized terthiophene monomers were designed for binding and polymerization on the surface of silicon quantum dots. The syntheses of silicon quantum dots and the chemical reactions that have been carried out on their surface are discussed in Section (2.35).

The key building blocks are 3'-formylterthiophene derivatives which were synthesized by Suzuki coupling of aromatic halides with aryl boronic acids, and used to prepare the

functionalized *β'*-substituted terthiophenes. Wittig reactions between 3'-formylterthiophene derivatives and ylides, derived from various phosphonium salts, gave four new *β'*-substituted terthiophenes (TT1, TT2, TT3, and TT4). These compounds were characterized using mass spectrometry and ^{1}H NMR.

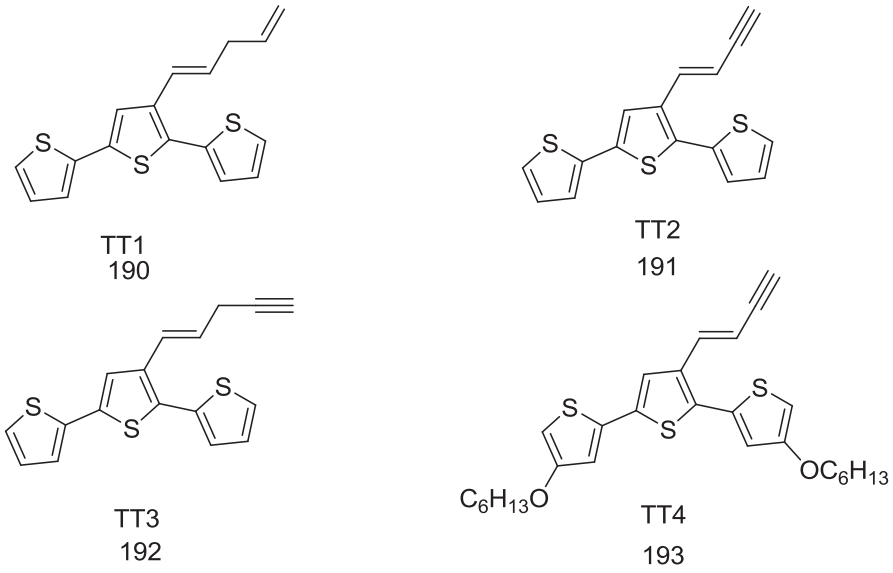

Figure 2.67 The structures of *β'*-substituted terthiophenes

2.33.1 Synthesis of Starting Materials: 3'-Formylterthiophene Derivatives

The first step towards the synthesis of the target molecules was the synthesis of the key building blocks: 3'-formylterthiophene and the alkoxy-chain substituted 3'-formylterthiophene, as depicted in Fig. (2.68). These materials were synthesized using standard procedures via Suzuki and Wittig chemistries.[76-78] 3'-formylterthiophene (91) was synthesized in 70% yield. An attempt to improve the solubility of the terthiophenes was made by attaching alkoxy groups at the β-positions in terthiophene. An alkoxy-chain substituted 3'-formylterthiophene was synthesized via the reaction of 2,5-dibromo-3-thiophenecarboxaldehyde (196) and 4-hexyloxy-2-thienyl boronic acid (200) in the presence of the tetrakis(triphenylphosphine)palladium catalyst. A yellow-orange solid containing the alkoxy-chain substituted 3'-formylterthiophene (201) was isolated in 65 % yield after column chromatography. Introducing alkoxy groups into 3'-formylterthiophene

enhanced the solubility of this material in most solvents. Furthermore, it was separated easily by column chromatography in a good yield (65%).

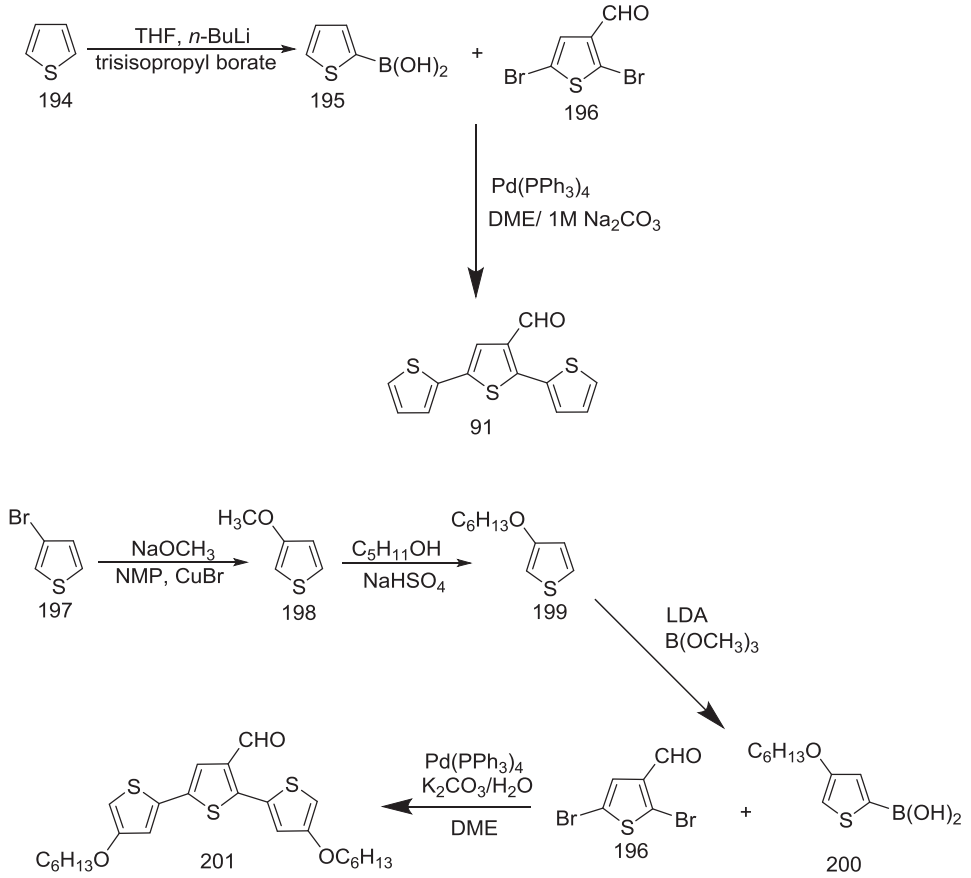

Figure 2.68 Synthesis of 3'-formylterthiophene starting materials. NMP is N-methyl-2-pyrrolidone, DME is dimethyl ether and LDA is lithium diisopropylamide.

2.33.2 Synthesis of Intermediate Compounds (205), (208) and (211)

Bromination of propargyl alcohol (202), butynyl alcohol (206), and butenyl alcohol (209) have been carried out according to the literature.[79] The appropriate alcohol was reacted with triphenylphosphite dibromide under mild conditions to give, after distillation in vacuo and condensation in a cold trap, the appropriate bromo derivative. Fractionation gave the pure products (propargyl bromide 66%, butynyl bromide 65%, and butenyl bromide 68%), as depicted in Fig. (2.69).

The appropriate phosphonium salts were prepared by refluxing triphenylphosphine in dry tetrahydrofuran (THF). After the reaction mixture became homogeneous, the appropriate

bromide was added. Recrystallization gave the appropriate phosphonium salts (47%, 32%, and 35% yield of (205), (208) and (211) respectively) as white crystals.

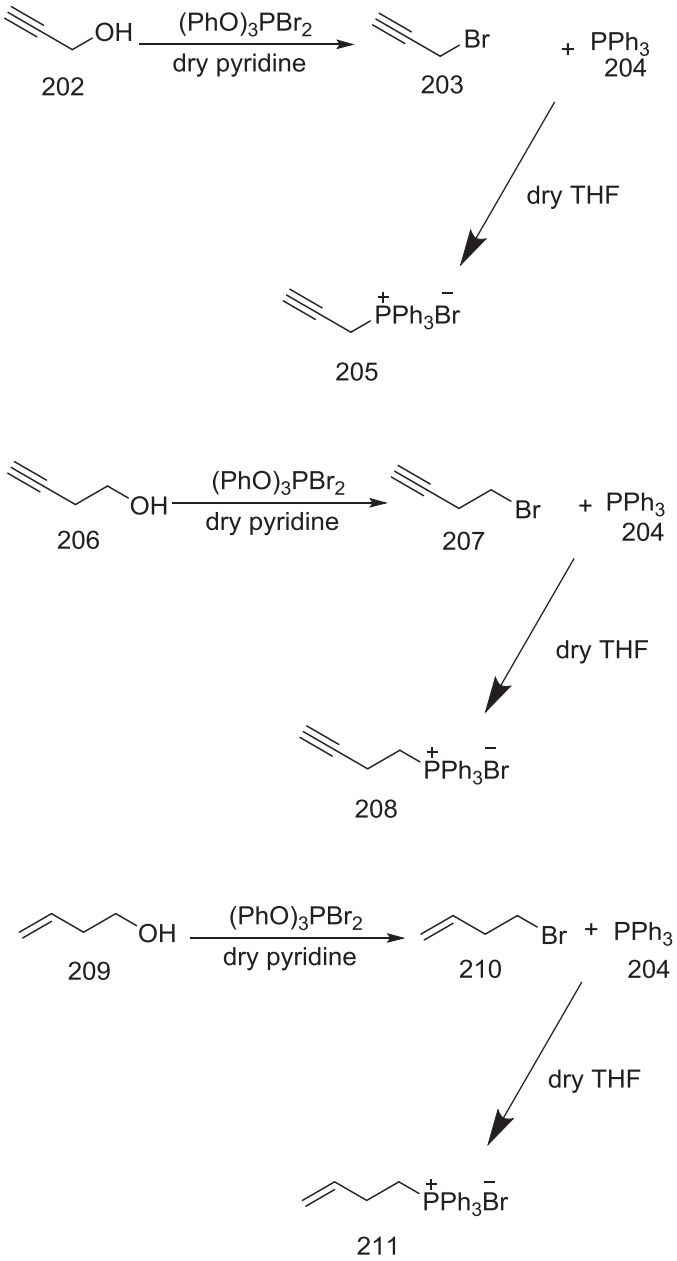

Figure 2.69 Synthesis of intermediate compounds: bromo derivatives (compounds (203), (207), and (210)) and phosphonium salt derivatives (compounds (205), (208), and (211)).

2.33.3 Synthesis of *β*'-Substituted Terthiophene Monomers

Syntheses of β'-substituted terthiophene monomers have been carried out using 1,8-diazabicycloundec-7-ene (DBU) as a catalyst under standard conditions. The solvent was evaporated from the reaction mixture. The resultant crude mixture was then purified by column chromatography to give the appropriate β'-substituted terthiophenes in yields of 65%, 52%, 48%, and 67% for (191), (192), (190), and (193) respectively, as depicted in Fig. (2.70).

Wittig chemistry is an important method for the synthesis of terthiophene derivatives. As described in Section (2.33.2), phosphonium salts have been prepared by treatment of triphenylphosphine with alkyl or alkenyl halides. A Wittig reagent (ylid) has been synthesized from the appropriate phosphonium salt by suspending it in THF followed by treatment with a non-nucleophilic base (DBU). Characterization of the β'-substituted terthiophene compounds was carried out with mass spectrometry and ^{1}H NMR.

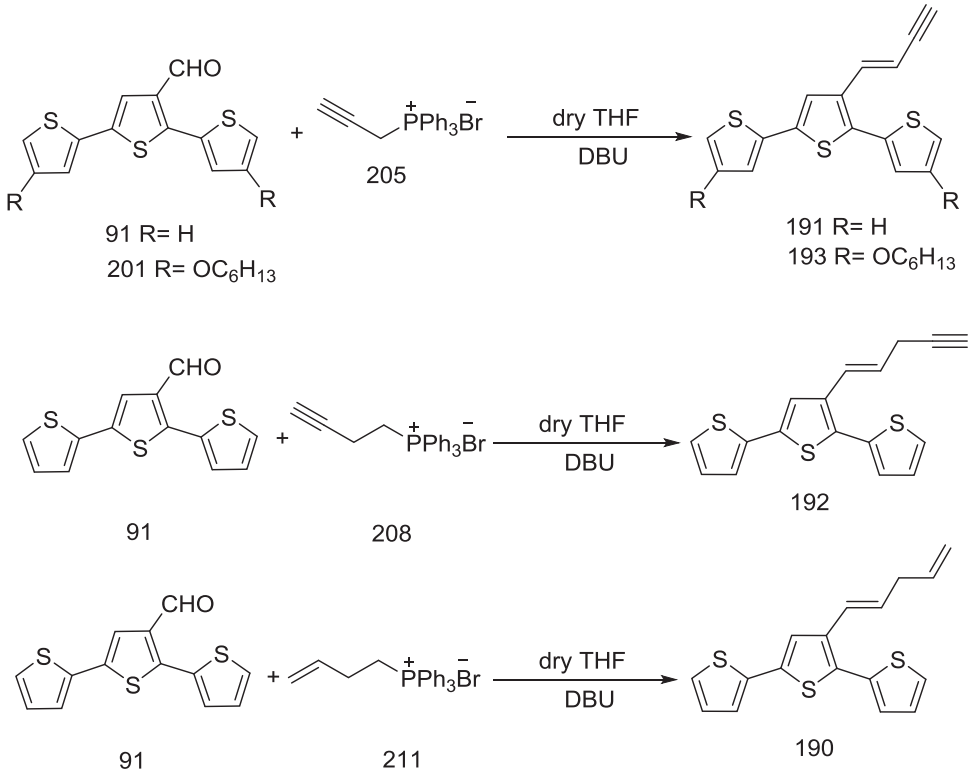

Figure 2.70 Synthetic routes of the functionalized *β*'-substituted terthiophene; (190), (191), (192) and (193).

The proposed mechanism of this reaction is shown in Figure (2.71). The nucleophilic addition of the ylid C to the electrophilic C in the polar carbonyl group in 3'-formylterthiophene forms a σ bond. Oxaphosphetane will be formed as a cyclic intermediate. The formation of the C=C π bond in the alkene and triphenyl phosphine oxide is achieved by breaking the C-P and C-O σ bonds in oxaphosphetane. [80] Attachment of unsaturated terminal groups within terthiophene should make this molecule capable of binding to quantum dots.

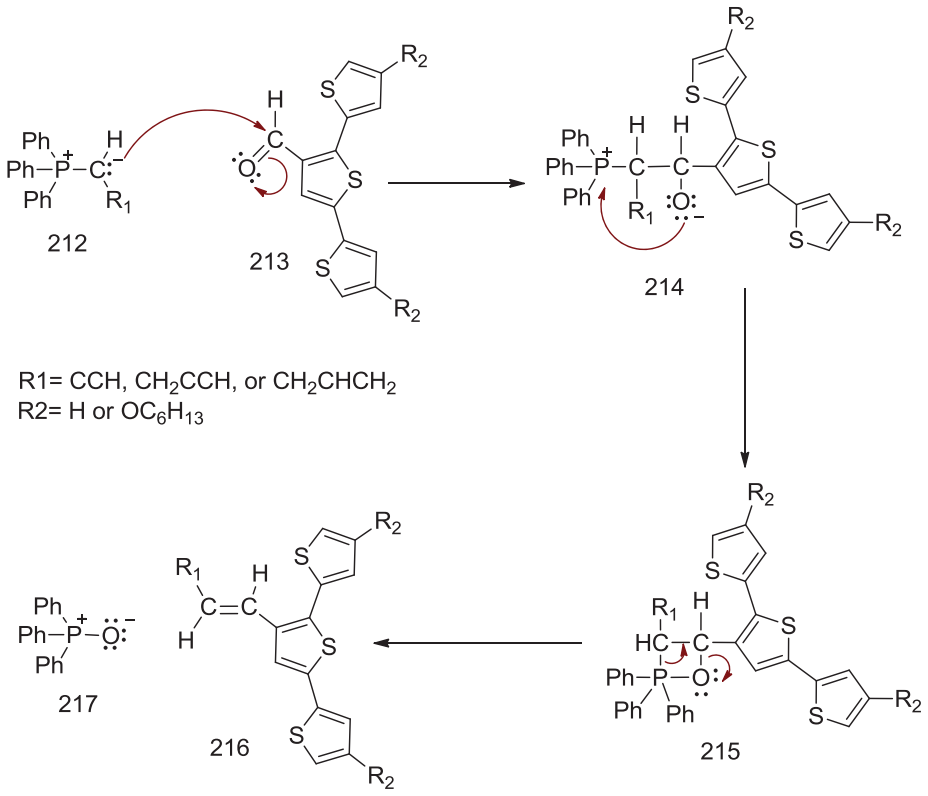

Figure 2.71 The proposed mechanism of the Wittig reaction for the formation of terthiophene derivatives (derived from the general mechanism of a Wittig reaction).

2.34 Synthesis of Ruthenium Complexes

Ruthenium complexes show an intense charge transfer band from metal to ligand in the visible spectrum. The most used Ru-complex in a dye-sensitized solar cell (DSSC) is the N3 dye (compound (222)), whose structure is shown in Fig. (2.72). This dye has two thiocyanate ligands and additional carboxylic acid groups as anchoring sites. The N3 dye has been known as a reference dye in DSSC, and its power conversion efficiency value in DSSCs was originally about 10% but this has been slightly improved since then.[81-85] Many attempts have made to tune up the electronic and optical properties of N3 dye by exchanging the bipyridyl ligands. Our intended approach was to attach Si-quantum dots (QDs) to one of the bipyridyl ligands in the N3 dye through the reaction of amine-terminated Si-QDs with the carboxylic acid groups on the bipyridyl ligand. Fig. (2.72) and Fig. (2.73) show the synthesis of standard ruthenium complexes and the proposed synthesis route of Ru-dye-Si-QDs. Ruthenium complexes having free carboxylic acid groups and phosphonic acid on bipyridyl units were synthesized using standard procedures.[86-89] The reaction of amine-terminated silicon quantum dots (QDs) with ruthenium complexes was carried out under standard conditions.

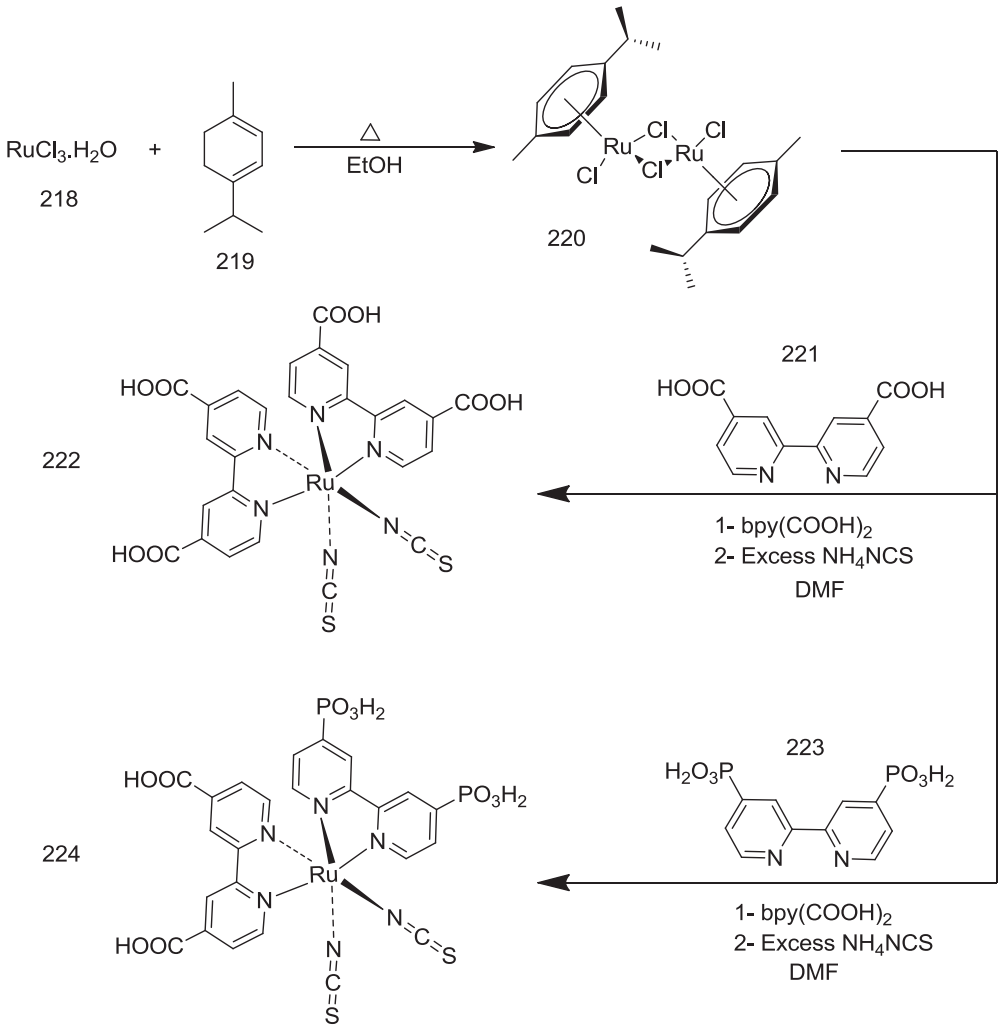

Figure 2.72 The syntheses of the standard ruthenium N3 dyes (222) and (224)

2.35 Synthesis of Silicon Quantum Dots and their Surface Modification

Quantum dots (QDs) are semiconductors (also called nano-crystals), in which excitons are confined in all three spatial dimensions. The confinement is realized by fabricating the semiconductor in very small size, usually several hundred to thousands of atoms per particle.[90] Quantum dots have unique electronic properties and show interesting phenomena such as narrow emission peaks, broad excitation ranges and size-dependent emission wavelengths. Quantum dots are intermediate between the bulk semiconductors and discrete molecules. The unique optical and electronic properties of the quantum dots are due to the quantum effects that appear at the nanoscale. These interesting characteristics have found many applications such as photovoltaics, photosensors, lasers and medical and biological fluorescent-imaging.[90-97]

Si-QDs were prepared by microemulsion synthesis at room temperature.[98] Fig. (2.73) shows the proposed plan for the modification of the surfaces of silicon quantum dots. Water-soluble silicon quantum dots were synthesized at room temperature by using hydride reducing-agents to produce hydrogen capped silicon quantum dots. These quantum dots showed a strong blue emission. Silicon quantum dots (Si-QDs) were characterized using energy dispersive spectrometry (EDS) and transmission electron microscopy (TEM). The purification of Si-QDs was carried out by liquid-phase separation and column chromatography. The purpose behind the modification of Si-QDs surface with thiophene derivatives was to allow Si-QDs to be used in photovoltaic applications. Only a few investigations of capped Si-QDs with small molecules, such as 1-heptene, acrylic acid and propionic acid had been carried out previously.[99-101]

The surfaces of Si-QDs can be modified by reacting the Si-H bond (on Si-QDs surface) with a compound having a double bond via a platinum catalyst to form a Si-C bond, as shown through route a and b in Fig. (2.73). In route b, allylamine-capped Si-QDs are synthesized. Allylamine-capped Si-QDs were fully characterized using ^{1}H NMR and transmission electron microscopy (TEM) (a TEM image is shown in Fig. (2.74)). Allylamine was used to protect the silicon particles from oxidation and provide a functional group to allow Si-QDs to be covalently bound to carbon- or oxygen-containing molecules.

In route a, synthesis of terthiophene capped Si-QDs through the reaction of the functionalized β'-substituted terthiophene monomers was envisaged (as synthesized in Section (2.35)). The reaction did not lead to the desired product. Due to the limited supplies of the silicon quantum dots, further attempts to synthesize terthiophene capped Si-QDs were not made.

The synthesized allylamine-capped Si-QDs were reacted with ruthenium complexes to produced Dye-Si-QDs, as depicted in Fig. (2.73), route b. The preliminary results of the characterizations of the product dye-Si-QDs (compound (229)) confirmed that the reactions had succeeded, however the small quantities of each product limited further investigations. The limited supply of the starting material (Si-QDs) was the main obstacle to do any further studies.

The allylamine-capped Si-QDs were produced in the size range from 1.5 to 10 nm with an average diameter of 3.7 ± 0.9 nm. Analysis of the synthesized allylamine-capped Si-QDs using an energy dispersive spectrometer (EDS) showed a strong peak related to silicon. No platinum peaks were observed, which confirmed the purity of the quantum dots.

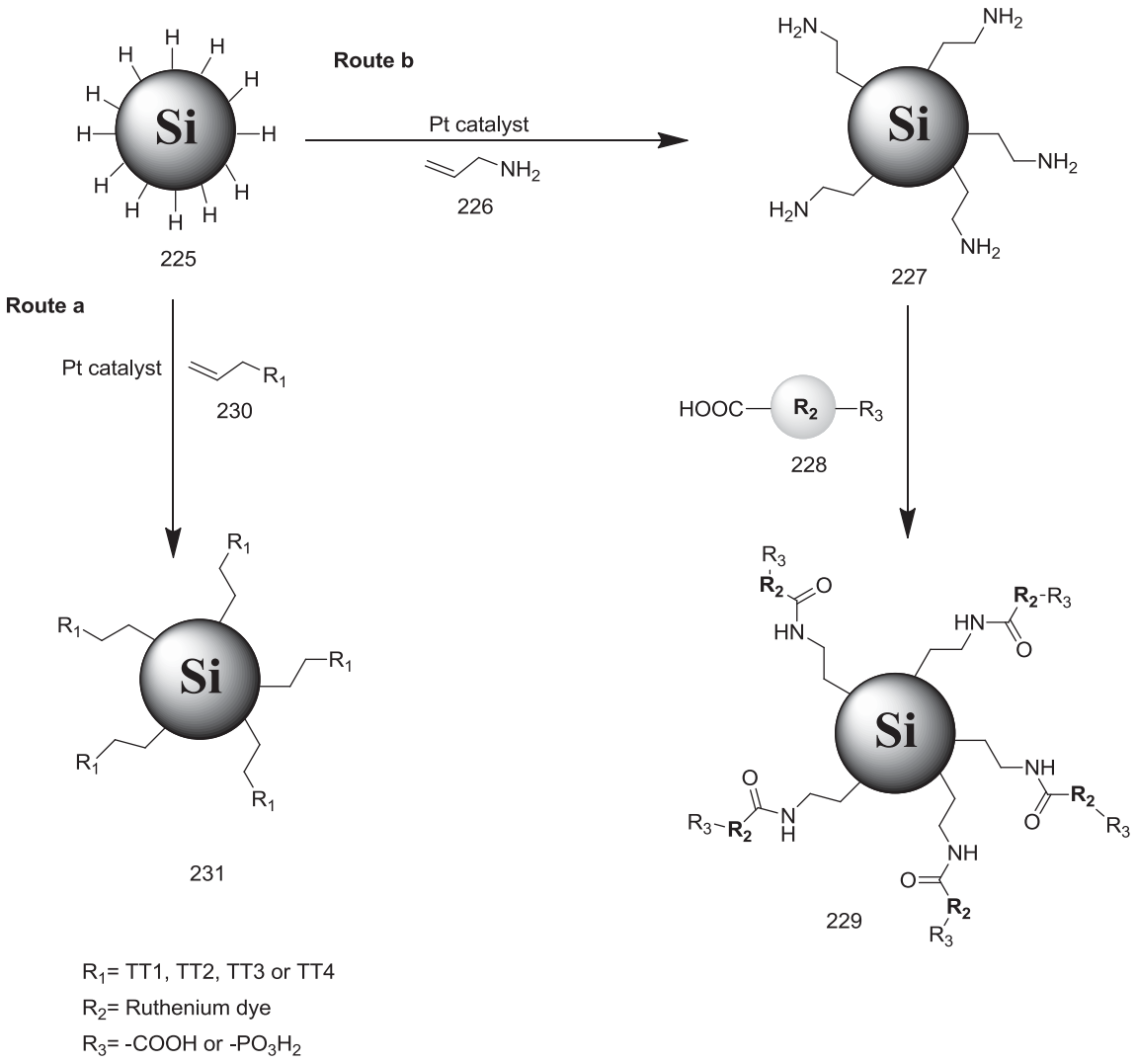

Figure 2.73 The proposed routes for modification of the silicon quantum dots.

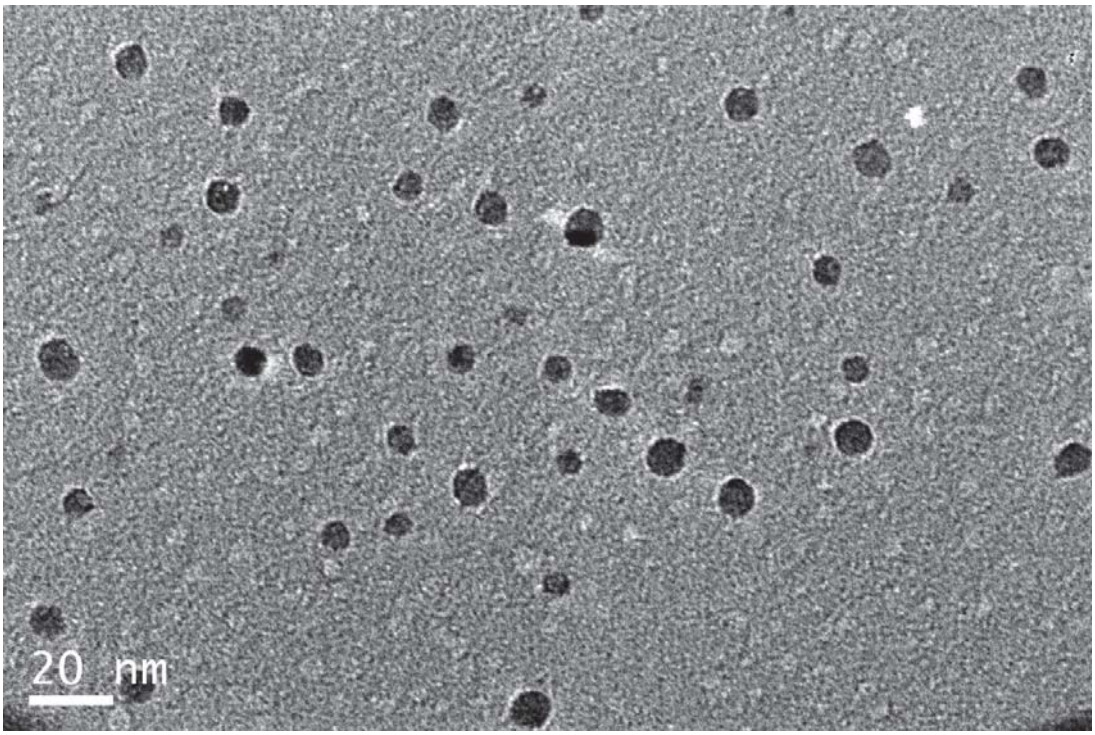

Figure 2.74 Transmission electron microscopy (TEM) image of amine-terminated silicon quantum dots.

2.36 Synthesis of BODIPY monomers as Building Blocks for Benzo-Dithiophene (BDT)-BODIPY Polymers

Numerous polymeric photovoltaic materials have been developed during the last few years for application in polymer solar-cells (PSCs). Benzo[1,2-b:4,5-b']dithiophene (BDT) has been one of the very important components of these polymeric materials.[102-110] Power conversion efficiency has reached 10% for BDT-based polymer solar-cells.[106] The strategy has been to tune the energy levels of BDT-based polymers, as well as the band gaps and absorption bands, by co-polymerizing BDT with different conjugated components and/or different functional side-groups. The energy levels and band gap of photovoltaic polymeric materials are the most important factors, and must be taken in consideration in order to achieve more highly efficient polymer solar-cells (PSCs). An improvement in the power conversion efficiency of PSCs has already been achieved by using low band-gap polymers.[110-112] In principle, the unique features of BODIPY dyes, such as the strong absorption and emission, tunable color characteristics and excellent photochemical and thermal stability, make them ideal components in co-polymers for application in polymer solar-cells. Some studies have been published where BODIPY-based polymers have been introduced to polymer solar-cell applications.[113-116]

The target was the synthesis of BODIPY monomers. The new thiophene-BODIPY monomer (compound (236)) was designed and successfully synthesized (see Fig. (2.75)). It was synthesized via[117] the condensation of 4-(3-thienyl)benzaldehyde (232) with 2,4-dimethylpyrrole (233) followed by coordination with the BF_3 etherate, and was readily obtained in a high yield. It was planned that the co-polymerization of this monomer with BDT would be carried out in a North America laboratory, but, due to unexpected difficulties, there has as yet been no progress. The synthesis of BODIPY monomers with ethyl and hexyl groups (Fig. 2.76) on the BODIPY core, which were intended to enhance its donor ability, was halted as the focus of the study shifted to the solution-processable small molecules based on aza-BODIPYs.

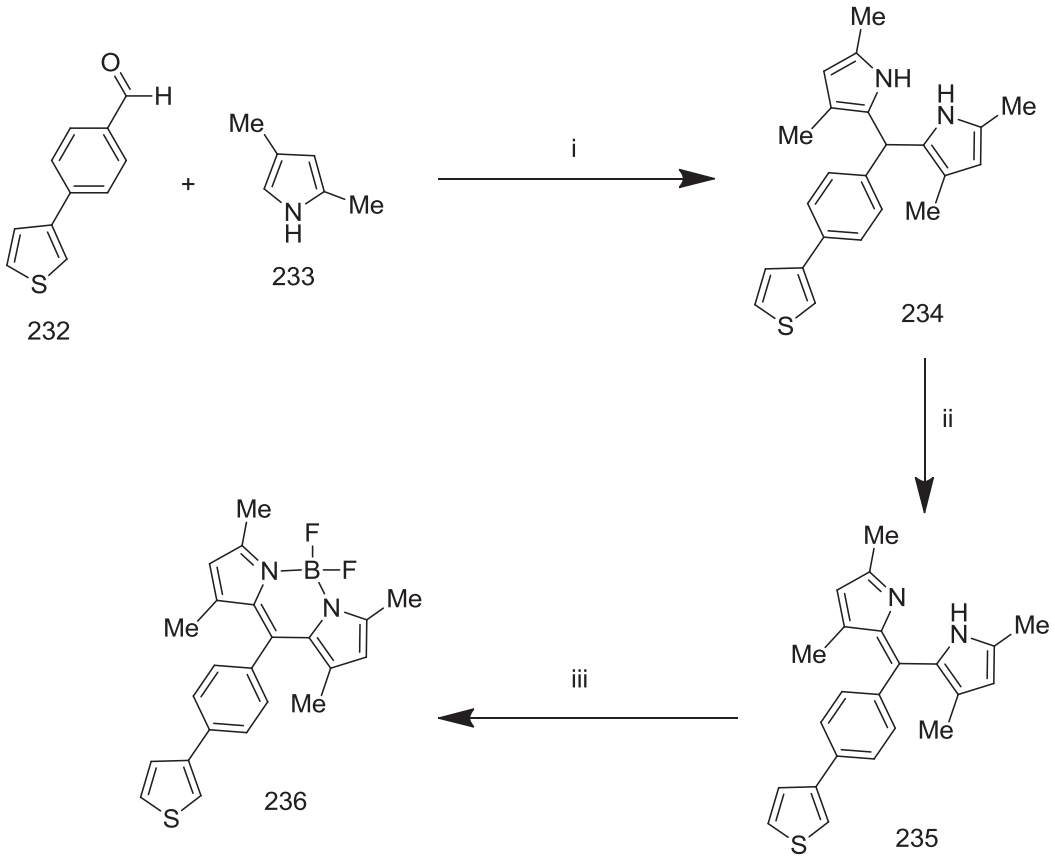

Figure 2.75 The proposed synthetic routes of thiophene-BODIPY based monomers. Reagents and conditions: (i) TFA, DCM. (ii) p-chloranil or DDQ, rt. (iii) DIEA, BF_3-OEt_2, DCM.

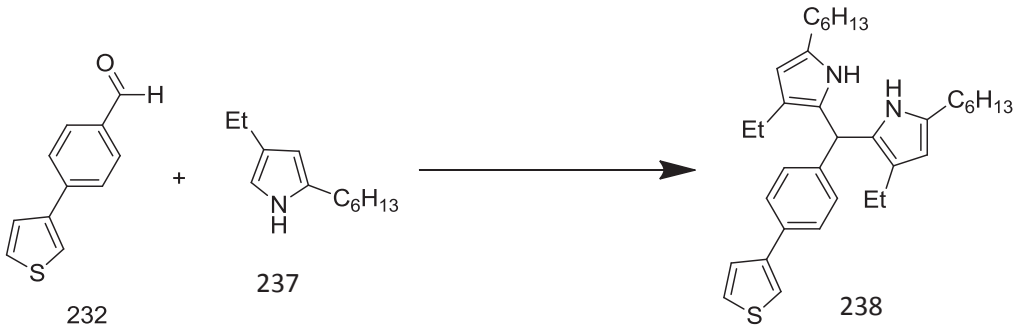

Figure 2.76 The proposed synthetic routes of thiophene-BODIPY based monomers. Reagents and conditions: TFA, DCM.

2.37 ^{1}H NMR and Mass Peaks Assignments

NMR Spectroscopy

The main characterization technique for the aza-BODIPY and thiophene compounds was ^{1}H NMR spectroscopy. Compound solutions of approximately 2 x 10^{-2} M in $CDCl_3$ or d_6-THF were prepared and ^{1}H NMR spectra were obtained on 400 or 500 MHz Brüker instruments using Topspin software. Chemical shifts given below are relative to tetramethylsilane (TMS) or the residual protium.

^{1}H NMR spectra are given for compounds (108), (109), (110), (106), (113), (112), (132) and (151) in Fig. (2.77), Fig. (2.79), Fig. (2.81), Fig. (2.83), Fig. (2.87), Fig. (2.91), Fig. (2.95) and Fig. (2.99) respectively, while the ^{13}C NMR spectra of compounds (106), (113), (112) and (132) are shown in Fig. (2.84), Fig. (2.88), Fig. (2.92) and Fig. (2.96) respectively.

The ^{1}H NMR spectra of the novel aza-BODIPYs synthesised in this study are perforce not available in the literature. Their ^{1}H NMR spectra are compared with those of compounds containing the same functional groups. The chemical shifts will differ, but the structures of the spectra should be similar.

The ^{1}H NMR spectrum of compound (106) (Fig. 2.83) showed a signal at 8.03 ppm, which corresponds to the four protons of the thiophene rings (H1, H19, H3 and H21), split into a doublet of triplets. The doublet of doublet signal at 7.93 ppm corresponds to the two protons of the thiophene rings (H2 and H20). These proton signals at 8.03 ppm and 7.93 ppm respectively are shifted slightly from the literature values (7.98 ppm and 7.48 ppm respectively) but still lie in the same range of the spectrum.[118] The usual signal of the two protons of the aza-BODIPY core (H4 and H22) is located at 7.00 ppm and it was a singlet as expected (nearly the same as in the literature 7.17 ppm).[119,120] The aromatic protons of the triphenyl amine (H5, H6, H7, H8, H9, H10, H11, H12, H13, H14, H15, H16, H17, H18, H23, H24, H25, H26, H27, H28, H29, H30, H31, H32, H33, H34, H35, H36) were located in between 7.07 ppm and 7.53 ppm (similar region to the one in literature of 7.00 ppm to 7.86 ppm).[121,122]

The multiplet signals of the protons of the benzothiadiazole unit in compound (112) (Fig. 2.91) (H1, H8, H2, H9, H3, H10) were located at 8.00 ppm as expected (nearly the same as the literature value of 8.11 ppm).[6] There was an interesting shift for the single signal of the two protons of the aza-BODIPY core (H4, H11) to 8.11 ppm in comparison to the literature (7.17 ppm).[119,123] The multiplet signals of the protons of the thiophene ring (H5, H12, H6, H13, H7, H14) at 7.69 ppm and 7.56 ppm were slightly shifted from the literature values (7.98 ppm and 7.48 ppm).[118]

The signals of the aromatic protons of the phenothiazine unit in compound (132) (H5, H17, H12, H24, H11, H23, H7, H19, H8, H20, H9, H21, H10, H22) were located in between 6.85 ppm and 6.56 ppm and were slightly shifted from the literature values (7.82 ppm and 6.84 ppm).[121,124] There was a shift for the single signal of the two protons of the aza-BODIPY core (H4 and H16) to 8.15 ppm from the literature (7.17 ppm).[119,123] The weak signal at 5.93 ppm corresponds to the two amine protons (H6 and H18) of the phenothiazine unit. The doublet of doublet signals at 7.20 ppm and 7.08 ppm corresponds to the protons of the thiophene rings (H1, H13, H3 and H15).

Mass Spectrometry

Mass spectrometry was used to support identification of the compounds. Molecular masses were obtained using a Waters Micromass time-of-flight instrument (MALDI) in the positive-ion mode. Mass spectra were obtained by matrix-assisted laser deposition ionization (MALDI) using either α-cyano-4-hydroxycinnamic acid (CHCA) or 2-(4'-hydroxybenzeneazo) benzoic acid (HABA) as a matrix.

The isotope distributions of the molecule ion $(M+H)^+$ for compounds (106), (112), (113), (132) and (151) have been calculated and compared with the experimental mass spectra as shown in Figs. (2.85), (2.86), (2.89), (2.90), (2.93), (2.94), (2.97) and (2.98) respectively. Good agreement has been found between the calculated and the experimental isotope distributions of molecule ion $(M+H)^+$ of compounds (106), (112) and (132). Compound (151) did not show the expected isotope distribution in its experimental mass spectrum. With compound (113), the monoisotopic peak was present in the experimental spectrum as expected, but the ^{13}C peaks appeared to have been influenced by an artifact. This comparison has been done at the School of Biological Sciences at the University of Auckland using Thermo Xcalibur © 2010 from Thermo Fisher Scientific Inc.

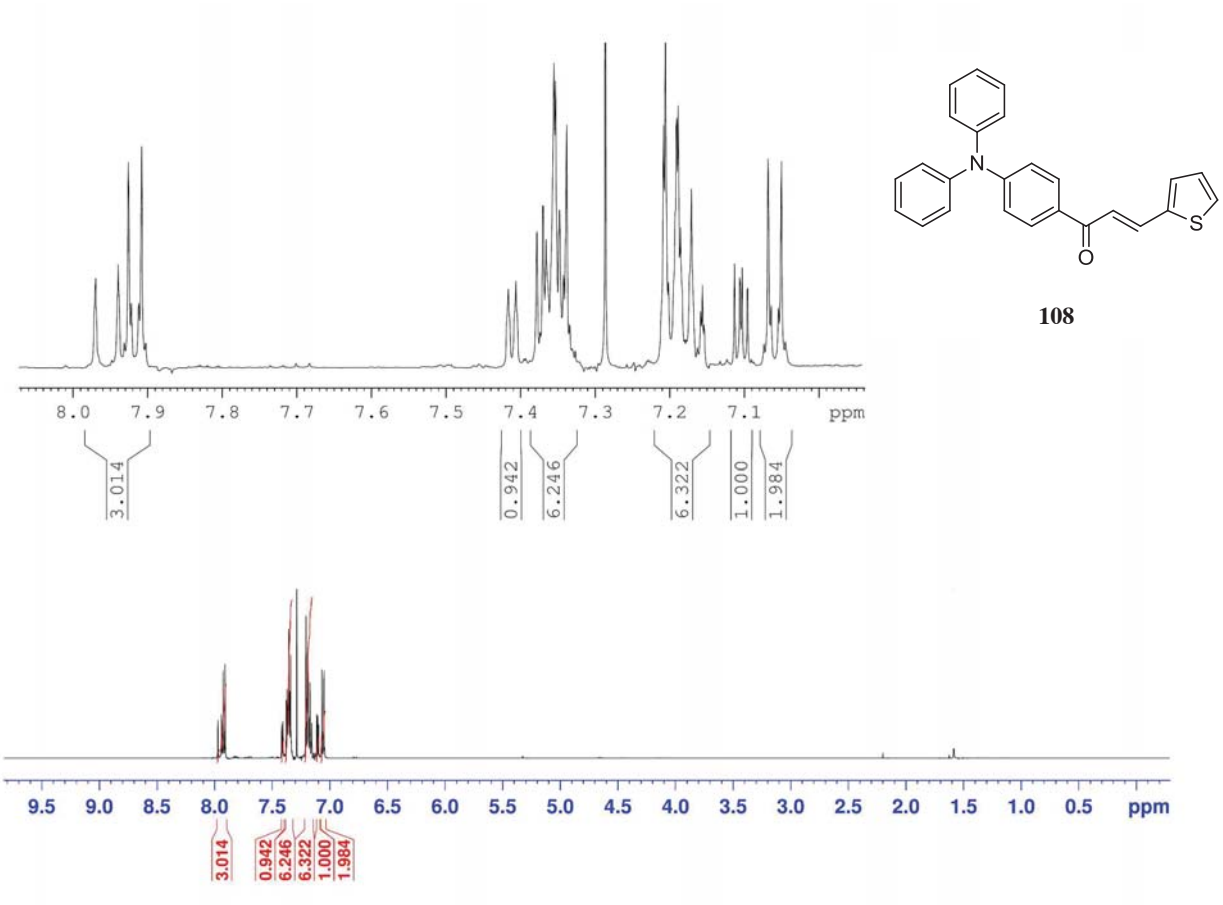

108

Figure 2.77 The ^{1}H NMR spectrum of compound (108)

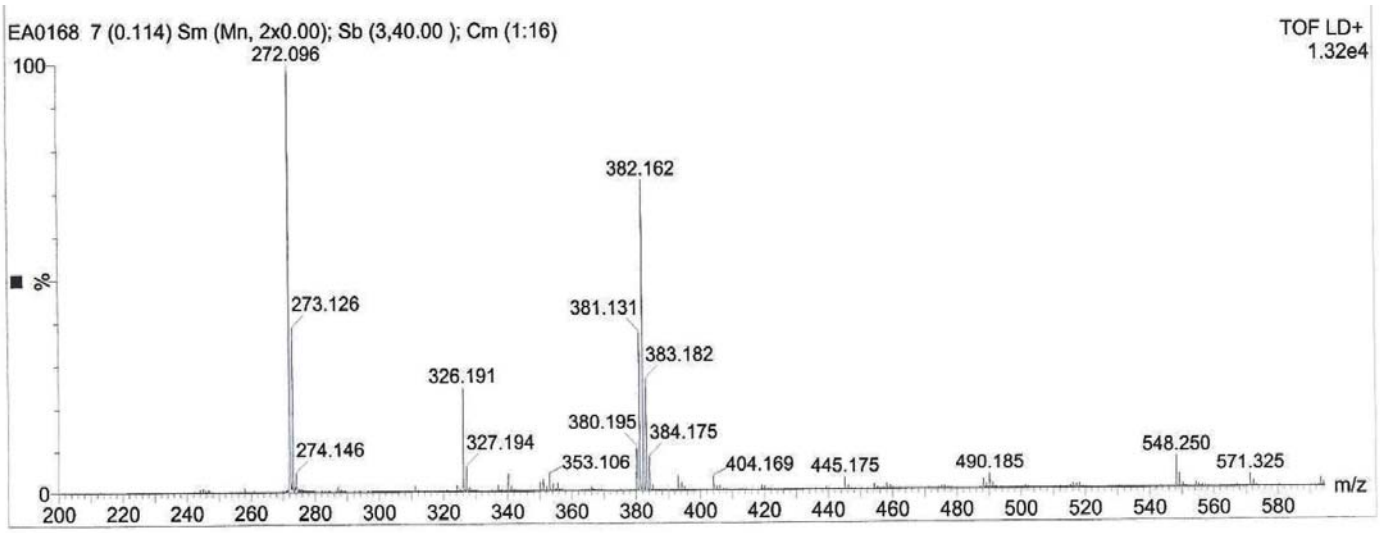

Figure 2.78 The mass spectrum of compound (108)

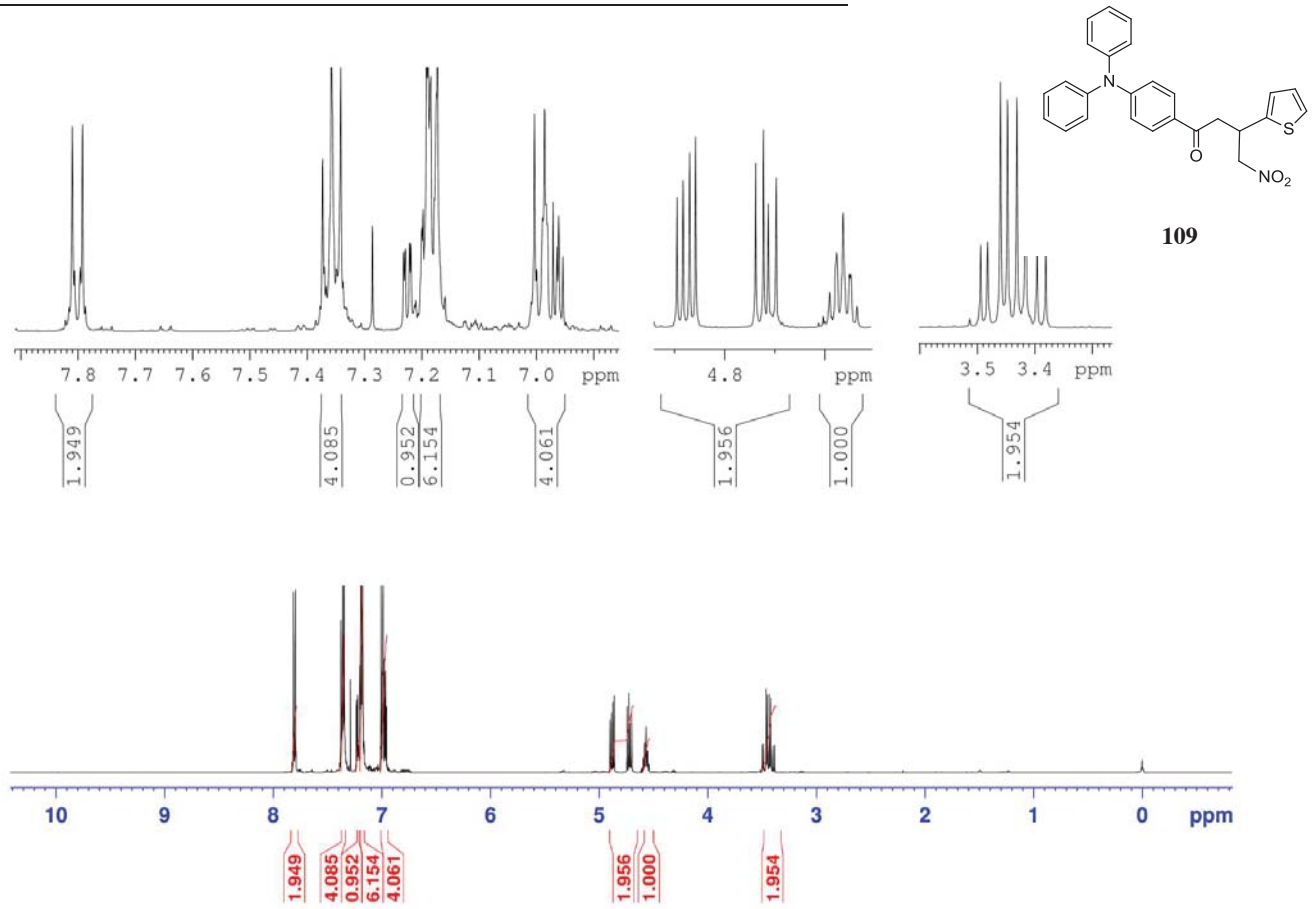

109

Figure 2.79 The ^{1}H NMR spectrum of compound (109)

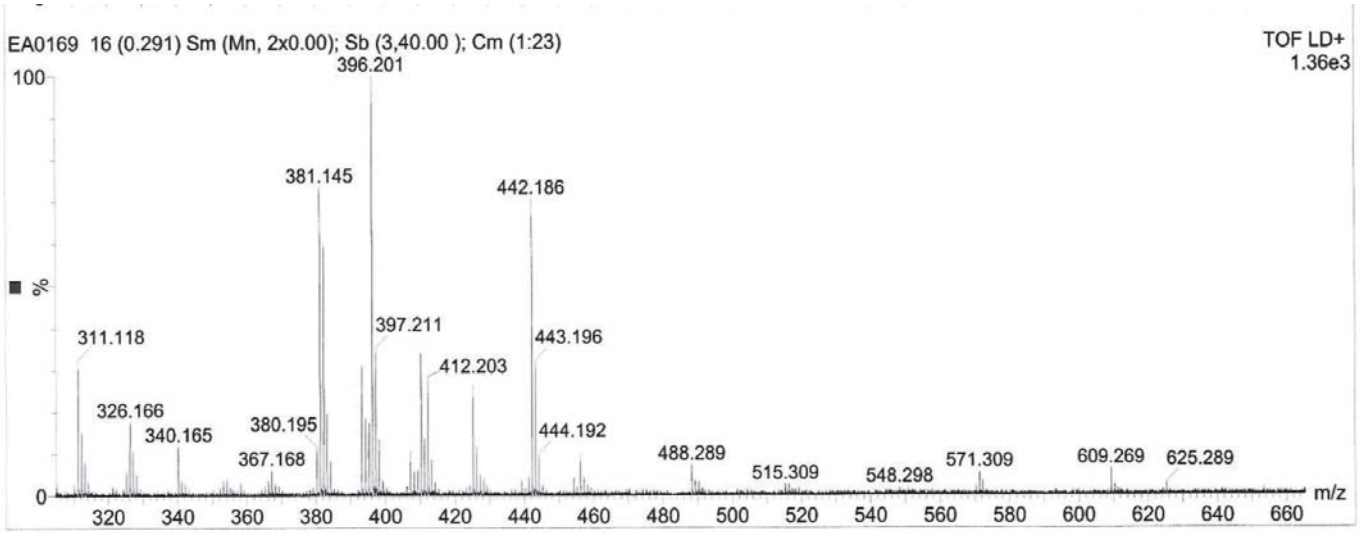

Figure 2.80 The mass spectrum of compound (109)

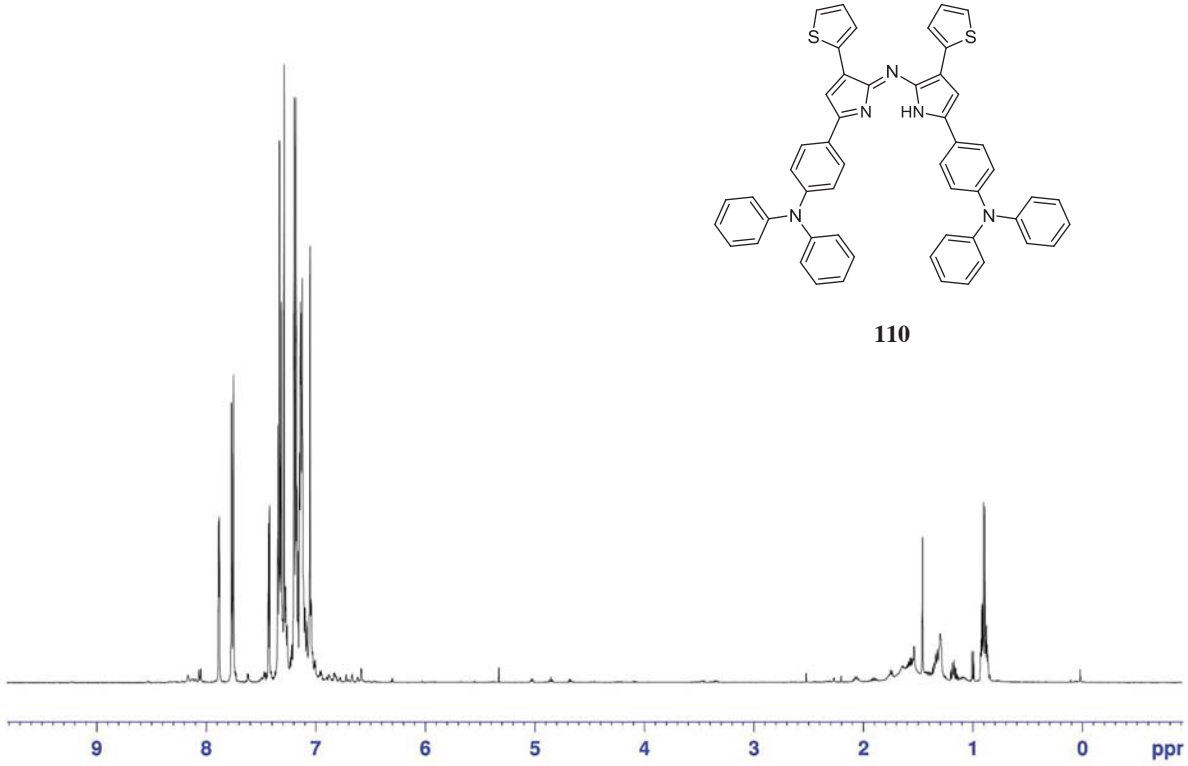

110

Figure 2.81 The ^{1}H NMR spectrum of compound (110)

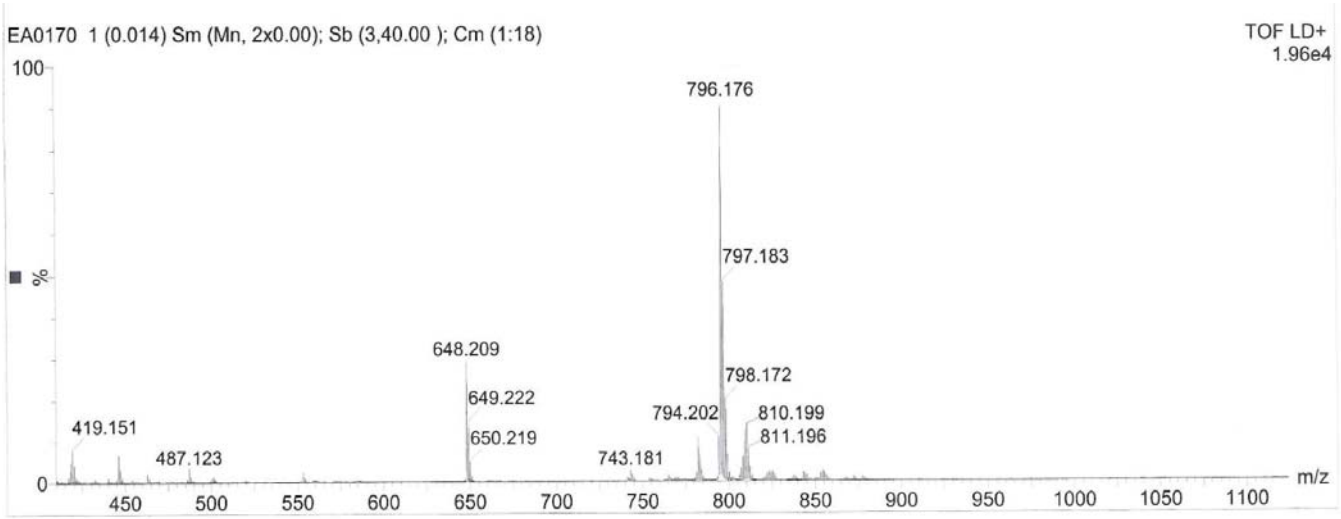

Figure 2.82 The mass spectrum of compound (110)

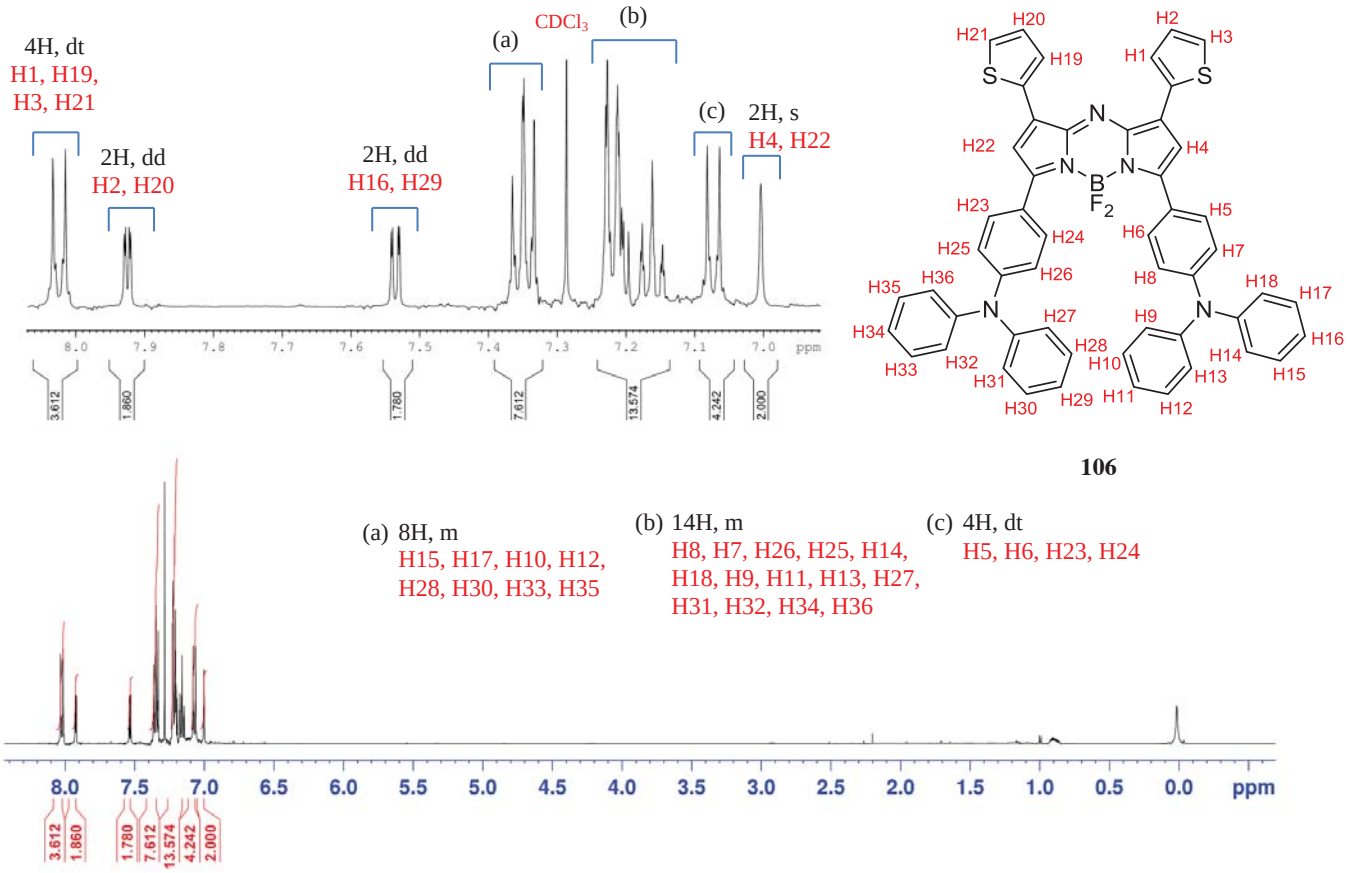

Figure 2.83 The ^{1}H NMR spectrum of compound (106)

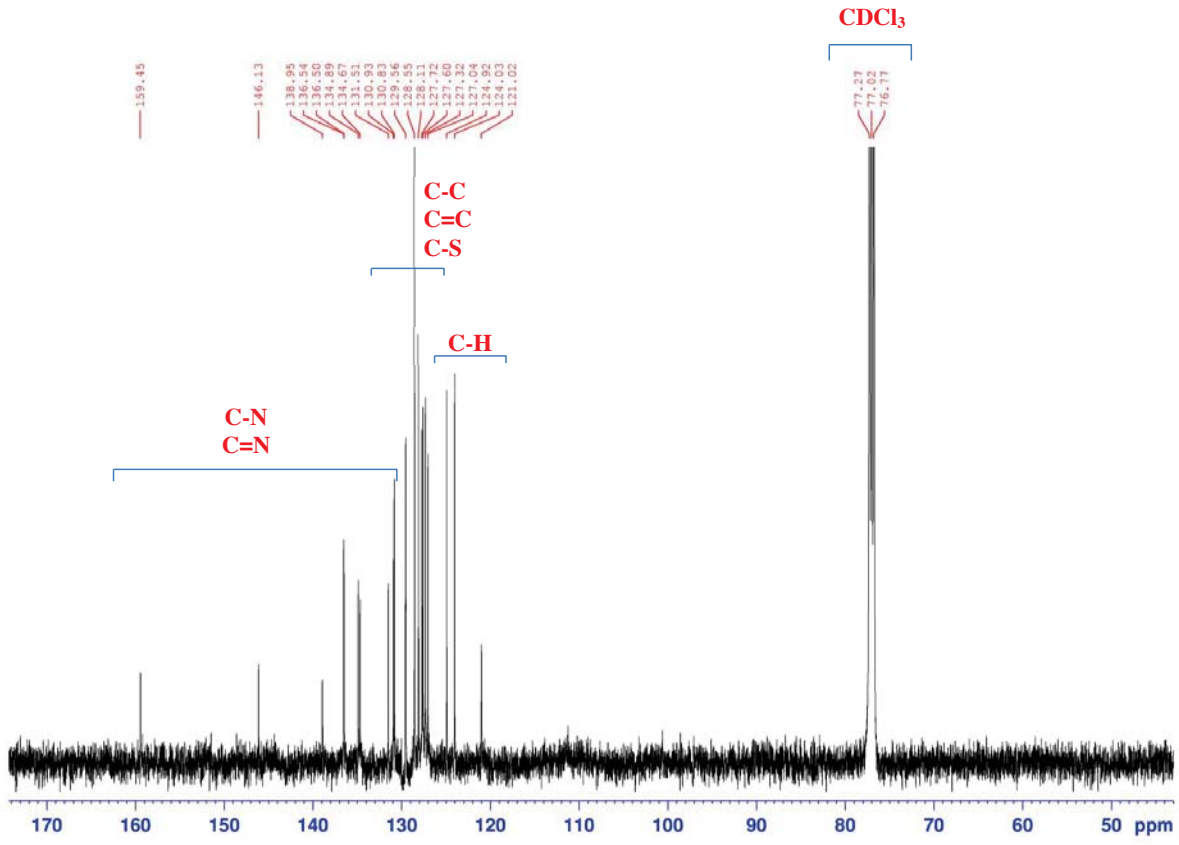

Figure 2.84 The ^{13}C NMR spectrum of compound (106)

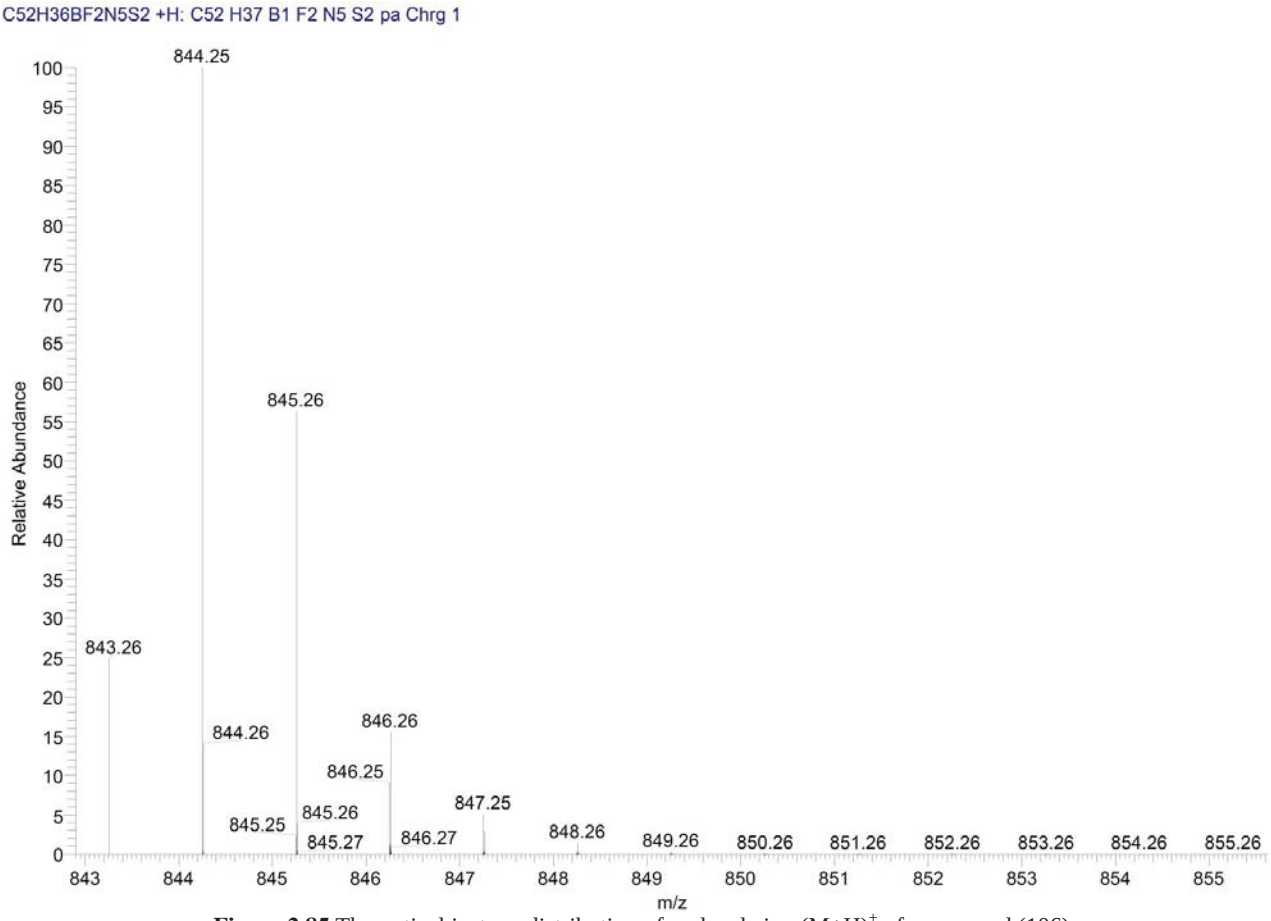

Figure 2.85 Theoretical isotope distribution of molecule ion $(M+H)^+$ of compound (106)

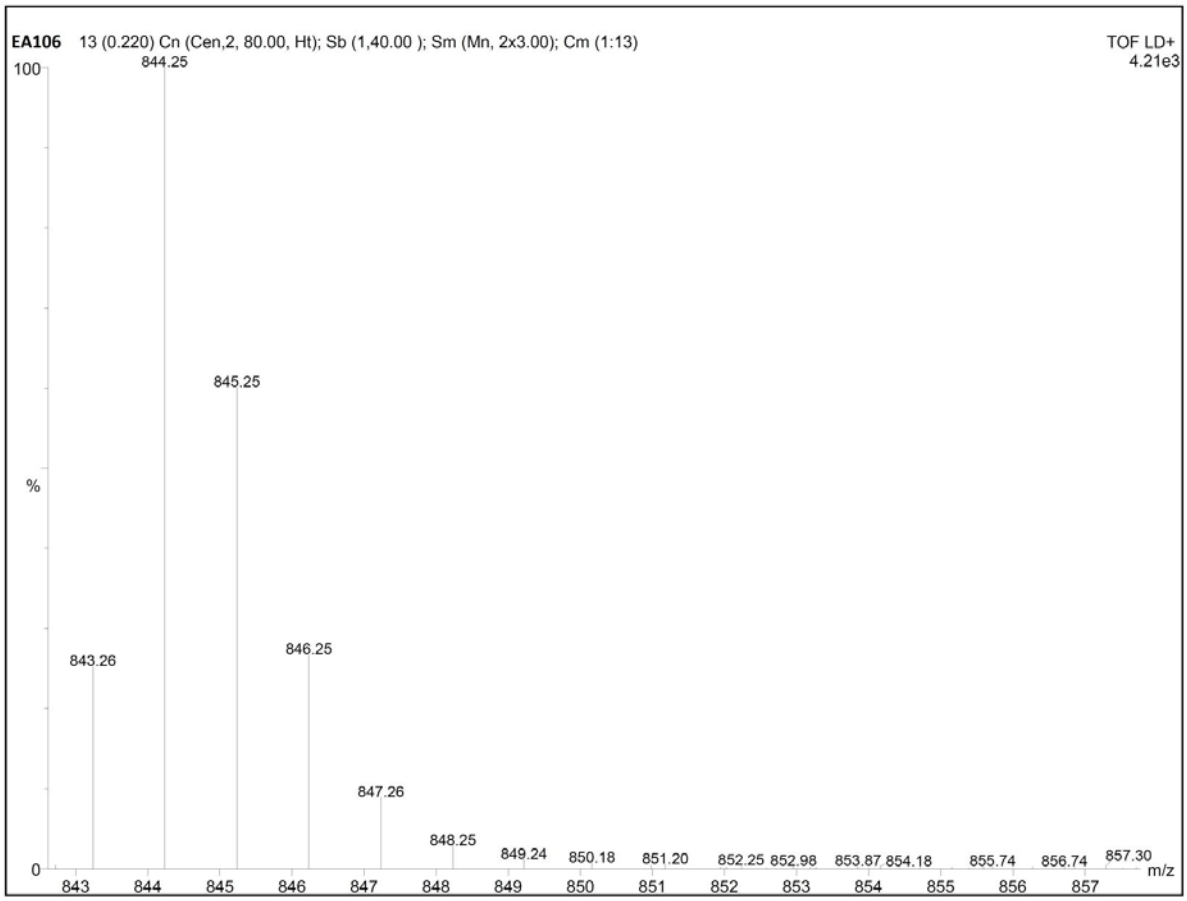

Figure 2.86 Experimental mass spectrum of compound (106)

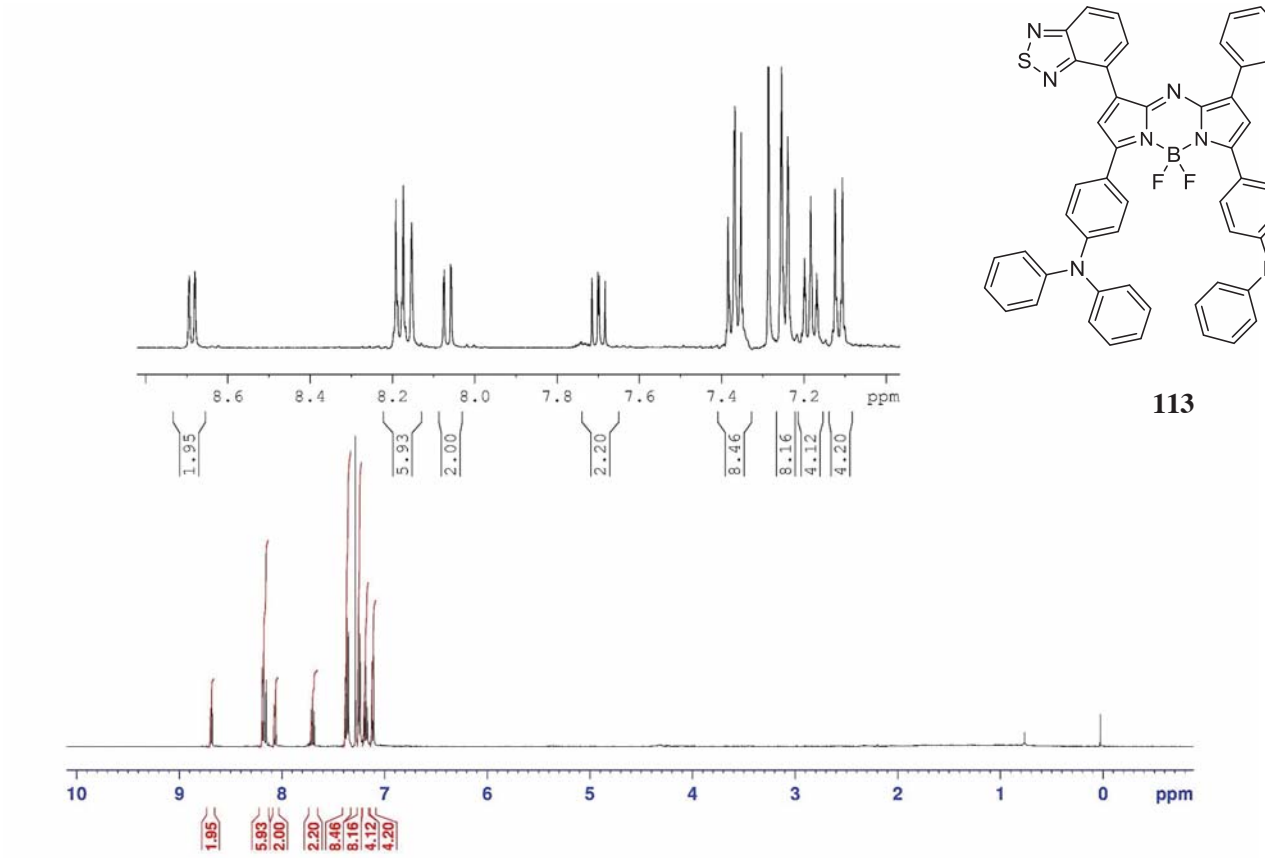

113

Figure 2.87 The ^{1}H NMR spectrum of compound (113)

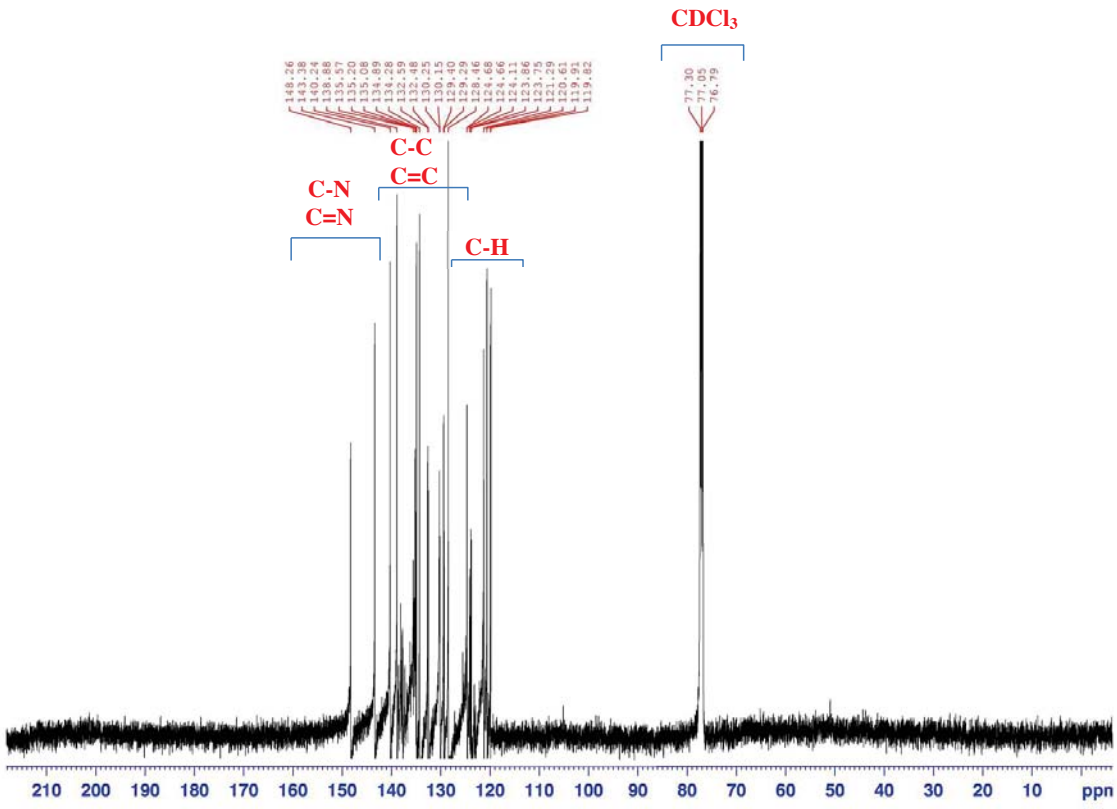

Figure 2.88 The ^{13}C NMR spectrum of compound (113)

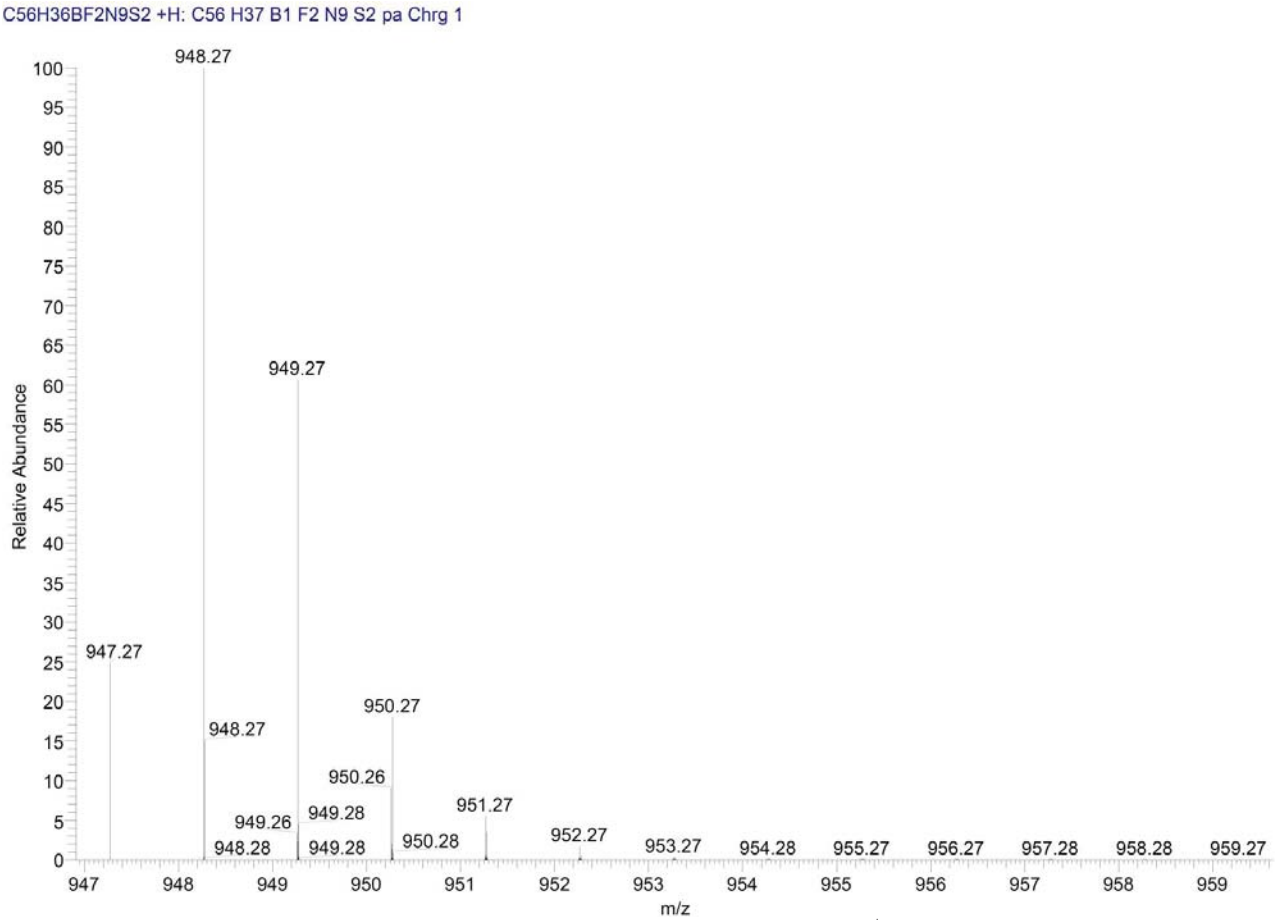

Figure 2.89 Theoretical isotope distribution of molecule ion $(M+H)^+$ of compound (113)

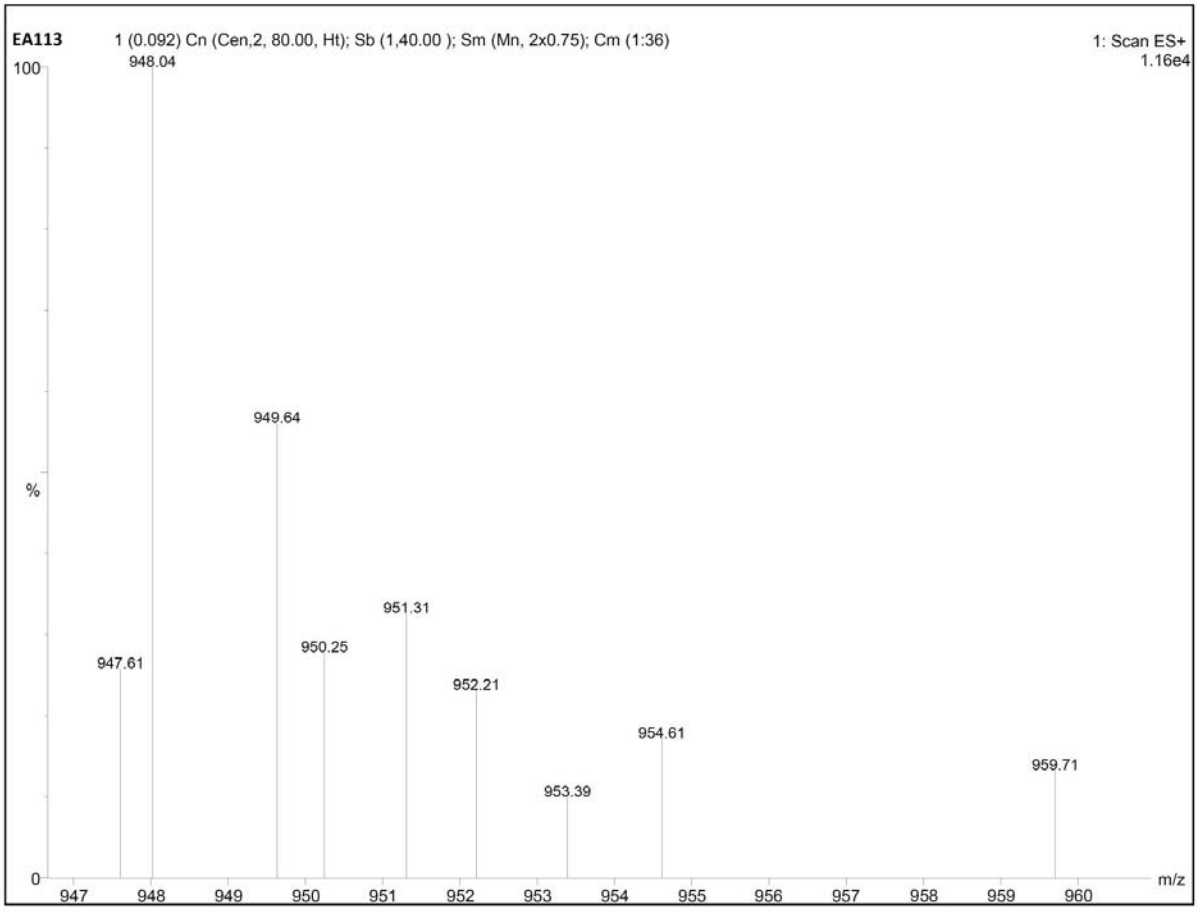

Figure 2.90 Experimental mass spectrum of compound (113)

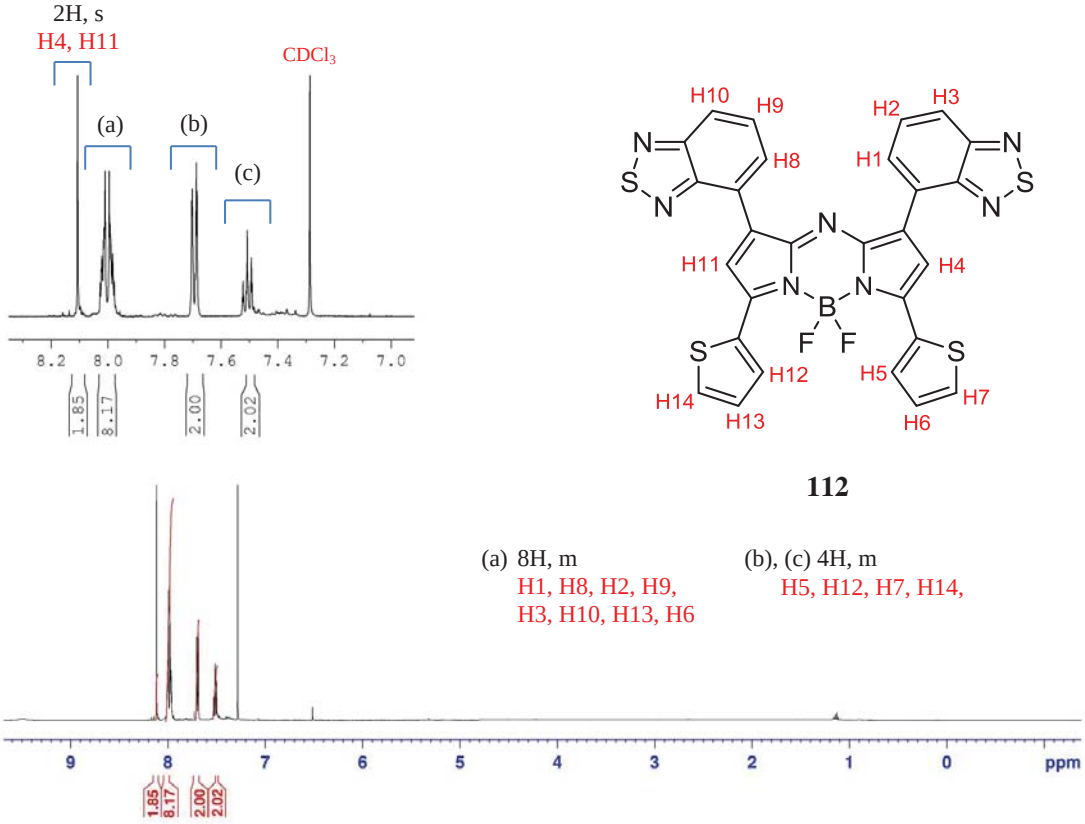

Figure 2.91 The ^{1}H NMR spectrum of compound (112)

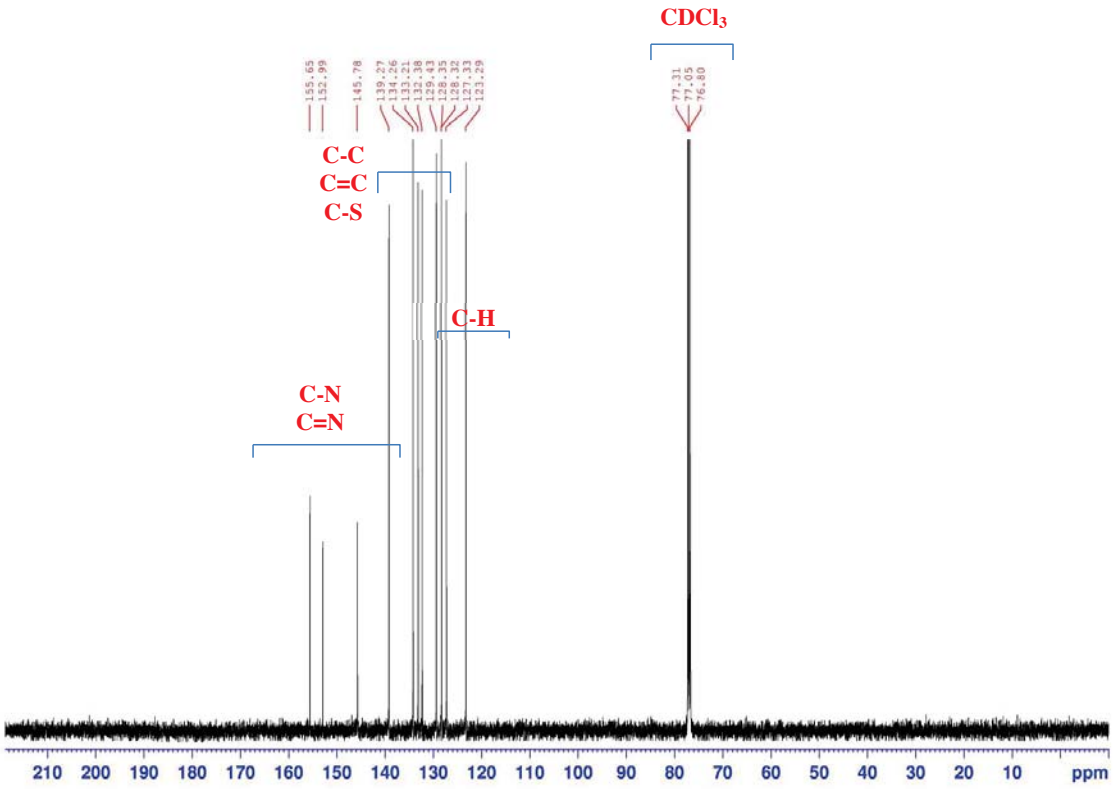

Figure 2.92 The ^{13}C NMR spectrum of compound (112)

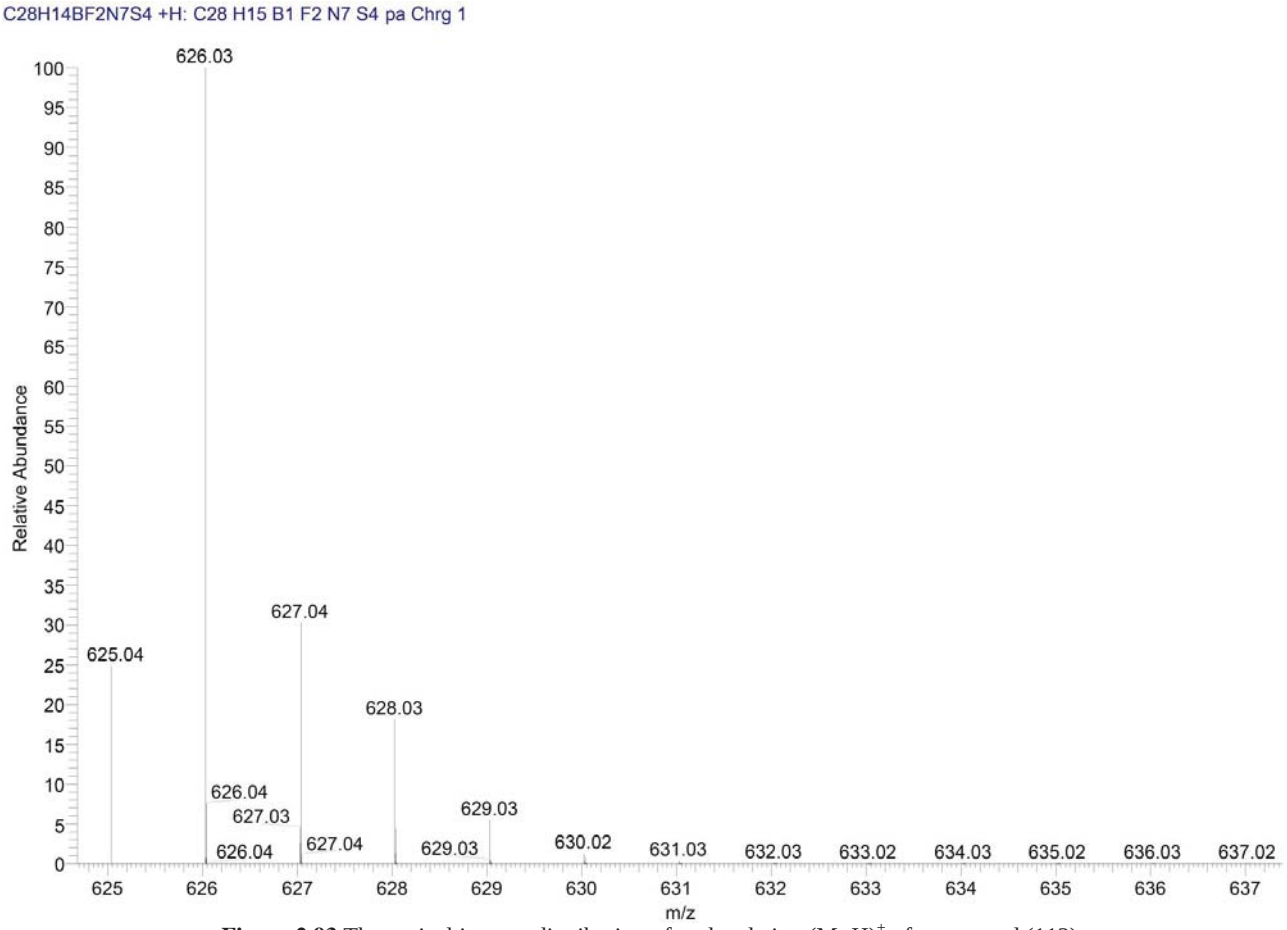

Figure 2.93 Theoretical isotope distribution of molecule ion $(M+H)^+$ of compound (112)

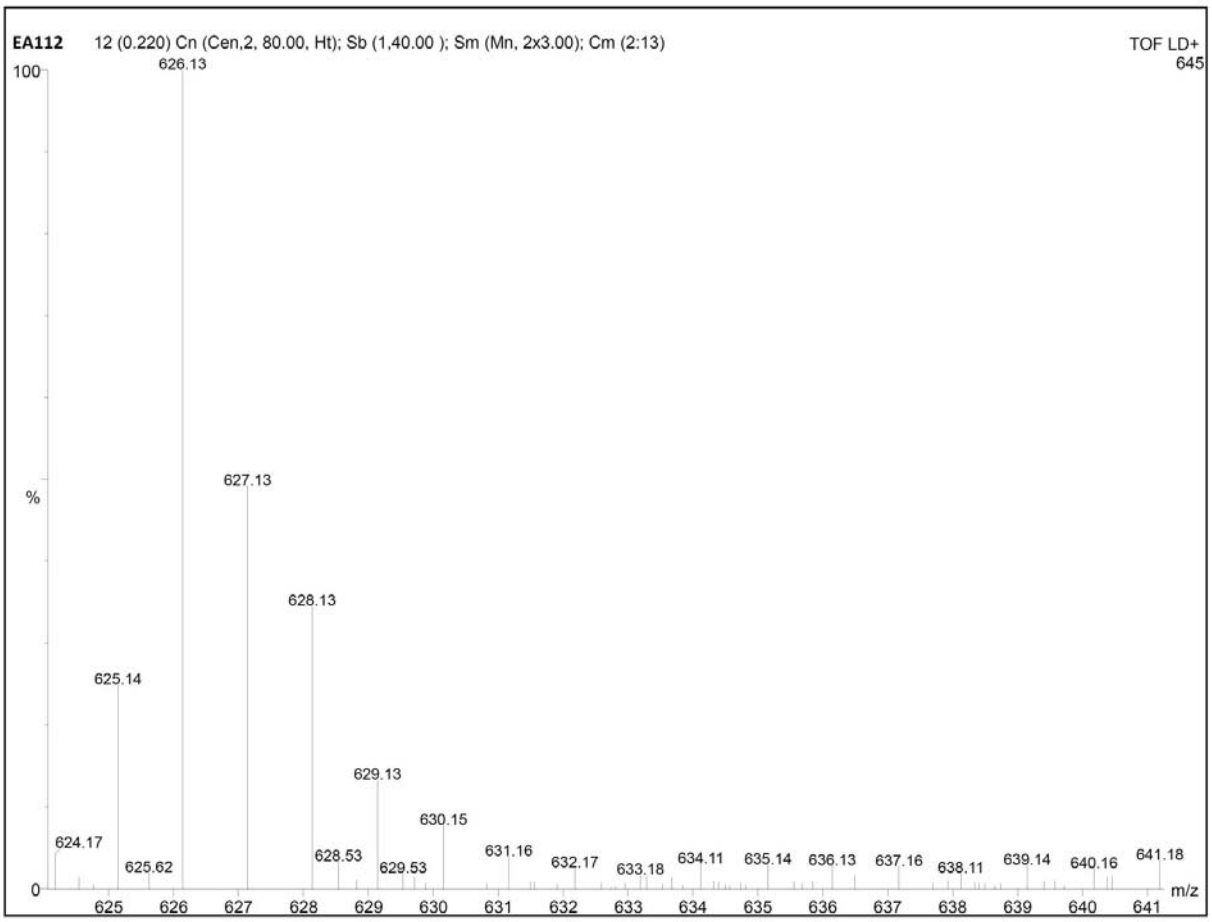

Figure 2.94 Experimental mass spectrum of compound (112)

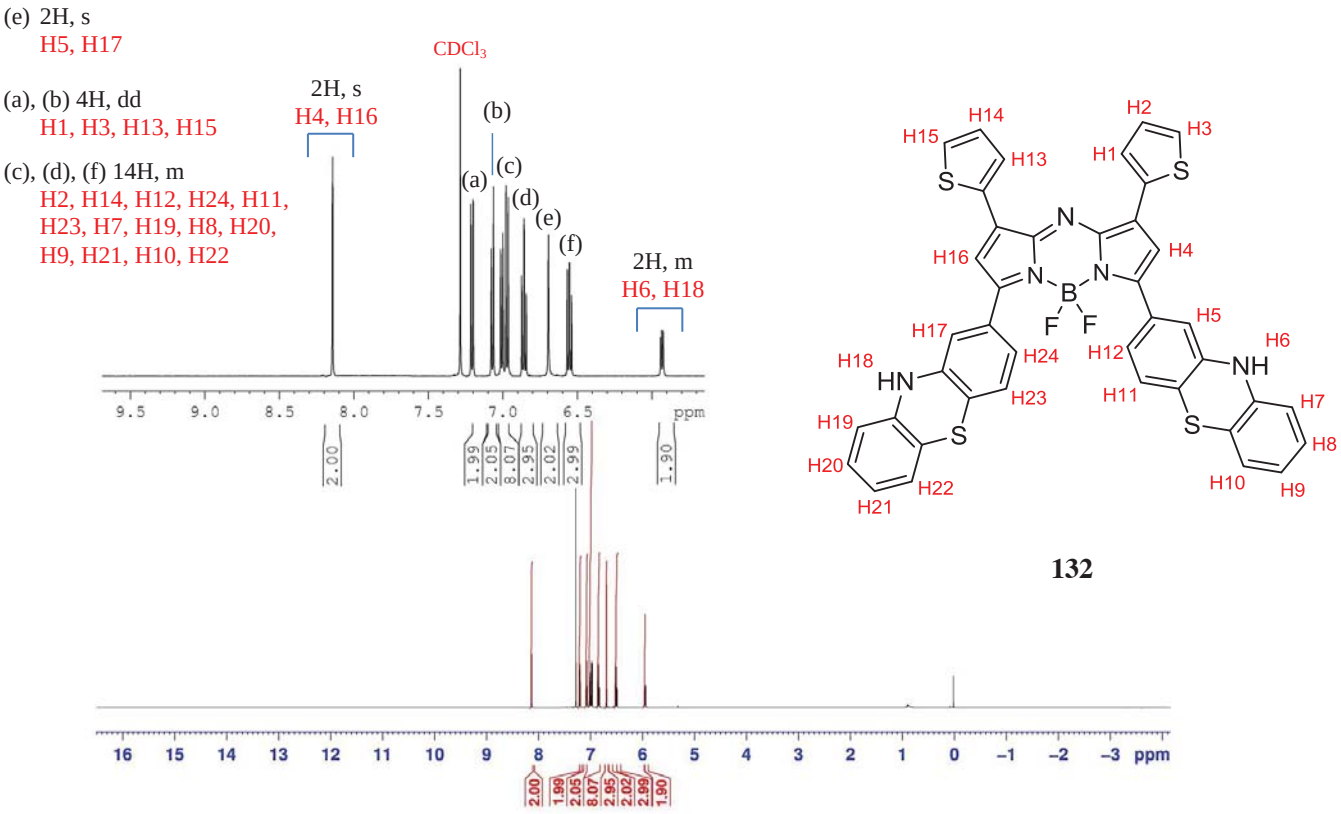

Figure 2.95 The ^{1}H NMR spectrum of compound (132)

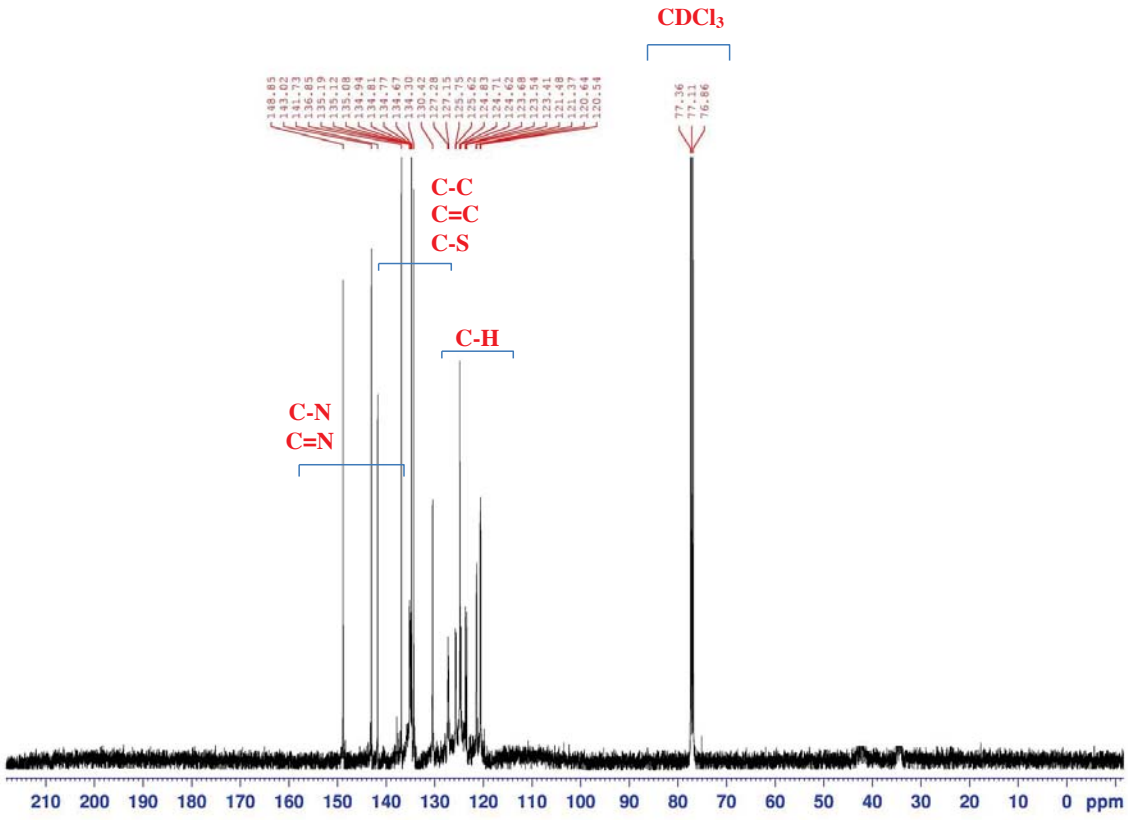

Figure 2.96 The ^{13}C NMR spectrum of compound (132)

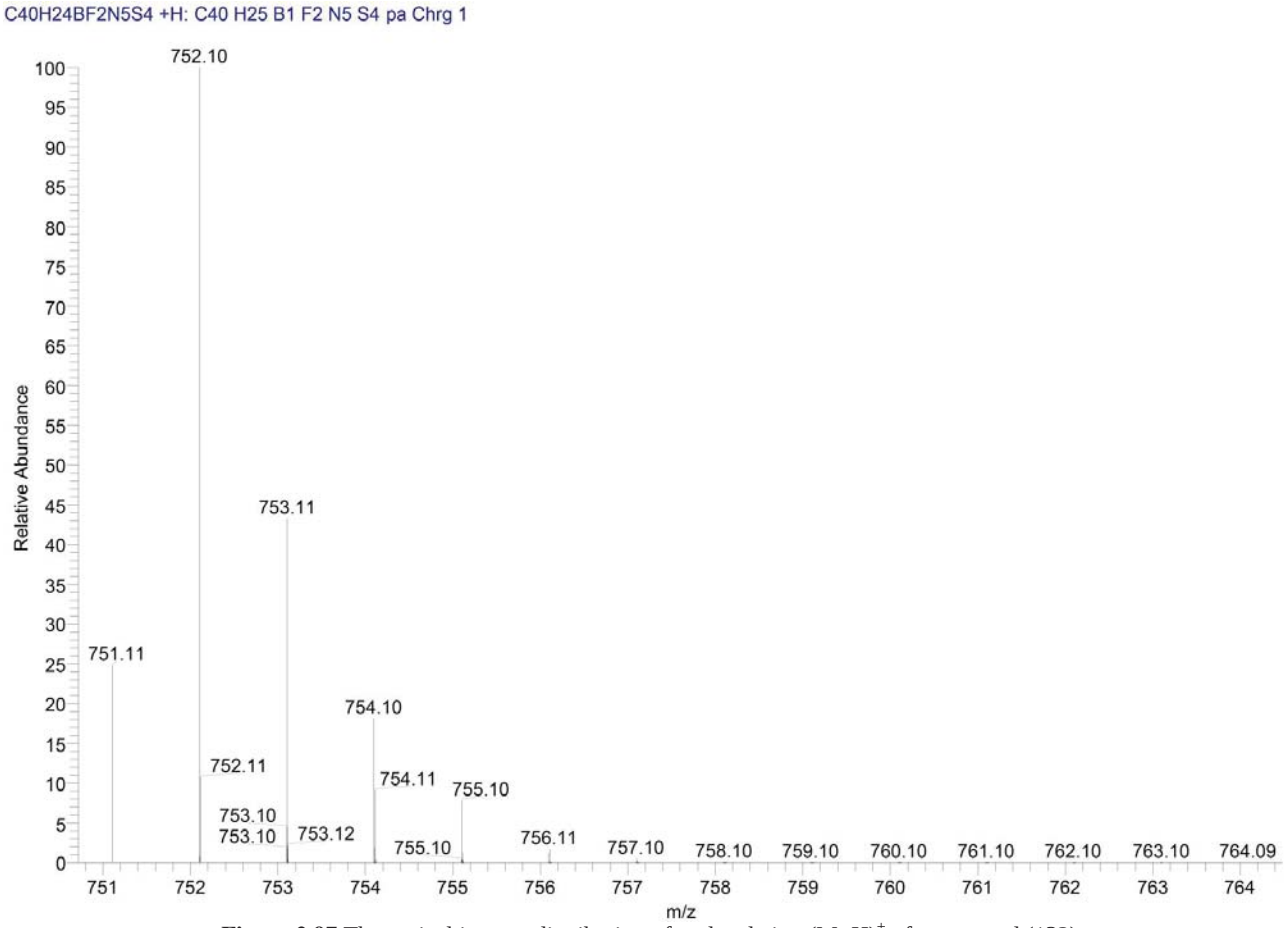

Figure 2.97 Theoretical isotope distribution of molecule ion $(M+H)^+$ of compound (132)

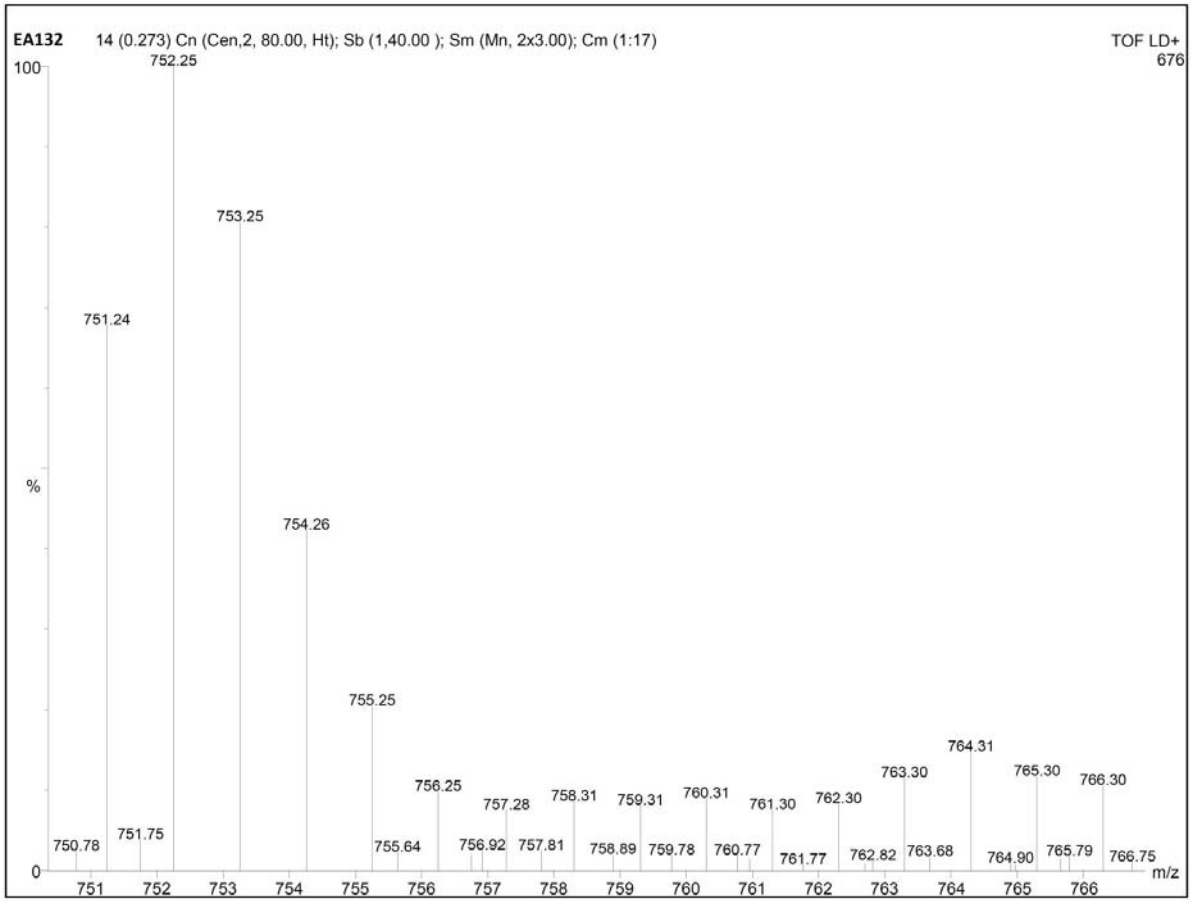

Figure 2.98 Experimental mass spectrum of compound (132)

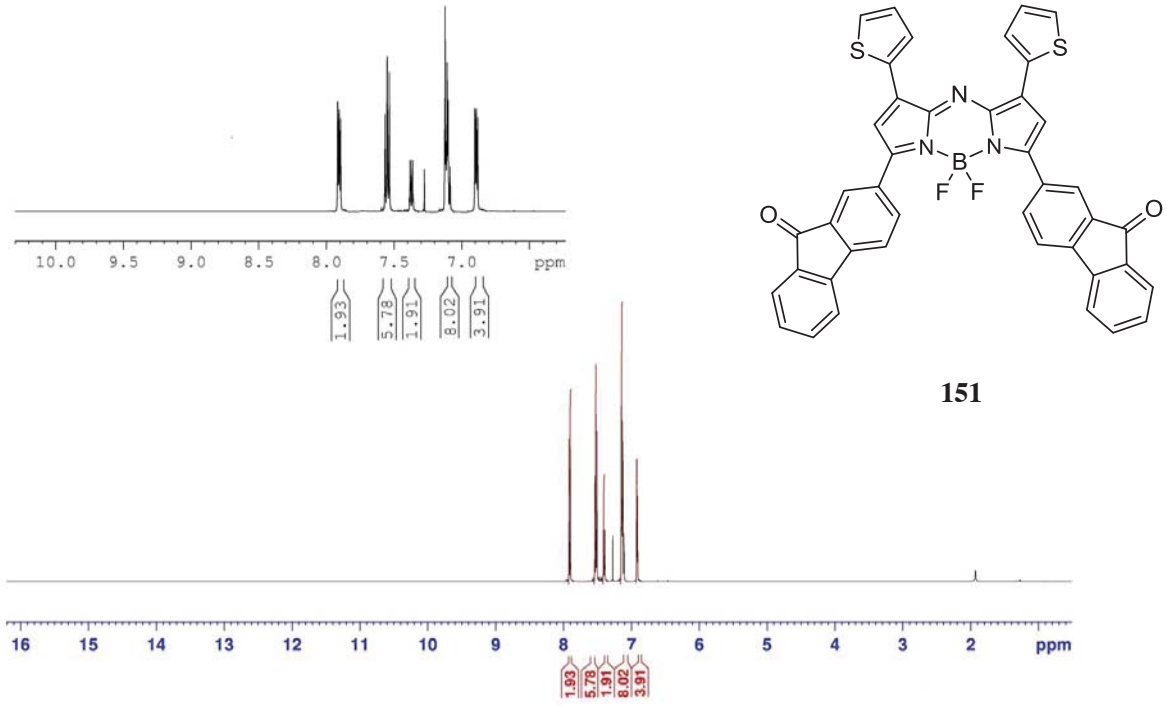

Figure 2.99 The ^{1}H NMR spectrum of compound (151)*

* ^{13}C NMR and Mass Spectrum were not reliable in terms of supporting evidence of purity and structure.

2.38 Experimental Methods

Solvents and reagents were purchased from Sigma-Aldrich, Merck and Acros Organics, generally as analytical reagent (AR) grade. Chromatography solvents were distilled laboratory grade. Dry dichloromethane (DCM) and dimethylformamide (DMF) were prepared by distilling AR grade solvent over CaH_2 under N_2 atmosphere. $CHCl_3$ was dried over K_2CO_3 and distilled under N_2 atmosphere. H_2O used in the aza-BODIPY synthesis was of reverse-osmosis grade. Dimethyl sulfoxide (DMSO) was dried over 4Å molecular sieves and distilled at reduced pressure. Tetrahydrofuran (THF) was dried by passing argon degassed solvent through activated alumina columns. For chromatography, silica gel (from Merck) and alumina have been used for all columns.

Reaction Monitoring

The intermediate compounds and the final aza-BODIPYs were coloured. Most of the reactions were easily monitored with thin layer chromatography (TLC) on silica TLC plates 60 F254 from Merck. Plates were visualized in UV light (254 nm) when necessary. The exceptions were the attempted reactions of aza-BODIPY discussed in Section (2.23) where the intermediate compounds and the crude mixture of aza-BODIPYs were monitored using both TLC and mass spectrometry.

2.38.1 General Experimental Procedures

2.38.1.1 General Procedure for the Synthesis of intermediate compounds (93), (97), (103), (108), (115), (119), (122), (128), (135), (142), (147), (157), (160), (165), (169), (172), (175), (178), (181), (183), (184), (186) and (187).

An appropriate aldehyde (0.05 mol) and ketone (0.05 mol) were dissolved in ethanol:H_2O (80:20 v/v, 25mL), then treated with potassium hydroxide (1.5 mmol) and stirred at room temperature for 24 h. During the course of the reaction, the product usually precipitated from the reaction mixture, and this was followed by filtration and recrystallization of the product from ethanol to yield a mostly yellow solid in a 7%-15% yield.

2.38.1.2 General Procedure for the Synthesis of intermediate compounds (94), (98), (104), (109), (116), (120), (123), (129), (136), (143), (148), (158), (161), (166), (170), (173), (176), (179), (182), (185) and (188).

The appropriate intermediate product from Section (2.38.1.1) (33.6 mmol), nitromethane (168 mmol) and diethylamine (168 mmol) were dissolved in dry methanol (25 mL), then heated under reflux for 24 h. The solution was cooled, acidified with 1M HCl and the resulting precipitate was isolated by filtration. Recrystallization from methanol gave the product as a white solid in a 35-85% yield.

2.38.1.3 General Procedure for the Synthesis of compounds (95), (99), (105), (110), (117), (121), (124), (130), (137), (144), (149), (159), (162), (167), (171), (174), (177), (180) and (189).

Method one: The appropriate intermediate product (3.71 mmol) from Section (2.38.1.2) was dissolved in 25 mL ethanol in round-bottomed flask and charged with ammonium formate (0.13 mol) and heated under reflux for 24 h. The product precipitated from the reaction mixture during the course of the reaction. The reaction mixture was cooled to room temperature and filtered and the isolated solid washed with ethanol (2x10 mL), and then purified by column chromatography to yield the appropriate product as a blue solid in a yield of 7%-33%.

Method two: The appropriate intermediate product (3.71 mmol) from Section (2.38.1.2) was dissolved in 25 mL ethanol in round-bottomed flask and charged with ammonium acetate (0.13 mol) and heated under reflux for 24 h. The product precipitated from the reaction mixture during the course of the reaction. The reaction mixture was cooled to room temperature and filtered and the isolated solid washed with ethanol (2x10 mL), and then purified by column chromatography to yield the appropriate product as a blue solid in a 7%-33% yield.

2.38.1.4 General Procedure for the Synthesis of compounds (87), (88), (100), (106), (111), (112), (113), (125), (132), (139), (145), (150) and (151).

The appropriate compound from Section (2.38.1.3) (0.45 mmol) was dissolved in dry DCM (20 mL) and treated with boron trifluoride diethyl etherate (8.13 mmol) and diisopropylethylamine (4.6 mmol), and the mixture stirred at room temperature under N_2 for 24 h. The mixture was washed with water (2x10 mL), and the organic layer was dried over magnesium sulfate and evaporated to dryness. Purification by column chromatography on silica gave the appropriate product as a metallic blue solid in a 35%-60% yield.

2.38.1.5 General Procedure for the Synthesis of compounds (205), (208) and (211).

A solution of 0.80 mmol of triphenylphosphine in 20 ml of dry THF in a flask fitted with reflux condenser. After the reaction mixture became homogeneous, 0.80 mmol of the appropriate bromide was added. The reaction mixture was stirred for 3 h and filtered. Re-crystallization gave the appropriate phosphonium salt (47%, 32%, and 35% yield of (205), (208), and (211) respectively) as white crystals.

2.38.1.6 General Procedure for the Synthesis of compounds (190), (191), (192) and (193).

A mixture of the appropriate 3'-formylterthiophene (0.44 mmol) and appropriate phosphonium salt (0.54 mmol) was dissolved in dry THF and degassed with argon for 30 minutes. DBU (0.53 mmol) was added and the mixture held at reflux under argon overnight. The solvent was evaporated from the reaction mixture. The resultant crude mixture was then purified by column chromatography (CH_2Cl_2/hexane 1:1) to give the appropriate β'-substituted terthiophene ((191), (192), (190), and (193)).

2.39 Characterization Data

2.39.1 ^{1}H NMR Spectra, MALDI Mass Spectra and Elemental Analysis Results

Compound (87)

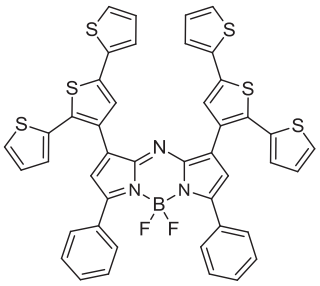

Yield: 75%
Chemical Formula: $C_{44}H_{26}BF_2N_3S_6$
Exact Mass: 837.05 Da
Molecular Weight: 837.90

MALDI: m/z = 838 $(M+H)^+$.

Elemental Analysis: Calculated: C, 62.10; H, 3.20;N, 6.01. Found: C 61.80, H 3.11, N 4.98.

^{1}H NMR (500 MHz, $CDCl_3$, TMS): δ 7.90 (m, 4H), 7.75 (s, 2H), 7.46 (m, 6H), 7.40 (dd, J=1.2, 5.3 Hz, 2H), 7.24 (dd, J=1.2, 3.6 Hz, 2H), 7.09 (m, 6H), 6.91 (dd, J=3.6, 5 Hz, 2H), 6.66 (s, 2H).

Compound (88)

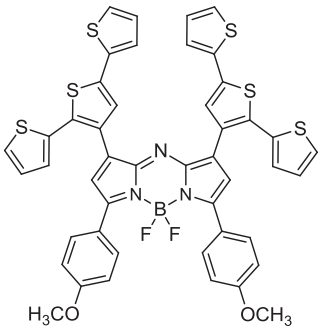

Yield: 77%

Chemical Formula: $C_{46}H_{30}BF_2N_3O_2S_6$

Exact Mass: 897.07 Da

Molecular Weight: 897.95

MALDI: m/z = 898.08 $(M+H)^+$.

^{1}H NMR (500 MHz, $CDCl_3$, TMS): δ 8.50 (d, J=9.2, 1H), 7.71 (dd, J=4.6, 2H), 7.66 (m, 10H), 7.31 (m, 6H), 7.23 (dd, J=3.6, 5.3 Hz, 3H), 7.1 (dd, J=3.4, 6.1 Hz, 2H), 2.50 (s, 6H).

Compound (93)

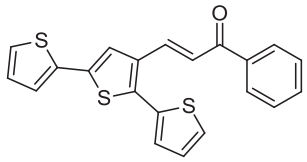

Yield: 70%
Chemical Formula: $C_{21}H_{14}OS_3$
Exact Mass: 378.02 Da
Molecular weight: 378.53

MALDI: m/z = 379.06 $(M+H)^+$.

^{1}H NMR (500 MHz, $CDCl_3$, TMS): δ 8.09 (s, 1H), 8.06 (dd, J=1.9, 6.1 Hz, 2H), 7.58 (m, 2H), 7.49 (s, 1H), 7.45 (d, J=15.5 Hz, 1H), 7.45 (dd, J=1.3, 5.2 Hz, 1H), 7.32 (dd, J=1.2, 5.1 Hz, 1H), 7.26 (dd, J=1.3, 3.7 Hz, 1H), 7.25 (dd, J=1.3, 3.7 Hz, 1H), 7.16 (dd, J=3.4, 5 Hz, 1H), 7.09 (dd, J=3.7, 5.1 Hz, 1H).

Compound (94)

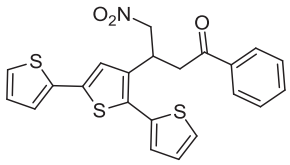

Yield: 75%
Chemical Formula: $C_{22}H_{17}NO_3S_3$
Exact Mass: 439.04 Da
Molecular weight: 439.57

MALDI: m/z = 440.2 $(M+H)^+$.

^{1}H NMR (500 MHz, $CDCl_3$, TMS): δ 7.94 (dd, J=1.2, 8.5 Hz, 2H), 7.60 (tt, J=1.2, 7.2 Hz, 1H), 7.48 (dt, J=1.8, 7.5 Hz, 2H), 7.42 (dd, J=1, 5 Hz, 1H), 7.26 (m, 2H), 7.18 (dd, J=1.2, 3.7 Hz, 1H), 7.13 (dd, J=3.5, 5.4 Hz, 1H), 7.08 (s, 1H), 7.04 (dd, J=3.4, 5 Hz, 1H), 4.80 (m, 2H), 4.66 (m, 1H), 3.48 (m, 2H).

Compound (95)

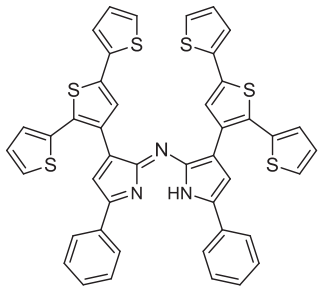

Yield: 14%
Chemical Formula: $C_{44}H_{27}N_3S_6$
Exact Mass: 789.05 Da
Molecular Weight: 790.10

MALDI: m/z = 790.09 $(M+H)^+$.

^{1}H NMR (500 MHz, $CDCl_3$, TMS): δ 7.70 (m, 4H), 7.45 (s, 2H), 7.36 (m, 8H), 7.14 (dd, J=1.4, 3.8 Hz, 2H), 7.01 (m, 8H), 6.86 (m, 3H).

Compound (97)

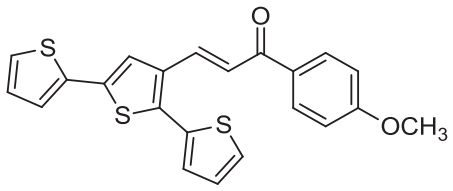

Yield: 69%

Chemical Formula: $C_{22}H_{16}O_2S_3$

Exact Mass: 408.03 Da

Molecular Weight: 408.56

MALDI: m/z = 409.02 $(M+H)^+$.

^{1}H NMR (500 MHz, $CDCl_3$, TMS): δ 7.81 (s, 1H), 7.60 (m, 4H), 7.61 (s, 1H), 7.42 (m, 4H), 7.15 (dd, J=1.2, 3.6 Hz, 1H), 7.01 (dd, J=2.4, 5.2 Hz, 1H), 6.90 (dd, J=2.4.7, 5.1 Hz, 1H), 3.71 (s, 3H).

Compound (98)

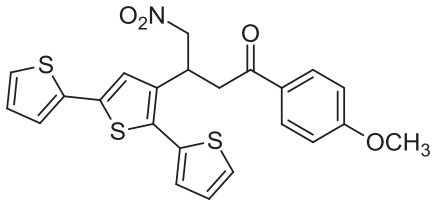

Yield: 80%

Chemical Formula: $C_{23}H_{19}NO_4S_3$

Exact Mass: 469.05 Da

Molecular Weight: 469.60

MALDI: m/z =470.03 $(M+H)^+$.

^{1}H NMR (500 MHz, $CDCl_3$, TMS): δ 7.88 (dd, J=2.2, 7 Hz, 2H), 7.40 (m, 2H), 7.15 (m, 3H), 7.02 (s, 1H), 6.93 (tt, J=1.9, 6.9 Hz, 2H), 6.73 (dd, J=9, 13.8 Hz, 1H), 4.74 (m, 2H), 4.57 (m, 1H), 3.87 (s, 3H), 3.35 (m, 2H).

Compound (99)

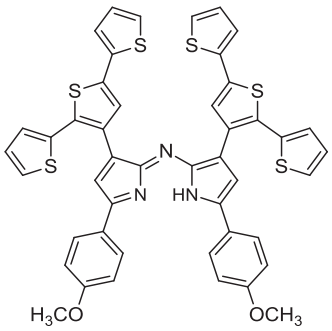

Yield: 19%

Chemical Formula: $C_{46}H_{31}N_3O_2S_6$

Exact Mass: 849.07 Da

Molecular Weight: 850.15

MALDI: m/z =850.09 $(M+H)^+$.

^{1}H NMR (500 MHz, $CDCl_3$, TMS): δ 8.40 (d, J=8.2, 1H), 7.92 (dd, J=6.1, 2H), 7.86 (m, 4H), 7.32 (m, 6H), 7.27 (m, 6H), 7.15 (dd, J=4.2, 6.3 Hz, 3H), 6.91 (dd, J=3.8, 6.1 Hz, 2H), 5.9 (s, 1H), 2.49 (s, 6H).

Triphenylamine-Substituted BF_2-aza-dipyrromethene (TPA-aza-BODIPY) (100)

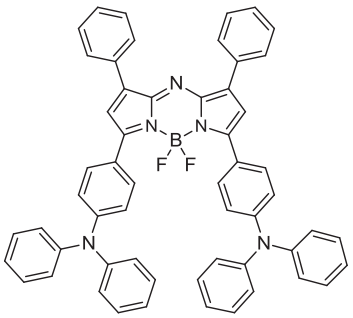

Yield: 18%

Chemical Formula: $C_{56}H_{40}BF_2N_5$

Exact Mass: 831.33 Da

Molecular Weight: 831.76

MALDI: m/z = 832.19 $(M+H)^+$.

Elemental Analysis: C, 81.01; H, 5.22; N, 9.03. Found: C 80.75, H 4.72, N 8.32.

^{1}H NMR (500 MHz, $CDCl_3$, TMS): δ 7.90 (dd, J=1.3, 6.1 Hz, 4H), 7.78 (m, 4H), 7.45 (m, 7H), 7.35 (p, J=3.1, 7.3 Hz, 9H), 7.24 (dd, 1.1, 8.4 Hz, 6H), 7.16 (m, 5H), 7.05 (dd, J=1.1, 7.8 Hz, 5H).

Compound (103)

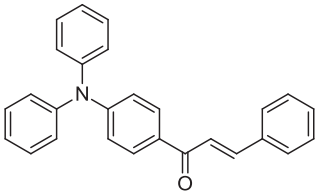

Yield: 65%

Chemical Formula: $C_{27}H_{21}NO$

Exact Mass: 375.16 Da

Molecular Weight: 375.46

MALDI: m/z =376.13 $(M+H)^+$.

^{1}H NMR (500 MHz, $CDCl_3$, TMS): δ 7.95 (dt, J=1.9, 6.8 Hz, 2H), 7.84 (d, J=15.6 Hz, 1H), 7.66 (dd, J=2.3, 7.5 Hz, 2H), 7.57 (d, J=15.6 Hz, 1H), 7.44 (m, 3H), 7.36 (m, 4H), 7.19 (m, 6H), 7.07 (dt, J=1.9, 6.7 Hz, 2H).

Compound (104)

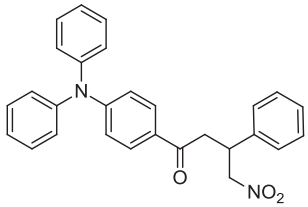

Yield: 70%

Chemical Formula: $C_{28}H_{24}N_2O_3$

Exact Mass: 436.18 Da

Molecular Weight: 436.50

MALDI: m/z = 437.20 $(M+H)^+$.

^{1}H NMR (500 MHz, $CDCl_3$, TMS): δ 7.80 (dt, J= 1.8, 7.1 Hz, 2H), 7.36 (m, 9H), 7.18 (m, 6H), 6.99 (dt, J=1.8, 7.1 Hz, 2H), 4.87 (dd, J=6.3, 12.4 Hz, 1H), 4.71 (dd, J=8.3, 12.4 Hz, 1H), 4.25 (p, J=7.7, 14.2 Hz, 1H), 3.38 (qd, J=6, 16.7 Hz, 2H).

Triphenylamine-Substituted Aza-dipyrromethene (TPA-aza-DIPY) (105)

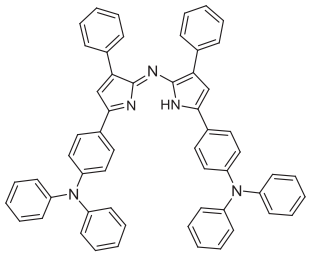

Yield: 10%-16%

Chemical Formula: $C_{56}H_{41}N_5$

Exact Mass: 783.34 Da

Molecular Weight: 783.96

MALDI: m/z =784.35 $(M+H)^+$.

^{1}H NMR (500 MHz, $CDCl_3$, TMS): δ 7.80 (dd, J=1.2, 6.1 Hz, 4H), 7.69 (m, 4H), 7.34 (m, 7H), 7.25 (p, J=4.1, 6.2 Hz, 9H), 7.12 (dd, J=1.0, 6.3 Hz, 6H), 7.00 (m, 5H), 6.90 (dd, J=1.2, 7.1 Hz, 5H), 6.1 (s, 1H).

Thiophene-Triphenylamine-Substituted BF_2-Aza-dipyrromethene (T-TPA-aza-BODIPY) (106)

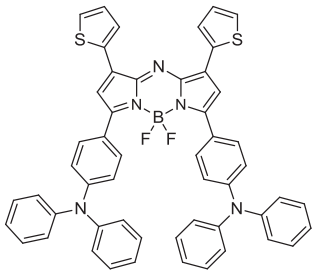

Yield: 20%

Chemical Formula: $C_{52}H_{36}BF_2N_5S_2$

Exact Mass: 843.25 Da

Molecular Weight: 843.81

MALDI: m/z = 844.25 $(M+H)^+$.

Elemental analysis: C, 73.11; H, 5.20; N, 7.50. Found: C 73.01, H 4.11, N 7.76.

^{1}H NMR (500 MHz, $CDCl_3$, TMS): δ 8.03 (dt, J=2, 7.1 Hz, 4H), 7.93 (dd, J=1.1, 3.6 Hz, 2H), 7.53 (dd, J=1.1, 5 Hz, 2H), 7.36 (m, 8H), 7.19 (m, 14H), 7.07 (dt, J=2, 7 Hz, 4H), 7.00 (s, 2H).

Compound (108)

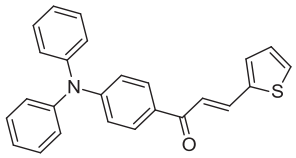

Yield: 80%

Chemical Formula: $C_{25}H_{19}NOS$

Exact Mass: 381.12 Da

Molecular Weight: 381.49

MALDI: m/z = 382.16 $(M+H)^+$.

^{1}H NMR (500 MHz, $CDCl_3$, TMS): δ 7.96 (d, J=15.24 Hz, 1H), 7.91 (dt, J=2.9, 6.9 Hz, 2H), 7.41 (d, J=5.2 Hz, 1H), 7.36 (m, 6H), 7.18 (m, 6H), 7.10 (dd, 3.5, 5.1 Hz, 1H), 7.06 (dt, J=2.9, 6.2 Hz, 2H).

Compound (109)

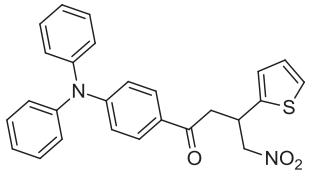

Yield: 65%

Chemical Formula: $C_{26}H_{22}N_2O_3S$

Exact Mass: 442.14 Da

Molecular Weight: 442.53

MALDI: m/z = 443.19 $(M+H)^+$.

^{1}H NMR (500 MHz, $CDCl_3$, TMS): δ 7.81 (dt, J=2.5, 6.9 Hz, 2H), 7.36 (m, 4H), 7.22 (dd, J=1.3, 5 Hz, 1H), 7.18 (m, 6H), 6.98 (m, 6H), 4.87 (dd, J=6, 12.6 Hz, 1H), 4.72 (dd, J=7.8, 12.6 Hz, 1H), 4.57 (q, J=6.8, 13.4 Hz, 1H), 3.44 (qd, J=6.1, 17.5 Hz, 2H).

Thiophene-Triphenylamine-Substituted Aza-dipyrromethene (T-TPA-aza-DIPY) (110)

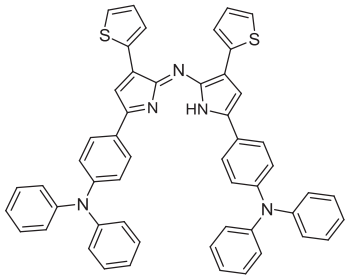

Yield: 18%

Chemical Formula: $C_{52}H_{37}N_5S_2$

Exact Mass: 795.25 Da

Molecular Weight: 796.01

MALDI: m/z = 796.18 $(M+H)^+$.

^{1}H NMR (500 MHz, $CDCl_3$, TMS): δ 7.93 (d, J=1.8, 6.1 Hz, 3H), 7.80 (dd, J=1.2, 4.3 Hz, 6H), 7.43 (m, 4H), 7.35 (m, 20H), 7.1 (m, 4H).

Benzothiadiazole-Substituted BF_2-Aza-dipyrromethene (BTZ-aza-BODIPY) (111)

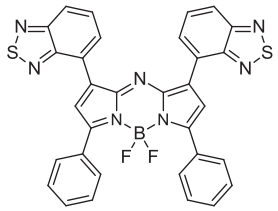

Yield: 50%

Chemical Formula: $C_{32}H_{18}BF_2N_7S_2$

Exact Mass: 613.11 Da

Molecular Weight: 613.47

MALDI: m/z = 614.21 $(M+H)^+$.

Elemental Analysis: C, 61.50; H, 3.20;N, 17.00. Found: C 61.10, H 2.87, N 16.89.

^{1}H NMR (500 MHz, $CDCl_3$, TMS): δ 8.31 (s, 2H), 8.27 (m, 4H), 8.15 (dd, J=0.9, 8.7 Hz, 2H), 7.95 (dd, J=0.9, 6.9 Hz, 2H), 7.79 (dd, J=6.9, 8.9 Hz, 2H), 7.56 (m, 4H), 7.49 (m, 2H).

Benzothiadiazole-Thiophene-Substituted BF_2-Aza-dipyrromethene (BTZ-T-aza-BODIPY) (112)

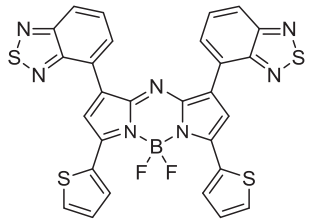

Yield: 40%

Chemical Formula: $C_{28}H_{14}BF_2N_7S_4$

Exact Mass: 625.03 Da

Molecular Weight: 625.53

MALDI: m/z = 626.13 $(M+H)^+$.

Elemental Analysis: C, 55.00; H, 2.30; N, 17.1. C 53.40, H 2.21, N 15.33.

^{1}H NMR (500 MHz, $CDCl_3$, TMS): δ 8.11 (s, 2H), 8.00 (m, 8H), 7.69 (dd, J=6.0, 4.8 Hz, 2H), 7.56 (m, 2H).

Benzothiadiazole-Triphenylamine-Substituted BF_2-Aza-dipyrromethene (BTZ-TPA-aza-BODIPY) (113)

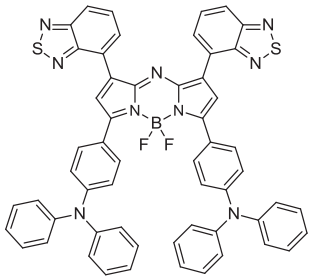

Yield: 35%

Chemical Formula: $C_{56}H_{36}BF_2N_9S_2$

Exact Mass: 947.26 Da

Molecular Weight: 947.88

MALDI: m/z = 948.04 $(M+H)^+$.

Elemental Analysis: C, 71.00; H, 4.20; N, 12.60. Found: C 70.66, H 4.71, N 12.51.

^{1}H NMR (500 MHz, $CDCl_3$, TMS): δ 8.69 (d, J=1.2 Hz, 2H), 8.18 (t, J=1.6, 2.4 Hz, 6H), 8.78 (d, J=3.1 Hz, 2H), 7.51 (dd, J=1.3, 4.6 Hz, 2H), 7.37 (m, 8H), 7.23 (d, J=8.9 Hz, 8H), 7.18 (t, J=2.1, 5.3 Hz, 4H), 7.11 (d, J=2.1 Hz, 4H).

Compound (115)

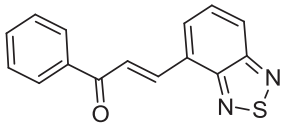

Yield: 60%

Chemical Formula: $C_{15}H_{10}N_2OS$

Exact Mass: 266.05 Da

Molecular Weight: 266.32

MALDI: m/z = 267.01 $(M+H)^+$.

^{1}H NMR (500 MHz, $CDCl_3$, TMS): δ 7.97 (m, 3H), 7.85 (dt, J=1.2, 7.1 Hz, 1H), 7.52 (m, 3H), 7.43 (t, J=7.7 Hz, 3H).

Compound (116)

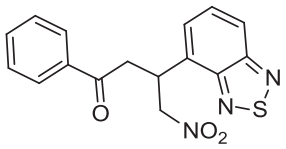

Yield: 70%

Chemical Formula: $C_{16}H_{13}N_3O_3S$

Exact Mass: 327.07 Da

Molecular Weight: 327.36

MALDI: m/z = 328.05 $(M+H)^+$.

^{1}H NMR (500 MHz, $CDCl_3$, TMS): δ 8.10 (m, 3H), 7.95 (dt, J=1.2, 6.1 Hz, 1H), 7.62 (m, 4H), 5.23 (dd, J=6.1, 11.1 Hz, 1H), 5.12 (dd, J=8.8, 11.6 Hz, 1H), 4.10 (p, J=6.2, 12.9 Hz, 1H), 3.74 (qd, J=6.1, 15.2 Hz, 2H).

Benzothiadiazole-Substituted Aza-dipyrromethene (BTZ-aza-DIPY) (117)

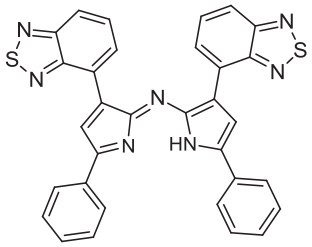

Yield: 8%

Chemical Formula: $C_{32}H_{19}N_7S_2$

Exact Mass: 565.11 Da

Molecular Weight: 565.67

MALDI: m/z = 566.13 $(M+H)^+$.

^{1}H NMR (500 MHz, $CDCl_3$, TMS): δ 8.20 (s, 1H), 8.11 (m, 8H), 7.81 (dd, J=6.5, 7.9 Hz, 3H), 7.51 (m, 6H), 6.2 (s, 1H).

Compound (119)

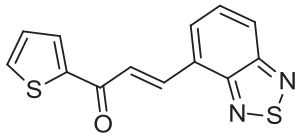

Yield: 40%

Chemical Formula: $C_{13}H_8N_2OS_2$

Exact Mass: 272.01 Da

Molecular Weight: 272.35

MALDI: m/z = 273.10 $(M+H)^+$.

^{1}H NMR (500 MHz, $CDCl_3$, TMS): δ 8.70 (d, J=15.5 Hz, 1H), 8.11 (s, 1H), 8.10 (dt, J=1, 5.3 Hz, 1H), 8.04 (dd, J=1, 3.8 Hz, 1H), 7.81 (d, J=7 Hz, 1H), 7.75 (dd, J=1.2, 4.8 Hz, 1H), 7.68 (dd, J=7, 8.8 Hz, 1H), 7.25 (dd, J=3.8, 4.8 Hz, 1H).

Compound (120)

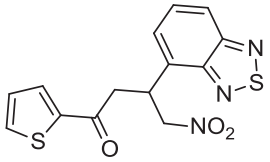

Yield: 50%

Chemical Formula: $C_{14}H_{11}N_3O_3S_2$

Exact Mass: 333.02 Da

Molecular Weight: 333.39

MALDI: m/z = 334.12 $(M+H)^+$.

^{1}H NMR (500 MHz, $CDCl_3$, TMS): δ 7.88 (dd, J=1.4, 8.6 Hz, 1H), 7.67 (dd, J=1.1, 3.7 Hz, 1H), 7.59 (dd, J=1.1, 5 Hz, 1H), 7.50 (m, 2H), 7.05 (dd, J=3.9, 4.9 Hz, 1H), 5.23 (dd, J=8.5, 12.9 Hz, 1H), 5.11 (dd, J=5.9, 12.9 Hz, 1H), 4.75 (p, J=6.9, 13.3 Hz, 1H), 3.74 (qd, J=6.9, 17.4 Hz, 2H).

Benzothiadiazole-Thiophene-Substituted Aza-dipyrromethene (BTZ-T-aza-DIPY) (121)

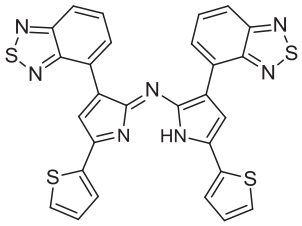

Yield: 10%

Chemical Formula: $C_{28}H_{15}N_7S_4$

Exact Mass: 577.03 Da

Molecular Weight: 577.73

MALDI: m/z = 578.02 $(M+H)^+$.

^{1}H NMR (500 MHz, $CDCl_3$, TMS): δ 8.20 (s, 2H), 7.88 (m, 10H), 7.56 (m, 2H), 6.1 (s, 1H).

Compound (122)

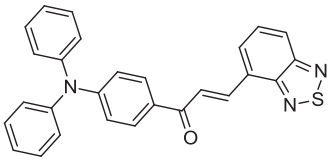

Yield: 40%

Chemical Formula: $C_{27}H_{19}N_3OS$

Exact Mass: 433.12 Da

Molecular Weight: 433.52

MALDI: m/z = 434.14 $(M+H)^+$.

^{1}H NMR (500 MHz, $CDCl_3$, TMS): δ 8.84 (d, J=15.58 Hz, 1H), 8.06 (m, 4H), 7.79 (d, J=6.87 Hz, 1H), 7.67 (dd, J=6.91, 8.81 Hz, 1H), 7.37 (m, 4H), 7.20 (m, 6H), 7.10 (dt, 1.89, 6.93 Hz, 2H)

Compound (123)

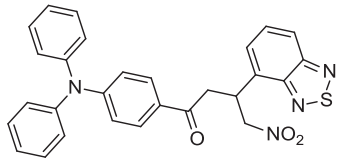

Yield: 45%

Chemical Formula: $C_{28}H_{22}N_4O_3S$

Exact Mass: 494.14 Da

Molecular Weight: 494.56

MALDI: m/z = 495.09 $(M+H)^+$.

^{1}H NMR (500 MHz, $CDCl_3$, TMS): δ 7.93 (dd, J=2.8, 7.2 Hz, 1H), 7.75 (dt, J=2.1, 7.2 Hz, 2H), 7.54 (m, 2H), 7.34 (tt, J=1.7, 6.4 Hz, 4H), 7.15 (tt, J=1.2, 7.4 Hz, 6H), 6.94 (dt, J=2.1, 7.1 Hz, 2H), 5.24 (dd, J=8.7, 12.7 Hz, 1H), 5.11 (dd, J=5.9, 12.7 Hz, 1H), 4.76 (p, J=7.1, 13.6 Hz, 1H), 3.72 (qd, J=6.7, 17.7 Hz, 2H).

Benzothiadiazole-Triphenylamine-Substituted Aza-dipyrromethene (BTZ-TPA-aza-DIPY) (124)

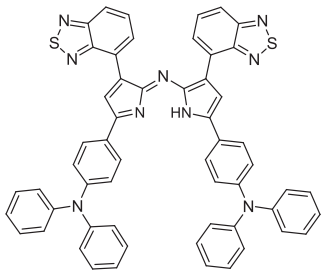

Yield: 7%

Chemical Formula: $C_{56}H_{37}N_9S_2$

Exact Mass: 899.26 Da

Molecular Weight: 900.08

MALDI: m/z = 900.12 $(M+H)^+$.

^{1}H NMR (500 MHz, $CDCl_3$, TMS): δ 8.68 (d, J=1.3 Hz, 2H), 8.12 (m, 6H), 8.08 (d, J=3.2 Hz, 2H), 7.41 (m, 10H), 7.13 (d, J=10.9 Hz, 8H), 6.92 (t, J=3.0, 6.3 Hz, 4H), 6.85 (d, J=3.1 Hz, 4H), 6.00 (s, 1H).

Ethylenedioxythiophene-Substituted BF_2-Aza-dipyrromethene (EDOT-aza-BODIPY) (125)

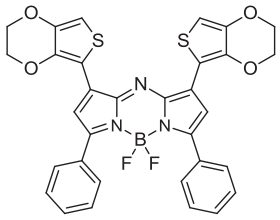

Yield: 50%

Chemical Formula: $C_{32}H_{22}BF_2N_3O_4S_2$

Exact Mass: 625.11 Da

Molecular Weight: 625.47

MALDI: m/z = 626.09 $(M+H)^+$.

^{1}H NMR (500 MHz, THF-d8, TMS): δ ^{1}H NMR (500 MHz, $CDCl_3$, TMS): δ 8.01 (s, 2H), 7.75 (m, 8H), 7.23 (m, 4H), 3.61 (m, 4H), 3.43 (m, 4H).

Compound (128)

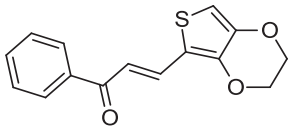

Yield: 60%

Chemical Formula: $C_{15}H_{12}O_3S$

Exact Mass: 272.05 Da

Molecular Weight: 272.32

MALDI: m/z = 273 $(M+H)^+$.

^{1}H NMR (500 MHz, THF-d8, TMS): δ 8.02 (d, J=2.3 Hz, 2H), 7.86 (d, J=6.2 Hz, 1H), 7.53 (m, 3H), 7.37 (d, J=6.8 Hz, 1H), 6.51 (s, 1H), 4.57 (qd, J=1.1, 3.6 Hz, 2H), 4.26 (qd, J=1.1, 3.6 Hz, 2H).

Compound (129)

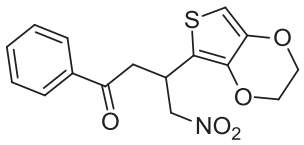

Yield: 50%

Chemical Formula: $C_{16}H_{15}NO_5S$

Exact Mass: 333.07 Da

Molecular Weight: 333.36

MALDI: m/z = 334.06 $(M+H)^+$.

^{1}H NMR (500 MHz, THF-d8, TMS): δ 7.98 (d, J=3.6 Hz, 2H), 7.61 (t, J=2.6 Hz, 1H), 7.50 (t, J=4.2 Hz, 2H), 6.21 (s, 1H), 4.82 (qd, J=1.2, 4.3 Hz, 2H), 4.39 (m, 1H), 4.20 (m, 4H), 3.56 (dd, J=1.3, 4.6 Hz, 1H), 3.48 (dd, J=1.3, 4.6 Hz, 1H).

Ethylenedioxythiophene-Substituted Aza-dipyrromethene (EDOT-aza-DIPY) (130)

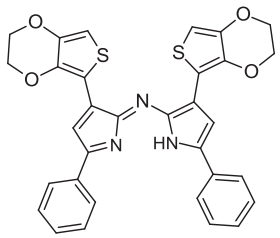

Yield: 10%

Chemical Formula: $C_{32}H_{23}N_3O_4S_2$

Exact Mass: 577.11 Da

Molecular Weight: 577.67

MALDI: m/z = 578.03 $(M+H)^+$.

^{1}H NMR (500 MHz, THF-d8, TMS): δ 7.99 (s, 2H), 7.55 (m, 12H), 6.00 (s, 1H), 3.59 (m, 4H), 3.20 (m, 4H).

Thiophene-Phenothiazine-Substituted BF_2-Aza-dipyrromethene (T-PTZ-aza-BODIPY) (132)

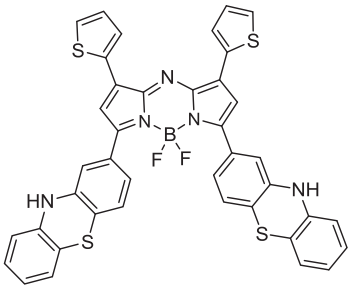

Yield: 20%

Chemical Formula: $C_{40}H_{24}BF_2N_5S_4$

Exact Mass: 751.10 Da

Molecular Weight: 751.72

MALDI: m/z = 752.25 $(M+H)^+$.

Elemental Analysis: C, 64.40; H, 3.00; N, 8.73. Found: C 63.20, H 2.80, N 8.71.

^{1}H NMR (500 MHz, $CDCl_3$, TMS): δ 8.15 (s, 2H), 7.20 (d, J=4.9 Hz, 2H), 7.08 (dd, J=3.2, 4.9 Hz, 2H), 7.00 (m, 8H), 6.85 (m, 3H), 6.70 (s, 2H), 6.56 (m, 3H), 5.93 (m, 2H).

Compound (135)

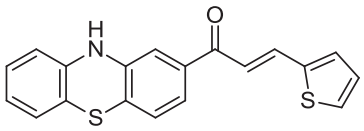

Yield: 54%

Chemical Formula: $C_{19}H_{13}NOS_2$

Exact Mass: 335.04 Da

Molecular Weight: 335.44

MALDI: m/z = 336.11 $(M+H)^+$.

^{1}H NMR (500 MHz, $CDCl_3$, TMS): δ 7.95 (d, J=15.2 Hz, 1H), 7.46 (m, 2H), 7.38 (d, J=3.4 Hz, 1H), 7.26 (d, J=15.5 Hz, 1H), 7.21 (d, J=1.6 Hz, 1H), 7.12 (dd, J=3.7, 5.1 Hz, 1H), 7.07 (d, J=7.9 Hz, 1H), 7.03 (dt, J=1.3, 7.5 Hz, 1H), 6.98 (d, J=7.3 Hz, 1H), 6.86 (dt, J=1.1, 7.2 Hz, 1H), 6.58 (dd, J=1.2, 8 Hz, 1H), 6.00 (s, 1H).

Compound (136)

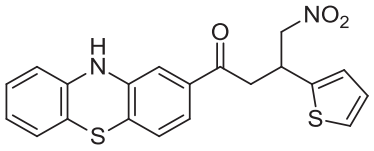

Yield: 45%

Chemical Formula: $C_{20}H_{16}N_2O_3S_2$

Exact Mass: 396.06 Da

Molecular Weight: 396.48

MALDI: m/z = 397.08 $(M+H)^+$.

^{1}H NMR (500 MHz, $CDCl_3$, TMS): δ 7.50 (m, 2H), 7.39 (d, J=4.6 Hz, 1H), 7.28 (d, J=1.5 Hz, 1H), 7.02 (dd, J=3.6, 6.1 Hz, 1H), 6.90 (m, 4H), 6.41 (m, 2H), 5.10 (dd, J=7.7, 11.7 Hz, 1H), 5.05 (dd, J=6.10, 12.2 Hz, 1H), 4.66 (p, J=6.1, 12.4 Hz, 1H), 3.52 (qd, J=7.7, 15.6 Hz, 2H).

Thiophene-Phenothiazine-Substituted Aza-dipyrromethene (T-PTZ-aza-DIPY) (137)

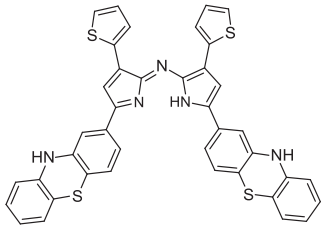

Yield: 9%

Chemical Formula: $C_{40}H_{25}N_5S_4$

Exact Mass: 703.10 Da

Molecular Weight: 703.92

MALDI: m/z = 704.27 $(M+H)^+$.

^{1}H NMR (500 MHz, $CDCl_3$, TMS): δ 8.01 (s, 2H), 7.10 (d, J=3.6 Hz, 2H), 6.92 (dd, J=3.2, 5.1 Hz, 2H), 6.8 (m, 13H), 6.61 (s, 2H), 6.03 (m, 5H).

Thiophene-MethylPyrrole-Substituted BF_2-Aza-dipyrromethene (T-MPy-aza-BODIPY) (139)

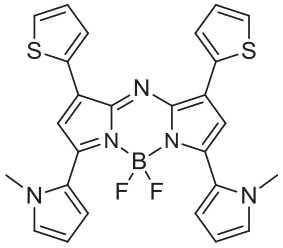

Yield: 60%

Chemical Formula: $C_{26}H_{20}BF_2N_5S_2$

Exact Mass: 515.12 Da

Molecular Weight: 515.41

MALDI: m/z = 516.18 $(M+H)^+$.

^{1}H NMR (500 MHz, THF-d8, TMS): δ 7.81 (d, J=5.2 Hz, 2H), 7.50 (d, J=2.2, 1 Hz, 2H), 7.32 (m, 6H), 6.90 (m, 4H), 4.00 (s, 6H).

Compound (142)

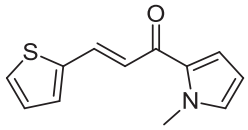

Yield: 40%

Chemical Formula: $C_{12}H_{11}NOS$

Exact Mass: 217.06 Da

Molecular Weight: 217.29

MALDI: m/z =218.18 $(M+H)^+$.

^{1}H NMR (500 MHz, $CDCl_3$, TMS): δ 7.87 (d, J=15.4 Hz, 1H), 7.39 (d, J=5 Hz, 1H), 7.32 (d, J=3.7, 1 Hz, 1H), 7.23 (d, J=15.4 Hz), 7.12 (dd, J=1.6, 4.2 Hz, 1H), 7.09 (dd, J=3.7, 5.1 Hz, 1H), 6.89 (t, J=2 Hz, 1H), 6.22 (dd, J=2.4, 4 Hz, 1H), 4.05 (s, 3H).

Compound (143)

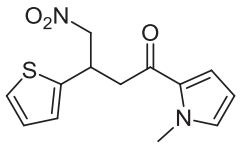

Yield: 40%

Chemical Formula: $C_{13}H_{14}N_2O_3S$

Exact Mass: 278.07 Da

Molecular Weight: 278.33

MALDI: m/z = 279.01 $(M+H)^+$.

^{1}H NMR (500 MHz, $CDCl_3$, TMS): δ 7.26 (d, J=4.1 Hz, 1H), 7.20 (d, J=3.6 Hz, 1H), 7.00 (m, 2H), 6.70 (m, 2H), 5.00 (dd, J=7.6, 12.6 Hz, 1H), 4.91 (dd, J=7.5, 12.2 Hz, 1H), 4.76 (p, J=6.2, 12.2 Hz, 1H), 4.00 (s, 3H), 3.51 (qd, J=7.6, 15.1 Hz, 2H).

Thiophene-MethylPyrrole-Substituted Aza-dipyrromethene (T-MPy-aza-DIPY) (144)

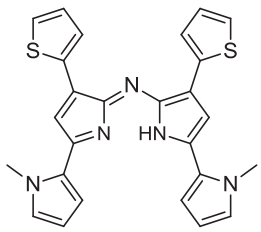

Yield: 10%

Chemical Formula: $C_{26}H_{21}N_5S_2$

Exact Mass: 467.12 Da

Molecular Weight: 467.61

MALDI: m/z = 468.04 $(M+H)^+$.

^{1}H NMR (500 MHz, THF-d8, TMS): δ 7.70 (d, J=4.2 Hz, 2H), 7.42 (d, J=2.2, 1 Hz, 2H), 7.30 (m, 6H), 7.02 (m, 4H), 5.91 (s, 1H), 4.05 (s, 6H).

Thiophene-Carbazole-Substituted BF_2-Aza-dipyrromethene (T-Cz-aza-BODIPY) (145)

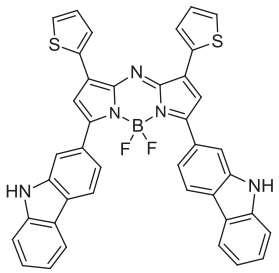

Yield: 35%

Chemical Formula: $C_{40}H_{24}BF_2N_5S_2$

Exact Mass: 687.15 Da

Molecular Weight: 687.59

MALDI: m/z = 688.02 $(M+H)^+$.

Elemental Analysis: C, 69.00; H, 3.90; N, 11.00. Found: C 68.32, H 3.33, N 10.06.

^{1}H NMR (500 MHz, THF-d8, TMS): δ 8.38 (d, J=11.5 Hz, 2H), 7.98 (m, 6H), 7.71 (dd, J=1.5, 8.3 Hz, 2H), 7.62 (qd, J=1.2, 7.3 Hz, 2H), 7.37 (m, 2H), 7.33 (m, 1H), 7.26 (m, 4H), 7.19 (dt, J=1.1, 5 Hz, 3H), 7.05 (s, 2H).

Compound (147)

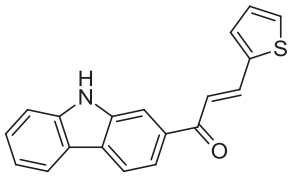

Yield: 46%

Chemical Formula: $C_{19}H_{13}NOS$

Exact Mass: 303.07 Da

Molecular Weight: 303.38

MALDI: m/z = 304.15 $(M+H)^+$.

^{1}H NMR (500 MHz, $CDCl_3$, TMS): δ 8.30 (t, J=9.7 Hz, 1H), 8.22 (dd, J=8.7, 17.9 Hz, 3H), 8.00 (t, J=7.2 Hz, 1H), 7.88 (d, J=8.2 Hz, 1H), 7.65 (m, 3H), 7.49 (dd, J=6.5, 13.6 Hz, 1H), 7.24 (m, 2H), 5.64 (s, 1H).

Compound (148)

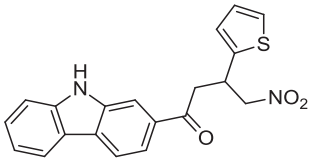

Yield: 60%

Chemical Formula: $C_{20}H_{16}N_2O_3S$

Exact Mass: 364.09 Da

Molecular Weight: 364.42

MALDI: m/z = 365.12 $(M+H)^+$.

^{1}H NMR (500 MHz, THF-d8, TMS): δ 8.10 (t, J=10.1 Hz, 1H), 7.70 (d, J=6.2 Hz, 1H), 7.55 (m, 8H), 6.81 (s, 1H), 5.11 (dd, J=5.1, 8.3 Hz, 1H), 5.12 (dd, J=6.0, 8.6 Hz, 1H), 4.45 (m, 1H), 3.91 (qd, J=5.1, 12.2 Hz, 2H).

Thiophene-Carbazole-Substituted Aza-dipyrromethene (T-Cz-aza-DIPY) (149)

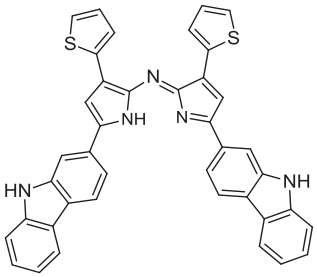

Yield: 10%

Chemical Formula: $C_{40}H_{25}N_5S_2$

Exact Mass: 639.16 Da

Molecular Weight: 639.79

MALDI: m/z = 640.16 $(M+H)^+$.

^{1}H NMR (500 MHz, THF-d8, TMS): δ 8.30 (d, J=11.1 Hz, 2H), 8.00 (m, 6H), 7.61 (m, 4H), 7.31 (m, 6H), 7.19 (dt, J=1.1, 5 Hz, 3H), 7.10 (s, 2H), 6.3 (s, 1H).

Fluorenone-Substituted BF_2-Aza-dipyrromethene (FN-aza-BODIPY) (150)

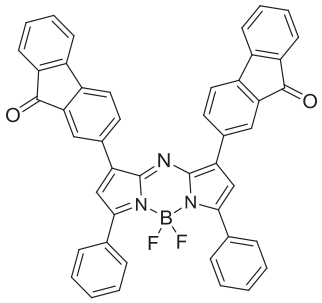

Yield: 31%

Chemical Formula: $C_{46}H_{26}BF_2N_3O_2$

Exact Mass: 701.21 Da

Molecular Weight: 701.53

MALDI-MS: m/z = 702.23 $(M+H)^+$.

^{1}H NMR (500 MHz, $CDCl_3$, TMS): δ 8.00 (d, J=1.2 Hz, 2H), 7.75 (d, J=6.2 Hz, 5H), 7.05 (m, 14H), 6.8 (m, 5H).

Thiophene-Fluorenone-Substituted BF_2-Aza-dipyrromethene (T-FN-aza-BODIPY) (151)

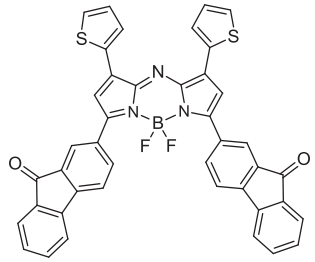

Yield: 65%

Chemical Formula: $C_{42}H_{22}BF_2N_3O_2S_2$

Exact Mass: 713.12 Da

Molecular Weight: 713.58

MALDI and ^{13}C NMR: these measurements were not reliable in terms of supporting evidence of purity and structure.

^{1}H NMR (500 MHz, $CDCl_3$, TMS): δ 7.90 (m, 2H), 7.56 (dd, J=4.2, 8.2 Hz, 6H), 7.38 (m, 2H), 7.10 (dd, J=2.3, 6.2 Hz, 8H), 6.90 (m, 4H).

Compound (157)

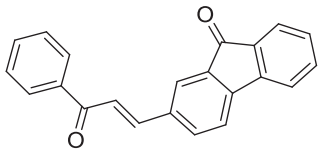

Yield: 28%

Chemical Formula: $C_{22}H_{14}O_2$

Exact Mass: 310.10 Da

Molecular Weight: 310.35

MALDI: m/z = 311.22 $(M+H)^+$.

^{1}H NMR (500 MHz, $CDCl_3$, TMS): δ 8.08 (m, 2H), 8.04 (d, J=1.6 Hz, 1H), 7.85 (d, J=15.4 Hz, 1H), 7.74 (dd, J=1, 7.6 Hz, 1H), 7.60 (m, 7H), 7.38 (dt, J=1.23, 7.6 Hz, 1H).

Compound (158)

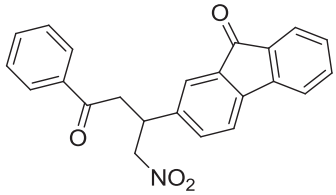

Yield: 56%

Chemical Formula: $C_{23}H_{17}NO_4$

Exact Mass: 371.12 Da

Molecular Weight: 371.39

MALDI: m/z = 372.02 $(M+H)^+$.

^{1}H NMR (500 MHz, $CDCl_3$, TMS): δ 7.95 (m, 2H), 7.68 (dd, J=1, 6.3 Hz, 1H), 7.61 (dt, J=1.5, 7.5 Hz, 2H), 7.51 (m, 6H), 7.32 (dt, J=2.2, 6.2 Hz, 1H), 4.87 (dd, J=6.4, 12.6 Hz, 1H), 4.72 (dd, J=8.3, 13.1 Hz, 1H), 4.31 (p, J=6.9, 13.8 Hz, 1H), 3.50 (qd, J=6.7, 17.6 Hz, 2H).

Fluorenone-Substituted Aza-dipyrromethene (FN-aza-DIPY) (159)

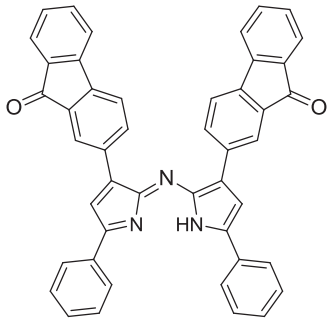

Yield: 5%

Chemical Formula: $C_{46}H_{27}N_3O_2$

Exact Mass: 653.21 Da

Molecular Weight: 653.73

MALDI: m/z = 654.03 $(M+H)^+$.

^{1}H NMR (500 MHz, $CDCl_3$, TMS): δ 7.75 (d, J=1.3 Hz, 2H), 7.56 (d, J=2.4 Hz, 4H), 7.15 (m, 14H), 6.9 (m, 4H), 6.75 (d, J=3.6 Hz, 2H), 6.1 (s, 1H).

Compound (160)

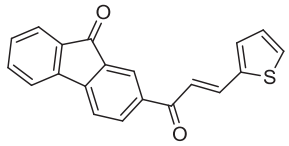

Yield: 46%

Chemical Formula: $C_{20}H_{12}O_2S$

Exact Mass: 316.06 Da

Molecular Weight: 316.37

MALDI: m/z = 317.05 $(M+H)^+$.

^{1}H NMR (500 MHz, $CDCl_3$, TMS): δ 8.31 (d, J=1.3 Hz), 8.26 (dd, J=1.6, 7.7 Hz, 1H), 8.03 (d, J=15.3 Hz, 1H), 7.72 (m, 3H), 7.59 (dt, J=1.2, 7.6 Hz, 1H), 7.50 (d, J=5 Hz, 1H), 7.40 (m, 3H), 7.14 (dd, J=3.6, 5 Hz, 1H).

Compound (161)

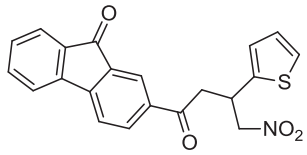

Yield: 60%

Chemical Formula: $C_{21}H_{15}NO_4S$

Exact Mass: 377.07 Da

Molecular Weight: 377.41

MALDI: m/z = 378.17 $(M+H)^+$.

^{1}H NMR (500 MHz, $CDCl_3$, TMS): δ 8.19 (d, J=1.2 Hz, 1H), 8.16 (dd, J=1.8, 7.9 Hz, 1H), 7.75 (dt, J=1, 6.5 Hz, 1H), 7.64 (t, J=8 Hz, 2H), 7.58 (dt, J=1.1, 7.5 Hz, 1H), 7.42 (dt, J=1.1, 7.5 Hz, 1H), 7.24 (dd, J=1.1, 5 Hz, 1H), 7.01 (d, J=3.2 Hz, 1H), 6.97 (dd, J=3.5, 5.1 H, 1H), 4.90 (dd, J=6.4, 12.5 Hz, 1H), 4.76 (dd, J=7.7, 12.9 Hz, 1H), 4.59 (p, J=6.9, 13.7 Hz, 1H), 3.55 (qd, J=5.9, 17.4 Hz, 2H).

Thiophene-Fluorenone-Substituted Aza-dipyrromethene (T-FN-aza-DIPY) (162)

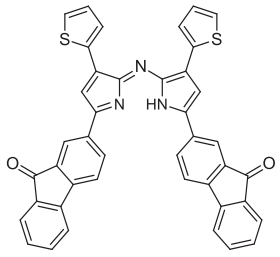

Yield: 15%

Chemical Formula: $C_{42}H_{23}N_3O_2S_2$

Exact Mass: 665.12 Da

Molecular Weight: 665.78

MALDI: m/z = 666.10 $(M+H)^+$.

^{1}H NMR (500 MHz, $CDCl_3$, TMS): δ 7.72 (m, 2H), 7.56 (dd, J=4.2, 9.2 Hz, 6H), 7.38 (t, J=2.3 Hz, 2H), 7.15 (dd, J=2.3, 6.1 Hz, 8H), 6.81 (m, 4H), 6.62 (s, 1H).

Compound (165)

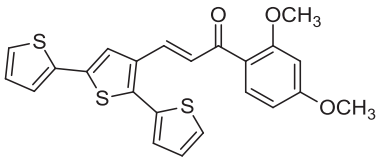

Yield: 50%

Chemical Formula: $C_{23}H_{18}O_3S_3$

Exact Mass: 438.04 Da

Molecular Weight: 438.58

MALDI: m/z = 439.05 $(M+H)^+$.

^{1}H NMR (500 MHz, $CDCl_3$, TMS): δ 7.70 (s, 1H), 7.51 (m, 5H), 7.32 (m, 4H), 7.10 (dd, J=1.3, 3.2 Hz, 1H), 7.00 (m, 1H), 3.82 (s, 6H).

Compound (166)

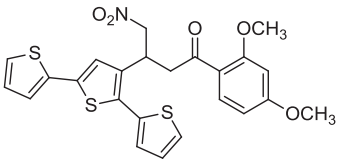

Yield: 57%

Chemical Formula: $C_{24}H_{21}NO_5S_3$

Exact Mass: 499.06 Da

Molecular Weight: 499.62

MALDI-MS: m/z = 500.10 $(M+H)^+$.

^{1}H NMR (500 MHz, $CDCl_3$, TMS): δ 7.71 (d, J=2.2, Hz, 2H), 7.26 (m, 5H), 7.00 (s, 1H), 6.83 (3H), 4.64 (m, 2H), 4.50 (m, 1H), 3.87 (s, 3H), 3.80 (s, 6H), 3.35 (m, 2H).

Terthiophene-Substituted Aza-dipyrromethene (TT-aza-DIPYs) (167)

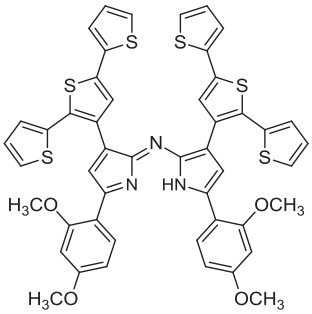

Chemical Formula: $C_{48}H_{35}N_3O_4S_6$

Exact Mass: 909.10 Da

Molecular Weight: 910.20

MALDI: m/z = 910.03 $(M+H)^+$.

^{1}H NMR (500 MHz, $CDCl_3$, TMS): Not Possible.

Compound (169)

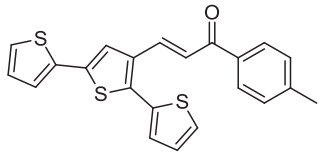

Yield: 48%

Chemical Formula: $C_{22}H_{16}OS_3$

Exact Mass: 392.04 Da

Molecular Weight: 392.56

MALDI: m/z = 393.02 $(M+H)^+$.

^{1}H NMR (500 MHz, THF-d8, TMS): δ 7.71 (s, 1H), 7.45 (m, 6H), 7.10 (d, J=1.2, 5.2 Hz, 1H), 7.00 (m, 5H), 3.80 (s, 3H).

Compound (170)

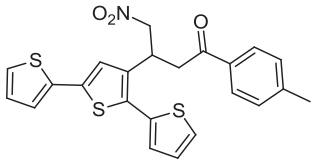

Yield: 40%

Chemical Formula: $C_{23}H_{19}NO_3S_3$

Exact Mass: 453.05 Da

Molecular Weight: 453.60

MALDI: m/z = 454.01 $(M+H)^+$.

^{1}H NMR (500 MHz, THF-d8, TMS): δ 7.69 (s, 1H), 7.50 (m, 6H), 7.32 (m, 4H), 4.54 (m, 3H), 3.72 (s, 3H), 3.40 (m, 2H).

Compound (172)

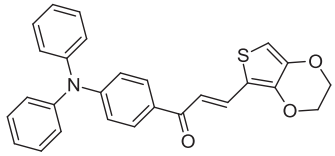

Yield: 45%

Chemical Formula: $C_{27}H_{21}NO_3S$

Exact Mass: 439.12 Da

Molecular Weight: 439.53

MALDI: m/z = 440.13 $(M+H)^+$.

^{1}H NMR (500 MHz, $CDCl_3$, TMS): δ 7.89 (dt, J=2, 6.9 Hz, 2H), 7.84 (d, J=15.4 Hz, 1H), 7.37 (s, 1H), 7.33 (m, 5H), 7.17 (m, 6H), 7.04 (dt, J=2, 6.9 Hz, 2H), 4.35 (p, J=2.4, 3.8 Hz, 2H), 4.25 (p, J=1.8, 4.2 Hz, 2H).

Compound (173)

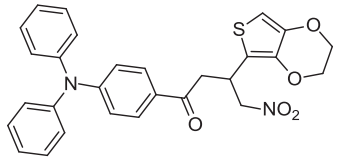

Yield: 35%

Chemical Formula: $C_{28}H_{24}N_2O_5S$

Exact Mass: 500.14 Da

Molecular Weight: 500.57

MALDI: m/z = 501.09 $(M+H)^+$.

^{1}H NMR (500 MHz, $CDCl_3$, TMS): δ 7.81 (d, J=3.6, 2H), 7.37 (m, 4H), 7.19 (m, 6H), 6.99 (d, J=2.4, 2H), 6.31 (s, 1H), 4.82 (m, 2H), 4.35 (dt, J=1.2, 4.1, 1H), 4.2 (m, 4H), 3.52 (m, 2H).

Ethylenedioxythiophene-triphenylamine-substituted Aza-dipyrromethene (EDOT-TPA-aza-DIPY) (174)

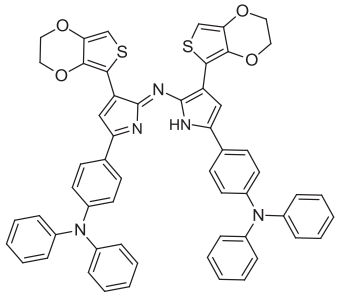

Chemical Formula: $C_{56}H_{41}N_5O_4S_2$

Exact Mass: 911.26 Da

Molecular Weight: 912.09

MALDI: m/z = 912.05 $(M+H)^+$.

^{1}H NMR (500 MHz, THF-d8, TMS): Not Possible.

Compound (175)

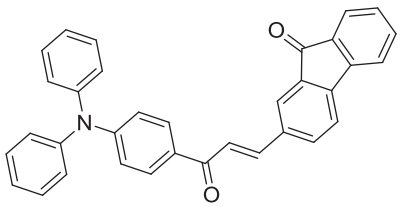

Yield: 35%

Chemical Formula: $C_{34}H_{23}NO_2$

Exact Mass: 477.17 Da

Molecular Weight: 477.55

MALDI: m/z = 478.08 $(M+H)^+$.

^{1}H NMR (500 MHz, $CDCl_3$, TMS): δ 8.02 (d, J=1.5 Hz, 1H), 7.96 (dt, J=2, 7 Hz, 2H), 7.83 (d, J=15.5 Hz, 1H), 7.72 (m, 2H), 7.60 (m, 4H), 7.37 (tt, J=2, 7 Hz, 5H), 7.19 (m, 6H), 7.07 (dt, J=2, 7 Hz, 2H).

Compound (176)

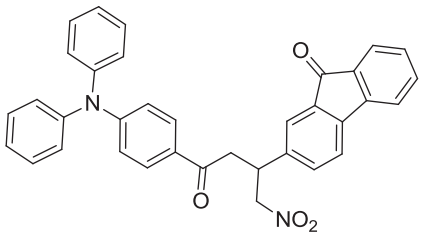

Yield: 38%

Chemical Formula: $C_{35}H_{26}N_2O_4$

Exact Mass: 538.19 Da

Molecular Weight: 538.59

MALDI: m/z = 539.08 $(M+H)^+$.

^{1}H NMR (500 MHz, $CDCl_3$, TMS): δ 7.77 (dt, J=2, 7 Hz, 2H), 7.67 (dt, J=1, 6.5 Hz, 1H), 7.60 (d, J=1.4 Hz, 1H), 7.50 (m, 4H), 7.34 (m, 5H), 7.17 (m, 6H), 6.97 (dt, J=1.8, 7 Hz, 2H), 4.87 (dd, J=6.2, 12.7 Hz, 1H), 4.7 (dd, J=8.5, 12.7 Hz, 1H), 4.29 (p, J=6.5, 14 Hz, 1H), 3.38 (qd, J=7, 17.7 Hz, 2H).

Compound (178)

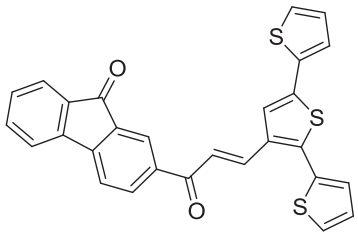

Yield: 47%

Chemical Formula: $C_{28}H_{16}O_2S_3$

Exact Mass: 480.03 Da

Molecular Weight: 480.62

MALDI: m/z = 481.03 $(M+H)^+$.

^{1}H NMR (500 MHz, $CDCl_3$, TMS): δ 8.34 (d, J=1.4 Hz, 1H), 8.27 (dd, J=1.7, 7.8 Hz, 1H), 8.11 (d, J=15.6 Hz, 1H), 7.77 (d, J=7.3 Hz, 1H), 7.71 (dd, J=0.7, 7.9 Hz, 1H), 7.66 (m, 1H), 7.59 (dt, J=1.2, 7.6 Hz, 1H), 7.54 (s, 1H), 7.45 (m, 3H), 7.35 (dd, J=1, 5 Hz, 1H), 7.31 (dd, J=1, 3.6 Hz, 1H), 7.26 (dd, J=1.2, 3.5 Hz, 1H), 7.17 (dd, J=3.6, 5.2 Hz, 1H), 7.11 (dd, J=3.6, 5.2 Hz, 1H).

Compound (179)

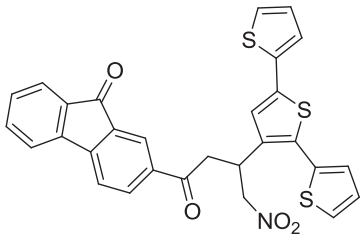

Yield: 40%

Chemical Formula: $C_{29}H_{19}NO_4S_3$

Exact Mass: 541.05 Da

Molecular Weight: 541.66

MALDI: m/z = 542.03 $(M+H)^+$.

^{1}H NMR (500 MHz, $CDCl_3$, TMS): δ 8.18 (d, J=1.3 Hz, 1H), 8.13 (dd, J=1.6, 7.8 Hz, 1H), 7.75 (d, J=7.3 Hz, 1H), 7.64 (d, J=7.6 Hz, 2H), 7.58 (dd, J=1.2, 7.5 Hz, 1H), 7.42 (dt, J=1, 7.5 Hz, 2H), 7.27 (m, 2H), 7.19 (dd, J=1.2, 3.7 Hz, 1H), 7.14 (dd, J=3.6, 5.2 Hz, 1H), 7.08 (s, 1H), 7.04 (dd, J=3.7, 5.2 Hz, 1H), 4.85 (dd, J=6.8, 12.5 Hz, 1H), 4.76 (dd, J=7.3, 12.7 Hz, 1H), 4.67 (p, J=7, 13.5 Hz, 1H), 3.50 (qd, J=7.5, 17.6 Hz, 2H).

Compound (181)

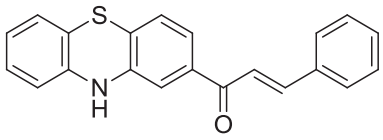

Yield: 35%

Chemical Formula: $C_{21}H_{15}NOS$

Exact Mass: 329.09 Da

Molecular Weight: 329.41

MALDI: m/z = 330.13 $(M+H)^+$.

^{1}H NMR (500 MHz, $CDCl_3$, TMS): δ 7.82 (d, J=15.2 Hz, 1H), 7.67 (d, J=3.6 Hz, 1H), 7.65 (d, J=2.2 Hz, 1H), 7.55 (dd, J=1.7, 8.1 Hz, 1H), 7.52 (s, 1H), 7.49 (d, J=13.8 Hz, 1H), 7.44 (m, 3H), 7.19 (m, 2H), 7.12 (dd, J=1.4, 7.6 Hz, 1H), 6.95 (dd, J=1.1, 7.4 Hz, 1H), 6.90 (m, 1H), 6.63 (s, 1H).

Compound (184)

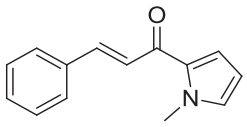

Yield: 40%

Chemical Formula: $C_{14}H_{13}NO$

Exact Mass: 211.10 Da

Molecular Weight: 211.26

MALDI: m/z = 212.04 $(M+H)^+$.

^{1}H NMR (500 MHz, THF-d8, TMS): δ 7.77 (d, J=15.7 Hz, 1H), 7.64 (dd, J=1.6, 7.7 Hz, 2H), 7.43 (m, 4H), 7.14 (dd, J=1.6, 4.1 Hz, 1H), 6.90 (t, J=1.8 Hz, 1H), 6.23 (dd, J=2.5, 4.1 Hz, 1H), 4.06 (s, 3H).

Compound (187)

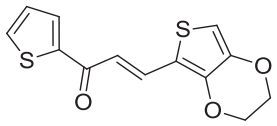

Yield: 15%

Chemical Formula: $C_{13}H_{10}O_3S_2$

Exact Mass: 278.01 Da

Molecular Weight: 278.35

MALDI: m/z = 279.04 $(M+H)^+$.

^{1}H NMR (500 MHz, $CDCl_3$, TMS): δ 7.95 (s, 1H), 7.76 (d, J=14.6, 1H), 7.28 (m, 4H), 4.50 (qd, J=1.2, 2.8 Hz, 2H), 4.33 (qd, J=1.2, 2.7 Hz, 2H).

Compound (188)

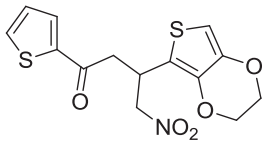

Yield: 9%

Chemical Formula: $C_{14}H_{13}NO_5S_2$

Exact Mass: 339.02 Da

Molecular Weight: 339.39

MALDI: m/z = 340.10 $(M+H)^+$.

^{1}H NMR (500 MHz, $CDCl_3$, TMS): 7.85 (s, 1H), 7.40 (m, 3H), 4.51 (qd, J=1.2, 2.6 Hz, 2H), 4.33 (qd, J=1.2, 2.7 Hz, 2H), 4.21 (m, 5H).

Compound TT1 (190)

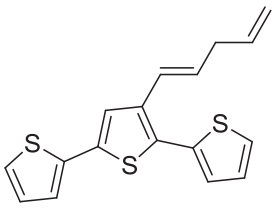

Yield: 48%

Chemical Formula: $C_{17}H_{14}S_3$

Exact Mass: 314.03 Da

Molecular Weight: 314.49

MALDI: m/z = 315.02 $(M+H)^+$.

^{1}H NMR (500 MHz, THF-d_8, TMS): δ 7.68 (s, 1H), 7.43 (dd, J=5, 1.2 Hz, 1H), 7.21 (m, 6H), 6.8 (dt, J=16, 5.5 Hz, 1H), 6.33 (m, 3H), 4.8 (m, 2H).

Compound TT2 (191)

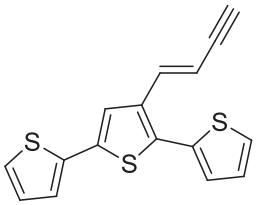

Yield: 65%

Chemical Formula: $C_{16}H_{10}S_3$

Exact Mass: 297.99 Da

Molecular Weight: 298.45

MALDI: m/z = 299 $(M+H)^+$.

^{1}H NMR (500 MHz, THF-d_8, TMS): δ 7.88 (s, 1H), 7.70 (dd, J=5.2, 2 Hz, 1H), 7.41 (m, 4H), 7.19 (dd, J=5.5, 3 Hz, 1H), 7.08 (m, 2H), 2.08 (s, 1H).

Compound TT3 (192)

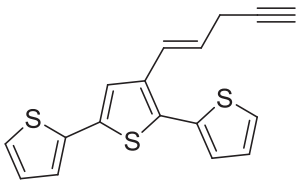

Yield: 52%

Chemical Formula: $C_{17}H_{12}S_3$

Exact Mass: 312.01 Da

Molecular Weight: 312.47

MALDI: m/z = 313.04 $(M+H)^+$.

^{1}H NMR (500 MHz, THF-d_8, TMS): δ 7.78 (s, 1H), 7.47 (dd, J=5.2, 1.2 Hz, 1H), 7.16 (m, 4H), 7.01 (dd, J=6.5, 4.8 Hz, 1H), 6.6 (m, 2H), 2.1 (s, 1H), 1.8 (d, J=6 Hz, 2H).

Compound TT4 (193)

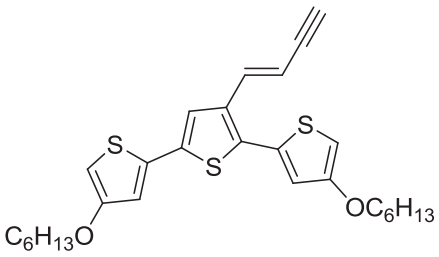

Yield: 67%

Chemical Formula: $C_{28}H_{34}O_2S_3$

Exact Mass: 498.17 Da

Molecular Weight: 498.76

MALDI: m/z = 499.12 $(M+H)^+$.

^{1}H NMR (500 MHz, THF-d_8, TMS): δ 7.56 (s, 1H), 7.1 (m, 5H), 6.29 (dd, J=5, 2.1 Hz, 1H), 4.2 (s, 1H), 3.5 (m, 26H).

Compound (234)

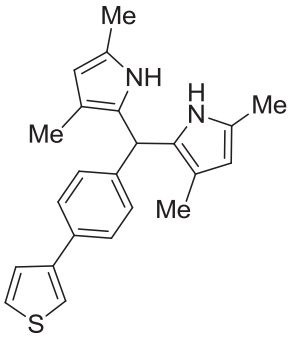

Yield: 60%

Chemical Formula: $C_{23}H_{24}N_2S$

Exact Mass: 360.17 Da

Molecular Weight: 360.52

MALDI: m/z = 361.01 $(M+H)^+$.

^{1}H NMR (500 MHz, THF-d8, TMS): δ 7.61 (s, 1H), 7.50 (m, 6H), 7.21 (s, 2H), 5.80 (s, 2H), 3.35 (m, 6H), 2.9 (m, 6H).

Compound (235)

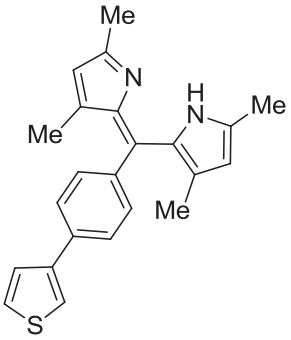

Yield: 78%

Chemical Formula: $C_{23}H_{22}N_2S$

Exact Mass: 358.15 Da

Molecular Weight: 358.50

MALDI: m/z = 359.01 $(M+H)^+$.

^{1}H NMR (500 MHz, THF-d8, TMS): δ 7.77 (s, 1H), 7.60 (m, 4H), 7.47 (m, 2H), 7.21 (s, 2H), 5.70 (s, 1H), 3.12 (m, 12H).

Compound (236)

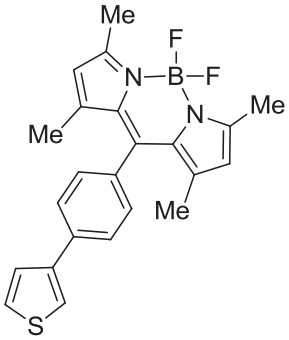

Yield: 70%

Chemical Formula: $C_{23}H_{21}BF_2N_2S$

Exact Mass: 406.15 Da

Molecular Weight: 406.30

MALDI: m/z = 407.09 $(M+H)^+$.

^{1}H NMR (500 MHz, THF-d8, TMS): δ 7.78 (s, 1H), 7.50 (m, 6H), 7.21 (s, 2H), 3.30 (m, 12H).

Compound (238)

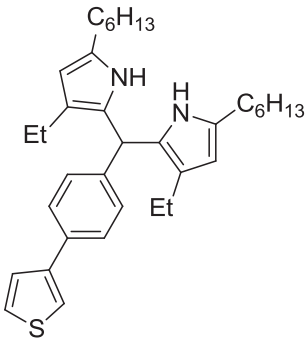

Yield: 37%

Chemical Formula: $C_{35}H_{48}N_2S$

Exact Mass: 528.35 Da

Molecular Weight: 528.83

MALDI-MS: m/z = 529.12 $(M+H)^+$.

^{1}H NMR (500 MHz, $CDCl_3$, TMS): Not possible.

2.39.2 Crystal data and structure refinement for compound (87)

All aspects of data collection, reduction, solution and refinement were performed using SHELXS97 (*Sheldrick, G. M. SHELXS97. program for the Solution of Crystal Structures. University of Göttingen: Göttingen, Germany, 1997*).

Table 2.2 Crystal data and structure refinement for compound (87).

Empirical formula	C44 H26 B F2 N3 S6	
Formula weight	837.85	
Temperature	426(2) K	
Wavelength	1.54178 Å	
Space group	P2(1)/c	
Unit cell dimensions	a= 14.0473(3) Å	α= 90°.
	b= 13.1343(2) Å	β= 96.707(7)°.
	c= 20.9339(15) Å	γ= 90°.
Volume	3835.9(3) $Å^3$	
Z	4	
Density (calculated)	1.451 Mg/m^3	
Absorption coefficient	3.686 mm^{-1}	
F(000)	1720	
Theta range for data collection	6.54 to 54.24°	
Index ranges	-14<=h<=14, -13<=k<=13, -22<=l<=22	
Reflections collected	35178	
Independent reflections	4668 [R(int) = 0.0533]	
Refinement method	SHELXL-97 (Sheldrick, 1997).	
Data / restraints / parameters	4668 / 282 / 506	
Goodness-of-fit	1.744	
Final R indices [I>2sigma(I)]	R1 = 0.1017, wR2 = 0.3543	
R indices (all data)	R1 = 0.1083, wR2 = 0.3678	
Largest diff. peak and hole	1.722 and -0.973 $e.Å^{-3}$	

Table 2.3 Atomic coordinates and equivalent isotropic displacement parameters ($Å^2$) for compound (87). U(eq) is defined as one third of the trace of the orthogonalized U^{ij} tensor.

	x	y	z	U(eq)
C50	0.7684(4)	-0.1834(4)	0.0549(3)	0.0379(16)
H50	0.728	-0.209	0.0832	0.046
C51	0.7459(4)	0.2917(4)	-0.0196(2)	0.0241(13)
H51	0.7218	0.2506	0.0135	0.029
C52	0.5311(3)	0.7023(3)	0.0719(2)	0.0095(11)
H52	0.556	0.7421	0.0386	0.011
C45	0.3745(6)	0.2554(10)	0.1099(5)	0.090(3)
H45	0.3084	0.2586	0.1099	0.108
C44	0.4359(9)	0.3404(10)	0.1238(5)	0.107(5)
H44	0.4146	0.4057	0.1318	0.129
C42	0.5382(5)	0.2029(6)	0.1022(3)	0.0488(18)
C46	0.7851(4)	-0.0733(4)	0.0366(3)	0.0387(16)
C43	0.5358(3)	0.3130(3)	0.1239(2)	0.0165(12)
H43	0.5696	0.3205	0.1668	0.02
C40	0.8321(6)	-0.2386(6)	0.0167(5)	0.069(2)
H40	0.8381	-0.309	0.0192	0.083
C39	0.8803(7)	-0.1848(7)	-0.0212(4)	0.069(2)
H39	0.9203	-0.2138	-0.0485	0.083
S7	0.86373(18)	-0.05972(18)	-0.01600(11)	0.0790(9)
C20	0.7818(4)	0.0910(5)	0.1037(3)	0.0350(15)
C19	0.7152(4)	0.1657(5)	0.1200(3)	0.0395(16)
H19	0.7324	0.2224	0.1453	0.047
C21	0.7394(4)	0.0140(5)	0.0647(3)	0.0364(16)
C18	0.6213(4)	0.1446(5)	0.0940(3)	0.0445(18)
S1	0.61785(11)	0.03450(13)	0.04743(8)	0.0452(7)
S2	0.67167(11)	0.51018(13)	0.03681(8)	0.0452(7)
S3	0.92392(15)	0.36570(16)	-0.01026(10)	0.0646(8)

S4	0.42716(17)	0.1588(2)	0.09498(15)	0.0962(10)
N1	0.8986(3)	0.2773(4)	0.1354(2)	0.0341(13)
F2	1.1856(3)	0.2458(3)	0.1794(2)	0.0590(12)
F1	1.1028(3)	0.2377(3)	0.26585(18)	0.0558(12)
N3	1.0481(3)	0.3514(3)	0.1792(2)	0.0295(12)
N4	1.0287(3)	0.1619(4)	0.1690(2)	0.0309(12)
C31	0.9336(4)	0.1835(4)	0.1449(3)	0.0328(15)
C1	1.1804(4)	0.4776(5)	0.2069(3)	0.0366(16)
C28	1.0070(4)	0.5170(5)	0.1599(3)	0.0348(15)
H28	1.0111	0.5876	0.1587	0.042
C27	1.0825(5)	0.4484(5)	0.1839(3)	0.0353(15)
C30	0.9542(4)	0.3565(4)	0.1509(3)	0.0318(15)
C29	0.9268(4)	0.4591(4)	0.1387(3)	0.0337(15)
C2	1.2339(5)	0.4343(5)	0.2604(3)	0.0415(16)
H2	1.2075	0.3826	0.2831	0.05
C32	0.8834(4)	0.0945(5)	0.1285(3)	0.0358(16)
C34	1.0373(4)	0.0581(5)	0.1659(3)	0.0347(16)
C33	0.9492(5)	0.0148(5)	0.1415(3)	0.0379(16)
H33	0.9366	-0.0542	0.1352	0.045
C17	0.7834(4)	0.4535(5)	0.0551(3)	0.0387(16)
C15	0.7777(4)	0.5690(4)	0.1374(3)	0.0382(16)
H15	0.8006	0.6032	0.175	0.046
C22	0.8111(5)	0.3759(5)	0.0100(3)	0.0418(17)
C7	1.1227(4)	-0.0036(5)	0.1870(3)	0.0359(16)
C6	1.2232(5)	0.5554(5)	0.1734(3)	0.0480(18)
H6	1.1882	0.5864	0.1383	0.058
C16	0.8316(4)	0.4939(5)	0.1089(3)	0.0364(16)
C14	0.6894(4)	0.5867(5)	0.1050(3)	0.0389(16)
C12	1.1070(5)	-0.1074(5)	0.2071(3)	0.0425(17)
H12	1.0448	-0.1312	0.208	0.051
C3	1.3262(5)	0.4680(5)	0.2798(3)	0.0465(18)

H3	1.3608	0.4398	0.3162	0.056
C11	1.1827(5)	-0.1701(5)	0.2249(3)	0.0466(18)
H11	1.1718	-0.2372	0.2364	0.056
C10	1.2744(6)	-0.1356(5)	0.2259(3)	0.052(2)
H10	1.3255	-0.1787	0.2392	0.063
C8	1.2175(5)	0.0259(5)	0.1880(4)	0.054(2)
H8	1.2304	0.0916	0.1748	0.065
C9	1.2921(5)	-0.0360(6)	0.2073(4)	0.064(2)
H9	1.3547	-0.0125	0.2081	0.076
B1	1.0968(5)	0.2473(5)	0.1993(3)	0.0326(17)
C4	1.3672(5)	0.5426(6)	0.2460(4)	0.057(2)
H4	1.4294	0.5642	0.2593	0.069
C5	1.3161(5)	0.5858(5)	0.1921(4)	0.059(2)
H5	1.3444	0.635	0.1686	0.07
C25	0.8972(6)	0.2630(6)	-0.0548(4)	0.059(2)
H25	0.942	0.23	-0.0769	0.071
C24	0.8075(7)	0.2314(6)	-0.0567(4)	0.071(3)
H24	0.7851	0.1744	-0.0802	0.085
S6	0.61005(19)	0.6919(2)	0.19683(16)	0.0970(10)
C36	0.6155(4)	0.6553(5)	0.1237(3)	0.0447(17)
C38	0.4862(5)	0.7699(6)	0.1223(5)	0.074(3)
H38	0.4348	0.8129	0.1099	0.089
C37	0.5240(6)	0.7637(7)	0.1834(6)	0.077(3)
H37	0.4998	0.8005	0.2159	0.092

Table 2.4 Bond lengths [Å] for compound (87).

C50-C40	1.461(10)
C50-C46	1.522(8)
C51-C24	1.462(11)
C51-C22	1.521(8)
C52-C38	1.567(11)
C52-C36	1.630(8)
C45-C44	1.420(15)
C45-S4	1.519(11)
C44-C43	1.448(12)
C42-C18	1.423(9)
C42-C43	1.518(9)
C42-S4	1.654(7)
C46-C21	1.469(8)
C46-S7	1.657(7)
C40-C39	1.309(12)
C39-S7	1.664(9)
C20-C21	1.390(9)
C20-C19	1.424(8)
C20-C32	1.462(8)
C19-C18	1.394(9)
C21-S1	1.725(6)
C18-S1	1.741(7)
S2-C14	1.739(6)
S2-C17	1.739(6)
S3-C25	1.658(8)
S3-C22	1.694(7)
N1-C30	1.318(7)
N1-C31	1.333(7)
F2-B1	1.362(8)
F1-B1	1.392(8)

N3-C27	1.363(7)
N3-C30	1.384(7)
N3-B1	1.563(8)
N4-C34	1.371(7)
N4-C31	1.400(7)
N4-B1	1.560(8)
C31-C32	1.387(8)
C1-C2	1.394(9)
C1-C6	1.413(9)
C1-C27	1.454(9)
C28-C29	1.388(8)
C28-C27	1.438(8)
C30-C29	1.417(8)
C29-C16	1.480(8)
C2-C3	1.386(10)
C32-C33	1.401(9)
C34-C33	1.403(9)
C34-C7	1.472(8)
C17-C16	1.352(8)
C17-C22	1.472(9)
C15-C14	1.363(8)
C15-C16	1.417(9)
C7-C8	1.385(9)
C7-C12	1.451(9)
C6-C5	1.376(9)
C14-C36	1.463(9)
C12-C11	1.363(9)
C3-C4	1.375(10)
C11-C10	1.363(10)
C10-C9	1.396(11)
C8-C9	1.351(10)

C4-C5	1.386(11)
C25-C24	1.322(12)
S6-C37	1.533(9)
S6-C36	1.616(8)
C38-C37	1.328(13)

Table 2.5 Bond angles [°] for compound (87).

C40-C50-C46	102.2(6)
C24-C51-C22	104.2(6)
C38-C52-C36	94.9(5)
C44-C45-S4	113.6(7)
C45-C44-C43	111.7(8)
C18-C42-C43	126.6(6)
C18-C42-S4	125.4(6)
C43-C42-S4	107.9(4)
C21-C46-C50	123.5(5)
C21-C46-S7	122.6(5)
C50-C46-S7	113.8(4)
C44-C43-C42	107.0(7)
C39-C40-C50	117.2(7)
C40-C39-S7	114.0(7)
C39-S7-C46	92.7(4)
C21-C20-C19	113.2(5)
C21-C20-C32	124.4(5)
C19-C20-C32	122.3(5)
C18-C19-C20	112.8(6)
C20-C21-C46	128.8(5)
C20-C21-S1	110.8(5)
C46-C21-S1	120.4(4)
C19 C18 C42	126.7(7)

C19 C18 S1	110.3(5)
C42-C18-S1	123.0(5)
C21-S1-C18	92.9(3)
C14-S2-C17	91.6(3)
C25-S3-C22	92.7(4)
C45-S4-C42	99.5(5)
C30-N1-C31	119.6(5)
C27-N3-C30	107.3(5)
C27-N3-B1	131.2(5)
C30-N3-B1	121.5(5)
C34-N4-C31	105.8(5)
C34-N4-B1	132.9(5)
C31-N4-B1	120.9(5)
N1-C31-C32	125.0(6)
N1-C31-N4	124.2(5)
C32-C31-N4	110.7(5)
C2-C1-C6	118.2(6)
C2-C1-C27	124.0(6)
C6-C1-C27	117.8(5)
C29-C28-C27	107.9(5)
N3-C27-C28	108.7(5)
N3-C27-C1	125.7(6)
C28-C27-C1	125.6(5)
N1-C30-N3	125.1(5)
N1-C30-C29	124.4(5)
N3-C30-C29	110.4(5)
C28-C29-C30	105.7(5)
C28-C29-C16	128.7(5)
C30-C29-C16	125.6(5)
C3-C2-C1	120.3(6)
C33-C32-C31	106.1(5)

C33-C32-C20	129.7(6)
C31-C32-C20	124.2(6)
N4-C34-C33	109.9(5)
N4-C34-C7	127.4(5)
C33-C34-C7	122.7(5)
C32-C33-C34	107.6(5)
C16-C17-C22	131.5(6)
C16-C17-S2	111.5(5)
C22-C17-S2	117.0(4)
C14-C15-C16	114.1(6)
C17-C22-C51	125.0(6)
C17-C22-S3	122.7(5)
C51-C22-S3	112.1(4)
C8-C7-C12	115.9(6)
C8-C7-C34	126.8(6)
C12-C7-C34	117.3(5)
C5-C6-C1	120.9(6)
C17-C16-C15	112.6(5)
C17-C16-C29	124.7(6)
C15-C16-C29	122.5(5)
C15-C14-C36	127.3(6)
C15-C14-S2	110.2(5)
C36-C14-S2	122.5(5)
C11-C12-C7	120.5(6)
C4-C3-C2	120.7(7)
C10-C11-C12	120.6(7)
C11-C10-C9	120.4(6)
C9-C8-C7	123.2(7)
C8-C9-C10	119.4(7)
F2-B1-F1	110.8(5)
F2-B1-N3	108.5(5)

F1-B1-N3	108.8(5)
F2-B1-N4	113.9(5)
F1-B1-N4	107.7(5)
N3-B1-N4	107.0(5)
C3-C4-C5	120.2(6)
C6-C5-C4	119.7(7)
C24-C25-S3	115.1(6)
C25-C24-C51	115.8(7)
C37-S6-C36	97.6(5)
C14-C36-C52	122.7(6)
C14-C36-S6	123.4(5)
C52-C36-S6	114.0(4)
C37-C38-C52	117.8(7)
C38-C37-S6	115.6(8)

Table 2.6 Anisotropic displacement parameters ($Å^2$) for compound (87).

	U^{11}	U^{22}	U^{33}	U^{23}	U^{13}	U^{12}
C50	0.022(3)	0.016(3)	0.079(5)	-0.005(3)	0.019(3)	0.000(2)
C51	0.039(3)	0.028(3)	0.004(3)	0.009(2)	-0.005(2)	0.005(3)
C52	0.000(2)	0.003(2)	0.025(3)	0.0030(19)	-0.0038(19)	0.0092(17)
C45	0.036(5)	0.140(10)	0.097(8)	0.033(7)	0.021(5)	0.023(6)
C44	0.138(11)	0.125(10)	0.059(6)	0.015(6)	0.014(6)	0.095(9)
C42	0.041(4)	0.062(5)	0.042(4)	0.007(3)	0.000(3)	0.016(3)
C46	0.041(4)	0.034(4)	0.038(4)	-0.002(3)	-0.007(3)	-0.002(3)
C43	0.000(2)	0.015(3)	0.031(3)	0.002(2)	-0.013(2)	0.0033(19)
C40	0.069(5)	0.046(5)	0.096(7)	-0.002(5)	0.019(5)	0.004(4)
C39	0.080(6)	0.074(6)	0.053(5)	0.003(4)	0.008(5)	0.030(5)
S7	0.0909(18)	0.0801(17)	0.0695(16)	0.0065(11)	0.0237(13)	0.0121(13)
C20	0.026(3)	0.039(4)	0.042(4)	0.008(3)	0.008(3)	0.002(3)
C19	0.031(4)	0.045(4)	0.041(4)	0.001(3)	-0.006(3)	-0.003(3)
C21	0.032(4)	0.037(4)	0.038(4)	0.000(3)	-0.006(3)	-0.002(3)

C18	0.029(4)	0.058(4)	0.047(4)	0.005(3)	0.005(3)	-0.007(3)
S1	0.0290(11)	0.0523(12)	0.0520(12)	-0.0036(8)	-0.0046(8)	-0.0047(7)
S2	0.0332(11)	0.0498(12)	0.0488(12)	0.0000(8)	-0.0118(8)	0.0038(7)
S3	0.0621(14)	0.0765(15)	0.0543(13)	-0.0076(10)	0.0027(10)	0.0066(10)
S4	0.0527(15)	0.116(2)	0.120(2)	0.0067(17)	0.0082(14)	-0.0064(14)
N1	0.032(3)	0.039(3)	0.031(3)	0.007(2)	0.001(2)	0.009(2)
F2	0.033(2)	0.042(2)	0.102(4)	-0.019(2)	0.010(2)	-0.0045(17)
F1	0.071(3)	0.044(2)	0.046(3)	0.0039(17)	-0.019(2)	0.0046(19)
N3	0.028(3)	0.031(3)	0.027(3)	0.001(2)	-0.004(2)	-0.004(2)
N4	0.027(3)	0.033(3)	0.032(3)	0.002(2)	-0.001(2)	-0.001(2)
C31	0.031(3)	0.035(4)	0.034(4)	0.003(3)	0.008(3)	0.001(3)
C1	0.029(3)	0.033(3)	0.045(4)	-0.005(3)	-0.009(3)	0.002(3)
C28	0.030(3)	0.027(3)	0.045(4)	-0.002(3)	-0.006(3)	-0.001(3)
C27	0.038(4)	0.039(4)	0.029(3)	0.000(3)	0.006(3)	-0.004(3)
C30	0.021(3)	0.036(4)	0.037(4)	0.009(3)	0.001(3)	-0.011(3)
C29	0.034(4)	0.036(4)	0.030(3)	-0.005(3)	0.000(3)	0.004(3)
C2	0.042(4)	0.038(4)	0.044(4)	-0.004(3)	0.003(3)	0.001(3)
C32	0.027(3)	0.038(4)	0.042(4)	-0.005(3)	-0.002(3)	-0.002(3)
C34	0.029(3)	0.040(4)	0.036(4)	-0.001(3)	0.006(3)	-0.005(3)
C33	0.038(4)	0.033(3)	0.041(4)	-0.003(3)	-0.004(3)	-0.001(3)
C17	0.031(3)	0.035(4)	0.048(4)	0.002(3)	-0.006(3)	0.009(3)
C15	0.039(4)	0.033(4)	0.042(4)	-0.004(3)	0.000(3)	-0.006(3)
C22	0.051(4)	0.045(4)	0.027(3)	0.000(3)	-0.010(3)	0.012(3)
C7	0.032(4)	0.032(3)	0.043(4)	-0.006(3)	0.002(3)	0.006(3)
C6	0.043(4)	0.048(4)	0.051(4)	0.007(3)	-0.005(3)	-0.010(3)
C16	0.030(4)	0.046(4)	0.031(4)	0.001(3)	-0.006(3)	0.000(3)
C14	0.027(3)	0.042(4)	0.046(4)	0.003(3)	-0.004(3)	0.002(3)
C12	0.045(4)	0.044(4)	0.040(4)	0.003(3)	0.012(3)	0.002(3)
C3	0.036(4)	0.042(4)	0.057(5)	-0.007(3)	-0.011(3)	0.004(3)
C11	0.052(4)	0.048(4)	0.040(4)	0.006(3)	0.006(3)	0.016(4)
C10	0.058(5)	0.052(5)	0.045(4)	0.004(3)	-0.002(4)	0.032(4)

C8	0.033(4)	0.036(4)	0.091(6)	-0.005(4)	0.005(4)	0.001(3)
C9	0.028(4)	0.070(6)	0.088(6)	-0.010(4)	-0.011(4)	0.001(4)
B1	0.026(4)	0.032(4)	0.038(4)	-0.002(3)	-0.003(3)	0.003(3)
C4	0.036(4)	0.058(5)	0.075(5)	-0.030(4)	-0.006(4)	-0.001(4)
C5	0.036(4)	0.049(4)	0.090(6)	0.006(4)	0.003(4)	-0.014(3)
C25	0.058(5)	0.062(5)	0.055(5)	-0.006(4)	0.001(4)	0.016(4)
C24	0.112(7)	0.042(4)	0.051(5)	0.003(4)	-0.020(5)	-0.008(5)
S6	0.0761(18)	0.093(2)	0.122(2)	-0.0110(16)	0.0133(16)	0.0071(14)
C36	0.029(4)	0.041(4)	0.062(5)	0.000(3)	-0.004(3)	0.001(3)
C38	0.038(4)	0.059(5)	0.123(8)	0.011(5)	-0.006(5)	0.002(4)
C37	0.045(5)	0.069(6)	0.116(8)	-0.030(5)	0.008(5)	-0.003(4)

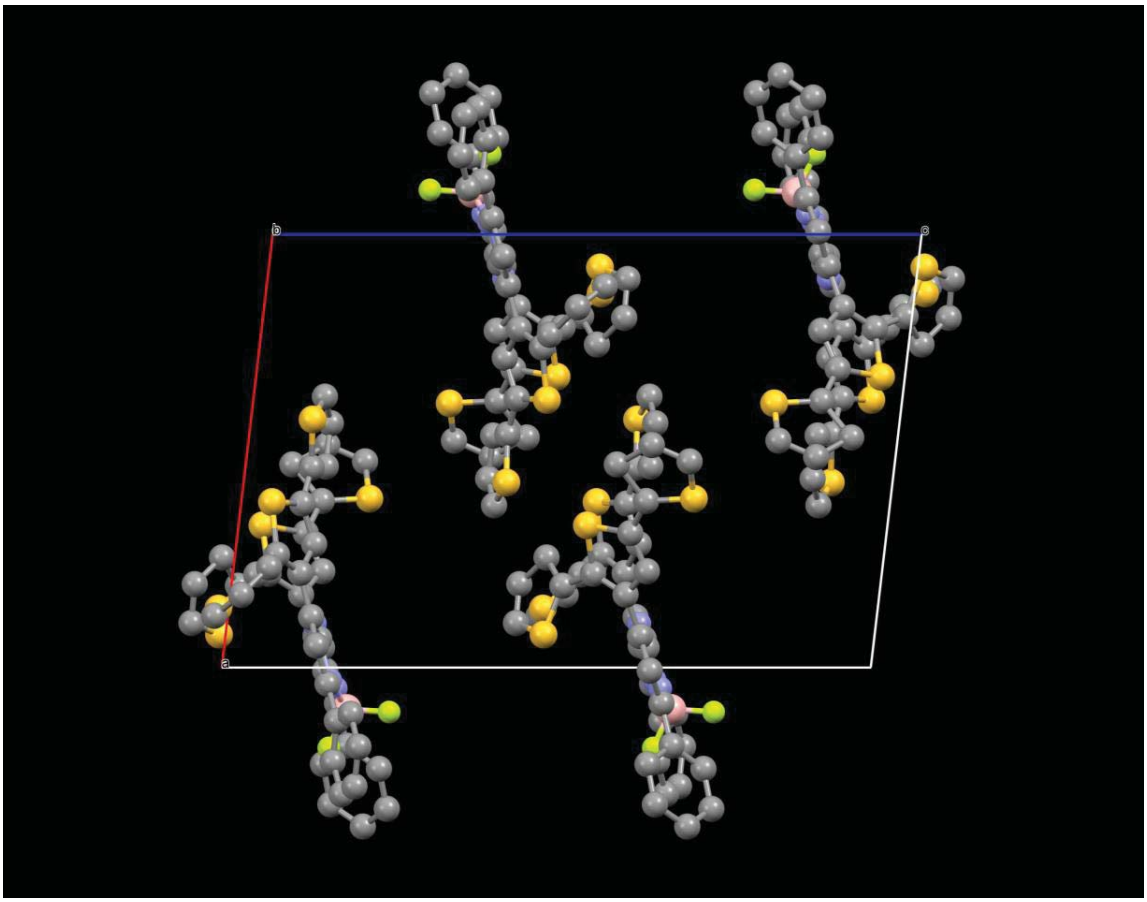

Figure 2.100 Crystal structure for compound (87).

2.40 References

(1) Gorman, A.; Killoran, J.; O'Shea, C.; Kenna, T.; Gallagher, W. M.; O'Shea, D. F. *Journal of the American Chemical Society* **2004**, *126*, 10619.

(2) Flavin, K.; Lawrence, K.; Bartelmess, J.; Tasior, M.; Navio, C.; Bittencourt, C.; O'Shea, D. F.; Guldi, D. M.; Giordani, S. *ACS Nano* **2011**, *5*, 1198.

(3) Hall, M. J.; McDonnell, S. O.; Killoran, J.; O'Shea, D. F. *J. Org. Chem.* **2005**, *70*, 5571.

(4) Wattanasin, S.; Murphy, W. S. *Synthesis* **1980**, 647.

(5) Gorman, A.; Killoran, J.; O'Shea, C.; Kenna, T.; Gallagher, W. M.; O'Shea, D. F. *J. Am. Chem. Soc.* **2004**, *126*, 10619.

(6) Gresser, R.; Hartmann, H.; Wrackmeyer, M.; Leo, K.; Riede, M. *Tetrahedron* **2011**, *67*, 7148.

(7) Ramesh, B.; Someswara, R. B. *E-J. Chem.* **2010**, *7*, 433.

(8) Ko, H.-H.; Tsao, L.-T.; Yu, K.-L.; Liu, C.-T.; Wang, J.-P.; Lin, C.-N. *Bioorganic & Medicinal Chemistry* **2003**, *11*, 105.

(9) Gorman, A.; Killoran, J.; O'Shea, C.; Kenna, T.; Gallagher, W. M.; O'Shea, D. F. *J. Am. Chem. Soc.* **2004**, *126*, 10619.

(10) Min, J.; Ameri, T.; Gresser, R.; Lorenz-Rothe, M.; Baran, D.; Troeger, A.; Sgobba, V.; Leo, K.; Riede, M.; Guldi, D. M.; Brabec, C. J. *ACS Applied Materials & Interfaces* **2013**, *5*, 5609.

(11) Zhao, W.; Carreira, E. M. *Angew. Chem., Int. Ed.* **2005**, *44*, 1677.

(12) Li, Y. *Acc. Chem. Res.* **2012**, *45*, 723.

(13) Dietrich, M.; Heinze, J.; Heywang, G.; Jonas, F. *Journal of Electroanalytical Chemistry* **1994**, *369*, 87.

(14) Wakim, S.; Beaupre, S.; Blouin, N.; Aich, B.-R.; Rodman, S.; Gaudiana, R.; Tao, Y.; Leclerc, M. *Journal of Materials Chemistry* **2009**, *19*, 5351.

(15) Scharber, M. C.; Mühlbacher, D.; Koppe, M.; Denk, P.; Waldauf, C.; Heeger, A. J.; Brabec, C. J. *Advanced Materials* **2006**, *18*, 789.

(16) Lincker, F.; Delbosc, N.; Bailly, S.; De Bettignies, R.; Billon, M.; Pron, A.; Demadrille, R. *Advanced Functional Materials* **2008**, *18*, 3444.

(17) Ulrich, G.; Goeb, S.; De, N. A.; Retailleau, P.; Ziessel, R. *Synlett* **2007**, 1517.

(18) Benniston, A. C.; Copley, G.; Harriman, A.; Rewinska, D. B.; Harrington, R. W.; Clegg, W. *J. Am. Chem. Soc.* **2008**, *130*, 7174.

(19) Goeb, S.; Ziessel, R. *Tetrahedron Lett.* **2008**, *49*, 2569.

(20) Zrig, S.; Remy, P.; Andrioletti, B.; Rose, E.; Asselberghs, I.; Clays, K. *J. Org. Chem.* **2008**, *73*, 1563.

(21) Rihn, S.; Retailleau, P.; Bugsaliewicz, N.; De, N. A.; Ziessel, R. *Tetrahedron Lett.* **2009**, *50*, 7008.

(22) Goeb, S.; Ziessel, R. *Org. Lett.* **2007**, *9*, 737.

(23) Collis, G. E.; Burrell, A. K.; Scott, S. M.; Officer, D. L. *The Journal of Organic Chemistry* **2003**, *68*, 8974.

(24) Cravino, A.; Roquet, S.; Leriche, P.; Aleveque, O.; Frere, P.; Roncali, J. *Chem. Commun. (Cambridge, U. K.)* **2006**, 1416.

(25) Roquet, S.; Cravino, A.; Leriche, P.; Aleveque, O.; Frere, P.; Roncali, J. *J. Am. Chem. Soc.* **2006**, *128*, 3459.

(26) Cravino, A.; Leriche, P.; Aleveque, O.; Roquet, S.; Roncali, J. *Adv. Mater. (Weinheim, Ger.)* **2006**, *18*, 3033.

(27) Preat, J.; Michaux, C.; Jacquemin, D.; Perpete, E. A. *J. Phys. Chem. C* **2009**, *113*, 16821.

(28) Xu, W.; Peng, B.; Chen, J.; Liang, M.; Cai, F. *J. Phys. Chem. C* **2008**, *112*, 874.

(29) Wang, H. L.; Zhang, B.; Xu, W. Y.; Bai, Y. Q.; Wu, H. *Acta Crystallogr., Sect. E: Struct. Rep. Online* **2007**, *E63*, o2648.

(30) Higashihara, T.; Wu, H.-C.; Mizobe, T.; Lu, C.; Ueda, M.; Chen, W.-C. *Macromolecules (Washington, DC, U. S.)* **2012**, *45*, 9046.

(31) Hu, X.-L.; Zuo, L.-J.; Nan, Y.-X.; Helgesen, M.; Hagemann, O.; Bundgaard, E.; Shi, M.-M.; Krebs, F. C.; Chen, H.-Z. *Synth. Met.* **2012**, *162*, 2005.

(32) Jia, J.; Zhang, Y.; Xue, P.; Zhang, P.; Zhao, X.; Liu, B.; Lu, R. *Dyes Pigm.* **2013**, *96*, 407.

(33) Okubo, Y.; Hattori, T.; Konica Minolta Holdings, Inc., Japan . 2012, p 43pp.

(34) Tamilavan, V.; Cho, N.; Kim, C.; Ko, J.; Hyun, M. H. *Synth. Met.* **2012**, *162*, 2155.

(35) Zhang, Z.; Han, J.; Li, X.; Cai, S.; Su, J. *Chin. J. Chem.* **2012**, *30*, 2779.

(36) King, W. J.; Nord, F. F. *J*. *Org*. *Chem*. **1948**, *13*, 635.

(37) Wang, H. L.; Zhang, B.; Xu, W. Y.; Bai, Y. Q.; Wu, H. *Acta Crystallogr*., *Sect*. *E: Struct*. *Rep*. *Online* **2007**, *63*, o2648.

(38) Bundgaard, E.; Krebs, F. C. *Proc*. *SPIE-Int*. *Soc*. *Opt*. *Eng*. **2005**, *5938*, 59380Q/1.

(39) Kim, Y.; Cook, S.; Choulis, S. A.; Nelson, J.; Durrant, J. R.; Bradley, D. D. C. *Chem*. *Mater*. **2004**, *16*, 4812.

(40) Gieseking, B.; Jaeck, B.; Preis, E.; Jung, S.; Forster, M.; Scherf, U.; Deibel, C.; Dyakonov, V. *Adv*. *Energy Mater*. **2012**, *2*, 1477.

(41) Behramand, B.; Molin, F.; Gallardo, H. *Dyes Pigm*. **2012**, *95*, 600.

(42) Karpicz, R.; Puzinas, S.; Sulskus, J.; Malickaja, S.; Grigalevicius, S.; Gulbinas, V. *Chem*. *Phys*. **2012**, *404*, 82.

(43) Peng, Q.; Lim, S.-L.; Wong, I. H.-K.; Xu, J.; Chen, Z.-K. *Chem*.*--Eur*. *J*. **2012**, *18*, 12140.

(44) Vanelle, P.; Liegeois, C. T.; Meuche, J.; Maldonado, J.; Crozet, M. P. *Heterocycles* **1997**, *45*, 955.

(45) Komoto, I.; Matsuo, J.-I.; Kobayashi, S. *Top*. *Catal*. **2002**, *19*, 43.

(46) Roncali, J.; Blanchard, P.; Frere, P. *J*. *Mater*. *Chem*. **2005**, *15*, 1589.

(47) Turbiez, M.; Frere, P.; Allain, M.; Videlot, C.; Ackermann, J.; Roncali, J. *Chem*.*--Eur*. *J*. **2005**, *11*, 3742.

(48) Turbiez, M.; Frere, P.; Roncali, J. *J*. *Org*. *Chem*. **2003**, *68*, 5357.

(49) Feng, Z.-Q.; Wu, J.; Cho, W.; Leach, M. K.; Franz, E. W.; Naim, Y. I.; Gu, Z.-Z.; Corey, J. M.; Martin, D. C. *Polymer* **2013**, *54*, 702.

(50) Levon, K.; Nasybulin, E.; Wei, S.; Albuquerque, I.; Polytechnic Institute of New York University, USA . 2011, p 47pp.

(51) Lin, C.; Ma, B.; Xia, C.; Wu, Y.; Kwong, R.; Universal Display Corporation, USA . 2010, p 65pp.

(52) Nishimura, K.; Onaka, K.; Miwa, H.; Isobe, K.; Konica Minolta Business Technologies, Inc., Japan . 2012, p 46pp.

(53) Sim, J. H.; Sato, H. *Macromol*. *Res*. **2009**, *17*, 714.

(54) Song, I. Y.; Park, S.-H.; Lim, J.; Kwon, Y. S.; Park, T. *Chem*. *Commun*. *(Cambridge, U*. *K*.*)* **2011**, *47*, 10395.

(55) Jessing, M.; Brandt, M.; Jensen, K. J.; Christensen, J. B.; Boas, U. *J*. *Org*. *Chem*. **2006**, *71*, 6734.

(56) Ma, D.; Geng, Q.; Zhang, H.; Jiang, Y. *Angew*. *Chem*., *Int*. *Ed*. **2010**, *49*, 1291.

(57) Shen, P.; Liu, X.; Jiang, S.; Huang, Y.; Yi, L.; Zhao, B.; Tan, S. *Org*. *Electron*. **2011**, *12*, 1992.

(58) Liang, Y.; Peng, B.; Chen, J. *J*. *Phys*. *Chem*. *C* **2010**, *114*, 10992.

(59) Xin, G.; Gong, S.; Kim, N.; Kim, J.; Hwang, W.; Nam, J.; Cho, Y.-H.; Cho, S. M.; Chae, H. *Sens*. *Actuators*, *B* **2013**, *176*, 81.

(60) Abbotto, A.; Calderon, E. H.; Manfredi, N.; Mari, C. M.; Marinzi, C.; Ruffo, R. *Synth*. *Met*. **2011**, *161*, 763.

(61) Damaceanu, M. D.; Bruma, M. *J*. *Optoelectron*. *Adv*. *Mater*. **2008**, *10*, 3086.

(62) Santos, C. S.; Liang, M.; Maroncelli, M.; Castner, E. W.; American Chemical Society: 2012, p PHYS.

(63) Tamayo, A. B.; Dang, X.-D.; Walker, B.; Seo, J.; Kent, T.; Nguyen, T.-Q. *Appl*. *Phys*. *Lett*. **2009**, *94*, 103301/1.

(64) Walker, B.; Tamayo, A.; Duong, D. T.; Dang, X.-D.; Kim, C.; Granstrom, J.; Nguyen, T.-Q. *Adv*. *Energy Mater*. **2011**, *1*, 221.

(65) He, F.; Wu, H.; Chen, J.; Su, W. *Synth*. *Commun*. **2008**, *38*, 255.

(66) Blouin, N.; Michaud, A.; Leclerc, M. *Adv*. *Mater*. *(Weinheim, Ger.)* **2007**, *19*, 2295.

(67) Beaupre, S.; Belletete, M.; Durocher, G.; Leclerc, M. *Macromol*. *Theory Simul*. **2011**, *20*, 13.

(68) Beaupre, S.; Boudreault, P.-L. T.; Leclerc, M. *Adv*. *Mater*. *(Weinheim, Ger.)* **2010**, *22*, E6.

(69) Blouin, N.; Michaud, A.; Gendron, D.; Wakim, S.; Blair, E.; Neagu-Plesu, R.; Belletete, M.; Durocher, G.; Tao, Y.; Leclerc, M. *J*. *Am*. *Chem*. *Soc*. **2008**, *130*, 732.

(70) Demadrille, R.; Firon, M.; Leroy, J.; Rannou, P.; Pron, A. *Adv*. *Funct*. *Mater*. **2005**, *15*, 1547.

(71) Lincker, F.; Heinrich, B.; De, B. R.; Rannou, P.; Pecaut, J.; Grevin, B.; Pron, A.; Donnio, B.; Demadrille, R. *J*. *Mater*. *Chem*. **2011**, *21*, 5238.

(72) Macor, L.; Gervaldo, M.; Fungo, F.; Otero, L.; Dittrich, T.; Lin, C.-Y.; Chi, L.-C.; Fang, F.-C.; Lii, S.-W.; Wong, K.-T.; Tsai, C.-H.; Wu, C.-C. *RSC Adv*. **2012**, *2*, 4869.

(73) Porzio, W.; Destri, S.; Pasini, M.; Giovanella, U.; Ragazzi, M.; Scavia, G.; Kotowski, D.; Zotti, G.; Vercelli, B. *New J*. *Chem*. **2010**, *34*, 1961.

(74) Qin, C.; Islam, A.; Han, L. *J*. *Mater*. *Chem*. **2012**, *22*, 19236.

(75) Dufresne, S.; Callaghan, L.; Skene, W. G. *J*. *Phys*. *Chem*. *B* **2009**, *113*, 15541.

(76) Collis, G. E.; Burrell, A. K.; Scott, S. M.; Officer, D. L. *J*. *Org*. *Chem*. **2003**, *68*, 8974.

(77) Gronowitz, S.; Peters, D. *Heterocycles* **1990**, *30*, 645.

(78) Zotti, G.; Gallazzi, M. C.; Zerbi, G.; Meille, S. V. *Synth*. *Met*. **1995**, *73*, 217.

(79) Black, D. K.; Landor, S. R.; Patel, A. N.; Whiter, P. F. *J*. *Chem*. *Soc*. *C* **1967**, 2260.

(80) Anon *Org*. *Process Res*. *Dev*. **1999**, *3*, 380.

(81) Chen, C.-L.; Yin, T.-C.; Chou, D.-G.; Everlight USA Inc., USA . 2010, p 33 pp.

(82) Hoskins, A. R.; Dent, D.; Donahoo, B.; Lau, L.; Hunt, A. W.; Pak, J. J.; Rodriguez, R. G.; American Chemical Society: 2008, p NWRM.

(83) Lin, C.-Y.; Lai, Y.-H.; Chen, H.-W.; Chen, J.-G.; Kung, C.-W.; Vittal, R.; Ho, K.-C. *Energy Environ*. *Sci*. **2011**, *4*, 3448.

(84) Song, H.-K.; Park, Y. H.; Han, C.-H.; Jee, J.-G. *J*. *Ind*. *Eng*. *Chem*. *(Amsterdam, Neth.)* **2009**, *15*, 62.

(85) Yin, J.-F.; Chen, J.-G.; Lu, Z.-Z.; Ho, K.-C.; Lin, H.-C.; Lu, K.-L. *Chem*. *Mater*. **2010**, *22*, 4392.

(86) Song, H.-K.; Park, Y. H.; Han, C.-H.; Jee, J.-G. *J*. *Ind*. *Eng*. *Chem*. *(Amsterdam, Neth.)* **2009**, *15*, 62.

(87) Jensen, S. B.; Rodger, S. J.; Spicer, M. D. *J*. *Organomet*. *Chem*. **1998**, *556*, 151.

(88) James, B. R.; Ochiai, E.; Rampel, G. L. *Inorg*. *Nucl*. *Chem*. *Lett*. **1971**, *7*, 781.

(89) Oki, A. R.; Morgan, R. J. *Synth*. *Commun*. **1995**, *25*, 4093.

(90) Alivisatos, A. P. *Science (Washington, D. C.)* **1996**, *271*, 933.

(91) Zrenner, A.; Beham, E.; Stufler, S.; Findeis, F.; Bichler, M.; Abstreiter, G. *Nature (London, U. K.)* **2002**, *418*, 612.

(92) Harman, T. C.; Taylor, P. J.; Walsh, M. P.; LaForge, B. E. *Science (Washington, DC, U. S.)* **2002**, *297*, 2229.

(93) Santori, C.; Fattal, D.; Vuckovic, J.; Solomon, G. S.; Yamamoto, Y. *Nature (London, U. K.)* **2002**, *419*, 594.

(94) Svrcek, V.; Slaoui, A.; Muller, J. C. *Thin Solid Films* **2004**, *451-452*, 384.

(95) Hanaki, K.-I.; Momo, A.; Oku, T.; Komoto, A.; Maenosono, S.; Yamaguchi, Y.; Yamamoto, K. *Biochem. Biophys. Res. Commun.* **2003**, *302*, 496.

(96) Hoshino, A.; Hanaki, K.-I.; Suzuki, K.; Yamamoto, K. *Biochem. Biophys. Res. Commun.* **2004**, *314*, 46.

(97) Mattoussi, H.; Mauro, J. M.; Goldman, E. R.; Anderson, G. P.; Sundar, V. C.; Mikulec, F. V.; Bawendi, M. G. *J. Am. Chem. Soc.* **2000**, *122*, 12142.

(98) Warner, J. H.; Hoshino, A.; Yamamoto, K.; Tilley, R. D. *Angew. Chem., Int. Ed.* **2005**, *44*, 4550.

(99) Tilley, R. D.; Warner, J. H.; Yamamoto, K.; Matsui, I.; Fujimori, H. *Chem. Commun. (Cambridge, U. K.)* **2005**, 1833.

(100) Li, Z. F.; Ruckenstein, E. *Nano Lett.* **2004**, *4*, 1463.

(101) Sato, S.; Swihart, M. T. *Chem. Mater.* **2006**, *18*, 4083.

(102) Blouin, N.; Mitchell, W.; Topley, A.; Tierney, S.; Merck Patent GmbH, Germany . 2012, p 98pp.

(103) Jones, D. J.; Wong, W. H. W.; Holmes, A. B.; Seyler, H.; The University of Melbourne, Australia . 2013, p 29pp.

(104) Peng, Q.; Huang, Q.; Hou, X.; Chang, P.; Xu, J.; Deng, S. *Chem. Commun. (Cambridge, U. K.)* **2012**, *48*, 11452.

(105) Qin, H.; Li, L.; Liang, T.; Peng, X.; Peng, J.; Cao, Y. *J. Polym. Sci., Part A: Polym. Chem.*, Ahead of Print.

(106) Qu, B.; Tian, D.; Cong, Z.; Wang, W.; An, Z.; Gao, C.; Gao, Z.; Yang, H.; Zhang, L.; Xiao, L.; Chen, Z.; Gong, Q. *J. Phys. Chem. C*, Ahead of Print.

(107) Qu, B.; Yang, H.; Tian, D.; Liu, H.; Cong, Z.; Gao, C.; Chen, Z.; Xiao, L.; Gao, Z.; Wei, W.; Gong, Q. *Synth. Met.* **2012**, *162*, 2020.

(108) Topley, A.; Blouin, N.; Mitchell, W.; Tierney, S.; Merck Patent GmbH, Germany . 2013, p 66pp.

(109) Wu, F.; Zha, D.; Chen, L.; Chen, Y. *J. Polym. Sci., Part A: Polym. Chem.*, Ahead of Print.

(110) Zhou, E.; Cong, J.; Hashimoto, K.; Tajima, K. *Macromolecules (Washington, DC, U. S.)* **2013**, *46*, 763.

(111) Tang, Y.; McNeill, C. R. *J. Polym. Sci., Part B: Polym. Phys.* **2013**, *51*, 403.

(112) Zhong, H.; Li, Z.; Deledalle, F.; Fregoso, E. C.; Shahid, M.; Fei, Z.; Nielsen, C. B.; Yaacobi-Gross, N.; Rossbauer, S.; Anthopoulos, T. D.; Durrant, J. R.; Heeney, M. *J. Am. Chem. Soc.* **2013**, *135*, 2040.

(113) Chi, C.-C.; Huang, Y.-J.; Chen, C.-T. *J. Chin. Chem. Soc. (Weinheim, Ger.)* **2012**, *59*, 305.

(114) Cortizo-Lacalle, D.; Howells, C. T.; Gambino, S.; Vilela, F.; Vobecka, Z.; Findlay, N. J.; Inigo, A. R.; Thomson, S. A. J.; Skabara, P. J.; Samuel, I. D. W. *J. Mater. Chem.* **2012**, *22*, 14119.

(115) Kim, B.-S.; Ma, B.; Donuru, V. R.; Liu, H.; Frechet, J. M. J. *Chem. Commun. (Cambridge, U. K.)* **2010**, *46*, 4148.

(116) Ma, B.; Liu, H.; Michigan Technological University, USA . 2010, p 152pp.

(117) Wagner, R. W.; Lindsey, J. S. *Pure Appl. Chem.* **1996**, *68*, 1373.

(118) Liu, M.; Johnston, M. B.; Snaith, H. J. *Nature (London, U. K.)* **2013**, *501*, 395.

(119) Lee, M. M.; Teuscher, J.; Miyasaka, T.; Murakami, T. N.; Snaith, H. J. *Science (Washington, DC, U. S.)* **2012**, *338*, 643.

(120) Loi, M. A.; Hummelen, J. C. *Nat. Mater.* **2013**, *12*, 1087.

(121) Gallazzi, M. C.; Toscano, F.; Paganuzzi, D.; Bertarelli, C.; Farina, A.; Zotti, G. *Macromolecular Chemistry and Physics* **2001**, *202*, 2074.

(122) Snaith, H. J. *The Journal of Physical Chemistry Letters* **2013**, *4*, 3623.

(123) Burschka, J.; Pellet, N.; Moon, S.-J.; Humphry-Baker, R.; Gao, P.; Nazeeruddin, M. K.; Graetzel, M. *Nature (London, U. K.)* **2013**, *499*, 316.

(124) Batat, P.; Cantuel, M.; Jonusauskas, G.; Scarpantonio, L.; Palma, A.; O'Shea, D. F.; McClenaghan, N. D. *The Journal of Physical Chemistry A* **2011**, *115*, 14034.

Chapter 3

Electronic and Fluorescence Properties of Aza-BODIPYs

Chapter 3

3.1 Introduction

Ultraviolet–visible spectroscopy is the most useful technique for the characterization of materials for solar cells applications. It provides essential information about the absorption of each part of the molecule and the amount of light absorbed in each part of the solar spectrum. These details are useful in designing or developing new materials for solar cells application.

The absorption and emission properties of the synthesized aza-BODIPYs were investigated, with a view to evaluating the potential use of aza-BODIPYs in solar cells. Quantum chemical calculations were performed to aid interpretation of the results. Electronic properties were calculated using time-dependent density functional theory (TD-DFT).

The interactions between aza-BODIPYs and fullerene derivatives ($PC_{60}BM$) were investigated using fluorescence and time-correlated single-photon counting (TCSPC) spectroscopy. Fluorescence quenching was studied in the presence and the absence of the acceptor ($PC_{60}BM$). The quenching constants and binding constants were determined from Stern-Volmer plots (discussed in Chapter 1). Fluorescence quantum yields were determined. The fluorescence lifetimes of aza-BODIPYs were determined from the analyses of the fluorescence decay curves.

3.2 Experimental Details

3.2.1 Absorption Measurements

Absorption measurements were carried out for all aza-BODIPYs using a Shimadzu UV-3101PC UV-VIS-NIR-scanning spectrophotometer. The absorption spectra were collected for samples in chloroform solutions. Quartz cells (1cm) were used for these measurements.

3.2.2 Quantum Chemical Calculations

Quantum chemical calculations were achieved with Gaussian09 program,[1] by means of the density functional theory (DFT) method using the B3LYP functional with the basis set 6-311++G (2d, P). Symmetry constraints were used in the geometry optimization of all compounds except compound (87), (88) and (113). The choice of computational procedures adopted to evaluate the spectral properties of aza-BODIPYs was guided by the literature (Section (3.3.1)).[2,3] The absorption energies and the principal orbital contributions of the excited states energies were calculated using the time-dependent DFT method. GaussSum 2.2.5[4] software was used to extract the calculated UV-VIS spectra and vibrational frequencies from DFT calculations.

3.2.3 Fluorescence measurements

Emission spectra were measured for aza-BODIPYs in de-gassed chloroform solutions using a FluoroMax-4 spectrofluorimeter from Horiba Scientific with FluorEssence software. The fluorescence cells were dried and purged with argon before any measurements. Fluorescence quantum yield measurements were performed using an integrating sphere. The configuration of the integrating sphere is depicted in Fig. (3.1). An integrating sphere is a hollow sphere coated internally with highly reflective but diffusing material. The light output at one aperture of the sphere is proportional to the total light produced by a sample within the sphere. Fluorescence quantum yield measurements were performed for selected highly emissive aza-BODIPYs. Rhodamine 101 and Nile Blue Chloride were used as standards for comparison purposes in fluorescence quantum yield measurements.

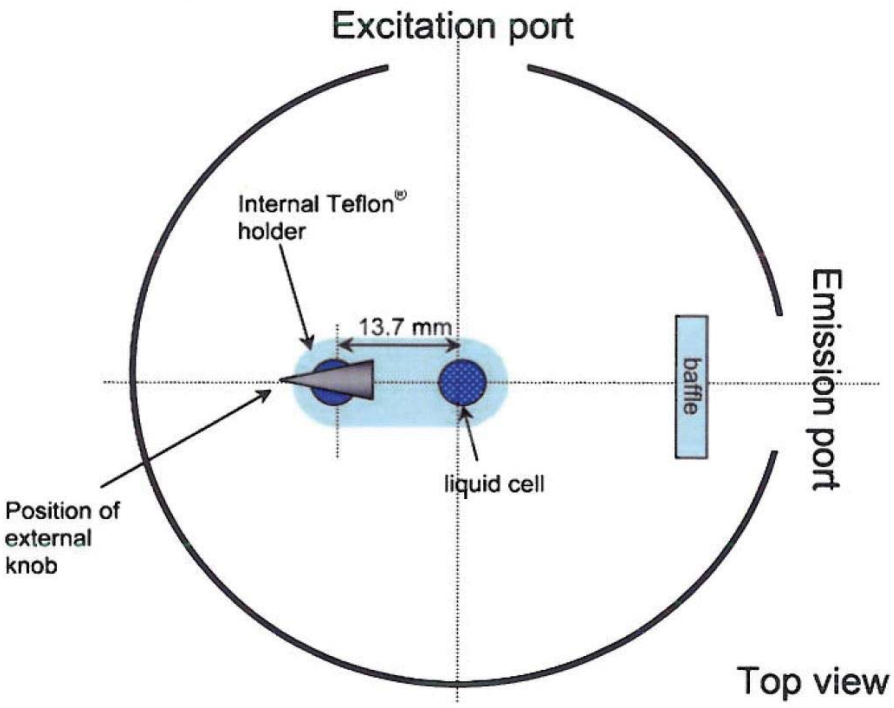

Figure 3.1 The configuration of the integrating sphere

3.2.4 Time-Correlated Single-Photon Counting (TCSPC) Measurements

Time-resolved measurements were performed with Fluorolog TCSPC from HORIBA Scientific combined with TBX Picosecond Photon Detection Module and a Pulsed laser source of DeltaDiode ^{TM} (Peak wavelength 452 nm with a laser repetition rate of 100 kHz). Data analysis of time-resolved measurements obtained from TCSPC was performed utilizing DAS6 Fluorescence decay analysis software. All measurements were performed in degassed chloroform solution and in a sealed and dry cell.

3.3 Results and Discussion

3.3.1 Quantum Chemical Calculations and UV-VIS Studies on Aza-BODIPYs

The energy of the ground state system can be calculated from the electron density $\rho(\vec{r})$, according to Kohn and Hohenberg:[5]

$$\rho(\vec{r}) = \sum_{i=1}^{N_e} \psi_l^*(\vec{r})\psi_l(\vec{r}), \quad (3.1)$$

$$E = f(\rho(\vec{r})). \quad (3.2)$$

By the means of the variational principle and according to equation 3.2, the Kohn-Sham equation can be derived for the one-electron orbitals as follows:[6]

$$E\rho(\vec{r}) = E^{\mathrm{T}}\rho(\vec{r}) + E^{\mathrm{V}}\rho(\vec{r}) + E^{\mathrm{J}}\rho(\vec{r}) + E^{\mathrm{XC}}\rho(\vec{r}). \quad (3.3)$$

Where, E^{T} corresponds to the kinetic energy of the electrons; E^{V} includes the nuclear electron interaction and the nuclear-nuclear repulsion; E^{J} represents the Coulomb interaction and E^{XC} is the exchange correlation energy.[7] E^{XC} is approximated by the local density approximation (LDA) or the generalized gradient approximation (GGA), and it depends on the total electron density of the whole molecule.[7]

The variation of electron density with position is taken into account in the exchange correlation functional of the GGA. This can be done by including the gradient of the electron density. B88, P, PW, B86 and PBE are widely used exchange GGA functionals (E_X), while PW91, B95, P86 and LYP are correlation functionals (E_C). The exchange correlation functional B3LYP is the most commonly used:[8,9]

$$E_{\mathrm{XC}}^{\mathrm{B3LYP}} = (1-a)E_{\mathrm{X}}^{\mathrm{LSDA}} + aE_{\mathrm{X}}^{\mathrm{HF}} + bE_{\mathrm{X}}^{\mathrm{B}} + (1-c)E_{\mathrm{C}}^{\mathrm{LSDA}} + cE_{\mathrm{C}}^{\mathrm{LYP}} \quad (3.4)$$

The values of a, b and c have been optimized by Becke[9] as 0.20, 0.72, and 0.81, respectively. The B3LYP exchange correlation functional has been used in this study for the quantum chemical calculations, as it is very good in the prediction of minimum-energy structures and transition state geometries.[8]

The intensity of the electronic transition is a proportional to the square of the transition dipole moment and indicated by the oscillator strength. The oscillator strength determines the transition probability to ψ_i and can be determined from experiment.[10] In terms of the accuracy/effort ratio, TD-DFT is considered as one of the most valuable approaches.[2] The system's response to the time-dependent perturbation is given by:

$$f \propto \langle \Psi_0 | r | \Psi_i \rangle^2 \qquad (3.5)$$

Where, Ψ_0 is the electronic ground state; Ψ_i is the electronic excited state; $f\alpha < \Psi_0|r|\Psi_i >^2$ corresponds to an intensity of an electronic transition.[10]

The polarizability α(ω) defines the transition from the electronic ground state Ψ_0 to the excited state Ψ_i, and is given by:

$$\alpha(\omega) = \sum_{i}^{\text{states}} \frac{|\langle \Psi_0 | r | \Psi_i \rangle|^2}{\omega - \omega_i} \qquad (3.6)$$

The extension of DFT to electronically excited-states is known as time-dependent density functional theory (TD-DFT). The interaction of electromagnetic radiation with the electron density can be computed within time-dependent perturbation theory. TD-DFT calculations using B3LYP functional have been employed in this study to predict the absorption energies of aza-BODIPYs. The $S_0 \rightarrow S_1$ electronic excitation was distinguished in terms of oscillator strength and was characterized as a highest occupied molecular orbital to the lowest unoccupied molecular orbital transition. This fundamental information complements spectroscopic data and is a valuable guide in the design and synthesis of promising materials for solar cells.

The excited-state energies of some aza-BODIPY derivatives have been investigated in the literature[11] with time-dependent density functional theory (TD-DFT). The results of these studies suggested which computational protocol was likely to be most efficient for making rapid semi-quantitative estimates of the λ_{max} for selected aza-BODIPY compounds. A comparison between the TD-DFT calculations in this thesis and those in the literature has been carried out in this Chapter. The B3LYP (Becke, three-parameter, Lee-Yang-Parr) exchange-correlation functional with a split-valence basis set of 6-311++G (2d, P) level of calculation delivered similar results to those in the literature (e.g. the mean absolute errors (MAE) value for selected bond lengths for compound (87) in comparison to compound (b)), but it showed higher MAE value for selected valence angles (for compound (87)) in comparison with compounds (a) and (b), see Table (3.1). It can be concluded from Table (3.1) that pure functionals (such as PBE) and range-separated hybrids relying on a large attenuation parameter (such as LC-PBE) were less satisfactory. Most hybrids yield reasonable estimates with MAE smaller than 0.010 Å and 1.0° for both molecules.[11]

It has been shown[11] that the PCM-TD-BMK/6-311+G(2d,p) approach delivers appropriate lower bounds of the experimental results regardless of the inherent limits of the vertical approximation. The experimental maximum absorption and emission wavelengths of aza-BODIPYs in the literature are shown in Fig. (3.2); the experimental wavelengths for the novel aza-BODIPYs synthesised in this study are shown in Fig. (3.3).

Pure functionals (PBE and TPSS) have been found to be inadequate because they predict much too small transition energies, see Table (3.2).[11] Range-separated hybrids (functionals in rows 12, 13, 14 and 15 in Table (3.2)) have estimated the λ_{max}, but underestimated the differences between compounds (c) and (d). They did not predict any significant transitions in the 400–600 nm range for compound (c). Global hybrids of exact exchange were accurate for compound (d) but less satisfactory for compound (c) as they yielded a too large λ_{max} and extra transitions that remain unseen experimentally.[11] The BMK hybrid slightly underestimated the wavelengths but recovered reasonable position and intensities for the different bands. It did predict a (c)–(d) shift (-64 nm) instead of the -47 nm measured value, while B3LYP gave -172 nm, which was an overstated value typical of charge transfer (CT) states, and ωB97 gave -16 nm.

Table 3.1 Mean absolute errors (DFT versus XRD) of compounds (a), (b) (literature)[12,13] and the new compound (87) calculated for selected bond lengths (Å) and valence angles (degrees).

	Functional	Bond lengths			Valence angles		
		Compounds			Compounds		
		(a)	(b)	(87)	(a)	(b)	(87)
1	B3LYP	0.006	0.008	0.008*	0.7	0.5	0.9*
2	PBE	0.009	0.013	-	0.8	0.5	-
3	TPSS	0.008	0.012	-	0.7	0.4	-
4	TPSSh	0.005	0.008	-	0.7	0.4	-
5	O3LYP	0.007	0.009	-	1.0	0.7	-
6	PBE0	0.005	0.007	-	0.8	0.5	-
7	BMK	0.009	0.009	-	0.8	0.6	-
8	M05-2X	0.007	0.009	-	0.9	0.4	-
9	LC-PBE	0.017	0.016	-	0.9	0.6	-
10	LC-ωPBE	0.009	0.011	-	1.0	0.8	-
11	CAM-B3LYP	0.005	0.008	-	0.8	0.6	-
12	ωB97	0.010	0.010	-	0.9	0.5	-
13	ωB97X	0.007	0.010	-	0.9	0.5	-
14	ωB97XD	0.009	0.009	-	0.9	0.5	-

* MAE values of compound (87) calculated for selected bond lengths ((C45-C44), (C44-C43), (C46-C21), (C40-C39), (C19-C18), (N3-C30), (N3-B1), (C29-C16), (C17-C16), (C52-C36), (C20-C19), (C17-C22), (C7-C8), (C11-C10) and (C34-C33)) and selected valence angles ((C21-C20-C19), (C6-C1-C27), (N3-C27-C1), (C28-C27-C1), (C28-C29-C30), (C3-C2-C1), (C33-C32-C31), (C31-C32-C20), (C32-C33-C34), (C16-C17-C22), (C15-C16-C29), (C11-C12-C7), (C4-C3-C2), (C14-C36-C52) and (C37-C38-C52)), see Table (2.4) and (2.5) in Chapter 2, Section (3.39.2).

Table 3.2 Comparison of the theoretical and experimental λ_{max} (nm) from the literature.[11,12,14] The theoretical values were computed using a variety (rows 1-15) with the PCM(CH_2Cl_2)-TD-DFT/6-311+G(2d,p)//PCM(CH_2Cl_2)-PBE0/6-311G(2d,p) level of approximation.[11] Oscillator strengths are given in brackets.

		Compound (c)	Compound (d)
	Experimental	745[12]	694[14]
	Theoretical		
1	B3LYP	885 (0.76)	713 (1.18)
2	PBE	1267 (0.54)	852 (0.92)
3	TPSS	1212 (0.55)	829 (0.95)
4	TPSSh	1021 (0.62)	750 (1.09)
5	O3LYP	1011 (0.62)	751 (1.09)
6	PBE0	834 (0.85)	690 (1.22)
7	M06	810 (0.91)	701 (1.20)
8	BMK	711 (1.14)	647 (1.27)
9	M05-2X	688 (1.22)	649 (1.24)
10	LC-PBE	672 (1.19)	655 (1.17)
11	LC-ωPBE	669 (1.18)	652 (1.16)
12	CAM-B3LYP	679 (1.21)	648 (1.22)
13	ωB97	673 (1.18)	657 (1.16)
14	ωB97X	665 (1.19)	647 (1.18)
15	ωB97XD	662 (1.21)	641 (1.20)

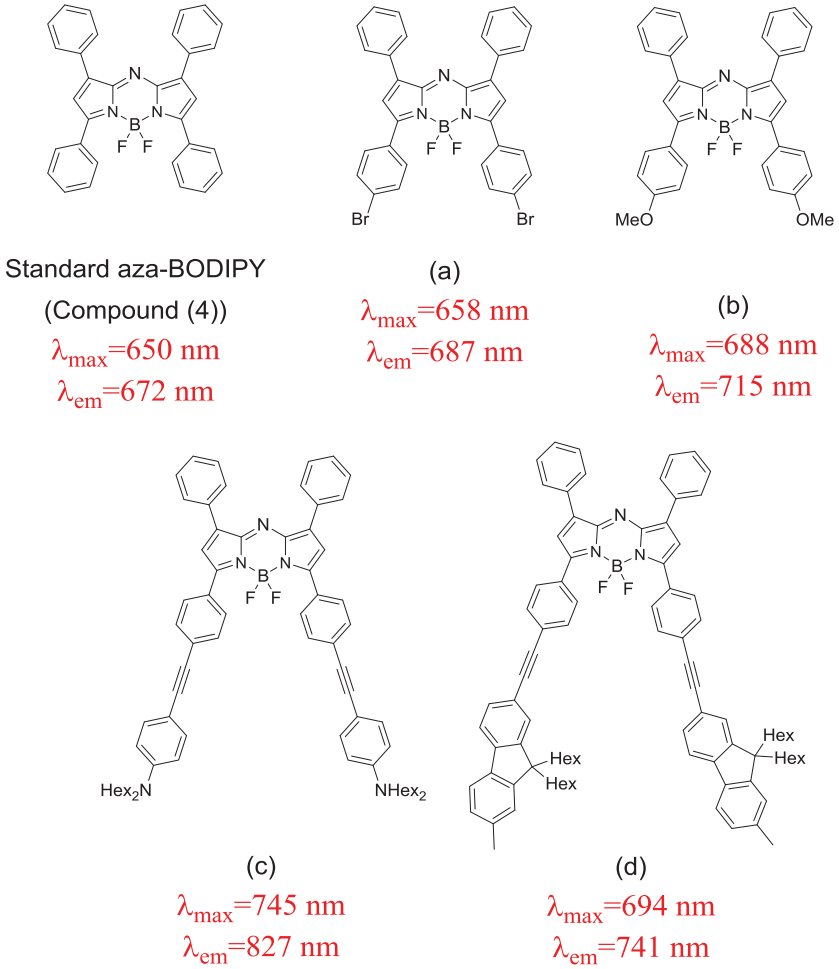

Figure 3.2 The experimental λ_{max} and λ_{em} values for selected aza-BODIPYs from the literature.[11-13,15]

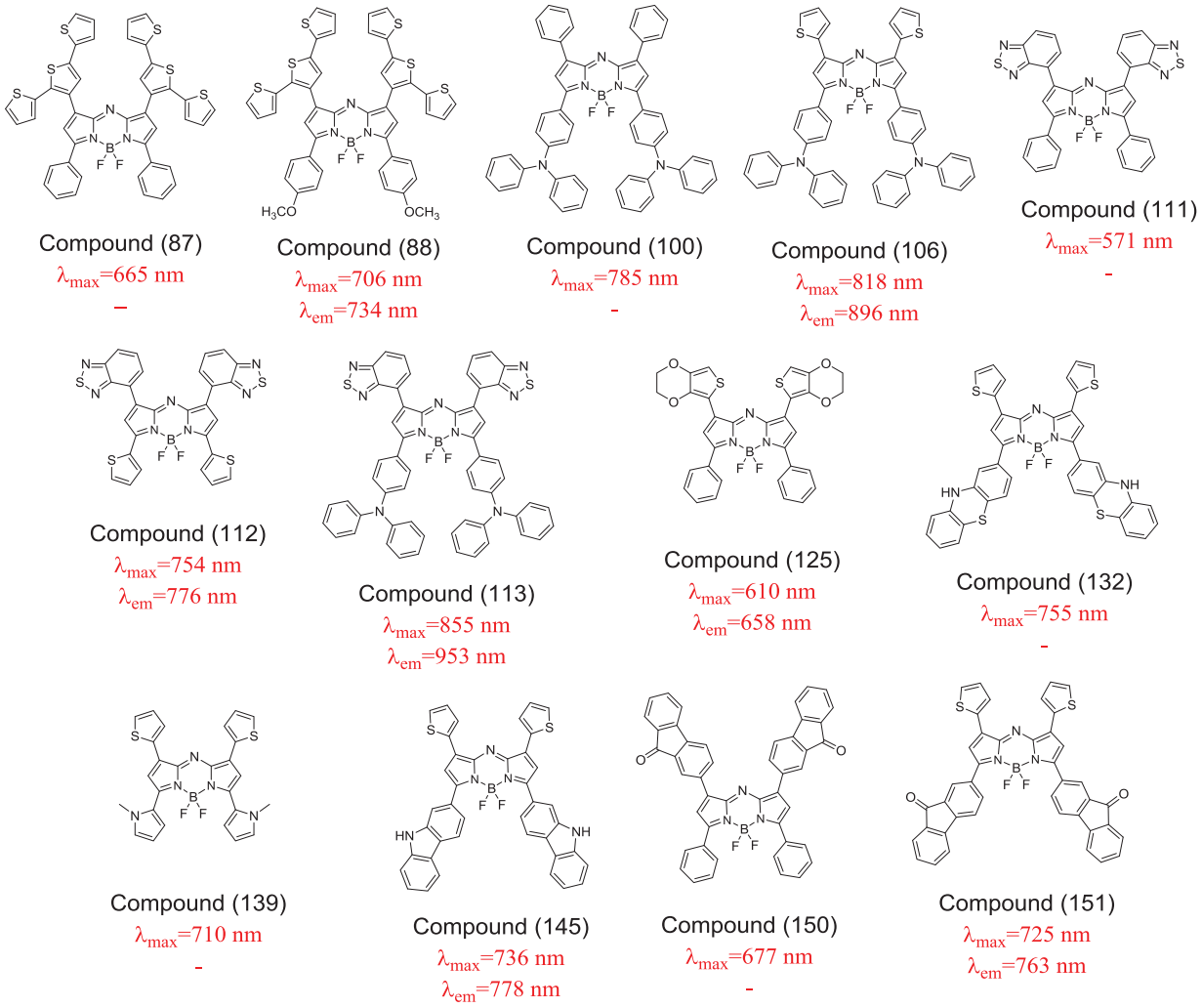

Figure 3.3 The experimental λ_{max} and λ_{em} values measured for the novel aza-BODIPYs.

The structural parameters of the gas-phase DFT/6-311G(2d,p) estimates and X-ray diffraction (XRD) data for compounds (a), (b) and (87) (Fig. (3.2) and Fig. (3.3)) have been compared in order to compute the MAE (Table (3.1)). MAE for the bond lengths and valence angles of these compounds are shown in Table (3.1). The average measured data for the two halves of the molecules has been used because the structures were not perfectly of C_2 symmetry and because of the influence of solid-state effects.[13]

The B3LYP functional was chosen in this study because it showed reasonable MAE values in the literature for bond lengths and valence angles (see Table 3.1, row (1); compounds (a) and (b)) and reasonable estimates for absorption wavelengths for some aza-BODIPYs, e.g. 19 nm shift in compound (d) (Table 3.3, row (2)). The advantage of using the B3LYP functional was the reasonable time frame of processing geometry optimization and TD-DFT calculations for aza-BODIPY molecules.

Absorption energies were calculated for the new aza-BODIPYs using the B3LYP/6-311++G (2d, P). The B3LYP/6-311++G (2d, P) level of calculation has delivered reasonable estimates of the absorption wavelengths for compounds (100), (106), (113), (150), (151) and (145), but it severely underestimated the absorption wavelengths of compounds (87), (88) and (112), and overestimated the absorption wavelengths of compounds (111), (125), (132) and (139), see Table (3.3) and Fig. (3.4) to Fig. (3.16). These findings were comparable to the literature, e.g. the absorption wavelengths of compound (d) have been reasonably estimated using the same level of theory, while the absorption wavelengths of compound (c) has been overestimated using the same level of theory.

Table 3.3 Comparison of the theoretical and experimental λ_{max} (nm). The theoretical values were computed using the B3LYP/6-311++G (2d, P) level of approximation. (Rows (1) and (2) are from literature; rows (3) to (15) were from this study).

	Compounds	Experimental	Calculated (TD-DFT) using the B3LYP functional
		λ_{max} (nm)	λ_{max} (nm)
1	(c)[12]	745	885
2	(d)[14]	694	713
3	(87)	665	590
4	(88)	706	650
5	(100)	785	795
6	(106)	818	813
7	(113)	855	880
8	(150)	677	641
9	(151)	725	700
10	(111)	571	654
11	(112)	754	701
12	(125)	610	697
13	(132)	755	829
14	(139)	710	720
15	(145)	736	701

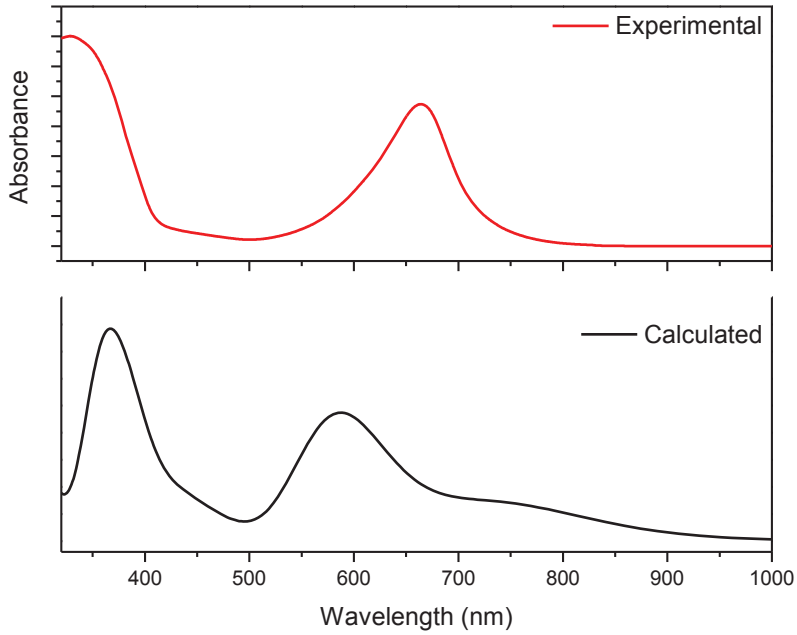

Figure 3.4 A comparison between the experimental and calculated absorption spectrum of compound (87) in chloroform.

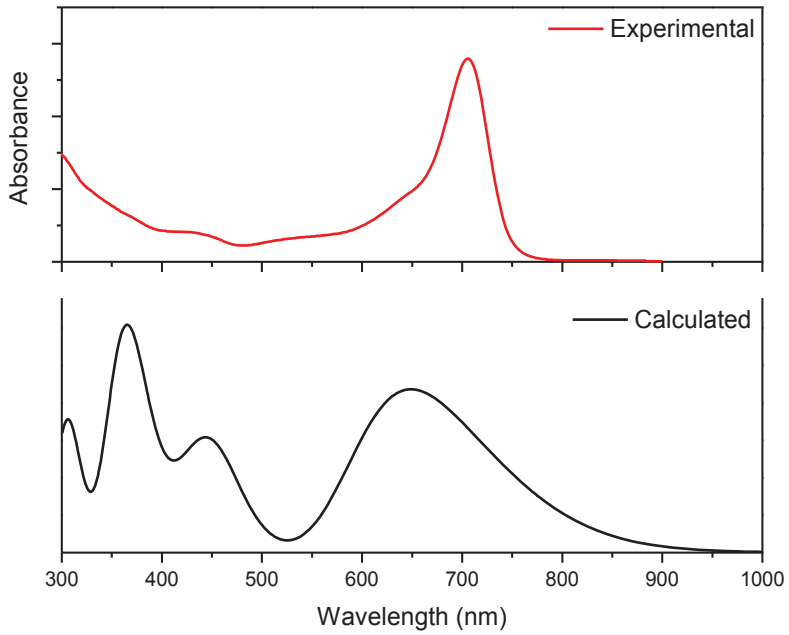

Figure 3.5 A comparison between the experimental and calculated absorption spectrum of compound (88) in chloroform.

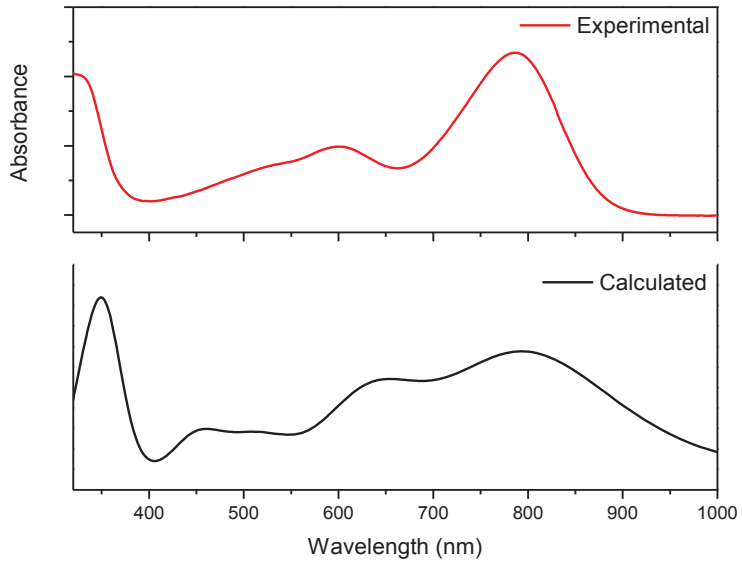

Figure 3.6 A comparison between the experimental and calculated absorption spectrum of compound (100) in chloroform.

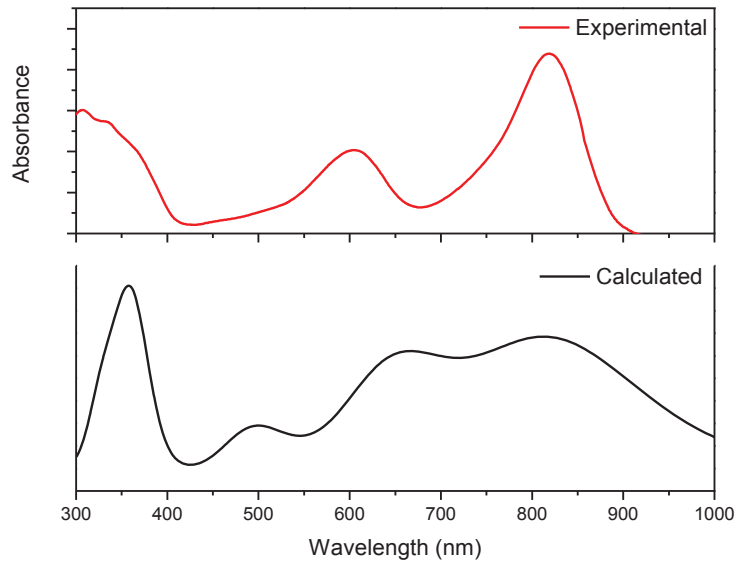

Figure 3.7 A comparison between the experimental and calculated absorption spectrum of compound (106) in chloroform.

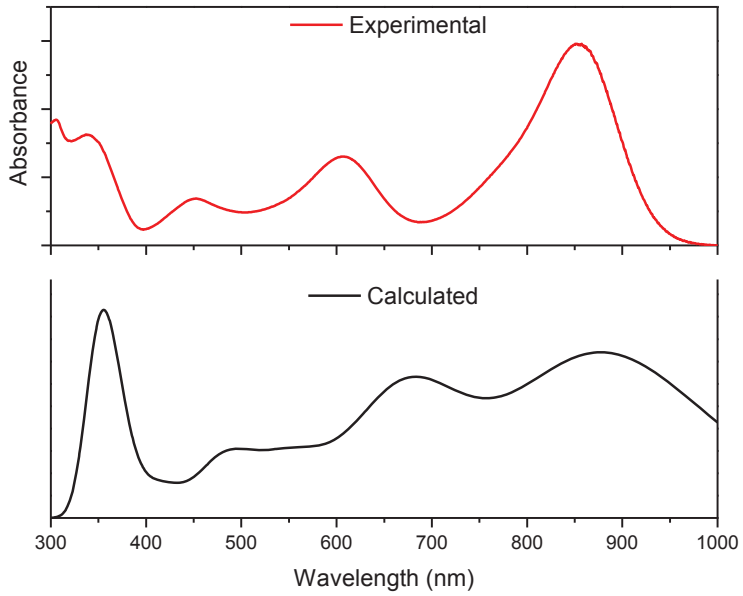

Figure 3.8 A comparison between the experimental and calculated absorption spectrum of compound (113) in chloroform.

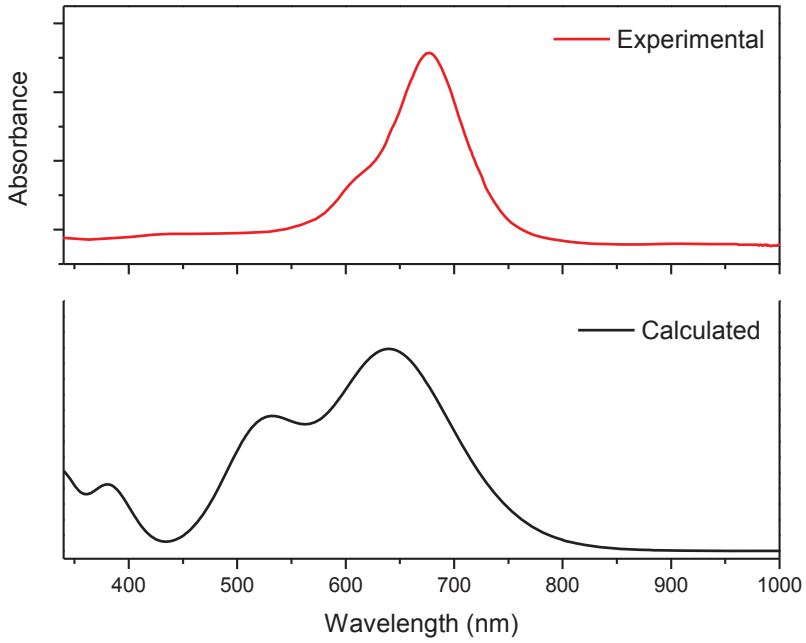

Figure 3.9 A comparison between the experimental and calculated absorption spectrum of compound (150) in chloroform.

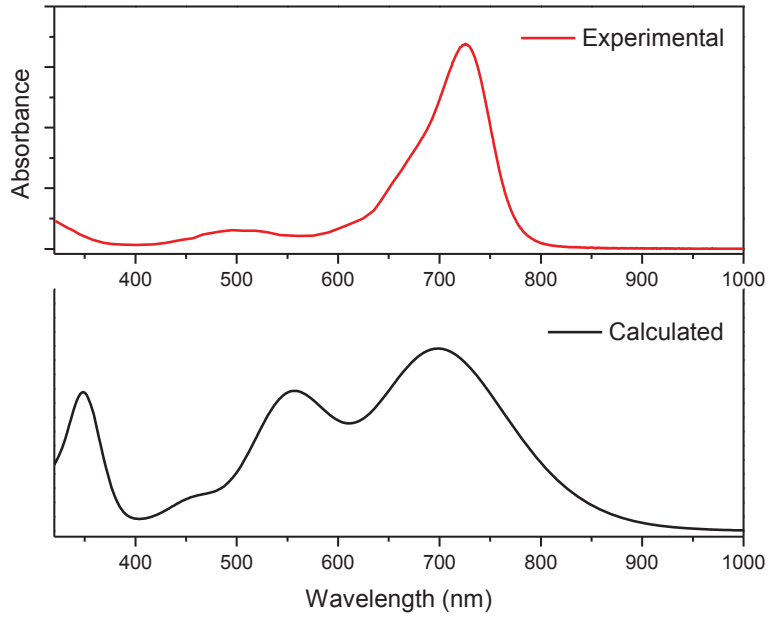

Figure 3.10 A comparison between the experimental and calculated absorption spectrum of compound (151) in chloroform.

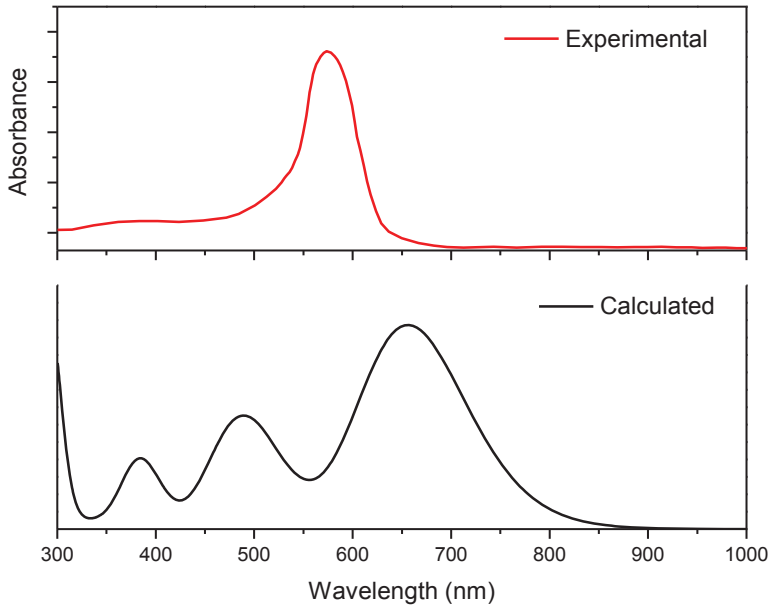

Figure 3.11 A comparison between the experimental and calculated absorption spectrum of compound (111) in chloroform.

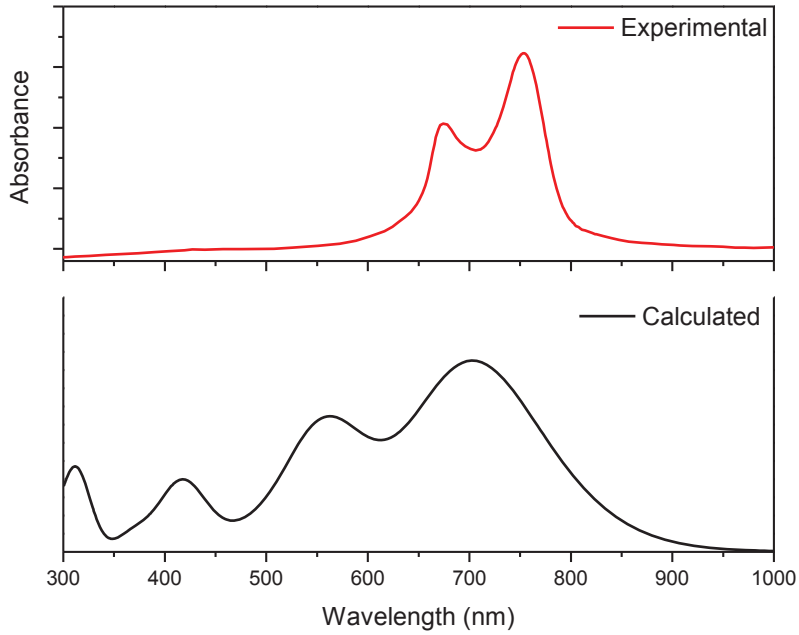

Figure 3.12 A comparison between the experimental and calculated absorption spectrum of compound (112) in chloroform.

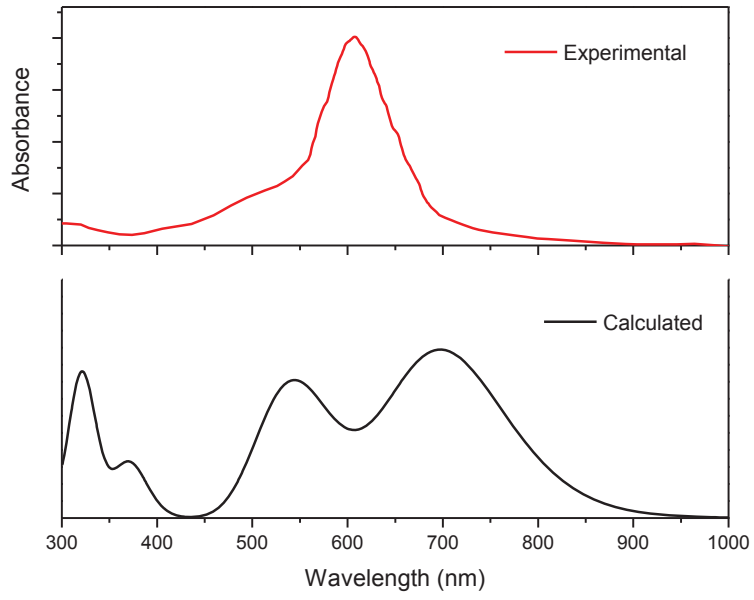

Figure 3.13 A comparison between the experimental and calculated absorption spectrum of compound (125) in chloroform.

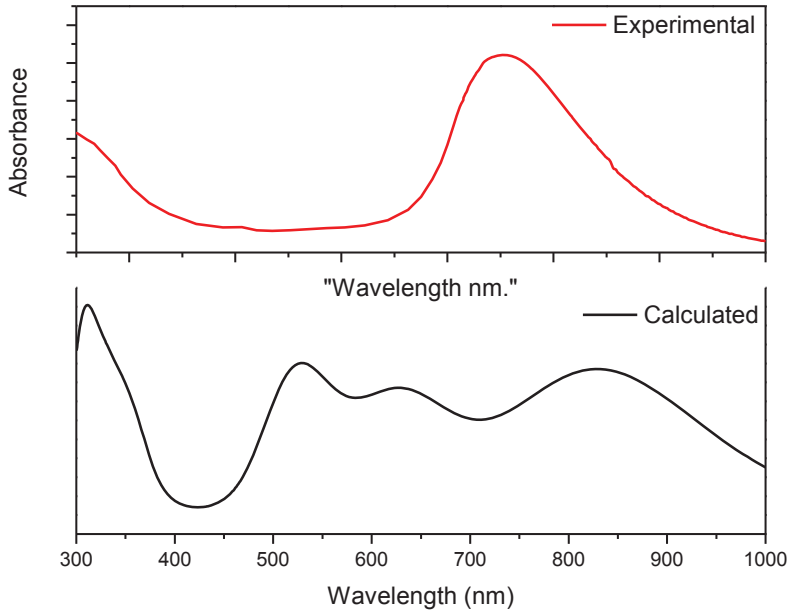

Figure 3.14 A comparison between the experimental and calculated absorption spectrum of compound (132) in chloroform.

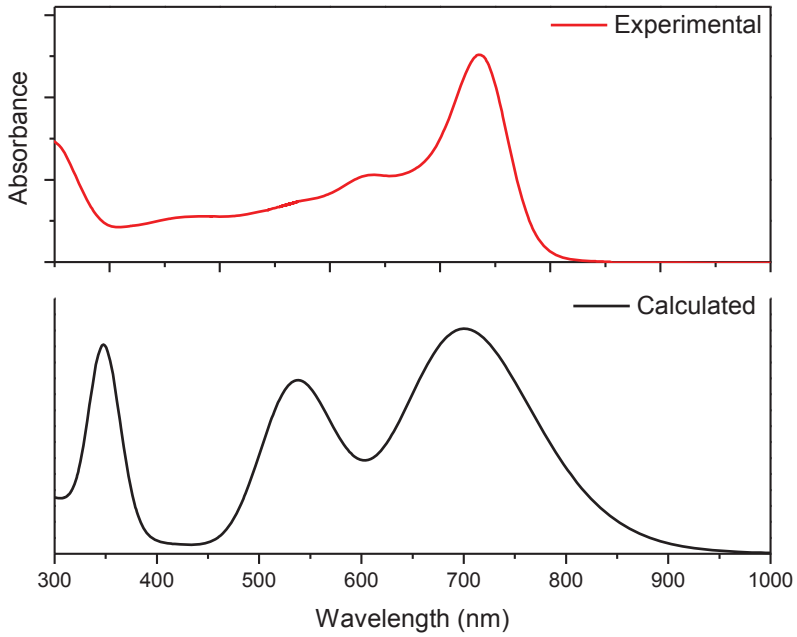

Figure 3.15 A comparison between the experimental and calculated absorption spectrum of compound (145) in chloroform.

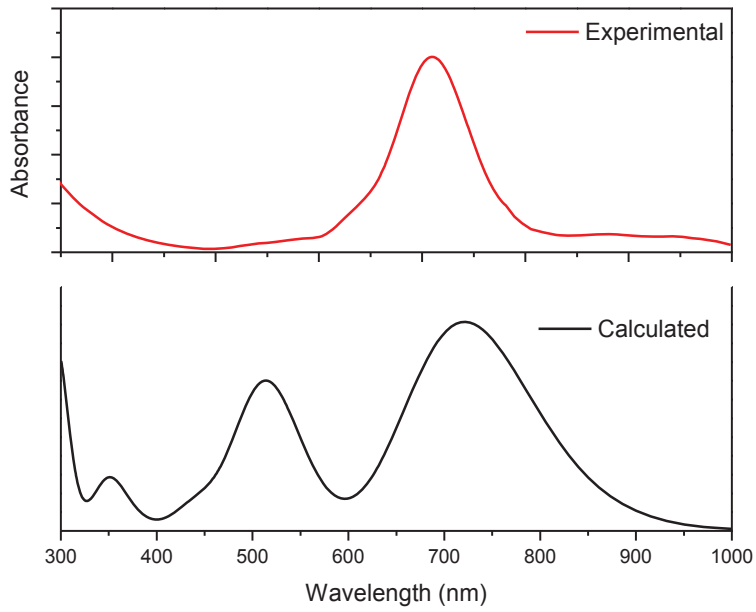

Figure 3.16 A comparison between the experimental and calculated absorption spectrum of compound (139) in chloroform.

The design of a high-efficiency donor for organic solar cells requires small energy gap, high hole mobility, and a relatively low-lying HOMO level.[16] It has also been found that broadening the absorption of the donor is an efficient strategy to improve the power conversion efficiency (η) in organic solar cells.[17] In this study, the introduction of electron donating and withdrawing groups on the aza-BODIPY has broadened and shifted the absorption wavelengths towards the near IR-region. For example, incorporation of electron-donating methoxy groups on the aryl rings (compound (88)) resulted in a small shift of 41 nm in comparison with compound (87). A significant red shift of 135 nm was observed when the electron donating triphenylamine (TPA) group was introduced onto the aza-BODIPY core structure (compound (100)) in comparison with compound (4) (1,3,5,7-tetraphenyl-aza-dipyrromethene boron difluoride). A remarkable red shift (284 nm) was found for compound (113) in comparison to compound (111) as a result of introducing electron donating triphenylamine (TPA) groups onto the aza-BODIPY structure.

Substitution with terthiophene units on both positions 1 and 7 of the aza-BODIPY core (compound (87)) had less impact on the absorption with a small shift of 15 nm in

comparison with the standard aza-BODIPY (compound (4)). Compound (87) exhibited two intense peaks at 335 nm and 665 nm (the maximum). The spectra of these aza-BODIPYs are shown in Fig. (3.17). The small difference between the standard aza-BODIPY (compound (4)) and compound (87) in terms of absorption range and onset might suggest that the optical band gaps of these compounds are almost the same, see Fig. (3.17) and Table (3.4).

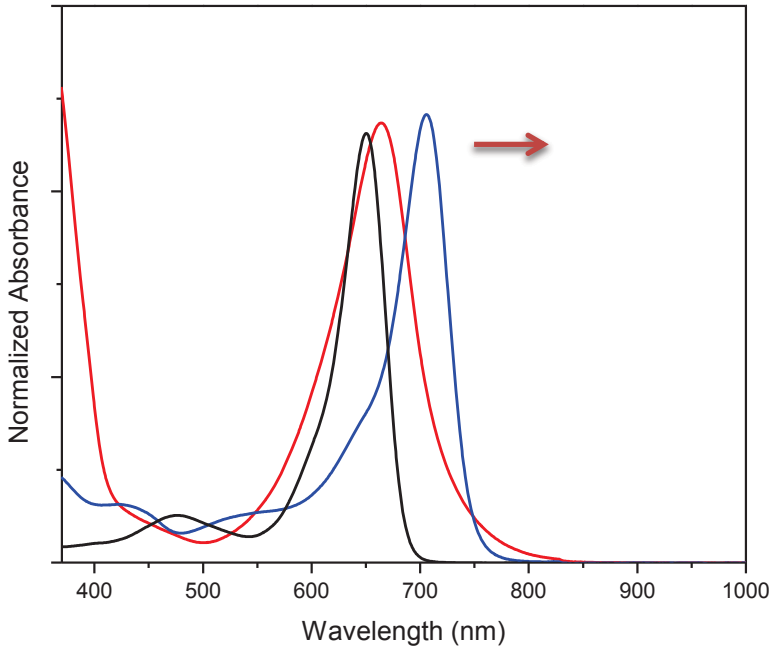

Figure 3.17 The experimental UV-visible spectra of compound (4), λ_{max}= 650 nm (black line), compound (87), λ_{max}= 665 nm (red line) and compound (88), λ_{max}= 706 nm (blue line) in chloroform.

Incorporation of electron-donating methoxy groups on the aryl rings (compound (88)) resulted in a small red shift of 41 nm in comparison with compound (87). Compound (88) exhibited two intense peaks at 295 nm and the maximum 706 nm. The UV-VIS results for the synthesized aza-BODIPYs are shown in Table (3.4).

The DFT calculations help explain the structure-optical property relationship of aza-BODIPY compounds. The optimized structures of the isolated molecules (87) and (88)

were obtained from DFT calculations (Fig. (3.18)). The aza-BODIPY core is a fully delocalised system and the boron difluoride (BF_2) units increase the planarity of the dipyrrin rings. The substituted terthiophene units at position 1 and 7, and the phenyl units at positions 3 and 5 are non-planar with the dipyrrin rings in both compounds (87) and (88).

Table 3.4: Experimental spectroscopic characteristics of compound (4) (literature)[15] and the synthesized aza-BODIPYs measured in chloroform.

	Compound number	Experimental	
		λ_{max} (nm)	ε (mol^{-1} cm^{-1})
1	(4)[15]	650	79000
2	(87)	665	15100
3	(88)	706	40300
4	(100)	785	28325
5	(106)	818	15236
6	(113)	855	25387
7	(150)	677	23884
8	(151)	725	38241
9	(111)	571	18240
10	(112)	754	22000
11	(125)	610	35042
12	(132)	755	20123
13	(139)	710	11325
14	(145)	736	33102

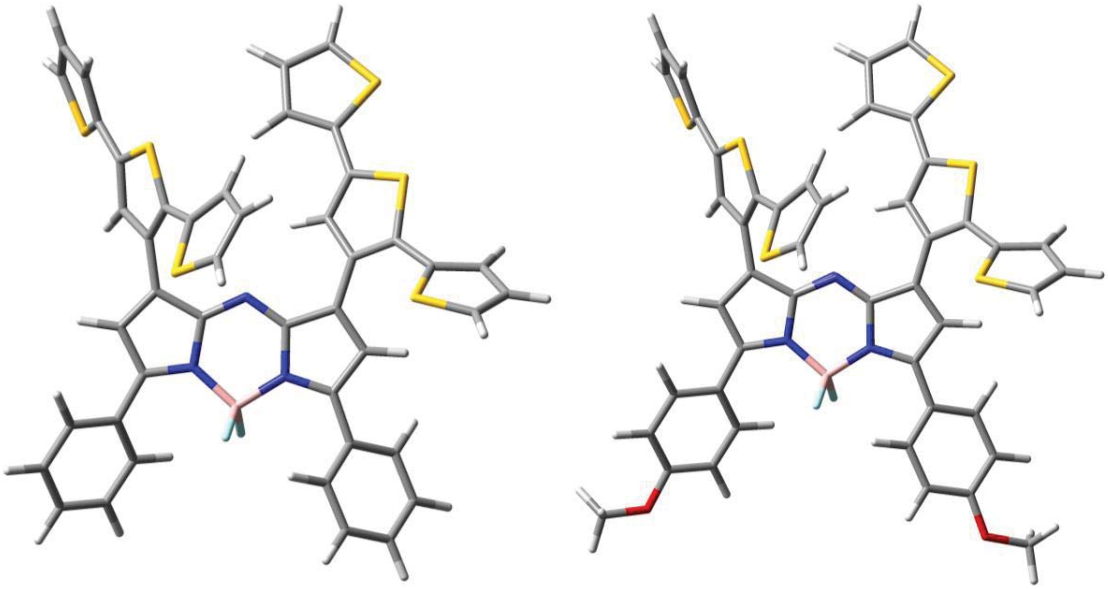

Figure 3.18 The optimized geometry of the isolated molecules (87) (left) and (88) (right) obtained from DFT calculations using DFT/B3LYP 6-311++G (2d, P) method.

Time-dependent DFT (TD-DFT) calculations have been used not only to predict the UV-VIS spectra, but also to determine the molecular orbitals involved in the electronic transitions. By replacing the phenyl groups at the 3 and 5 positions at the aza-BODIPY core with electron donating triphenylamine (TPA) groups (compound (100)), the absorption maxima has been significantly shifted by 135 nm when compared with compound (4) (see Fig. (3.19)), which is attributed to the electron donating ability as well as possibly to the extended conjugation lengths of the TPA groups. Compound (100) shows two major absorption bands at the visible region of the solar spectrum at 600 nm and 785 nm. From the TD-DFT calculation result, it is clear that both of the absorption bands are dominated by HOMO to LUMO electronic promotions, which correspond to charge-transfer from the triphenylamine arms to the phenyl rings through the central aza-BODIPY core. A further red shift occurs, of about 168 nm in comparison with compound (4), or 33 nm in comparison to compound (100), when the two phenyl groups at position 1 and 7 are replaced by thiophene rings (compound (106)). Compound (106) shows two absorption bands at the visible region (605 nm and 818 nm). These absorption bands are dominated by

HOMO to LUMO electronic promotions, which correspond to intramolecular charge-transfer (ICT) from the triphenylamine arms to the thiophene rings through the central aza-BODIPY core. These results suggest that the optical band gaps of compounds (100) and (106) are smaller in comparison to the band gaps of compounds (4), (87) and (88).

In push-pull-type molecules, incorporation of electron-rich and electron-deficient groups (specifically benzothiadazole-based groups) facilitates intramolecular charge transfer and such compounds exhibit a low band gap for a larger range of wavelengths of the solar spectrum.[17,18] This is in total agreement with the remarkable red shift observed for compound (113). Compound (113), which shows an absorption maximum at 855 nm represents the highest absorption maxima in this series of aza-BODIPY compounds. Introduction of the electron-deficient groups (benzothiadiazole groups) at positions 1 and 7 results in a significant red shift of about 205 nm in the absorption maxima in comparison with the standard aza-BODIPY (compound (4)), or 284 nm in comparison with compound (111). Fig. (3.19) shows the experimental UV-VIS spectrum of compounds (100), (106) and (113). It has been found in push-pull-type molecules that the HOMO level depends on the donor groups and these levels increase in energy, while the LUMO level is related to the acceptor groups and these decrease in energy.[16] These results suggest that the optical band gap of compound (113) is the smallest in comparison to the band gaps of the other synthesized aza-BODIPYs. From this it is concluded that the best strategy to tune the electronic energy levels and broaden the absorption of aza-BODIPY compounds is incorporation of suitable electron-rich and electron-deficient groups into the dipyrrin core. Replacement of the benzothiadiazole groups in compound (113) with the electron donating thiophene groups in compound (106) resulted in λ_{max}=818 nm, instead of 855 nm, suggesting that LUMO level has been raised in energy.

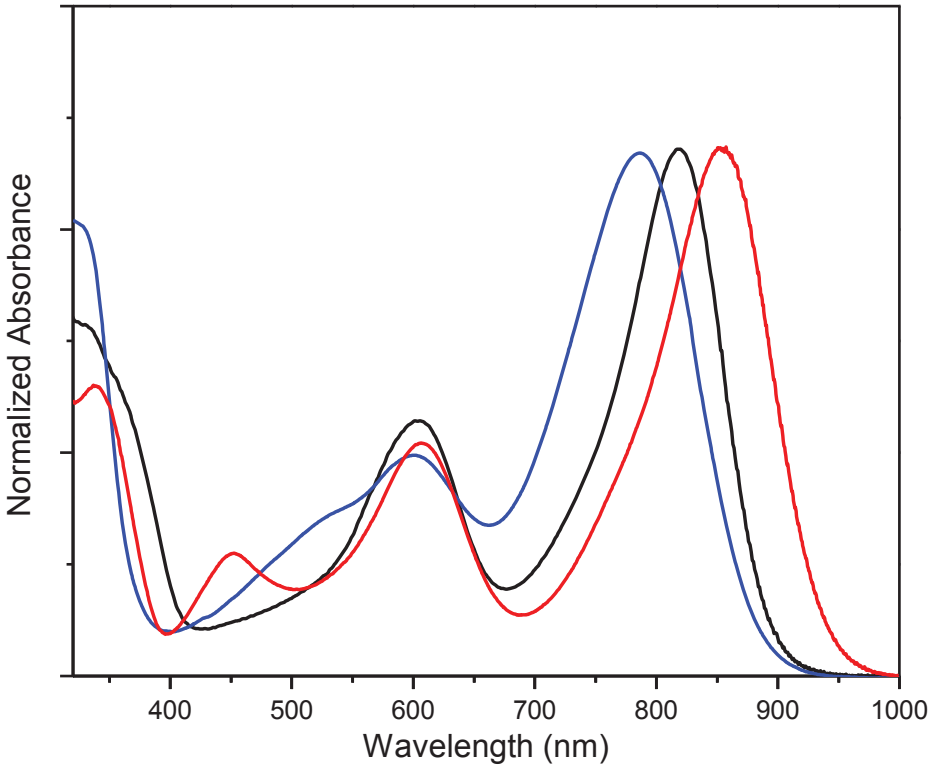

Figure 3.19 The experimental UV-VIS spectra of compound (100), λ_{max}=785 nm (blue line), compound (106), λ_{max}= 818 nm (black line) and compound (113), λ_{max}= 855 nm (red line) in chloroform.

The optimized structures of isolated compounds (100), (106) and (113) obtained from DFT calculations using the DFT/B3LYP 6-311++G (2d, p) method are shown in Fig. (3.20). For compound (106), it is obvious that the two thiophene rings (at 1 and 7 positions) are close to being parallel to the dipyrrin core, and it (106) showed a strong emission band at 890 nm. In the same compound, the sulphur atoms point away from each other, while the nitrogen atom at TPA has a trigonal pyramidal geometry. The phenyl groups at positions 1 and 7 of the dipyrrin core in compound (100) are non-planar, while the benzothiadiazole groups in compound (113) appear to be fairly close to being planar with the core and the two sulphur atoms are pointing away from each other. The experimental absorption spectra of these compounds are shown in Fig. (3.19).

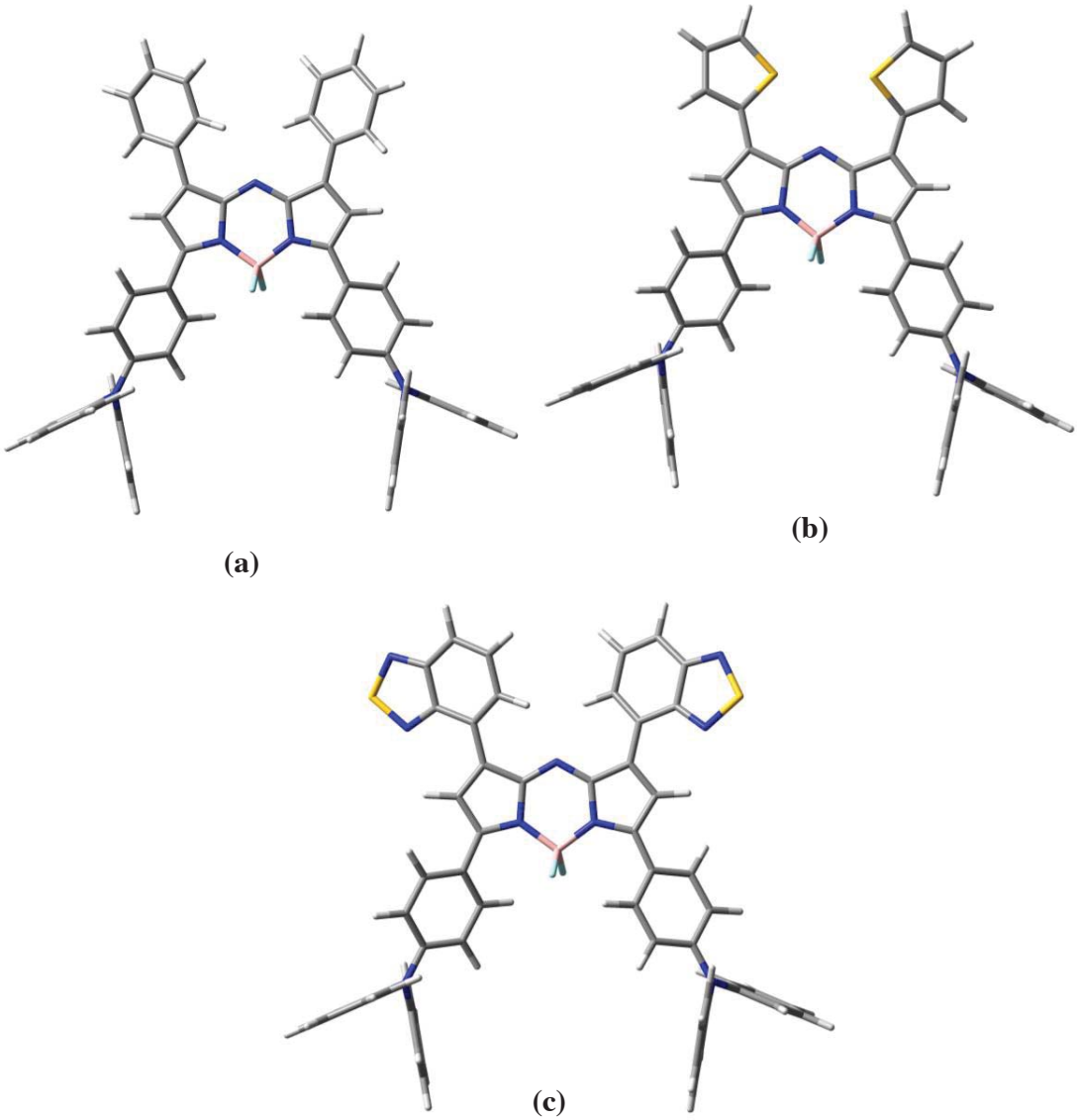

Figure 3.20 The optimized geometry of the isolated molecules (a) (100), (b) (106) and (c) (113) obtained from DFT calculations using DFT/B3LYP 6-311++G (2d, P) method.

Computed absorption energies for the excited states of compound (106) are shown in Table (3.5). The absorption energies have been calculated using the 6-311++G(2d,p) basis set and chloroform as a solvent. Compound (106) has been chosen to show the correlation between the electronic structure of aza-BODIPYs and their optical properties. Fig. (3.21), Fig. (3.22), Fig. (3.23) and Fig. (3.24) show the HOMO and LUMO orbitals.

Table 3.5: Calculated spectroscopic characteristics and frontier orbital energies of compounds (106), (125) and (151), calculated in chloroform.

Compound number	Main absorption wavelength (nm)	Energy [eV]	Principle orbital contribution	Oscillator strength	Contribution
(106)	825.1	1.5027	HOMO →LUMO (71%)	0.7659	0.70612
	658.35	1.8833	HOMO-1→LUMO (70%)	0.6417	0.70452
	385.96	3.2124	HOMO-10→LUMO (68%)	0.0251	0.67504
(125)	698.35	1.7754	HOMO → LUMO (70%)	0.6771	0.69947
	553.13	2.2415	HOMO-1→LUMO (68%)	0.3361	0.68048
	369.65	3.3541	HOMO-7→LUMO (68%)	0.2009	0.67561
(151)	700.33	1.7704	HOMO→LUMO (87%)	0.70573	0.8747
	553.99	2.2380	HOMO-2→LUMO (58%)	0.70105	0.5766
	349.22	3.5503	HOMO→LUMO+3 (58%)	0.63839	0.5783

The calculated λ_{max} at 825 nm, (818 nm, measured) is dominated by a HOMO to LUMO electronic promotion. It is evident from Fig. (3.21) and Fig. (3.22) that this absorption therefore corresponds to an intramolecular charge-transfer (ICT) from the triphenylamine arms to the thiophene rings through the central aza-BODIPYs core. The second band at 658 nm, calculated (605 nm, measured) is dominated by a HOMO-1 to LUMO transition. From Fig. (3.22) and Fig. (3.23) this absorption band corresponds to pure intramolecular charge transfer (ICT) from triphenylamine arms to the central aza-BODIPY core and thiophene rings. The absorption band at 386 nm, calculated (335 nm, measured) is dominated by a HOMO-10 to LUMO component. This corresponds to an intramolecular charge transfer (ICT) from thiophene rings to the central aza-BODIPY core, although there

is a small contribution from a HOMO-7 to LUMO, corresponding to an intramolecular charge transfer from the terminal phenyl rings in the triphenylamine arms to the central aza-BODIPY core and thiophene rings. The two absorption bands at 820 nm and 605 nm imply an intramolecular charge transfer from the triphenylamine arms towards the aza-BODIPY core and thiophene rings, whereas the 335 nm presents the opposite character (intramolecular charge transfer from thiophene rings to the central aza-BODIPY core).

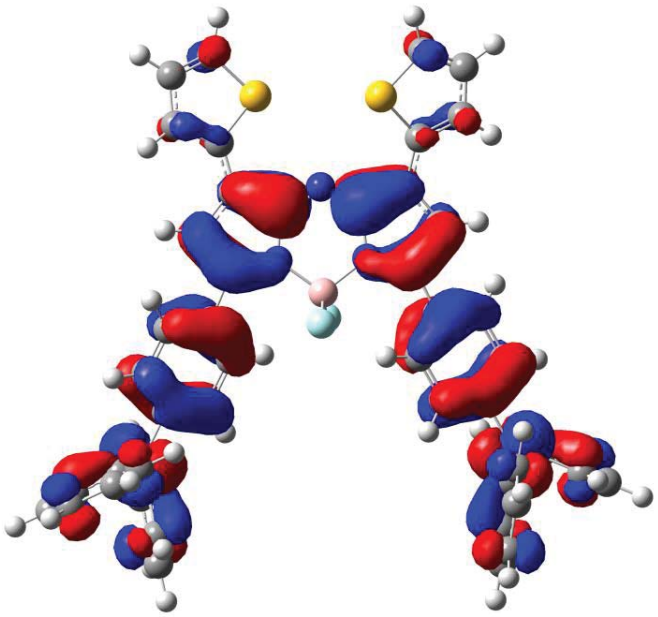

Figure 3.21 The HOMO frontier orbital of compound (106)

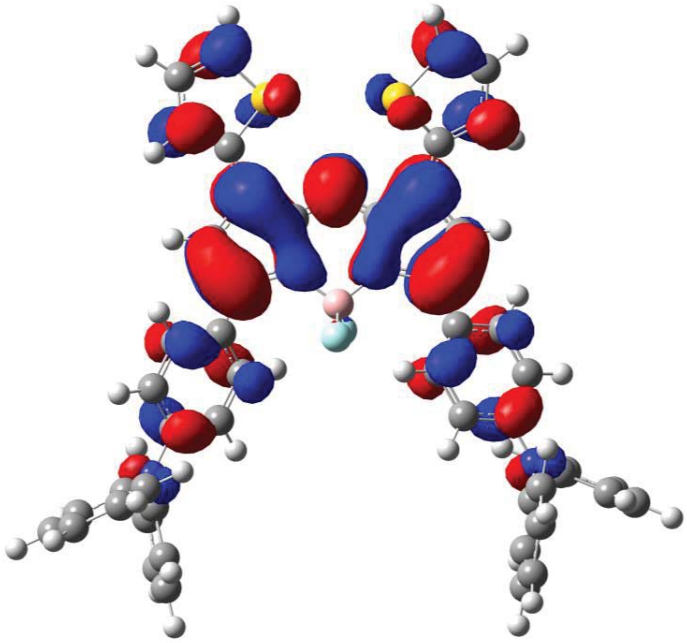

Figure 3.22 The LUMO frontier orbital of compound (106)

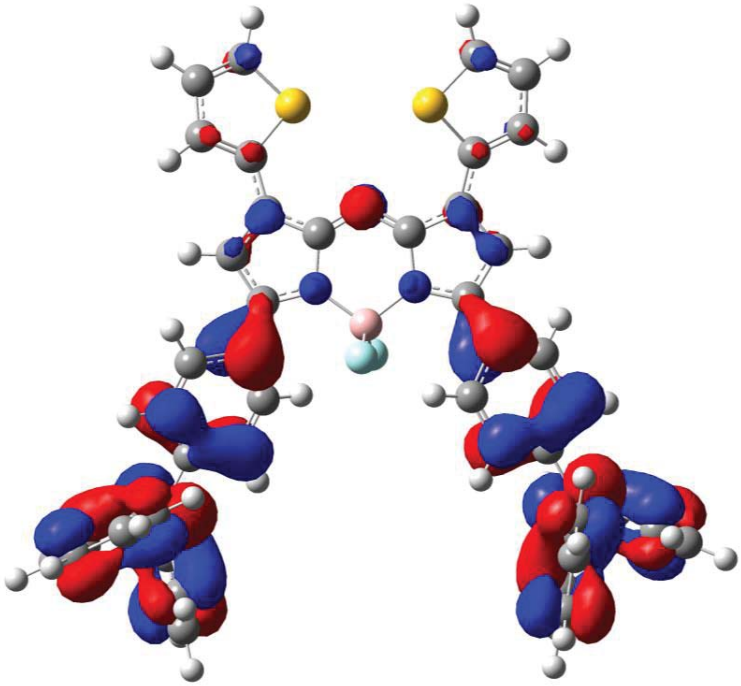

Figure 3.23 The HOMO-1 frontier orbital of compound (106)

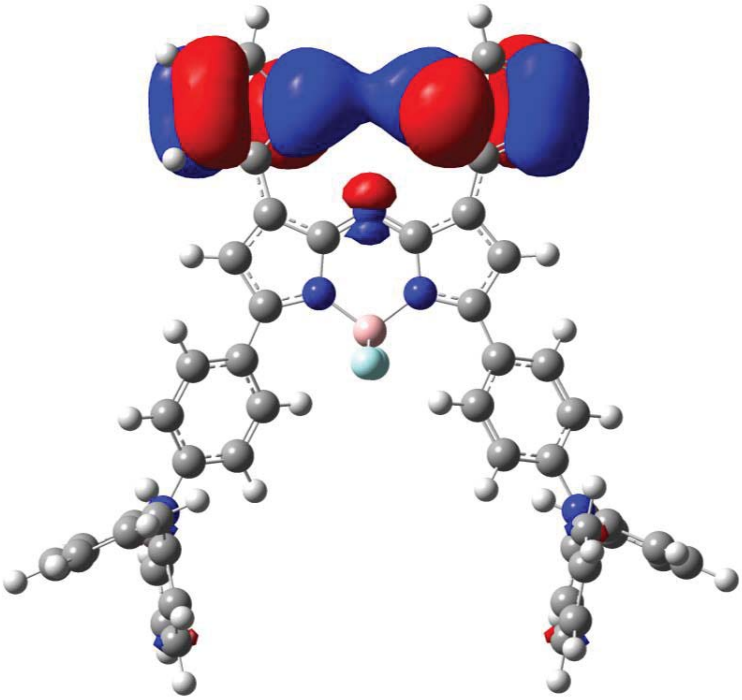

Figure 3.24 The HOMO-10 frontier orbital of compound (106)

Incorporation of fluorenone units at the 1 and 7 positions on the dipyyrin core (compound (150)) resulted in an absorption maximum at 670 nm. The very small shift (20 nm) in the absorption of compound (150) in comparison to compound (4) might be attributed to the weakly electron withdrawing property and steric hindrance of fluorenone groups. The fluorenone units appear to be slightly non-planar with the dipyrrin core, while the two oxygen atoms of the fluorenone units are pointing away from each other. The phenyl groups in the same compound are non-planar with the dipyrrin core. An interesting red shift (about 75 nm in comparison with compound (4)) occurred in compound (151), in which fluorenone units are located at the 3 and 5 and thiophene units are located at 1 and 7 positions. Compound (151) showed an absorption maximum at (λ_{max}) 725 nm and an interesting emission was observed at (λ_{em}) 762 nm. This moderate red-shift in the absorption of compound (151) is in agreement with the same push-pull-type argument that was invoked with compound (113). Fluorenone is a weak electron-withdrawing group and thiophene is an electron-donating group, which explains the moderate red-shift throughout the intramolecular charge transfer, being less intense compared with compound (113). The

optimized geometry of compound (151) suggests that the two thiophene units at 1 and 7 positions are planar with the dipyrrin core while the fluorenone units (at 3 and 5 positions) are not. The optimized structures of compounds (150) and (151) obtained from DFT calculations are shown in Fig. (3.26). The UV-VIS data is shown in Fig. (3.25) and Table (3.4).

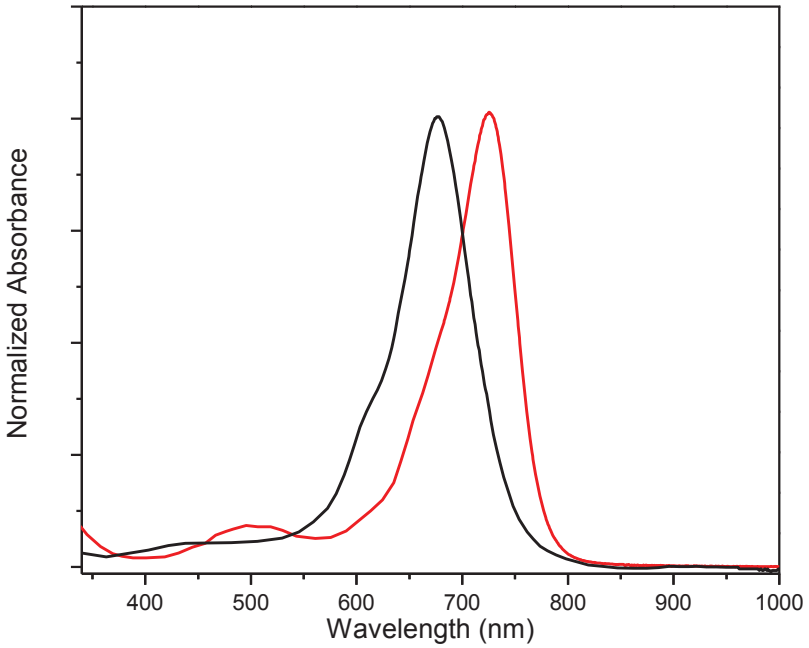

Figure 3.25 The experimental UV-visible spectra of compound (150), λ_{max}= 677 nm (black line) and compound (151), λ_{max}= 725 nm (red line) in chloroform.

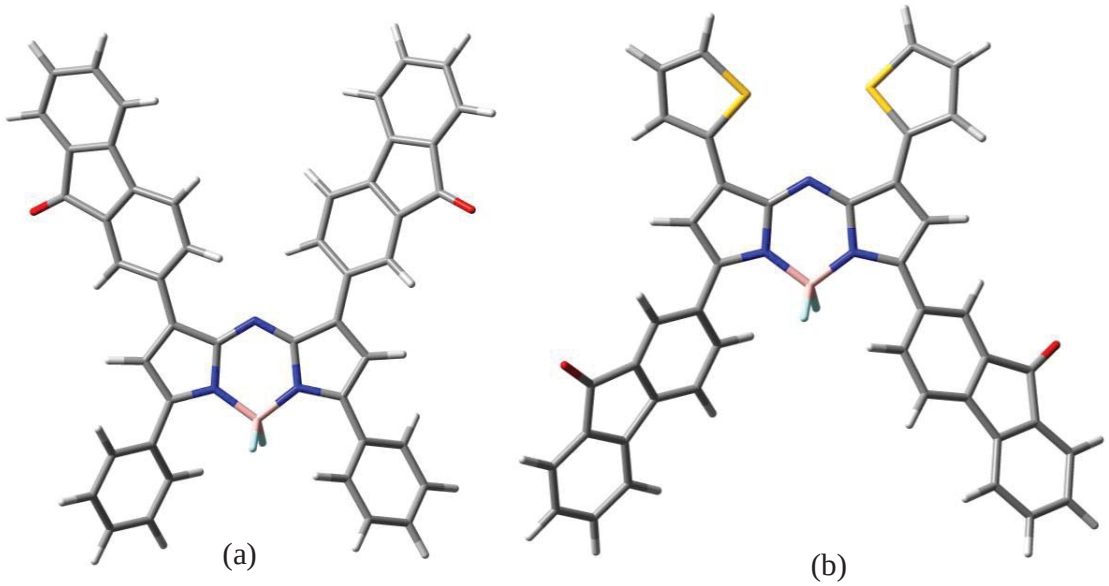

Figure 3.26 The optimized geometry of isolated molecules (a) (150) and (b) (151) obtained from DFT calculations using DFT/B3LYP 6-311++G (2d, P) method.

The HOMO and LUMO orbitals of compound (151) are shown in Fig. (3.26), Fig. (3.27), Fig. (3.28) and Fig. (3.29). The calculated absorption bands at 700 nm and 553 nm (727 nm and 500 nm measured) are dominated by HOMO to LUMO and HOMO-2 to LUMO electronic promotions. This absorption corresponds to intramolecular charge transfer (ICT) from the thiophene arms and a small contribution from the fluorenone arms to the central aza-BODIPY core. The calculated absorption band at 349 nm (320 nm, measured) is dominated by a HOMO to LUMO+3 component. This corresponds to an intramolecular charge transfer from thiophene rings and the aza-BODIPY core to fluorenone arms through the central aza-BODIPY core. The calculated absorption bands at 700 nm and 553 nm imply a charge transfer from the thiophene and fluorenone arms towards the aza-BODIPY core, whereas the 349 nm presents the opposite character (ICT from thiophene rings and aza-BODIPY core to fluorenone arms).

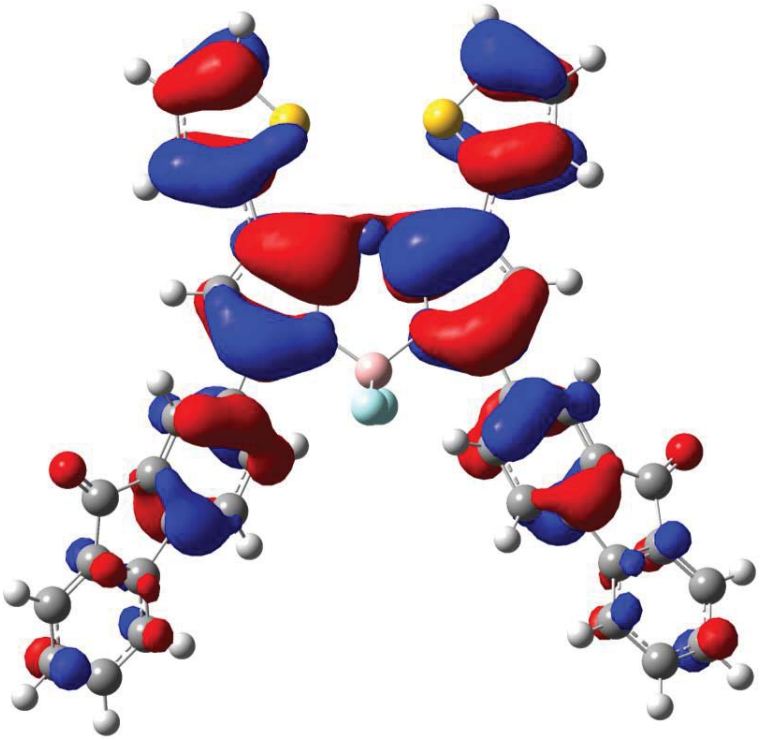

Figure 3.27 The HOMO frontier orbital of compound (151)

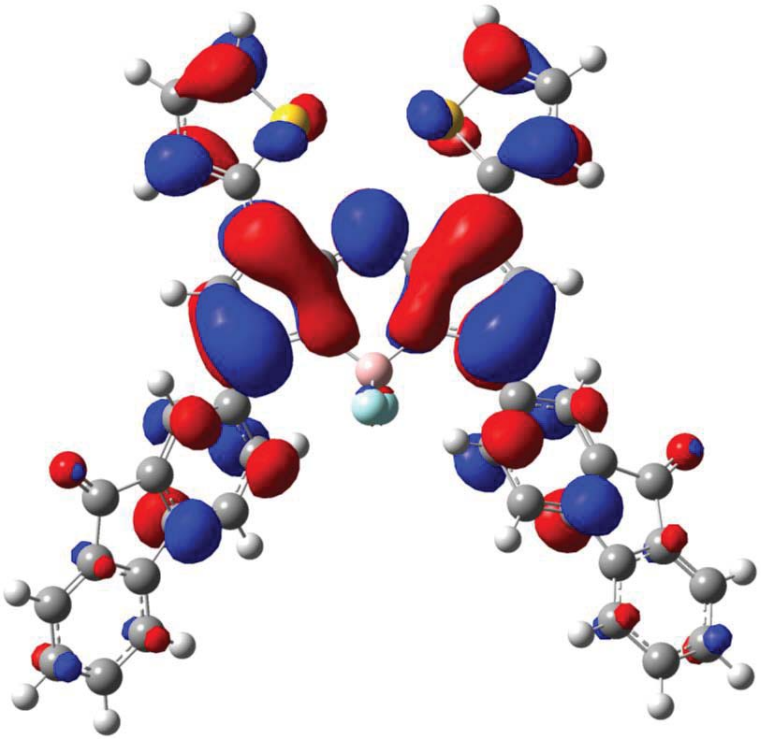

Figure 3.28 The LUMO frontier orbital of compound (151)

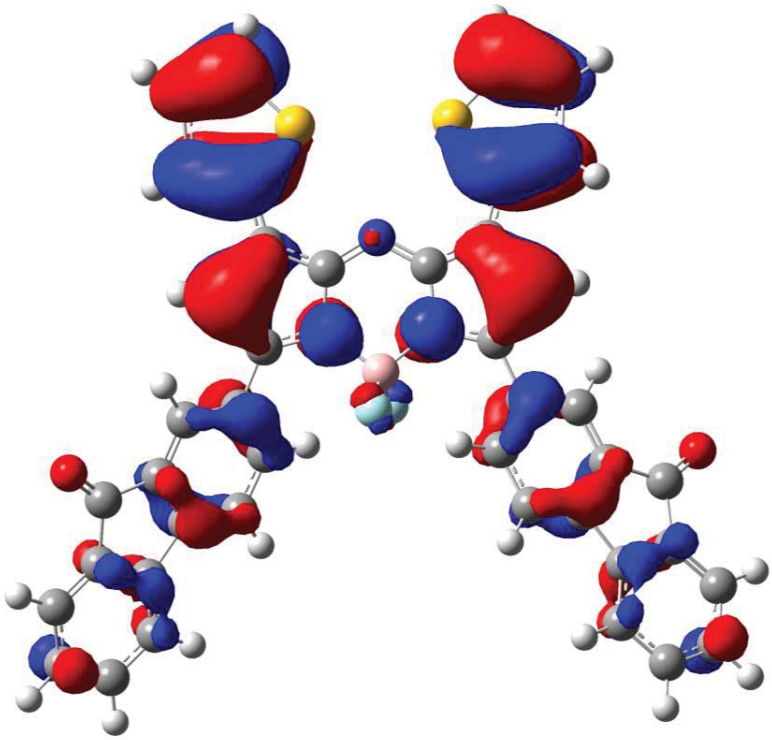

Figure 3.29 The HOMO-2 frontier orbital of compound (151)

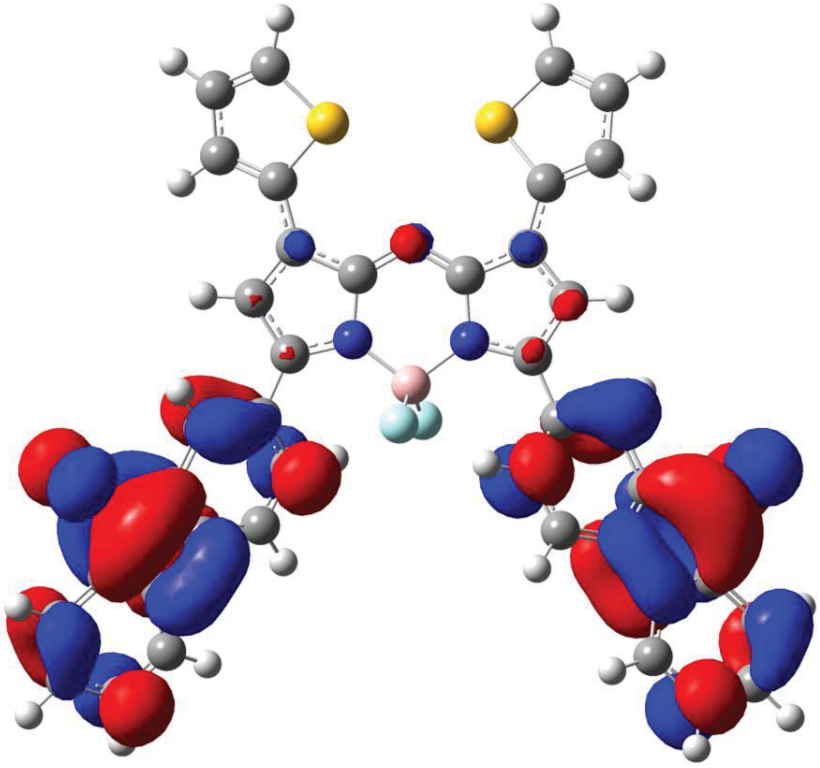

Figure 3.30 The LUMO+3 frontier orbital of compound (151)

Introducing benzothiadiazole units at the 1 and 7 positions of the dipyrrin core in compounds (111) and (112) resulted in absorption bands at 571 nm and 754 nm respectively. Incorporating thiophene units at positions 3 and 5 (compound (112)) red-shifted the absorption band by 104 nm when compared with compound (4), which might be explained by the same push-pull-type strategy as developed for compound (113). A blue-shift was observed (-79 nm) in compound (111) in comparison with compound (4), which might be attributable to the presence on the dipyrrin core of strong electron-deficient groups (benzothiadiazole) and the absence of a strong electron-rich groups such as thiophene and TPA found in compounds (112) and (113). Furthermore, the blue shift which resulted from incorporation of only strong electron-deficient groups into the dipyrrin core (e.g. compound (111)) reflects a negative effect in term of optical band gap, because the shift indicates a larger optical band gap. Incorporation of strong electron-deficient groups (benzothiadiazole) onto the dipyrrin core was predicted to lower the energy level of the LUMO and as a result reduce the band gap. This wasn't the case for compound (111), and might be a result of non-conjugation of R_1 or R_2 or both groups with the dipyrrin core. Further investigation is required, in particular measurements of the energy levels. From the optimized structure of compound (111) (Fig. (3.32) (a)), it can be seen that the benzothiadiazole units are not completely planar with the dipyrrin core. Also, the phenyl groups in the same compound (111) are not planar with the dipyrrin core. No emission bands were observed for compound (111). The opposite arises with compound (112): the benzothiadiazole units at the 1 and 7 positions are planar with the dipyrrin core, while the sulfur atoms are pointing away from each other. It seems also that the thiophene units are co-planar with the dipyrrin core and their sulfur atoms are pointing away from each other. Compound (112) showed an interesting emission band at λ_{em}=776 nm. In comparison with compound (4), a small unexpected blue-shift (-40 nm) was observed upon replacing benzothiadiazole groups at the 1 and 7 positions of compound (111) with EDOT groups (compound (125)), which suggests that the EDOT groups might have an unusual impact on the optical band gap. The geometry optimization of compound (125) shows that the EDOT units are non-planar as the rings containing the oxygen atoms inside the EDOT units are non-planar, but the thiophene rings of the EDOT units are essentially planar with the dipyrrin core. The phenyl groups at 3 and 5 positions are non-planar with the dipyrrin units.

Compound (125) showed an emission band at λ_{em}=660 nm. The UV-VIS spectrum of compounds (111), (112) and (125) are shown in Fig. (3.31), while the geometry optimized structures are shown in Fig. (3.32).

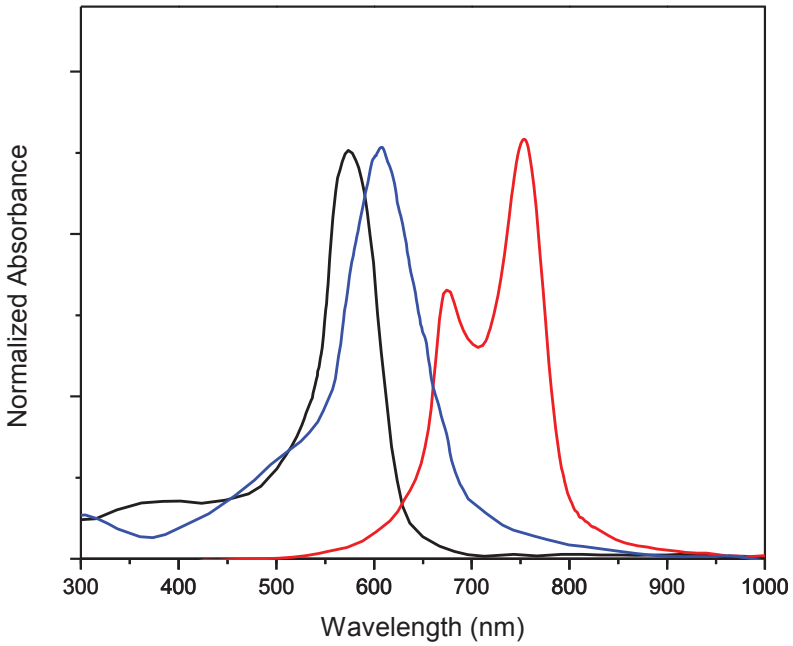

Figure 3.31 The experimental UV-visible spectra of compound (111), λ_{max}= 571 nm (black line), compound (112), λ_{max}= 754 nm (red line) and compound (125), λ_{max}= 610 nm (blue line) in chloroform.

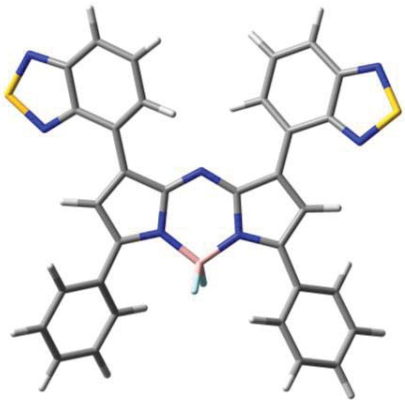

(a)

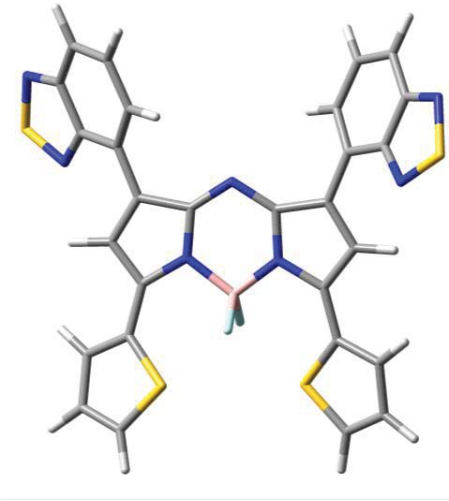

(b)

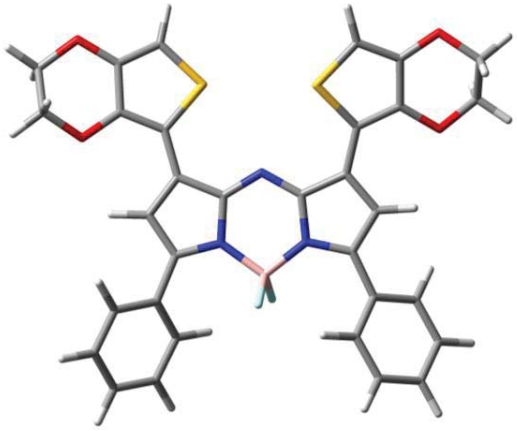

(c)

Figure 3.32 The optimized geometry of isolated molecules (a) (111) (b) (112) and (c) (125) obtained from DFT calculations using DFT/B3LYP 6-311++G (2d, P) method.

For compound (125), the HOMO and LUMO orbitals which contribute to the absorption spectrum are shown in Fig. (3.33), Fig. (3.34), Fig. (3.35) and Fig. (3.36). The calculated absorption bands at 698 nm and 553 nm (610 nm, measured) are dominated by HOMO to LUMO and HOMO-1 to LUMO electronic promotion. These two absorption bands therefore correspond to intramolecular-charge-transfers from the thiophene rings of EDOT arms to the phenyl arms through the central aza-BODIPY core. The third calculated absorption band at 369 nm (320 nm, measured) is dominated by a HOMO-7 to LUMO transition. This absorption band corresponds to pure charge transfer from phenyl arms to the central aza-BODIPY core and EDOT arms. The two absorption bands at 698 nm and 553 nm imply an intramolecular-charge-transfer from the EDOT arms towards the aza-BODIPY core and phenyl rings, whereas the 369 nm presents the opposite character (charge transfer from phenyl arms to the central aza-BODIPY core).

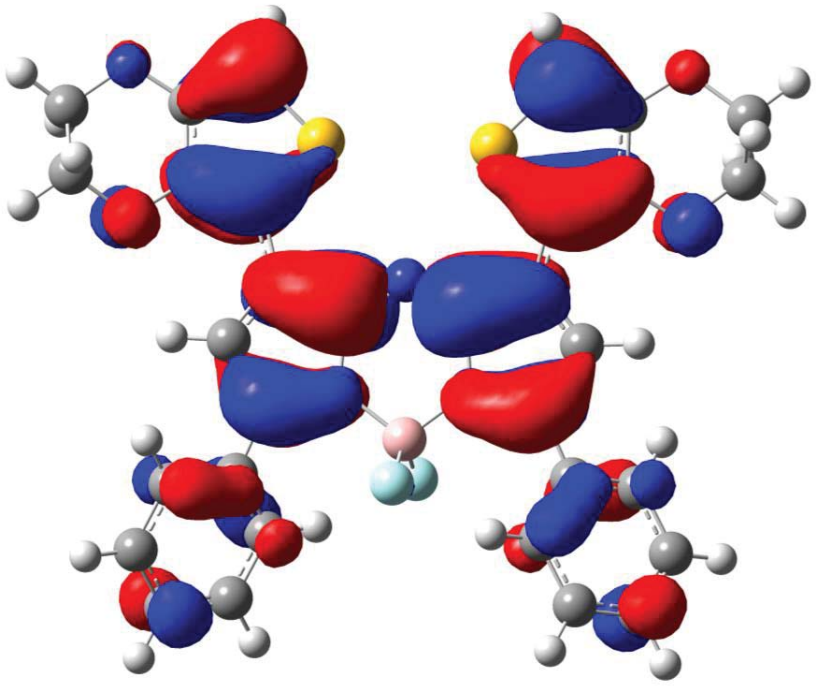

Figure 3.33 The HOMO frontier orbital of compound (125)

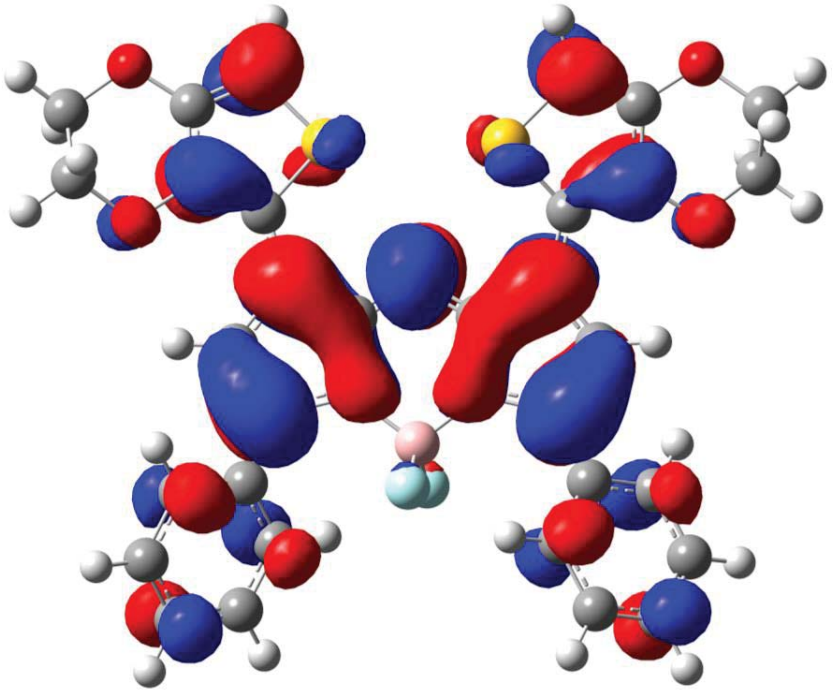

Figure 3.34 The LUMO frontier orbital of compound (125)

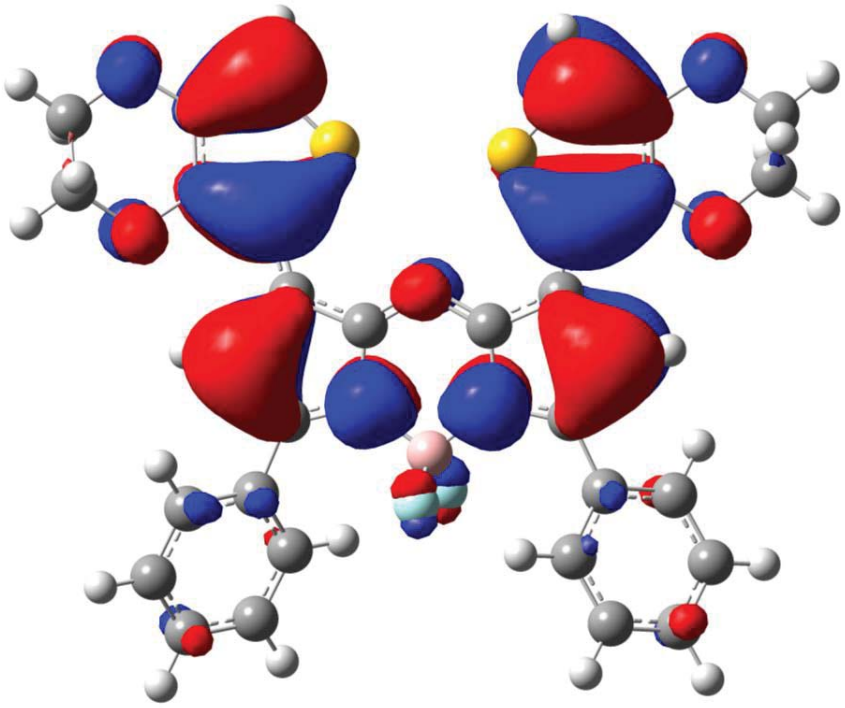

Figure 3.35 The HOMO-1 frontier orbital of compound (125)

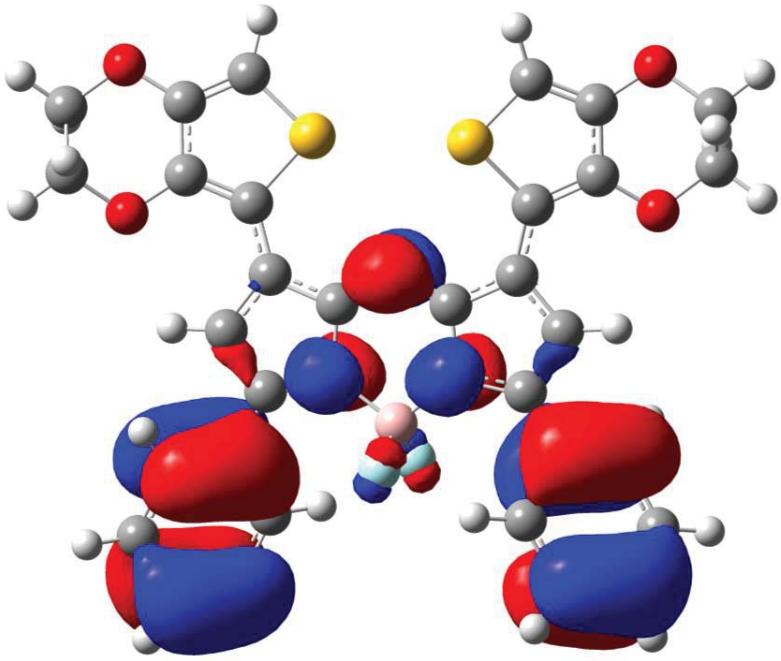

Figure 3.36 The HOMO-7 frontier orbital of compound (125)

Introducing thiophene groups at the 1 and 7 positions and varying the units at the 3 and 5 positions from phenothiazine to methylpyrrole to carbazole groups resulted in absorption bands at λ_{max}= 755 nm for compound (132), λ_{max}= 710 nm for compound (139) and λ_{max}= 736 nm for compound (145). Substitution with electron-deficient phenothiazine groups (compound (132)) resulted in the longest absorption wavelength, in comparison with substitution of methylpyrrole or carbazole groups, and this might be attributed to the possibility of the push-pull-type effect in compound (132). As a result, incorporation of phenothiazine and thiophene groups into a dipyrrin core has a moderately positive effect in terms of reducing the optical band gap. The geometry optimization showed that the thiophene units on compound (132) are close to planar with the dipyrrin core, while the phenothiazine units appear to be a slightly bent and not planar with the dipyrrin. Thiophene units are close to being planar with the dipyrrin core in compound (139) while methylpyrrole units are non-planar with the dipyrrin core, hence the methyl groups at pyrrole rings are pointing away from each other. The thiophene units are slightly planar with the dipyrrin core in compound (145), whereas the carbazole units are non-planar with the dipyrrin core. The UV-VIS spectra of compounds (132), (139) and (145) are shown in

Fig. (3.37). The geometry optimization structures obtained from DFT calculation are shown in Fig. (3.38) and Fig. (3.39).

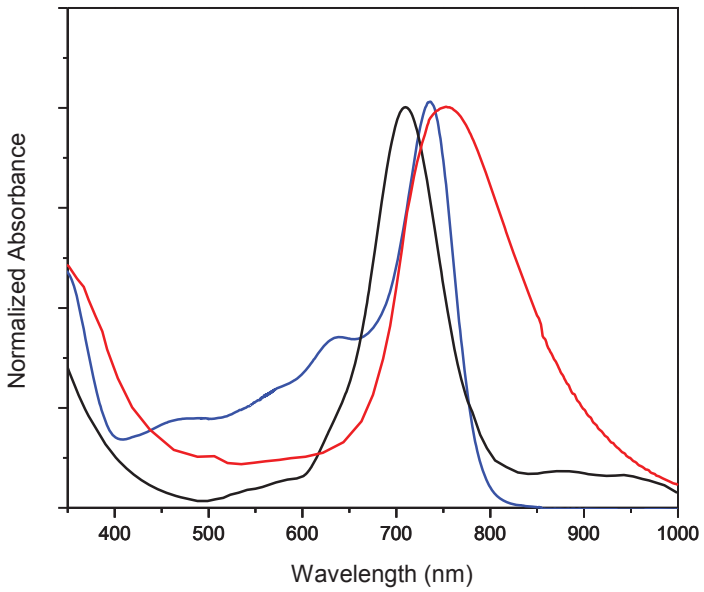

Figure 3.37 The experimental UV-visible spectra of compound (139), λ_{max}= 710 nm (black line), compound (132), λ_{max}= 755 nm (red line) and compound (145), λ_{max}= 736 nm (blue line) in chloroform.

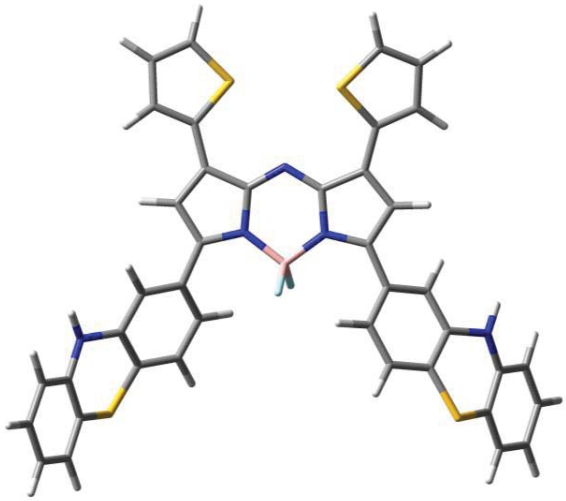

Figure 3.38 The optimized geometry of the isolated molecule (132) obtained from DFT calculations using DFT/B3LYP 6-311++G (2d, P) method.

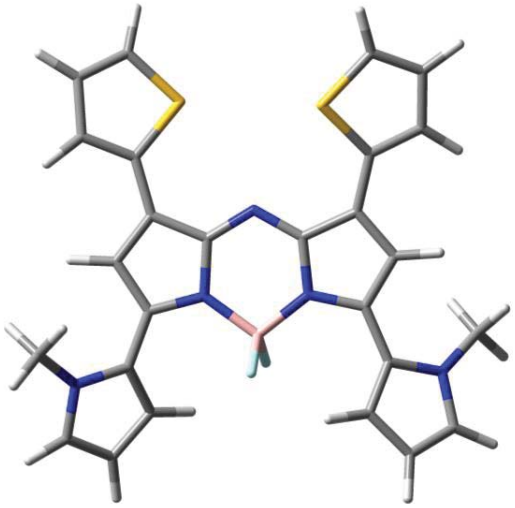

(a)

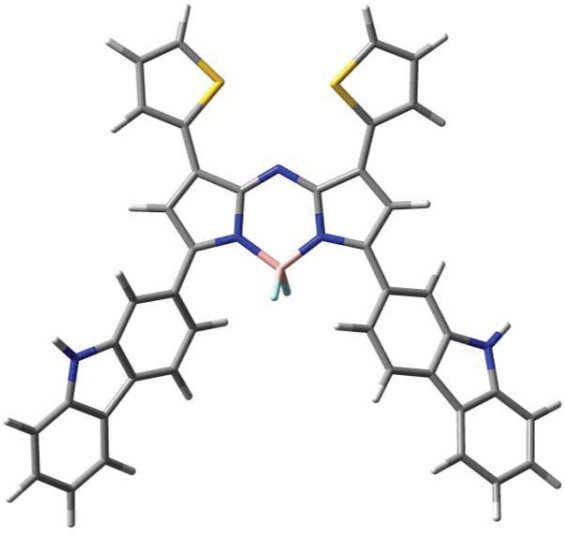

(b)

Figure 3.39 The optimized geometry of the isolated molecules (a) (139) and (b) (145) obtained from DFT calculations using DFT/B3LYP 6-311++G (2d, P) method.

3.3.2 Fluorescence Study

3.3.2.1 Fluorescence Spectra and Quantum yields

Fluorescence measurements of aza-BODIPYs were performed in chloroform solution in all cases. Several substituted aza-BODIPYs emitted in the red spectral region. The fluorescence spectra for compounds (88), (106), (112), (113), (125), (145) and (151) are shown in Fig. (3.39), Fig. (3.40), Fig. (3.41), Fig. (3.42), Fig. (3.43) and Fig. (3.44). Table (3.6) displays the fluorescence data for these compounds. The fluorescence spectra showed that the emission maxima varied from 658 nm for compound (125) to the remarkable emission at 953 nm for compound (113).

The fluorescence quantum yield (Φ)[19,20] is defined as the ratio of photons emitted to photons absorbed.

$$\Phi = \frac{\text{number of photons emitted}}{\text{number of photons absorbed}}$$

Table 3.6: Experimental fluorescence characteristics of compounds (88), (106), (112), (113), (125), (145), and (151) measured in chloroform, compared with compound (4).[15]

	Compound number	λ_{em} (nm)	Fluorescence Quantum Yield (Φ)[a]
1	(4)[15]	672	0.340
2	(88)	734	0.0648
3	(106)	896	0.1366
4	(112)	776	0.0931
5	(113)	953	0.0109
6	(125)	658	0.0254
7	(145)	778	0.0892
8	(151)	763	0.0298

[a] Fluorescence quantum yield measured relative to Rhodamine 101.

Fluorescence quantum yield measurements were performed using the integrating sphere (Fig. (3.1)). Rhodamine 101 and Nile Blue Chloride were used as standards for comparison in fluorescence quantum yield measurements. The fluorescence quantum yields provide an

upper limit for the emission efficiency within an organic layer. Fluorescence of photovoltaic materials is not desirable, because fluorescence is an energy-loss mechanism. For emissive applications such as LEDs, fluorescence behaviour is desired. For solar cells a low quantum yield is desired. Quantum yield measurements were determined for the emissive materials 88, 106, 112, 113, 125, 145, and 151 (Table 3.6). These compounds showed low quantum yields (in the range Φ= 0.0109 to 0.1366) in comparison to the standard aza-BODIPY (compound (4)) (Φ= 0.340, Table 3.6, entry 1). The low values of the quantum yields might be attributable to several reasons: the collision of excited molecule with non-excited molecule (energy loss), self-quenching or a solvent effect (the loss of fluorescence emission because of interactions between the fluorophore and the local molecular environment or with another fluorophore).

The absorption and emission spectra have shifted to significantly longer wavelengths on adding substituents to the aza-BODIPY core which yielded additional conjugation (Fig. (3.39) to Fig. (3.45)). An aza-BODIPY with a remarkable emission properties (λ_{em}= 953 nm for compound (113)) has been discovered in this study. The most effective substituents for producing red shifts in absorption and intense fluorescence in comparison to the aza-BODIPY parent molecule (4) were benzothiadiazole, thiophene and triphenylamine. Benzothiadiazole and triphenylamine-based dyes (compounds (106), (112) and (113)) displayed intense orange-red colour fluorescence in a region of 750–960 nm (compound (106), λ_{em}= 896 nm; compound (112), λ_{em}= 776; compound (113), λ_{em}= 953).

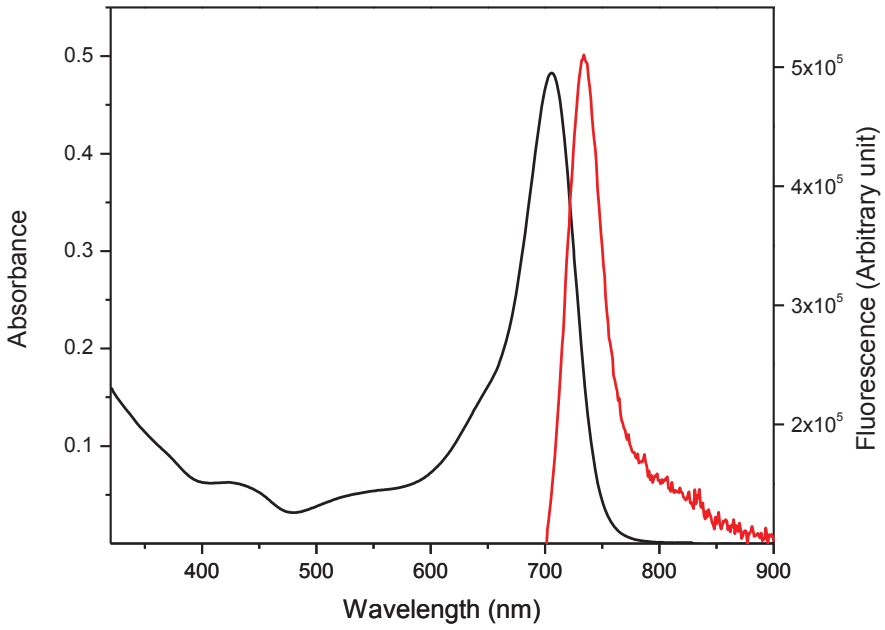

Figure 3.40 Absorption (black line) and emission spectra (red line) of compound (88) in chloroform, λ_{max}= 706 nm, λ_{ex}= 686 nm, λ_{em}= 734 nm.

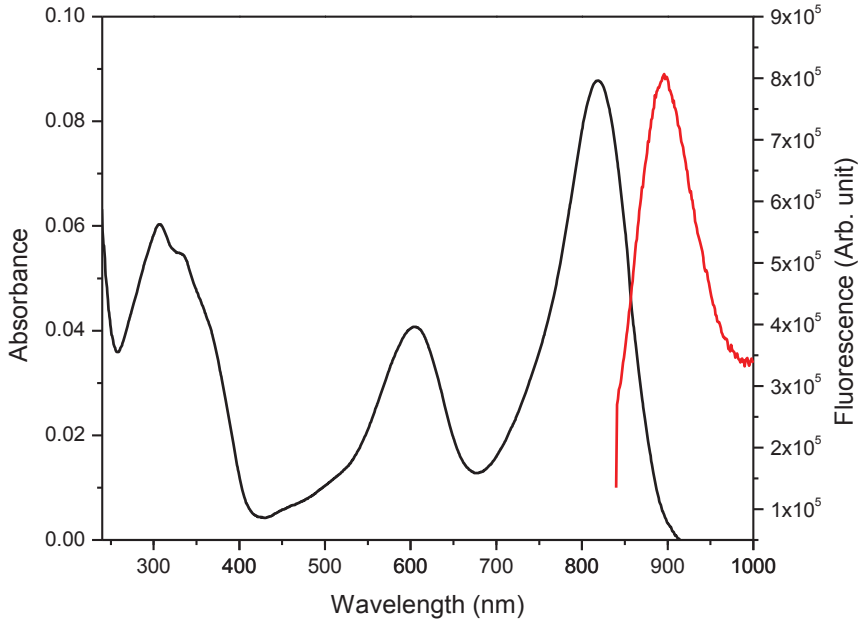

Figure 3.41 Absorption (black line) and emission spectra (red line) of compound (106) in chloroform, λ_{max}= 818 nm, λ_{ex}= 825 nm, λ_{em}= 896 nm.

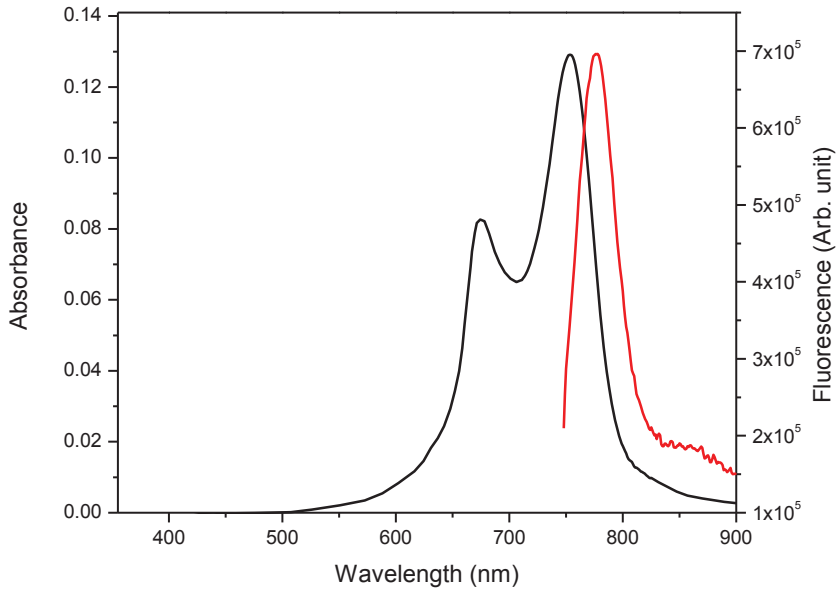

Figure 3.42 Absorption (black line) and emission spectra (red line) of compound (112) in chloroform, λ_{max}= 754 nm, λ_{ex}= 730 nm, λ_{em}= 776 nm.

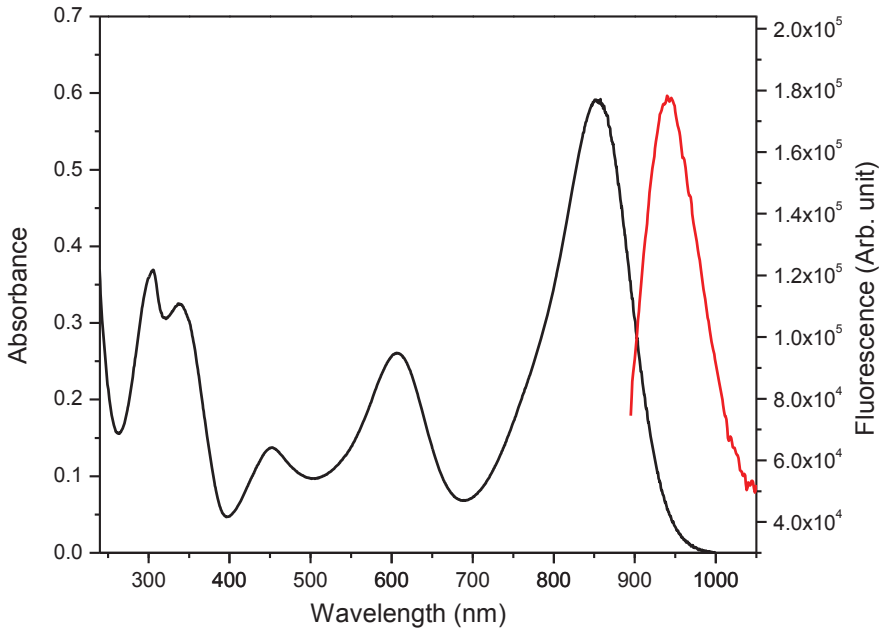

Figure 3.43 Absorption (black line) and emission spectra (red line) of compound (113) in chloroform, λ_{max}= 855 nm, λ_{ex}= 880 nm, λ_{em}= 953 nm.

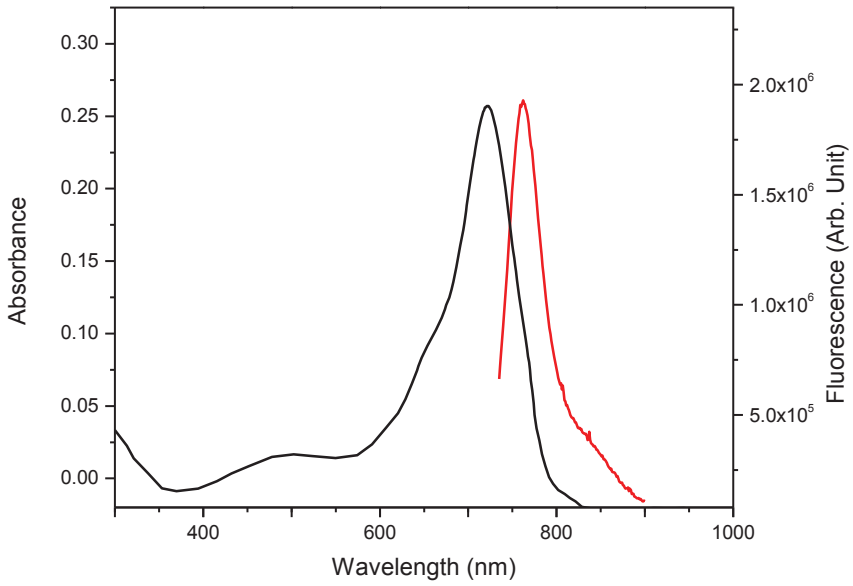

Figure 3.44 Absorption (black line) and emission spectra (red line) of compound (151) in chloroform, λ_{max}= 725 nm, λ_{ex}= 725 nm, λ_{em}= 763 nm.

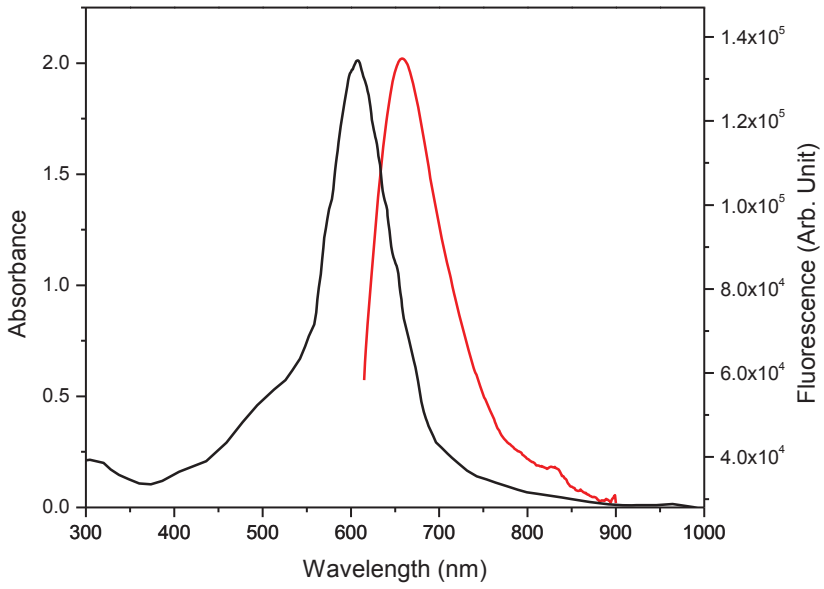

Figure 3.45 Absorption (black line) and emission spectra (red line) of compound (125) in chloroform, λ_{max}= 610 nm, λ_{ex}= 595 nm, λ_{em}= 658 nm.

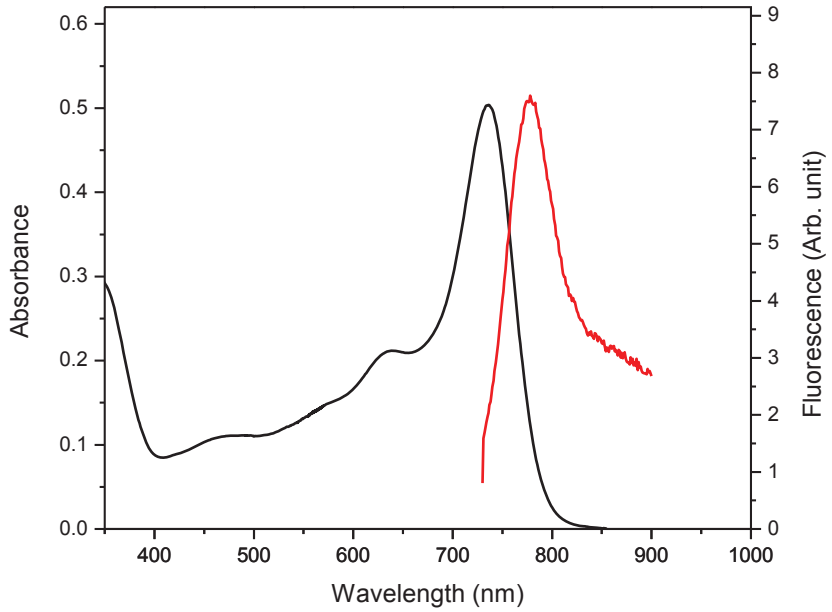

Figure 3.46 Absorption (black line) and emission spectra (red line) of compound (145) in chloroform, λ_{max}= 736 nm, λ_{ex}= 715 nm, λ_{em}= 778 nm.

3.3.2.2 Fluorescence Quenching

Charge transfer from a donor to an acceptor (e.g. the fullerene derivative ($PC_{60}BM$)) is central to the function of an efficient organic solar cell.[21-31] The electron transfer occurs in a very short time (sub-picosecond timeframe) inside the solar cell, which is faster than any other competing process. [32,33] Therefore, charge transfer quenches the fluorescence of the donor molecule.

Fluorescence quenching of selected compounds (compound (88) and (106)) in chloroform solution was studied at different concentrations of the quencher ($PC_{60}BM$) in closed containers under argon at room temperature. The concentration of the fluorophores (compounds (88) and (106)) was the same for all measurements. Fig. (3.46) shows the fluorescence of compounds (88) and (106) quenched by $PC_{60}BM$ in chloroform solution. It can be seen from Fig. (3.46) that the fluorescence intensities of these compounds decreased as a result of enhanced quenching on increasing $PC_{60}BM$ concentration. There are two important quenching processes: collisional (dynamic) quenching and static (complex formation) quenching.

Investigation of fluorescence quenching in the nanosecond timeframe using time-correlated single-photon counting (TCSPC) spectroscopy is described at the next Section (3.3.3).

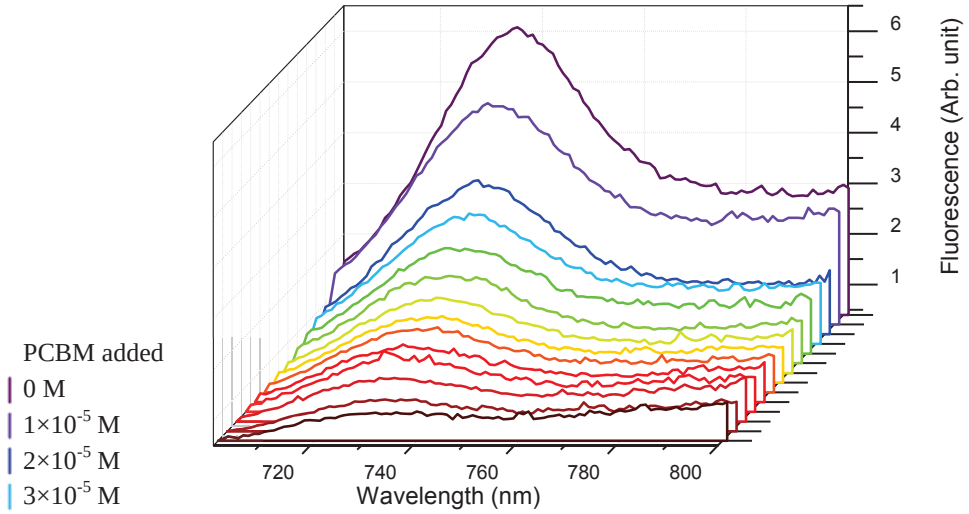

(a)

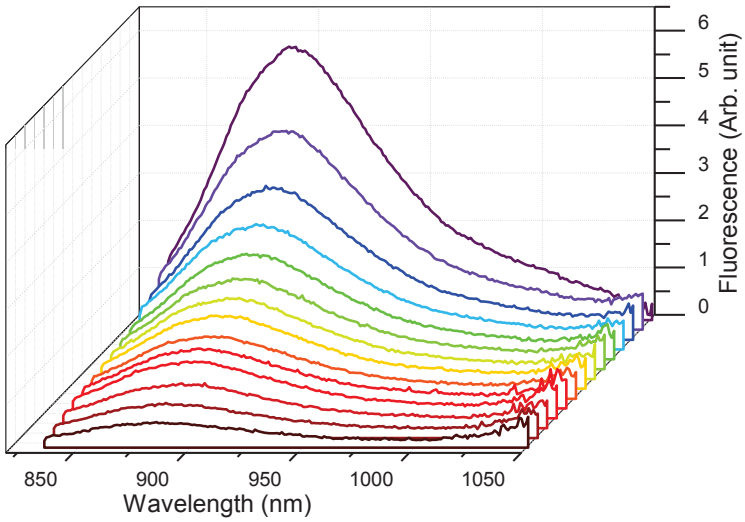

(b)

Figure 3.47 Fluorescence quenching by $PC_{60}BM$ of (a) compound (88) (λ_{ex}= 686 nm and λ_{em}= 734 nm) and (b) compound (106) (λ_{ex}= 825 nm and λ_{em}= 896 nm) in chloroform solution.

3.3.3 Time-Correlated Single-Photon Counting (TCSPC) Study

A pulsed laser was used to excite aza-BODIPYs in a chloroform solution. The measurement of fluorescence lifetimes of aza-BODIPYs is discussed in Section (3.3.3.1). Determination of the Stern-Volmer quenching constants and the nature of the quenching processes between the aza-BODIPYs and $PC_{60}BM$ are discussed in Section (3.3.3.2).

3.3.3.1 Fluorescence Lifetime Measurements

The fluorescence lifetime is the average time the fluorophore stays in its excited state before emitting a photon.[34] Fluorescence lifetimes were measured between aza-BODIPYs and $PC_{60}BM$ (in chloroform solution) and are shown in Table (3.7). The fluorescence intensity decays of aza-BODIPYs in chloroform solution at different concentrations of $PC_{60}BM$ are shown in figures from Fig. (3.47) to Fig. (3.58). The fluorescence lifetimes have been measured for all compounds except compound (139); this compound did not show enough fluorescence. It is obvious from these figures that there were steady decreases in the fluorescence intensities at a given lifetime with increasing concentrations of $PC_{60}BM$, which is attributed to the interactions between aza-BODIPYs and $PC_{60}BM$. Compounds (88), (125), (151) and (145) showed higher amplitudes in comparison with the other compounds, which reflected the greater populations of these species in solution. Medium values of amplitudes were observed for compounds (100), (113), (150), (112) and (132), lower values were attributed to compounds (87), (111), (106) and (139).

Table 3.7 Measured fluorescence lifetimes of aza-BODIPYs at different concentrations of $PC_{60}BM$ (in chloroform solution).

	$PC_{60}BM$ Concentration ($\times 10^{-5}$)					
	0 M	1M	3M	5M	10M	20M
Compound number	τ_0 (ns)	τ_1 (ns)	τ_2 (ns)	τ_3 (ns)	τ_4 (ns)	τ_5 (ns)
(87)	1.67	1.62	1.65	1.58	1.66	1.51
(88)	2.60	2.52	2.58	2.47	2.53	2.43
(100)	2.21	2.11	2.36	2.13	1.97	2.49
(106)	8.82	8.50	9.40	8.39	7.31	8.04
(111)	3.67	3.51	3. 61	3.28	3.60	3.09
(112)	5.38	5.60	5.59	5.13	5.06	5.01
(113)	10.61	9.73	9.46	9.82	9.71	9.69
(125)	2.02	1.98	1.85	2.04	2.31	2.09
(132)	3.10	2.96	2.55	3.37	3.36	3.25
(139)	-	-	-	-	-	-
(145)	6.32	6.86	6.42	6.52	5.73	5.25
(150)	2.89	2.88	2.61	2.73	2.40	2.98
(151)	9.68	8.06	9.77	8.16	8.25	9.56

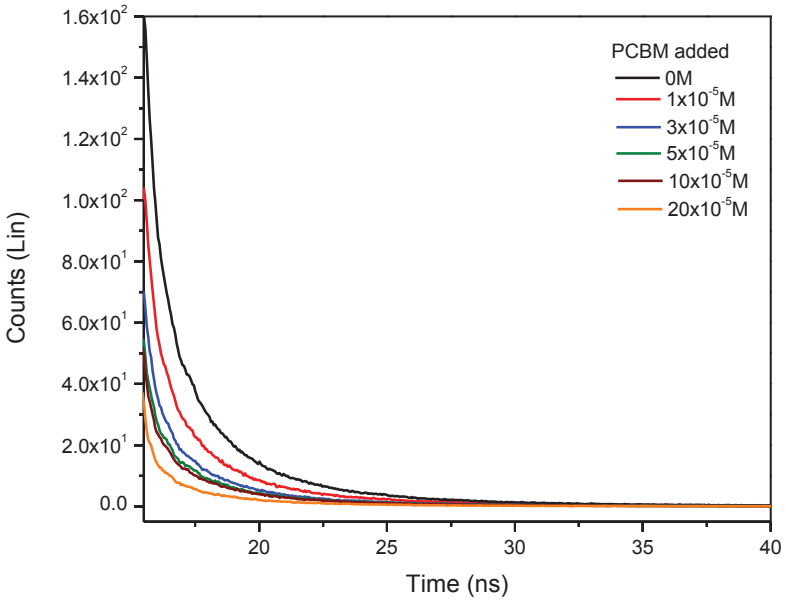

Figure 3.48 Fluorescence lifetime decay of compound (87) in the absence of $PC_{60}BM$ (black line) and the presence of $PC_{60}BM$ (colored lines).

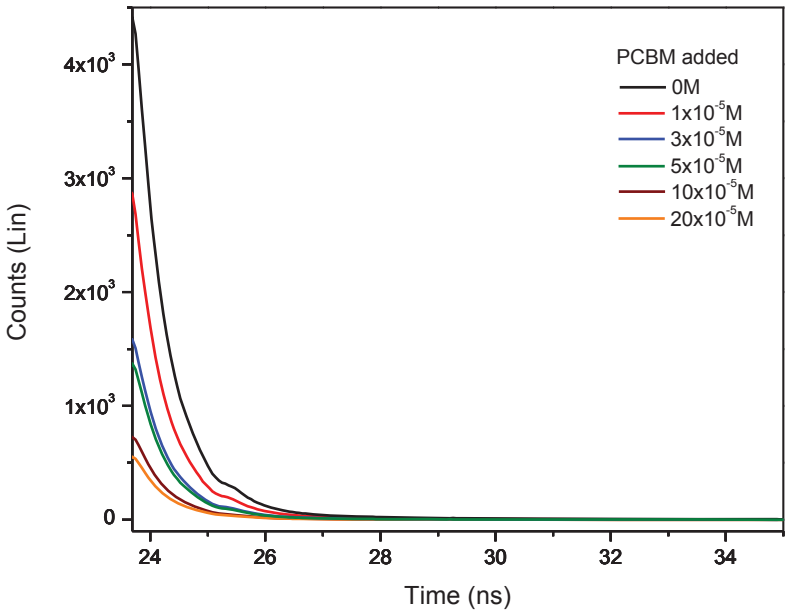

Figure 3.49 Fluorescence lifetime decay of compound (88) in the absence of $PC_{60}BM$ (black line) and the presence of $PC_{60}BM$ (colored lines).

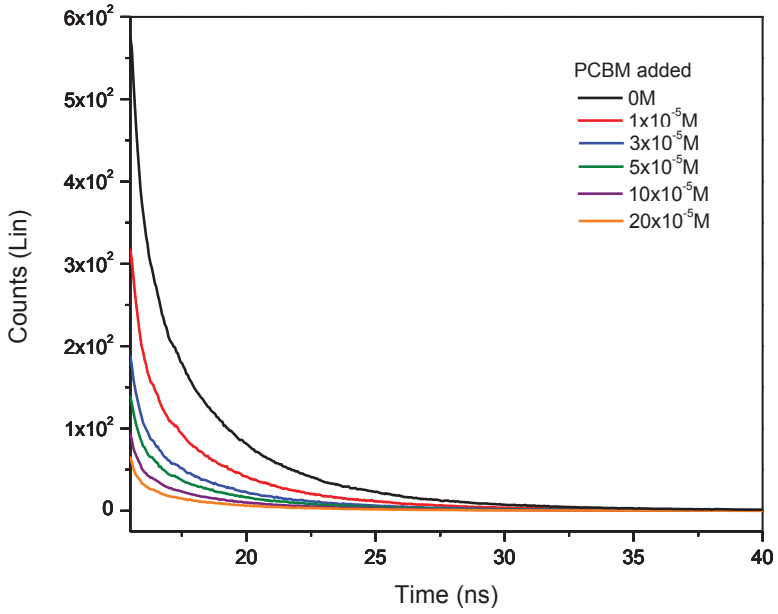

Figure 3.50 Fluorescence lifetime decay of compound (100) in the absence of $PC_{60}BM$ (black line) and the presence of $PC_{60}BM$ (colored lines).

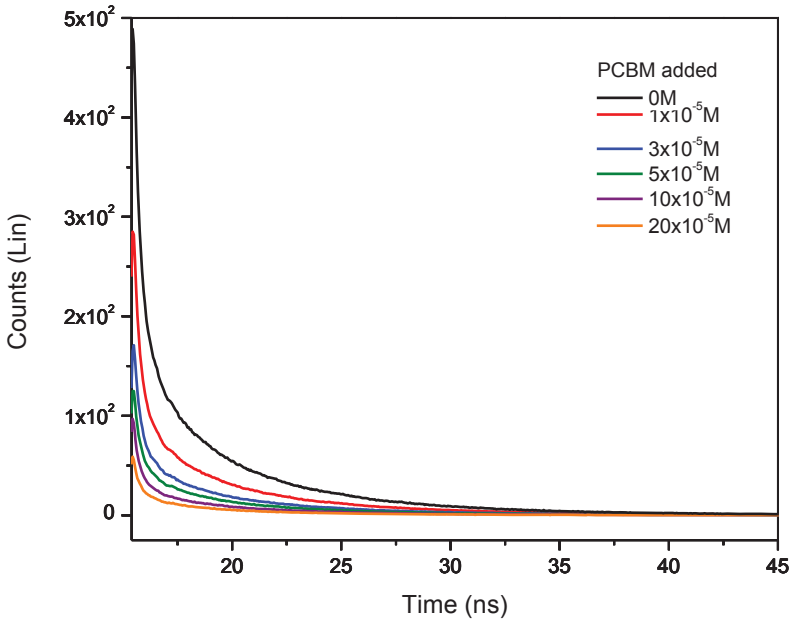

Figure 3.51 Fluorescence lifetime decay of compound (113) in the absence of $PC_{60}BM$ (black line) and the presence of $PC_{60}BM$ (colored lines).

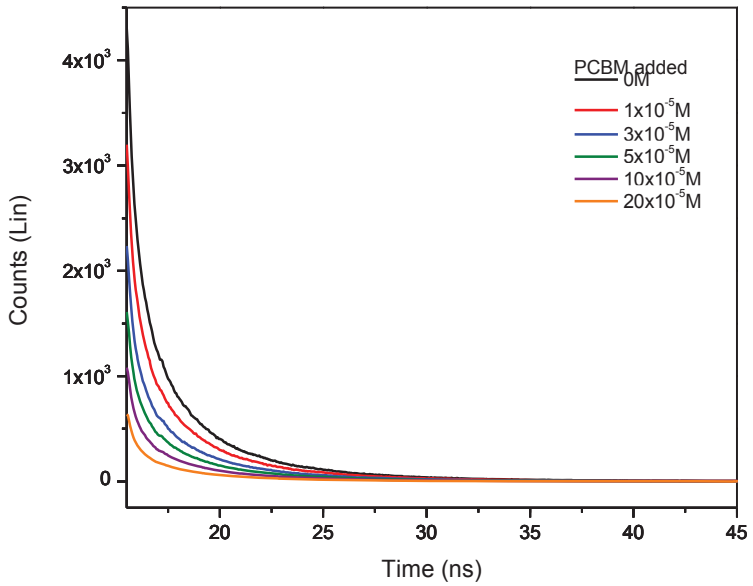

Figure 3.52 Fluorescence lifetime decay of compound (125) in the absence of $PC_{60}BM$ (black line) and the presence of $PC_{60}BM$ (colored lines).

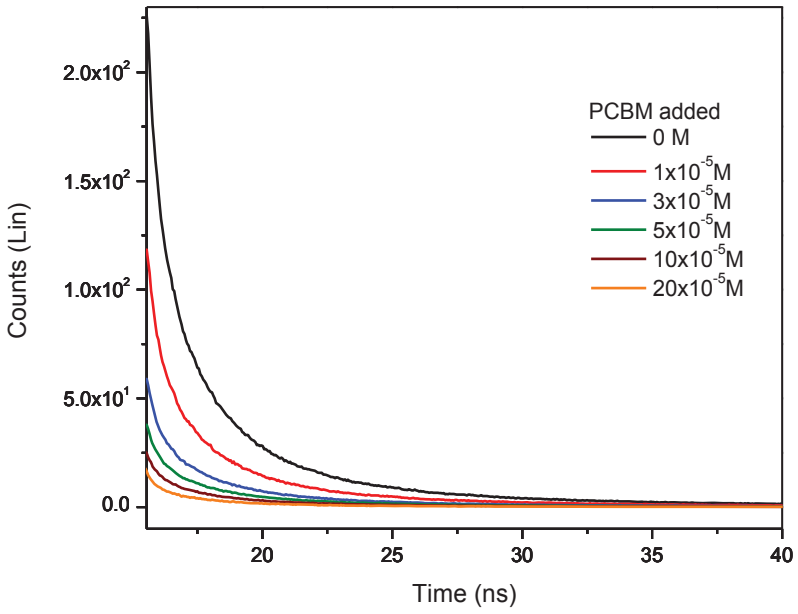

Figure 3.53 Fluorescence lifetime decay of compound (111) in the absence of $PC_{60}BM$ (black line) and the presence of $PC_{60}BM$ (colored lines).

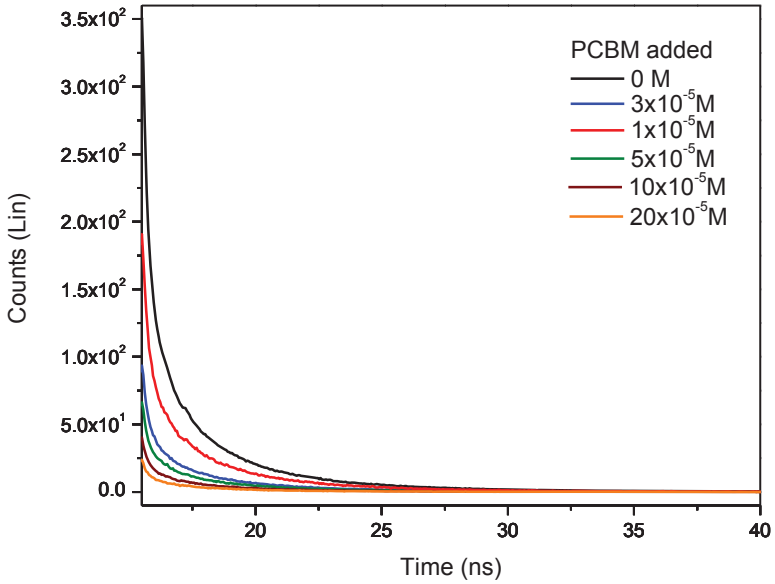

Figure 3.54 Fluorescence lifetime decay of compound (150) in the absence of $PC_{60}BM$ (black line) and the presence of $PC_{60}BM$ (colored lines).

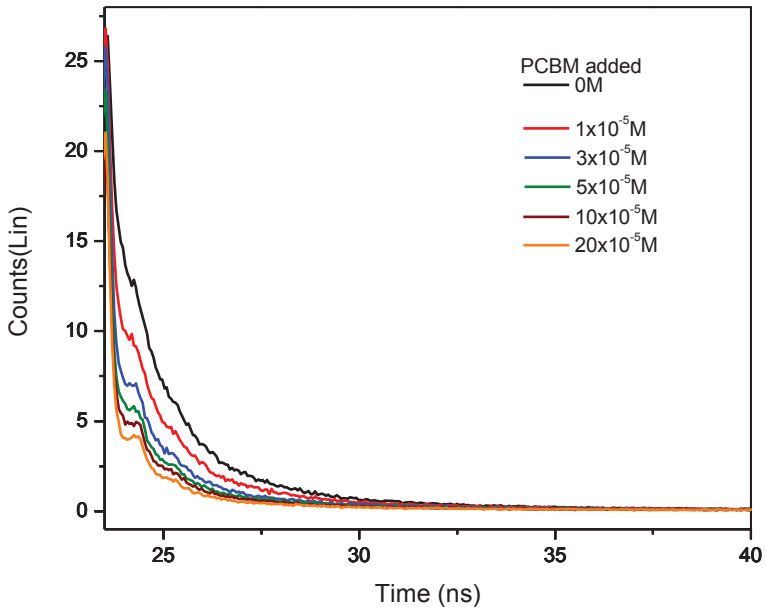

Figure 3.55 Fluorescence lifetime decay of compound (106) in the absence of $PC_{60}BM$ (black line) and the presence of $PC_{60}BM$ (colored lines).

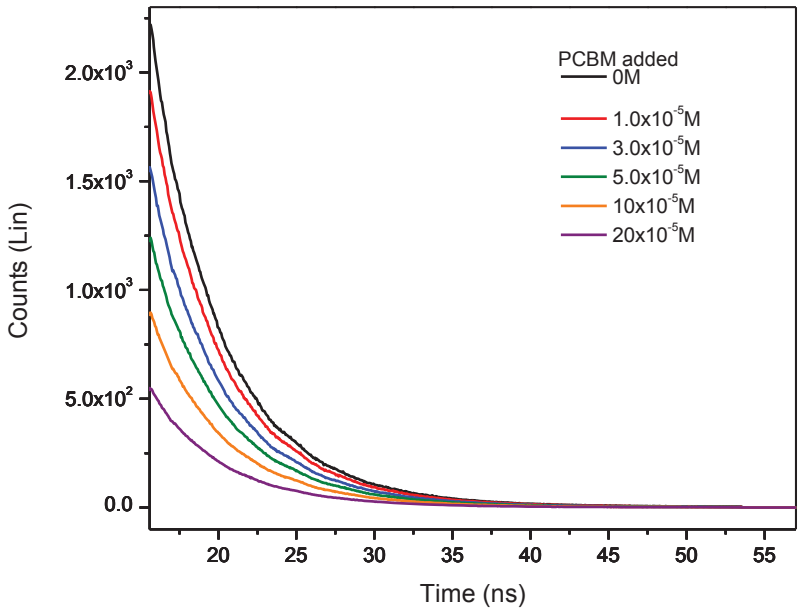

Figure 3.56 Fluorescence lifetime decay of compound (151) in the absence of $PC_{60}BM$ (black line) and the presence of $PC_{60}BM$ (colored lines).

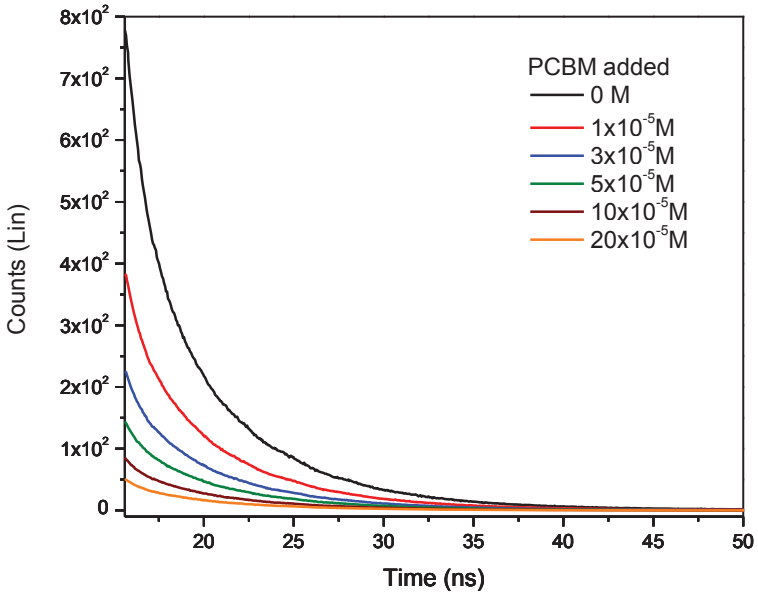

Figure 3.57 Fluorescence lifetime decay of compound (112) in the absence of $PC_{60}BM$ (black line) and the presence of $PC_{60}BM$ (colored lines).

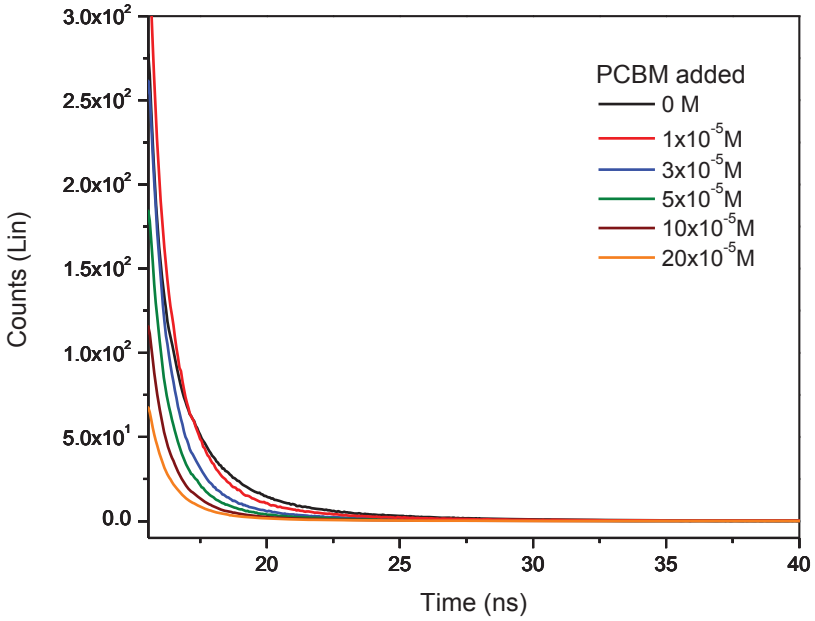

Figure 3.58 Fluorescence lifetime decay of compound (132) in the absence of $PC_{60}BM$ (black line) and the presence of $PC_{60}BM$ (colored lines).

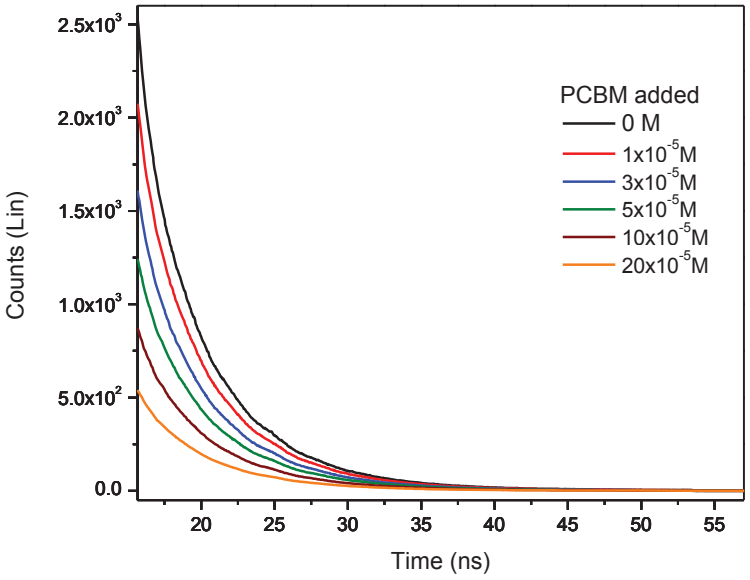

Figure 3.59 Fluorescence lifetime decay of compound (145) in the absence of $PC_{60}BM$ (black line) and the presence of $PC_{60}BM$ (colored lines).

The fluorescence lifetimes of aza-BODIPYs (Table (3.7)) were determined from the fluorescence decay curves (Fig. (3.47) to Fig. (3.58)). τ_0 refers to the intrinsic fluorescence lifetime, while τ_1, τ_2, τ_3, τ_4 and τ_5 refer to the lifetimes at difference concentrations of the quencher. Upon addition of $PC_{60}BM$ the lifetimes of compounds (87) and (88) showed very little variation: 1.67ns (τ_0) to 1.51ns (τ_5) for compound (87) and 2.60ns (τ_0) to 2.43ns (τ_5) for compound (88).

Compound (100) had lifetimes from 2.21 ns (τ_0) to 2.49 ns (τ_5); compound (111) shows a slightly higher lifetime varying between 3.67ns (τ_0) and 3.09ns (τ_5). Similarly compound (125) has a lifetime from 2.02 ns (τ_0) to 2.09 ns (τ_5); compound (132) from 3.10 ns (τ_0) to 3.25 ns (τ_5) and compound (150) from 2.89 ns (τ_0) to 2.98 ns (τ_5).

The highest lifetime was observed for compound (113) with 10.61ns for τ_0. This was followed by compounds (151) and (106) with lifetimes of 9.68 ns (τ_0) and 8.82 ns (τ_0) respectively, and then compounds (145) and (112) with lifetimes of 6.32ns (τ_0) and 5.38ns (τ_0) respectively. Compounds (106), (112), (113), (145) and (151) showed little variation in the lifetime.

3.3.3.2 Stern-Volmer Quenching Constants

The quenching constants (K_{sv}) and the binding constants (K_b) were determined using Stern-Volmer plots.[35-40] The ratio of emission intensities (I_0/I-1) was plotted as a function of quencher concentration. I_0 is the emission intensity in the absence of quencher and I is that in the presence of the quencher. The slope of a Stern-Volmer graph is the quenching constant (K_{sv}). The value of K_{sv} indicates there is a quenching process occurring, while the value of K_b gives an indication of how strong is the interaction between the aza-BODIPYs and the quencher ($PC_{60}BM$).

The Stern–Volmer plots of the fluorescence quenching of aza-BODIPYs by $PC_{60}BM$ are shown in Fig. (3.59) to Fig. (3.70). The dependences on quencher concentration ($PC_{60}BM$) are treated as being linear. The quenching constants were at the order of 10^4. The fluorescence quenching results alone are not enough to distinguish between dynamic or static quenching processes. In dynamic quenching, charge transfer occurs and the fluorescence is quenched when the electron acceptor collides with the excited fluorophore. The excited state of the fluorophore is affected only by the collision between the quencher and the fluorophore. No changes in the absorption spectrum are expected. The opposite scenario occurs for static quenching; the formation of ground-state complex alters the absorption spectra of the fluorophore. Therefore, only a careful examination of the absorption spectrum and measured lifetime can distinguish between static and dynamic quenching.[41]

Table 3.8 The quenching (K_b) and binding (K_{sv}) constants

Compound number	$K_b\,(M^{-1})$	$K_{sv}\,(M^{-1})$
(87)	8.26×10^{-3}	4.46×10^{-4}
(88)	1.2×10^{-4}	0.35×10^{-4}
(100)	9.8×10^{-5}	3.38×10^{-4}
(106)	1.6×10^{-4}	7.21×10^{-4}
(111)	5.3×10^{-5}	14.9×10^{-4}
(112)	2.2×10^{-4}	3.26×10^{-4}
(113)	6.47×10^{-4}	6.47×10^{-4}
(125)	1.68×10^{-4}	13.48×10^{-4}
(132)	5.3×10^{-4}	2.36×10^{-4}
(139)	-	-
(145)	4.1×10^{-4}	11.24×10^{-4}
(150)	3.5×10^{-4}	7.65×10^{-4}
(151)	1.4×10^{-4}	8.4×10^{-4}

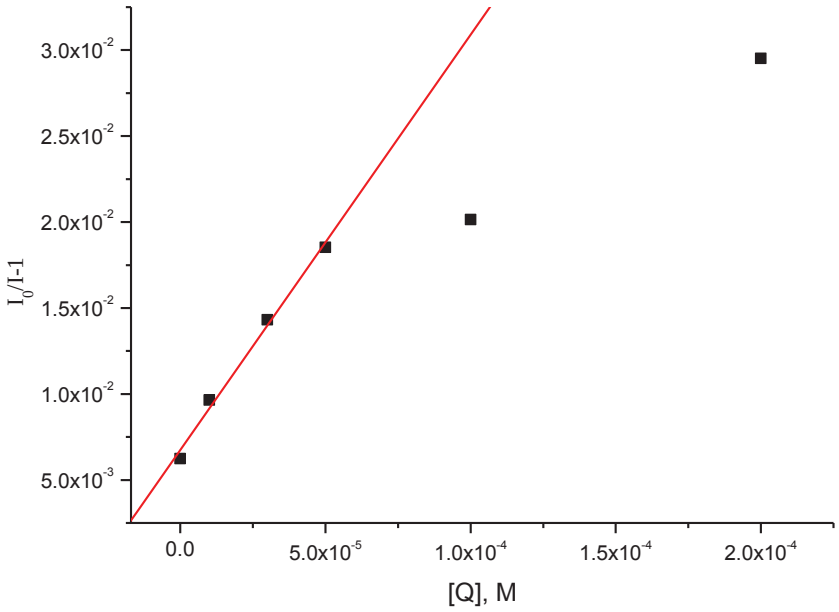

Figure 3.60 The ratio of fluorescence intensities of compound (87) versus quencher concentration [$PC_{60}BM$]

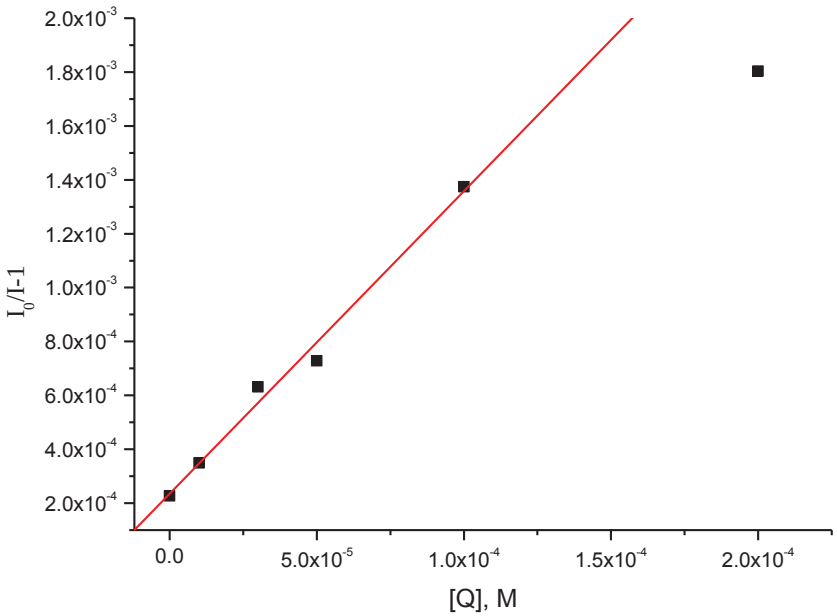

Figure 3.61 The ratio of fluorescence intensities of compound (88) versus quencher concentration [$PC_{60}BM$]

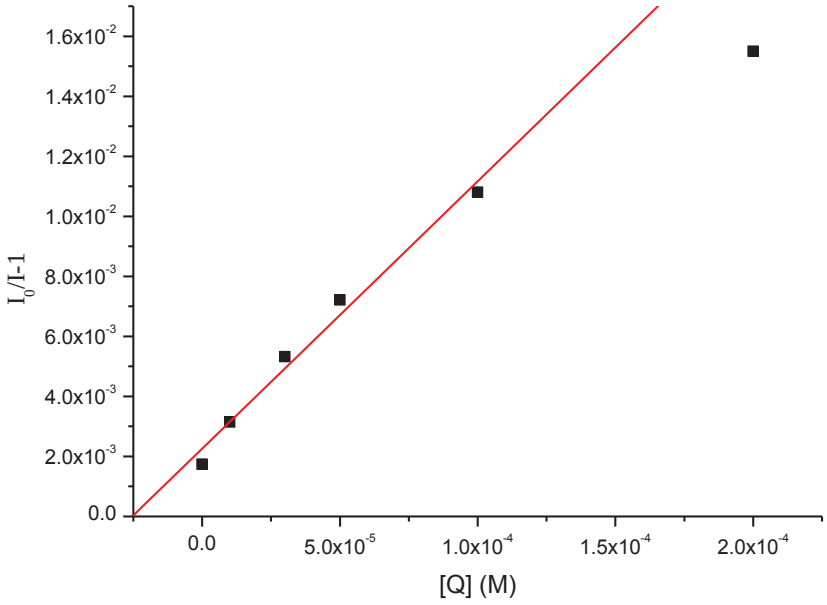

Figure 3.62 The ratio of fluorescence intensities of compound (100) versus quencher concentration [$PC_{60}BM$].

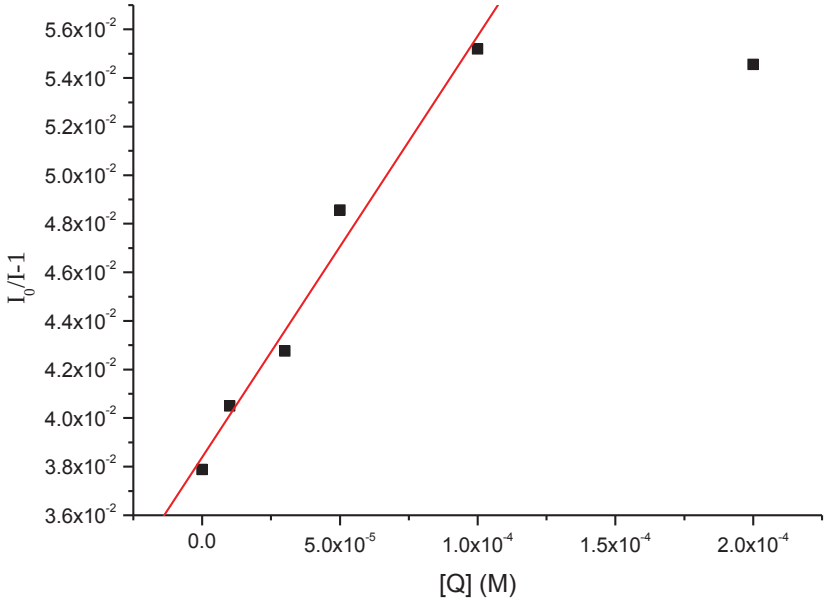

Figure 3.63 The ratio of fluorescence intensities of compound (106) versus quencher concentration [$PC_{60}BM$].

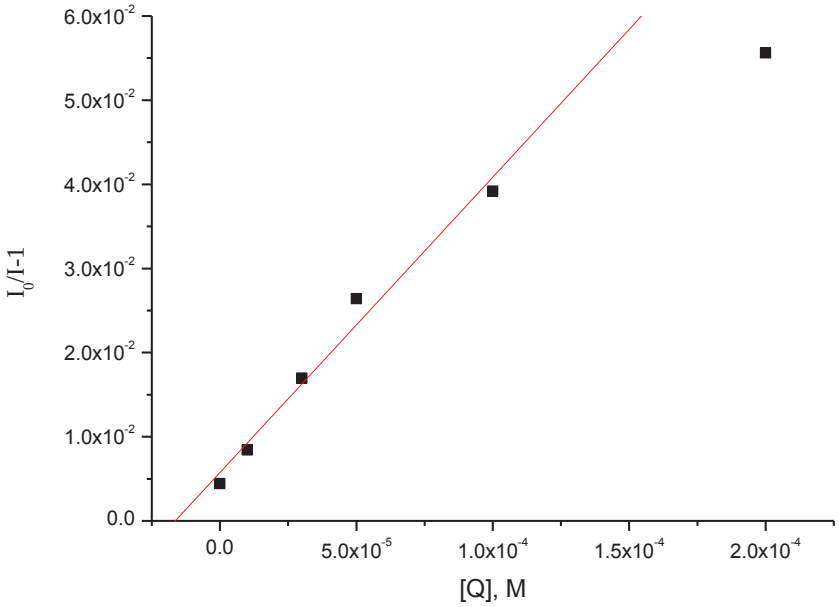

Figure 3.64 The ratio of fluorescence intensities of compound (111) versus quencher concentration [$PC_{60}BM$].

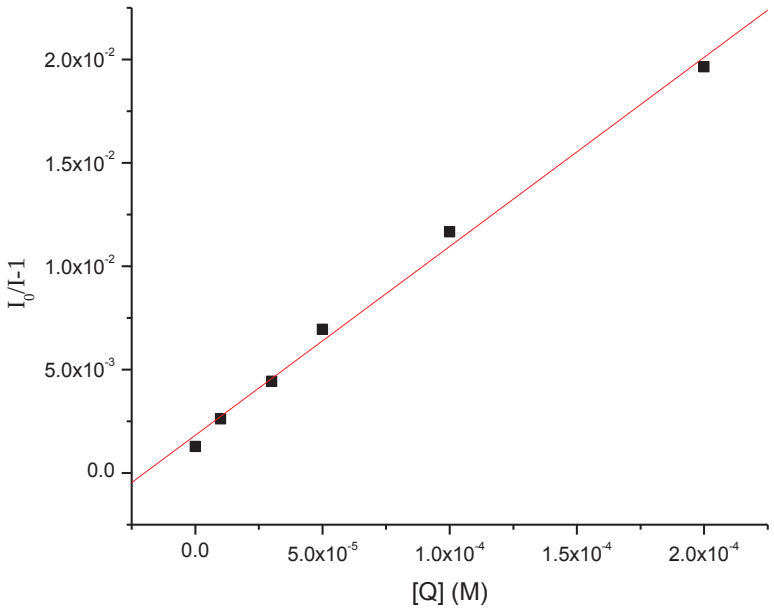

Figure 3.65 The ratio of fluorescence intensities of compound (112) versus quencher concentration [$PC_{60}BM$].

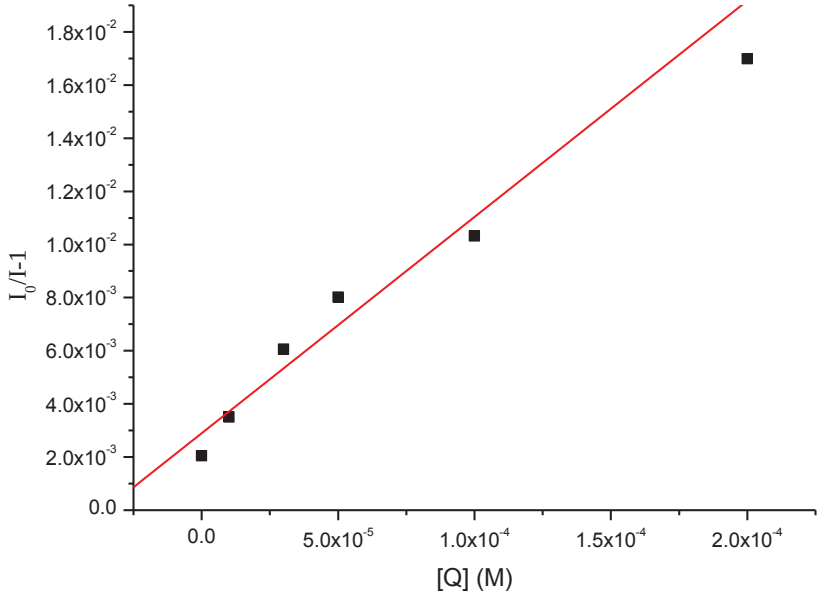

Figure 3.66 The ratio of fluorescence intensities of compound (113) versus quencher concentration [$PC_{60}BM$].

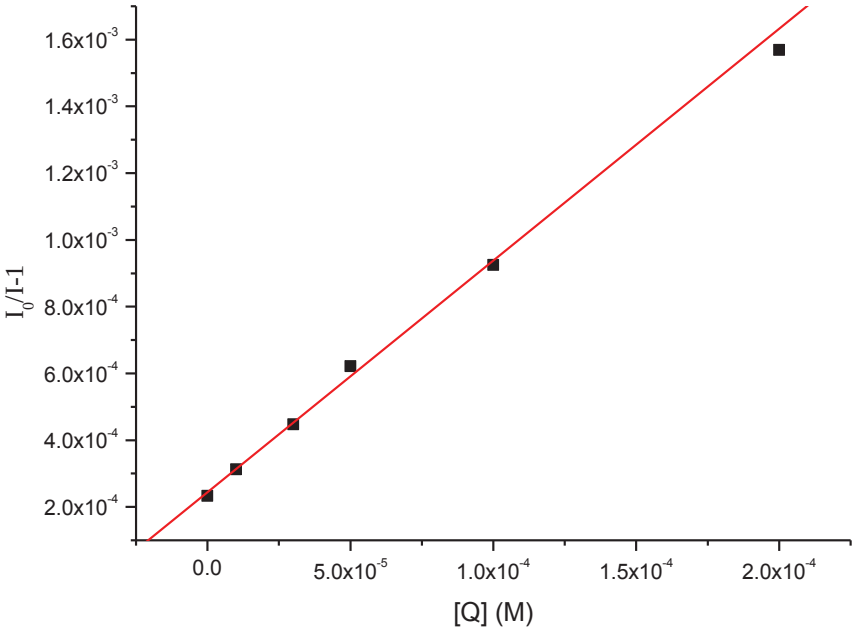

Figure 3.67 The ratio of fluorescence intensities of compound (125) versus quencher concentration [$PC_{60}BM$].

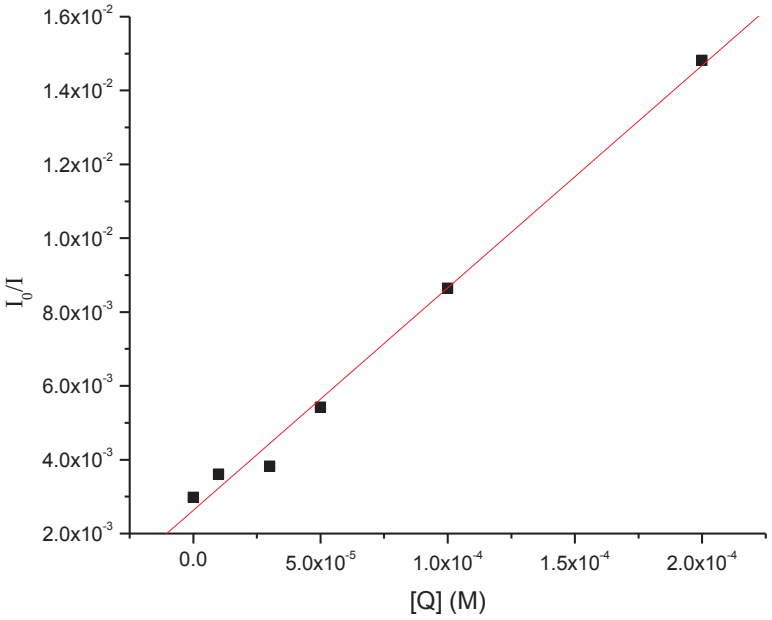

Figure 3.68 The ratio of fluorescence intensities of compound (132) versus quencher concentration [$PC_{60}BM$].

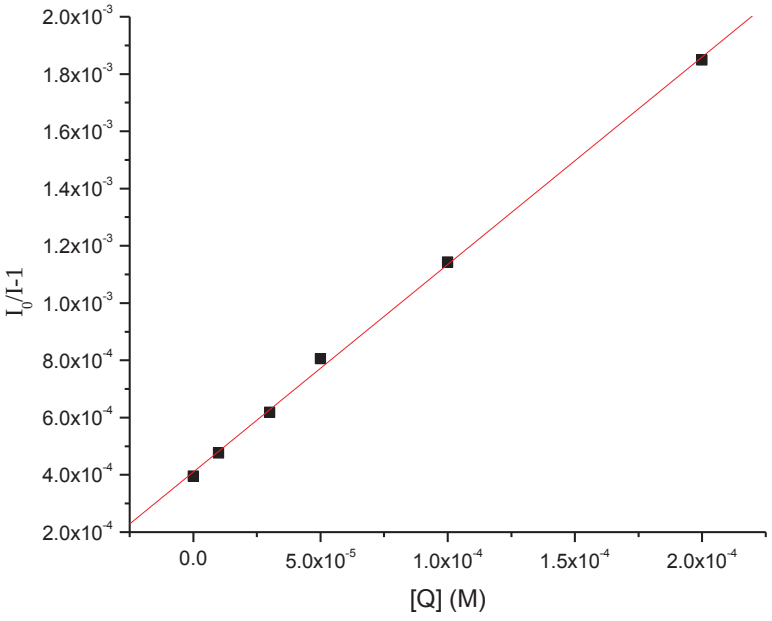

Figure 3.69 The ratio of fluorescence intensities of compound (145) versus quencher concentration [$PC_{60}BM$].

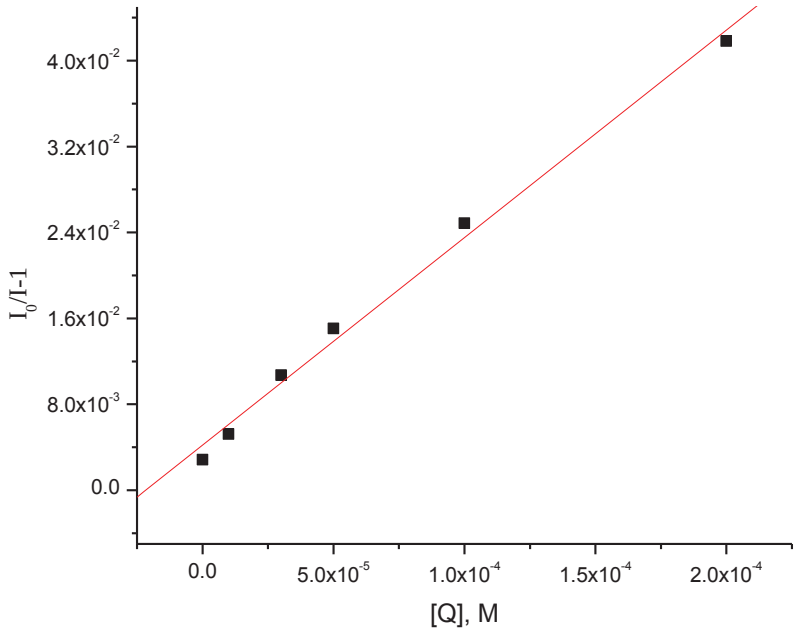

Figure 3.70 The ratio of fluorescence intensities of compound (150) versus quencher concentration [$PC_{60}BM$].

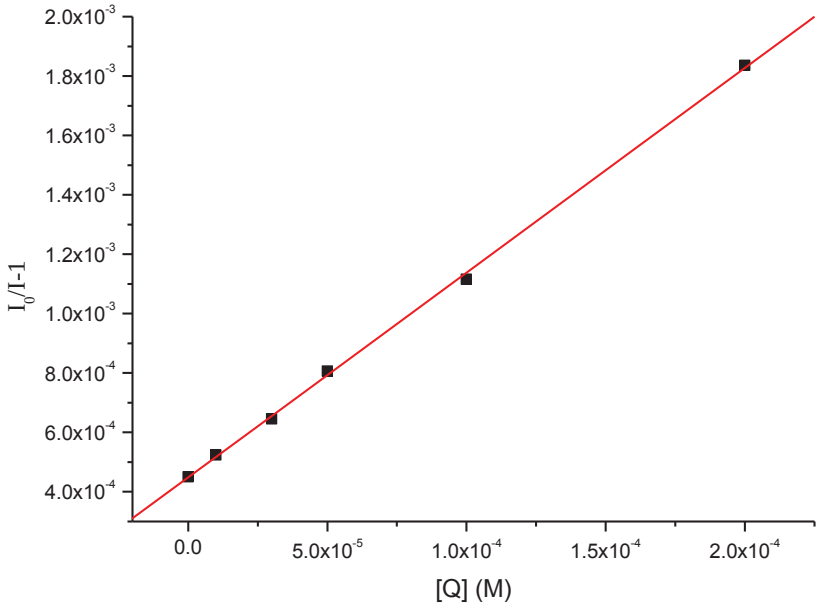

Figure 3.71 The ratio of fluorescence intensities of compound (151) versus quencher concentration [$PC_{60}BM$].

Both of the quenching mechanisms (dynamic or static) are expected to produce straight-line graphs of emission ratio is against quencher concentration (Fig. (3.59) to Fig. (3.70)), it is not clear which mechanism is the more appropriate description. In dynamic quenching, both emission intensity and lifetime are expected to reduce on increasing the quencher concentration because the fluorophore will collide with a quencher during its excited state lifetime. In static quenching, the fluorophore is bound to the quencher forming a non-emissive fluorophore-quencher complex, which results in the reduction in emission. The unbound fluorophores are free to emit. Therefore, increasing quencher concentration will affect emission intensity but not emission lifetime, because unbound fluorophore can emit in the absence of quencher. The two quenching mechanisms may be relevant simultaneously.

In this study, in order to determine which mechanism is appropriate to describe the quenching process, the τ_0/τ has been plotted against quencher concentration (Fig. (3.71) to Fig. (3.82)). It is obvious from these Figures that there was no significant change in the lifetimes. The τ_0/τ value fluctuated around 1. The almost horizontal line indicates static quenching. Hence, the relation between the fluorescence intensity and the quencher concentration [Q] can be given through the Stern-Volmer equation as follows:

$$\frac{I_0}{I} = 1 + K[Q]$$

Where I_0 is the inherent fluorescence intensity, I is quenched fluorescence intensity, K is a quenching constant and [Q] is the quencher concentration.

Table (3.8) summarises the Stern-Volmer quenching constant values determined from the slopes of the amplitude versus quencher concentration [$PC_{60}BM$] plots as well as binding constants.

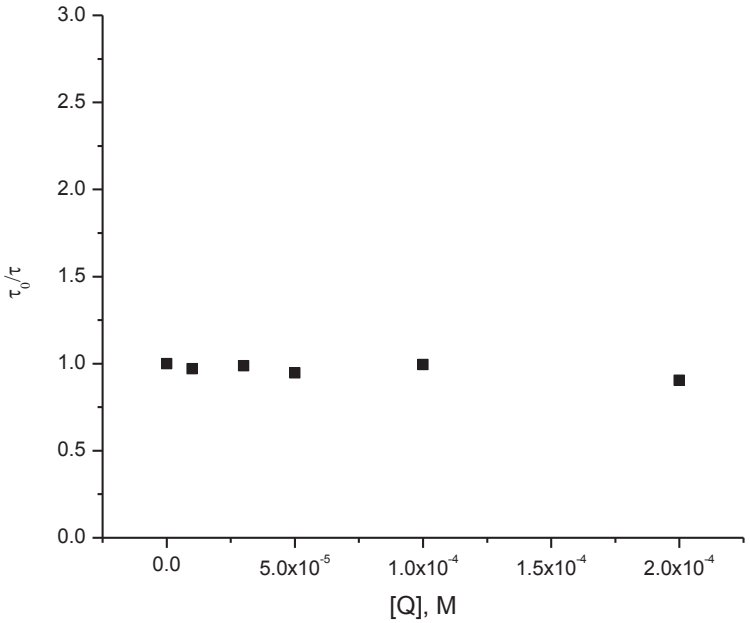

Figure 3.72 The fluorescence lifetimes of compound (87) versus quencher concentration [$PC_{60}BM$].

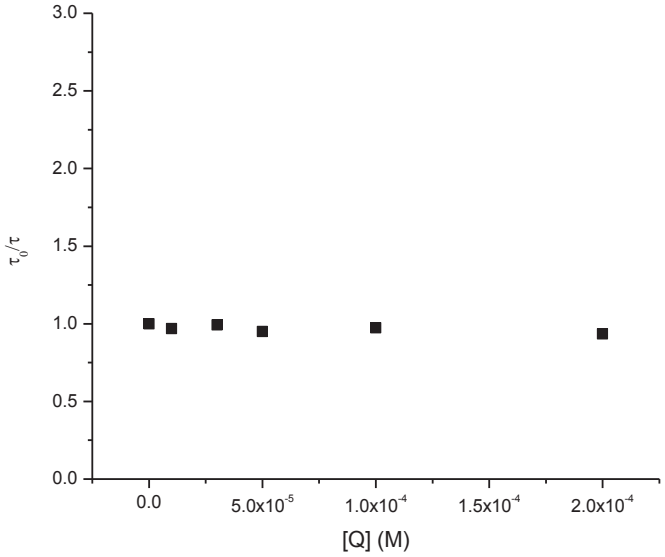

Figure 3.73 The fluorescence lifetimes of compound (88) versus quencher concentration [$PC_{60}BM$].

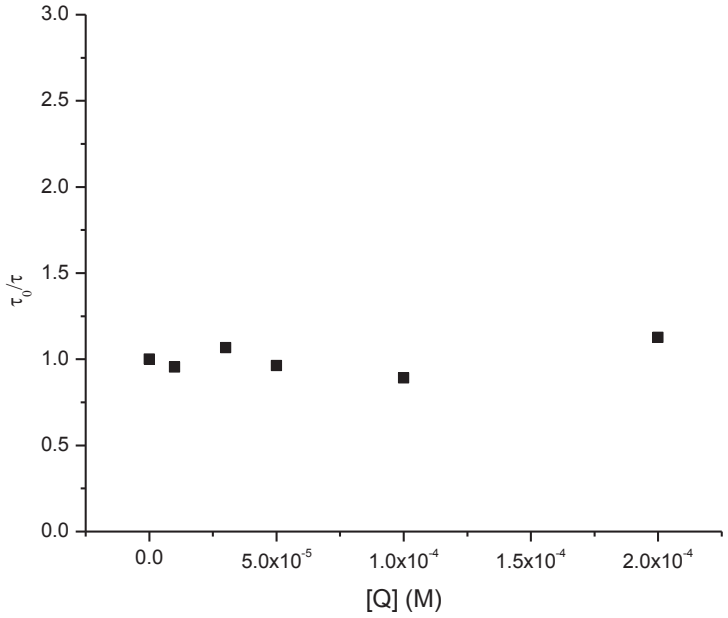

Figure 3.74 The fluorescence lifetimes of compound (100) versus quencher concentration [$PC_{60}BM$].

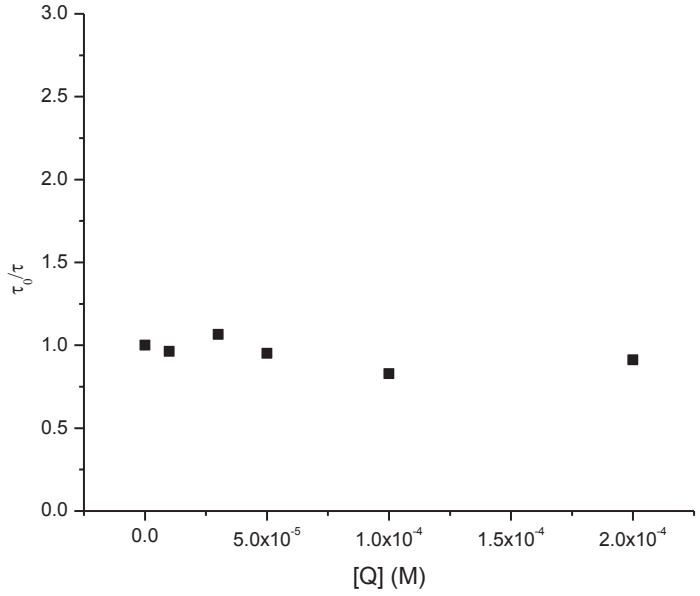

Figure 3.75 The fluorescence lifetimes of compound (106) versus quencher concentration [$PC_{60}BM$].

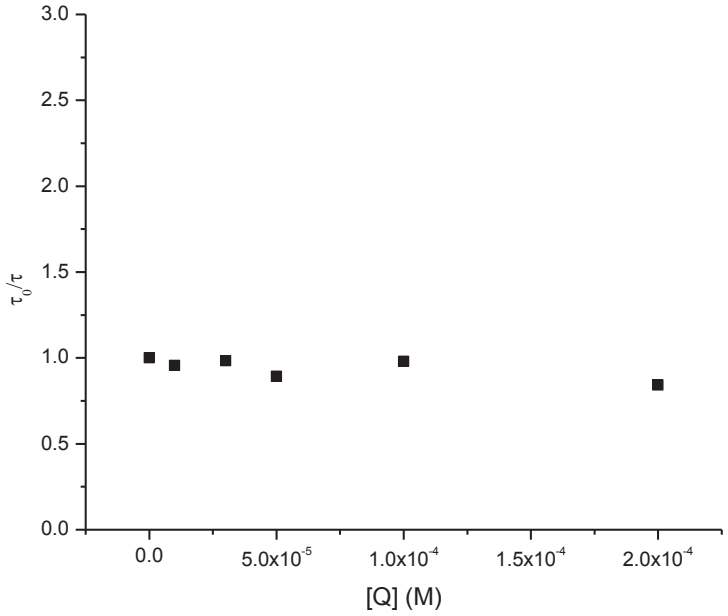

Figure 3.76 The fluorescence lifetimes of compound (111) versus quencher concentration [$PC_{60}BM$].

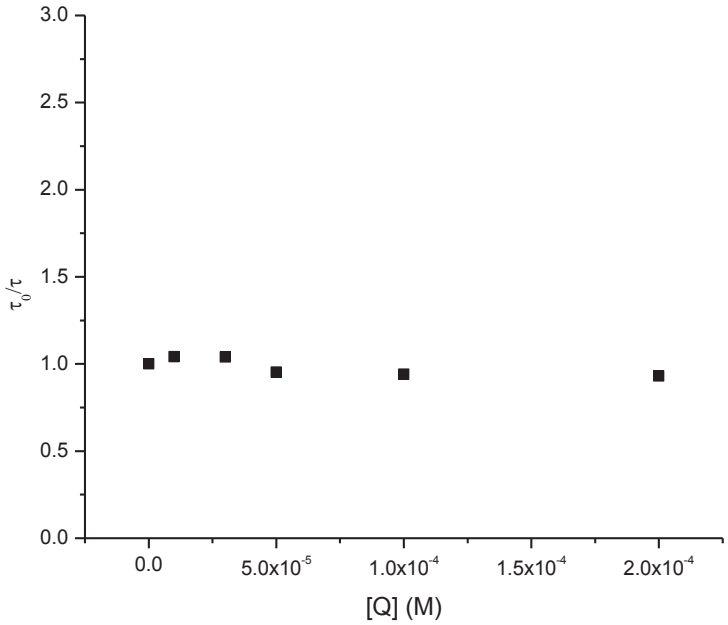

Figure 3.77 The fluorescence lifetimes of compound (112) versus quencher concentration [$PC_{60}BM$].

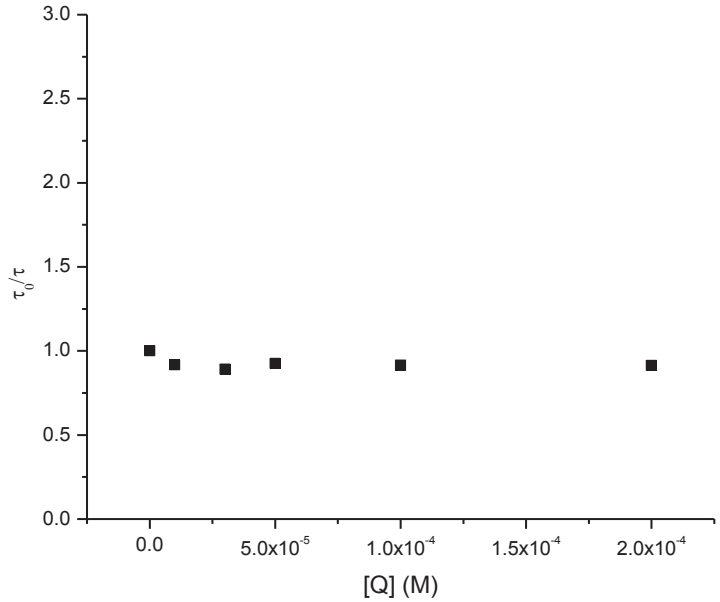

Figure 3.78 The fluorescence lifetimes of compound (113) versus quencher concentration [$PC_{60}BM$].

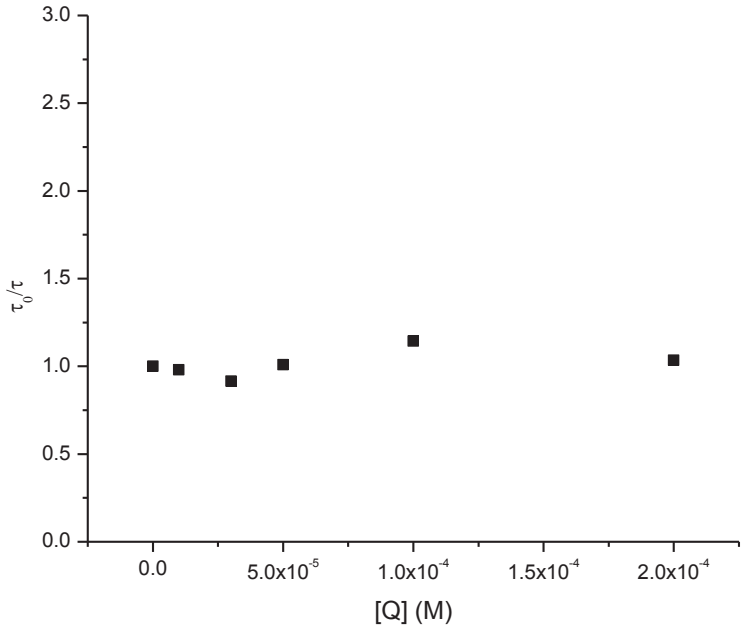

Figure 3.79 The fluorescence lifetimes of compound (125) versus quencher concentration [$PC_{60}BM$].

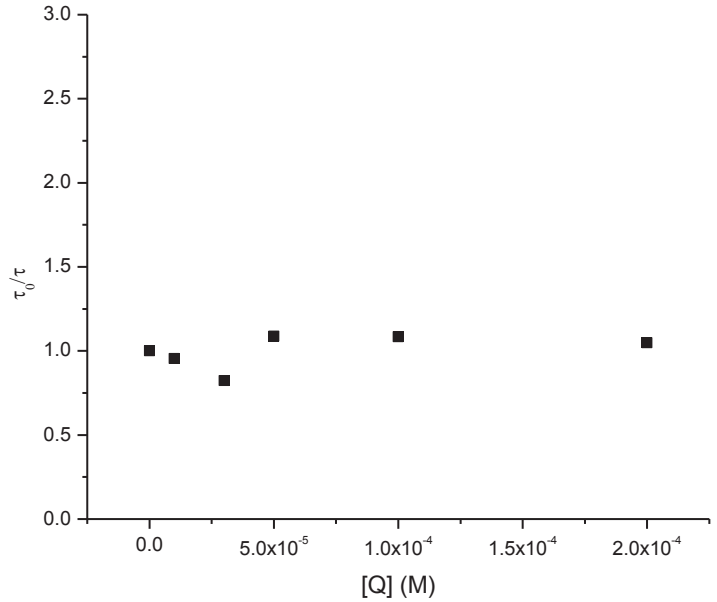

Figure 3.80 The fluorescence lifetimes of compound (132) versus quencher concentration [$PC_{60}BM$].

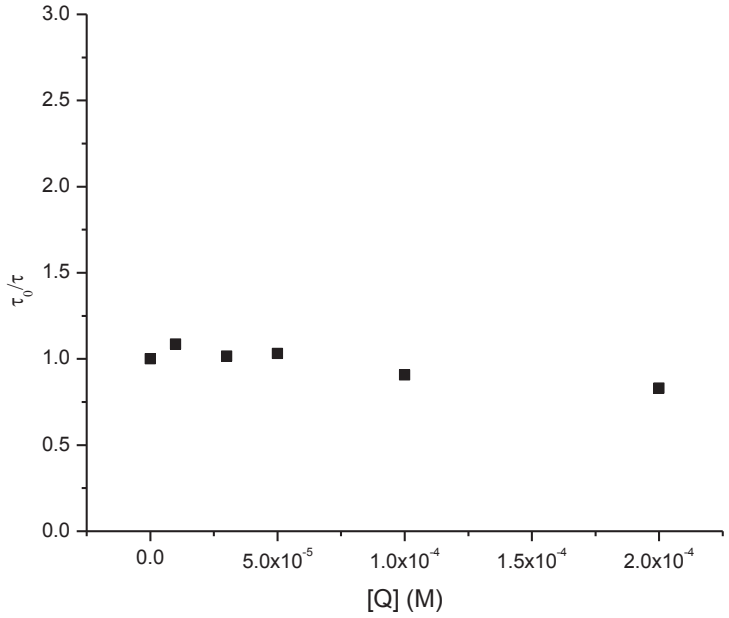

Figure 3.81 The fluorescence lifetimes of compound (145) versus quencher concentration [$PC_{60}BM$].

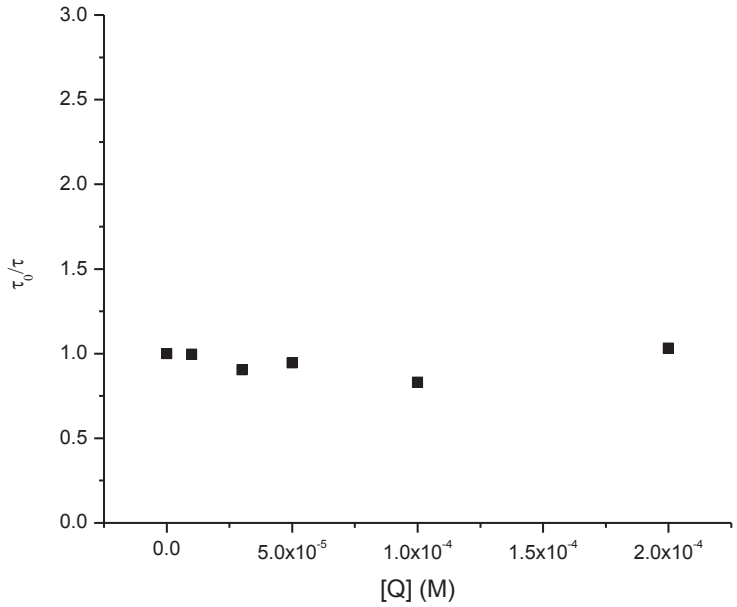

Figure 3.82 The fluorescence lifetimes of compound (150) versus quencher concentration [$PC_{60}BM$].

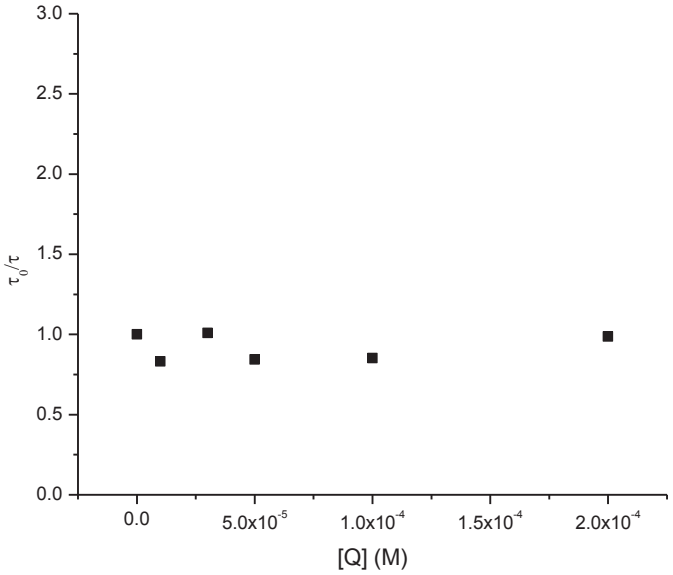

Figure 3.83 The fluorescence lifetimes of compound (151) versus quencher concentration [$PC_{60}BM$].

3.4 References

(1) Frisch, M. J. T., G. W.; Schlegel, H. B.; Scuseria, G. E.; Robb, M. A.; Cheeseman, J. R.; Scalmani, G.; Barone, V.; Mennucci, B.; Petersson, G. A.; Nakatsuji, H.; Caricato, M.; Li, X.; Hratchian, H. P.; Izmaylov, A. F.; Bloino, J.; Zheng, G.; Sonnenberg, J. L.; Hada, M.; Ehara, M.; Toyota, K.; Fukuda, R.; Hasegawa, J.; Ishida, M.; Nakajima, T.; Honda, Y.; Kitao, O.; Nakai, H.; Vreven, T.; Montgomery, J. A., Jr.; Peralta, J. E.; Ogliaro, F.; Bearpark, M.; Heyd, J. J.; Brothers, E.; Kudin, K. N.; Staroverov, V. N.; Kobayashi, R.; Normand, J.; Raghavachari, K.; Rendell, A.; Burant, J. C.; Iyengar, S. S.; Tomasi, J.; Cossi, M.; Rega, N.; Millam, N. J.; Klene, M.; Knox, J. E.; Cross, J. B.; Bakken, V.; Adamo, C.; Jaramillo, J.; Gomperts, R.; Stratmann, R. E.; Yazyev, O.; Austin, A. J.; Cammi, R.; Pomelli, C.; Ochterski, J. W.; Martin, R. L.; Morokuma, K.; Zakrzewski, V. G.; Voth, G. A.; Salvador, P.; Dannenberg, J. J.; Dapprich, S.; Daniels, A. D.; Farkas, Ö.; Foresman, J. B.; Ortiz, J. V.; Cioslowski, J.; Fox, D. J. *Gaussian 09*. **2009**, *Wallingford CT: Gaussian, Inc*.

(2) Le, G. B.; Maury, O.; Jacquemin, D. *Phys*. *Chem*. *Chem*. *Phys*. **2012**, *14*, 157.

(3) Chidthong, R.; Hannongbua, S. *J*. *Comput*. *Chem*. **2010**, *31*, 1450.

(4) O'Boyle, N. M.; Tenderholt, A. L.; Langner, K. M. *J*. *Comput*. *Chem*. **2008**, *29*, 839.

(5) Hohenberg, P.; Kohn, W. *Physical Review* **1964**, *136*, B864.

(6) Kohn, W.; Sham, L. J. *Physical Review* **1965**, *140*, A1133.

(7) Levine, I. N. *Quantum chemistry*; 5th ed.; Prentice Hall: Upper Saddle River, N.J., 2000.

(8) Cramer, C. J. *Essentials of computational chemistry : theories and models*; 2nd ed.; Wiley: Chichester, West Sussex, England ; Hoboken, NJ, 2004.

(9) Becke, A. D. *The Journal of Chemical Physics* **1993**, *98*, 5648.

(10) Gresser, R., Technischen Universitat Dresden, 2007.

(11) Le Guennic, B.; Maury, O.; Jacquemin, D. *Physical Chemistry Chemical Physics* **2012**, *14*, 157.

(12) Bellier, Q.; Pégaz, S.; Aronica, C.; Guennic, B. L.; Andraud, C.; Maury, O. *Organic Letters* **2010**, *13*, 22.

(13) Killoran, J.; Allen, L.; Gallagher, J. F.; Gallagher, W. M.; Oshea, D. F. *Chemical Communications* **2002**, 1862.

(14) Bouit, P.-A.; Kamada, K.; Feneyrou, P.; Berginc, G.; Toupet, L.; Maury, O.; Andraud, C. *Advanced Materials* **2009**, *21*, 1151.

(15) Gorman, A.; Killoran, J.; O'Shea, C.; Kenna, T.; Gallagher, W. M.; O'Shea, D. F. *J. Am. Chem. Soc.* **2004**, *126*, 10619.

(16) Li, Y. *Acc. Chem. Res.* **2012**, *45*, 723.

(17) Li, Y. *Accounts of Chemical Research* **2012**, *45*, 723.

(18) Ku, J.; Kim, D.; Ryu, T.; Jung, E.; Lansac, Y.; Jang, Y. H. *Bull. Korean Chem. Soc.* **2012**, *33*, 1029.

(19) Maritorena, S.; Morel, A.; Gentili, B. *Appl. Opt.* **2000**, *39*, 6725.

(20) Rurack, K. *Springer Ser. Fluoresc.* **2008**, *5*, 101.

(21) Asbury, J. B.; Pensack, R. D.; American Chemical Society: 2010, p PTC.

(22) Deibel, C.; Strobel, T.; Dyakonov, V. *Adv. Mater. (Weinheim, Ger.)* **2010**, *22*, 4097.

(23) Kopec, M.; Kruk, T.; Zapotoczny, S.; Laschewsky, A.; Holdcroft, S.; Mac, M.; Nowakowska, M. *J. Mater. Chem.* **2012**, *22*, 140.

(24) Lam, W. I.; Ivins, R. J.; Collier, G. S.; Walter, M. G.; American Chemical Society: 2012, p SERM.

(25) Lane, P. A. *ACS Symp. Ser.* **2010**, *1039*, 185.

(26) Noone, K. M.; Subramaniyan, S.; Zhang, Q.; Cao, G.; Jenekhe, S. A.; Ginger, D. S. *J. Phys. Chem. C* **2011**, *115*, 24403.

(27) Schwenn, P. E.; Gui, K.; Zhang, Y.; Burn, P. L.; Meredith, P.; Powell, B. J. *Org. Electron.* **2012**, *13*, 2538.

(28) Yang, S.; Liu, J.; Zhou, P.; Han, K.; He, G. *Chem. Phys. Lett.* **2011**, *512*, 66.

(29) Sariciftci, N. S.; Smilowitz, L.; Heeger, A. J.; Wudl, F. *Science (Washington, D. C., 1883-)* **1992**, *258*, 1474.

(30) Kang, T. E.; Cho, H.-H.; Cho, C.-H.; Kim, K.-H.; Kang, H.; Lee, M.; Lee, S.; Kim, B.; Im, C.; Kim, B. J. *ACS Appl. Mater. Interfaces* **2013**, *5*, 1.

(31) Luechai, A.; Gasiorowski, J.; Petsom, A.; Neugebauer, H.; Sariciftci, N. S.; Thamyongkit, P. *J. Mater. Chem.* **2012**, *22*, 23030.

(32) Kraabel, B.; Hummelen, J. C.; Vacar, D.; Moses, D.; Sariciftci, N. S.; Heeger, A. J.; Wudl, F. *J*. *Chem*. *Phys*. **1996**, *104*, 4267.

(33) Wang, J.; Wang, D.; Moses, D.; Heeger, A. J. *J*. *Appl*. *Polym*. *Sci*. **2001**, *82*, 2553.

(34) Albrecht, C. *Anal*. *Bioanal*. *Chem*. **2008**, *390*, 1223.

(35) Fraiji, E. K., Jr.; Cregan, T. R.; Werner, T. C. *Appl*. *Spectrosc*. **1994**, *48*, 79.

(36) Hamity, M.; Senz, A.; Gsponer, H. E. *J*. *Photochem*. *Photobiol*., *A* **2006**, *180*, 9.

(37) He, Y.-y.; Zhao, B.; Wang, X.-c.; Jin, P.-k. *Huanjing Huaxue* **2009**, *28*, 437.

(38) Seel, M.; Werner, T. C. *Appl*. *Spectrosc*. **2005**, *59*, 691.

(39) Senz, A.; Gsponer, H. E. *J*. *Sol-Gel Sci*. *Technol*. **2006**, *38*, 153.

(40) Tan, J.; Liu, X.; Li, L.; Liu, Z.; Tian, M.; Ma, Y.; Liu, K. *Sichuan Daxue Xuebao, Ziran Kexueban* **2009**, *46*, 1870.

(41) Wang, J.; Wang, D.; Moses, D.; Heeger, A. J. *Journal of Applied Polymer Science* **2001**, *82*, 2553.

Chapter 4

Organic Photovoltaic Device Fabrication and Testing

Chapter 4

4.1 Introduction

The fabrication and testing of photovoltaic devices incorporating BF_2-aza-dipyrromethenes as donor active layers are described in this Chapter. The device fabrication was carried out at Victoria University, Wellington. There were several steps each of which is disscussed here (Section (4.2)). The first step was to optimize the solutions used to deposit active layers of BF_2-aza-dipyrromethenes and $PC_{60}BM$ with the desired thicknesses (50–200 nm). The second step was the deposition of active layers on ITO (indium tin oxide). The final step was the thermal deposition of the aluminum electrode. The devices were fabricated in a laboratory which was in a clean room. A glove box was not available.

Two different types of bulk heterojunction devices were investigated. There were regular devices, which consisted of ITO(indium tin oxide)/PEDOT(poly(3,4-ethylenedioxythiophene) as an anode, a blend(BF_2-aza-dipyrromethenes and $PC_{60}BM$) as an active layer and aluminum/silver contact as a cathode on top. Then, there were inverted devices which consisted of ITO(indium tin oxide)/TiOx as a cathode, a blend(BF_2-aza-dipyrromethenes and $PC_{60}BM$) and MoO_3(molybdenum trioxide)/silver as an anode. As described below, certain of the regular devices functioned well, but none of the inverted devices worked satisfactorily. Device fabrication is discussed in Section (4.3.1). Experimental methods and techniques involved in testing the devices are discussed in Section (4.2.2).

External quantum efficiency (EQE) is the ratio of the number of charge carriers collected from the device to the incident photons at a given wavelength, as mentioned in Chapter 1. External quantum efficiencies were determined. The effects of various processing parameters on the external quantum efficiencies (EQE's) were investigated (Section 4.3.2.1). Current density-voltage (J-V) characteristics are covered in Section (4.3.2.2). The energy conversion efficiency (η) was determined under standard test condition (STC) of Air Mass 1.5 spectrum using a xenon arc lamp as a solar simulator.

4.2 Experimental Details

4.2.1 Device Fabrication

4.2.1.1 Preparation of the Solutions

The BF_2-aza-dipyrromethene and $PC_{60}BM$ solutions were prepared separately, and left for a few hours, and then both solutions mixed together briefly before spin coating. A total concentration of either 10 mg/mL, 20 mg/mL, 30 mg/mL or 40 mg/mL of BF_2-aza-dipyrromethene and $PC_{60}BM$ was used. A concentration of 40 mg/mL has been commonly used in the literature[1] on solution-processed small molecule devices. The lower concentrations (10 mg/mL, 20 mg/mL and 30 mg/mL) have been examined in this study to find the best concentration. Either chlorobenzene or chloroform was used to prepare the solutions. Blend ratios of 1:1, 1:2, 2:1, 2:3 or 1:4 of donor: $PC_{60}BM$ were used in the active layer. A TiO_x solution was prepared by diluting titanium(IV) isopropoxide (TIPT from Aldrich, 99.999%) in absolute ethanol to a concentration of 0.05 M and adding HCl (aq) to give a molar ratio of water-to-TIPT of 0.82 and a pH of 1.9. This was followed by stirring the precursor solution for 72 h at room temperature.

4.2.1.2 Substrate Preparation

Glass substrates patterned with a strip of ITO were purchased from Psiotech (S80110A-06-B). Substrates were always handled using tweezers. ITO substrates were peeled off from the plastic backings and the red photoresist was washed off the ITO surface using acetone. The edges of the ITO substrates were placed in a Teflon rack for sonication in a beaker with acetone (15 min) and then isopropyl alcohol (5 min). The substrates were dried using a gentle nitrogen flow. Numbers were scored on the back of each substrate using a diamond pen to distinguish easily the samples. ITO substrates for a batch of devices (up to 16 substrates, limited by the evaporator capacity, but generally 6-10) were placed in a Petri dish and cleaned in an oxygen plasma chamber in a cleanroom for 10 min using a Plasma Etch instrument. Plasma cleaning was expected to have the effect of increasing the work function of the ITO electrode, therefore further fabrication steps were undertaken as soon as possible after plasma cleaning to capture this beneficial effect.

4.2.1.3 Spin Coating

Immediately after the oxygen plasma etching, a layer of PEDOT:PSS (Sigma-Aldrich) was coated on top of the ITO substrates with a 50 μL aqueous dispersion at a speed of 6000 RPM for 60 sec using a WS-500 Series Spin Processor. The PEDOT:PSS layer was dried on a hot plate under a nitrogen flow for 20 minutes at 120 °C. For the active layer in chlorobenzene, a spin condition of 800 rpm and 60 s was used. The active layer was thermally annealed after spin coating on a ceramic hotplate under a nitrogen flow for about 20 min at 70 °C. These substrates were kept in a closed vacuum desiccator in the dark. Prior to evaporating metal electrodes, a thin strip of active layer and PEDOT:PSS, in the region where the top metal electrode was to be placed (see Section (4.2.1.4)), was carefully scratched to expose the end of the ITO strip such that one of the patterned metal electrodes made contacts with the ITO for ease of testing (see mask design).

For the inverted devices, 50 μL of the TiO_x solution (ambient atmosphere) was spin coated at 1000 rpm for 60 s and kept in air at room temperature for 2 hours for the film to oxidize. When the film started to solidify, the TiOx was scratched away from one end (~1 mm or less) in order to be able to make electrical contact with ITO later. This was followed by a thermal annealing of the coated TiO_x films (ambient atmosphere) on a hotplate at 150°C for 30 minutes. Then the active layer was coated using the same previously established spin-coating conditions. These substrates were kept in a closed vacuum desiccator in the dark prior to loading into the evaporator for metallization (typically within hours of active layer deposition).

4.2.1.4 Contact Evaporation

For evaporation of contact electrodes, a custom-made mask with a second mask over the top to ensure the mask sat flat was used. Substrates coated in active layers were arranged in an array (up to 4 × 4) and covered with the matching shadow mask shown in Fig. (4.1). Each mask defined two active pixels of ~18 mm^2 on each substrate and provided contacts which matched the test-clip designed for the purpose. The long electrode on the mask lined up with the scratch through to the ITO. The substrates were placed into the mask stack (4 pixels per device). Filaments or boats were prepared and loaded into the evaporator

(Angstrom Engineering instrument). Aluminum was evaporated from wire wrapped around tungsten filaments, silver was evaporated from pellets in a tungsten boat, and MoO_3 was evaporated from powder in a molybdenum boat.

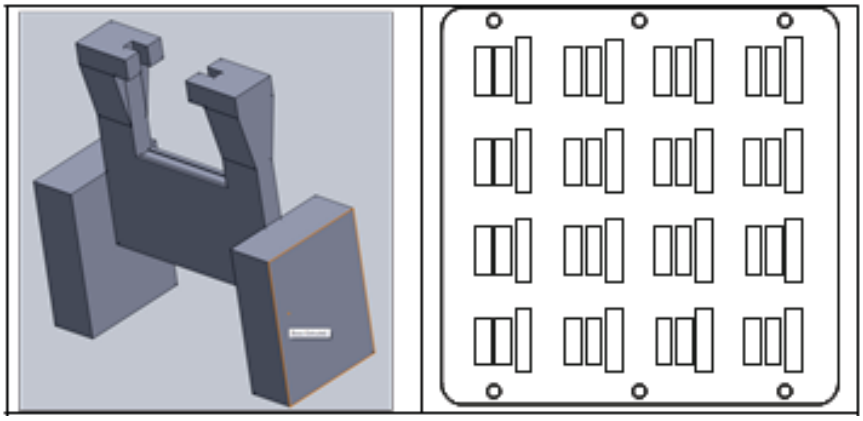

(a) (b)

(c)

Figure 4.1 (a) Mount designed for positioning devices (in top slot) appropriately for test clip. (b) Shadow mask for patterning electrodes. (c) OPV devices after aluminum and silver evaporation at the contacts.

4.2.2 Device Testing

The photovoltaic responses of devices were measured as soon as possible following metallization, typically on the same day. Two types of measurements were undertaken; spectrally resolved external quantum efficiency (EQE) measurements at short circuit (also called incident photon-to-current conversion efficiency), and current-voltage (J-V) response curves in the dark and under simulated solar illumination. EQE measurements were prioritized owing to the observation that devices were prone to short circuiting under mild applied voltages in J-V measurements.

EQE measurements were undertaken on an in-house measurement rig. The output of a Xe arc lamp was spectrally dispersed in a monochromater, and the monochromatic output (~5 nm spectral width) passed through a chopper to modulate the excitation at 137 Hz before being focused on the sample area. The sample was held in the purpose-built test clip, with the photocurrent measured as a function of scanned excitation wavelength via a lockin amplifier (Stanford Research Systems 830) referenced to the chopper modulation frequency. The raw output was converted to quantum efficiency by referencing to the spectrally resolved output of a calibrated silicon reference diode (Thorlabs) under identical conditions. Data acquisition and instrument control was facilitated through a LabVIEW software interface.

Current density-voltage (J-V) characteristics were measured with the samples in the same test clip and connected to a source measurement unit (Keithley 237). The voltage range scanned was generally limited to -0.5 V to +0.8 V to limit the risk of damage to the device. J-V curves were scanned in the dark, followed by simulated solar illumination. The output of the solar simulator (Sciencetech Inc) was adjusted to achieve AM1.5 conditions, as determined by the current output of a calibrated silicon reference PV device (Sciencetech Inc). Film thicknesses were measured by cleanly scratching through films to the substrate using the sharp point of tweezers, and measuring the depth profile of scratches using a Dektak profilometer (Veeco).

4.3 Results and Discussion

4.3.1 Device Fabrication

Bulk heterojunction devices were fabricated from the solutions of aza-BODIPYS (as donors) and $PC_{60}BM$ as the electron acceptor. Solar cell devices were made from six of the synthesized BF_2-aza-dipyrromethene compounds (compounds (88), (106), (112), (113), (132) and (151)) mainly focusing on optimization of device fabrication parameters of three compounds (compound (106), (112) and (113)) which showed highly encouraging signs during early stages of device testing. The six compounds tested were chosen on the basis of their broad absorption of the solar spectrum.

Two structures of bulk heterojunction devices were made, as mentioned. Firstly, these were the regular devices[2-6] with ITO(indium tin oxide)/PEDOT:PSS(poly(3,4-ethylenedioxythiophene): poly(styrenesulfonate)) as an anode, blend(BF_2-aza-dipyrromethenes and $PC_{60}BM$) and Al(aluminum)/Ag(silver) contact as a cathode on top. Secondly, the inverted devices[7-10] had the structure of ITO(indium tin oxide)/TiOx as a cathode, blend(BF_2-aza-dipyrromethenes and $PC_{60}BM$) and MoO_3(Molybdenum trioxide)/Ag (silver) as an anode on top, as depicted in Fig. (4.2).

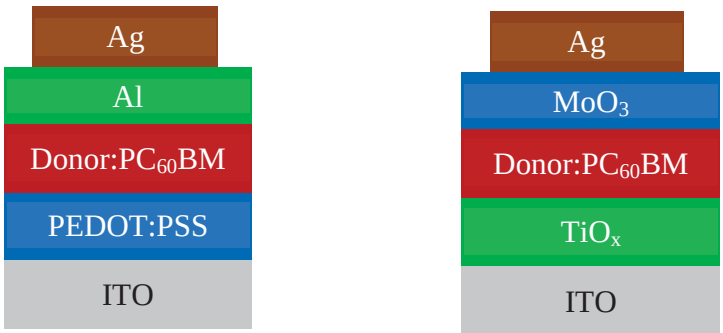

Figure 4.2 Schematic solar cell device architecture (a) regular device (b) inverted device.

A test-clip was designed based on a modified commercially available clip augmented with a 3D printed mount for holding the devices in place, as shown in Fig. (4.1). The test clip

had three pins that connected to the top electrodes of the two active pixels and the bottom electrode, respectively. A shadow mask was designed to match these three contacts, resulting in two 18 mm^2 active pixels and a space without electrodes to facilitate measuring film thickness. Each device pattern was replicated on a 4×4 array that fitted the evaporator baseplate. Fig. (4.6) shows how blend concentrations of 20-40 mg/mL led to films in the ideal thickness range of 80-200 nm when spin coated from chlorobenzene. Films were predictably thinner upon dilution. The materials studied extensively (compounds (106), (112), (113), (132) and (151)) produced uniform films most reliably.

On regular devices, the anode layer of PEDOT:PSS was coated from an aqueous dispersion, then dried on a hotplate under nitrogen. PEDOT:PSS was used for some devices to provide a more stable anode. The active layer of a mix solution of aza-BODIPYs and $PC_{60}BM$ was deposited on top of PEDOT:PSS layer. The active layer was thermally annealed under nitrogen at 70 °C to remove any residual solvent. The final step was the thermal deposition of 50-70 nm of Al on top of the active layer through a mask, followed by another thermal deposition of 30 nm of silver on top of aluminum layer in order to provide better electrode contacts. Both aluminum and silver evaporation were done under vacuum.

On inverted devices, a solution of TiO_x (titanium isopropoxide) was coated onto the ITO substrate. This was followed by thermal annealing of the substrate at 150 °C for 30 minutes. Similar conditions to regular devices were used to deposit the active layer on top of TiO_x. A 20 nm layer of MoO_3 was thermally evaporated on top of the active layer under vacuum, followed by deposition of an 80 nm silver layer. All of the inverted devices failed in the testing process. The reason behind the failures of the devices lay with the evaporation process of the MoO_3 layer on top of the active layer. It was found that the MoO_3 layers formed with less than 10 nm thickness, which was not enough thickness of the hole injection layer (MoO_3) for the device to work properly. Therefore, the focus was on the fabrication and testing of the regular architecture structure of bulk heterojunction solar cells (Fig. (4.2) (a)). The effects of active layer blend ratio, total concentration of a mixture solution, the solvent used for deposition, and the presence or absence of PEDOT:PSS were investigated by way of optimizing the device fabrication. Table (4.1) shows the variation of parameters used in the optimization of the solar cell device fabrication for selected devices.

Table 4.1 Selected devices with various fabrication parameters for compounds (88), (132), (112) and (151).

Device number	Compound Number	Solvent	Blend Ratio Donor:Acceptor	Total Solid Concentration (mg/mL)	PEDOT:PSS used
1	(88)	Chlorobenzene	2:1	40	yes
2	(132)	Chlorobenzene	1:2	20	yes
3	(151)	Chlorobenzene	1:2	20	Yes
4	(112)	Chlorobenzene	2:1	40	yes
5	(112)	Chlorobenzene	2:1	40	no
6	(112)	Chlorobenzene	1:2	20	yes
7	(106)	Chlorobenzene	2:1	40	yes
8	(106)	Chlorobenzene	2:1	40	no
9	(106)	Chlorobenzene	1:1	40	yes
10	(106)	Chlorobenzene	1:1	20	yes
11	(106)	Chlorobenzene	2:3	40	yes
12	(106)	Chlorobenzene	1:2	40	yes
13	(106)	Chlorobenzene	1:2	20	yes
14	(106)	Chlorobenzene	1:2	30	yes
15	(106)	Chlorobenzene	1:2	10	yes
16	(106)	Chlorobenzene	1:4	40	yes
17	(106)	Chlorobenzene	1:2	20	yes
18	(113)	Chlorobenzene	2:1	40	yes
19	(113)	Chlorobenzene	2:1	40	no
20	(113)	Chlorobenzene	1:1	40	yes
21	(113)	Chlorobenzene	1:1	20	yes
22	(113)	Chlorobenzene	2:3	40	yes
23	(113)	Chlorobenzene	1:2	40	yes
24	(113)	Chlorobenzene	1:2	20	yes
25	(113)	Chlorobenzene	1:2	30	yes
26	(113)	Chlorobenzene	1:2	10	yes
27	(113)	Chlorobenzene	1:4	40	yes
28	(113)	Chloroform	2:1	40	yes

4.3.2 Device Testing

4.3.2.1 External Quantum Efficiency (EQE) Measurements

4.3.2.1.1 Effect of Aza-BODIPYs as Donors

The external quantum efficiency (EQE)[11,12] was determined for devices with different compounds as donors (see Fig. (4.3)). Appropriate integration of EQE values reflects the photocurrent generation across the solar spectrum, and explains the value of the short circuit current density (J_{SC}) for the devices. Compounds (106), (112), (113), (132) and (151) exhibited the most promising quantum efficiencies. Interestingly, compounds (106), (113) and (151) exhibited substantial quantum efficiency in the red part of the spectrum (>600 nm), which is encouraging for broadband photocurrent generation. For other compounds exhibiting low efficiencies (e.g., compound (88)), the low efficiencies might be attributable to solvent impurities that were not easily removed prior to spin coating, thus compromising control over the actual concentrations and the film forming conditions. The EQE could not be measured above 750 nm because of the limitation of the testing equipment. The EQE values were very low (≤ 4.23%) in comparison with the standard P3HT:PCBM solar cell device (the EQE reported in the literature[13-18] for P3HT:PCBM exceeded 80%, see Section (1.3.2) in Chapter 1).

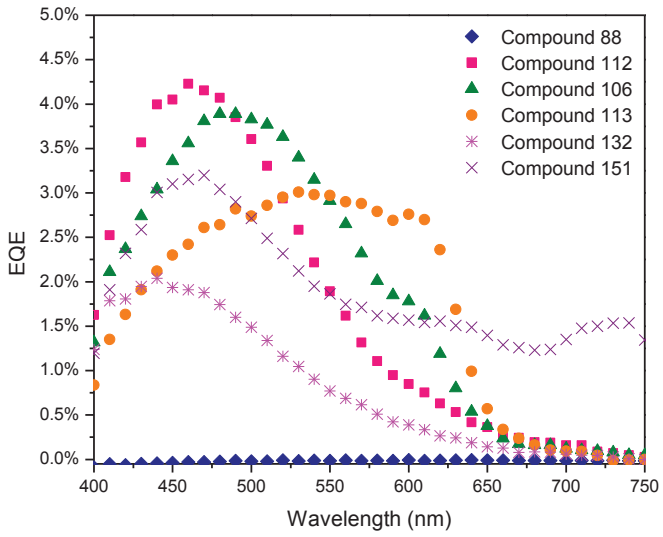

Figure 4.3 Effect of the electron donor (aza-BODIPY) for a series of devices with the same blend ratio and total concentration.

4.3.2.1.2 Effect of the PEDOT:PSS Interfacial Layer

Fig. (4.4), Fig. (4.5) and Fig. (4.6) represent the spectrally resolved photocurrent for devices made from compounds (112), (106) and (113) respectively, with and without the PEDOT:PSS interfacial layer. These results confirmed the beneficial effects of the PEDOT:PSS interfacial layer between the anode and active layer for hole extraction, consistent with experience in many other laboratories. All subsequent devices were made with the PEDOT:PSS layer.

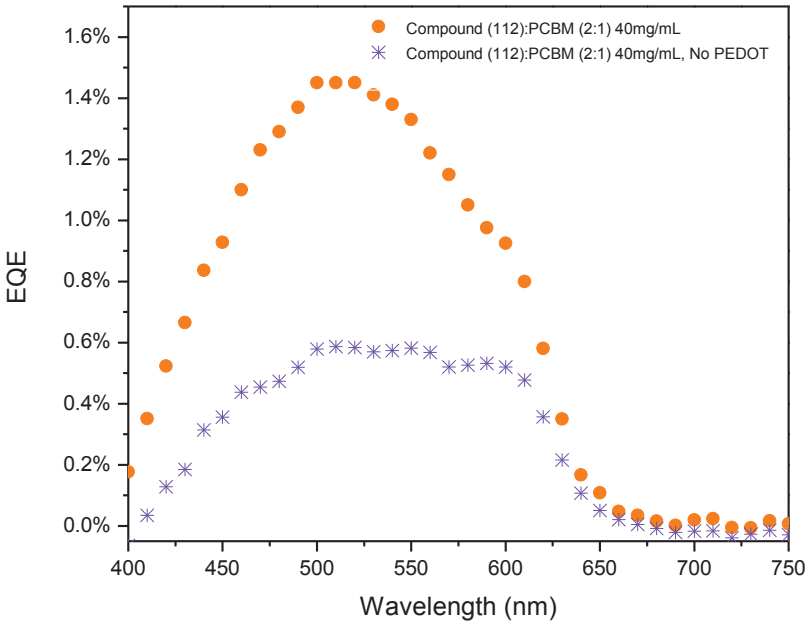

Figure 4.4 Spectrally resolved photocurrent for devices employing compound (112), examining the effect of the PEDOT:PSS interfacial layer.

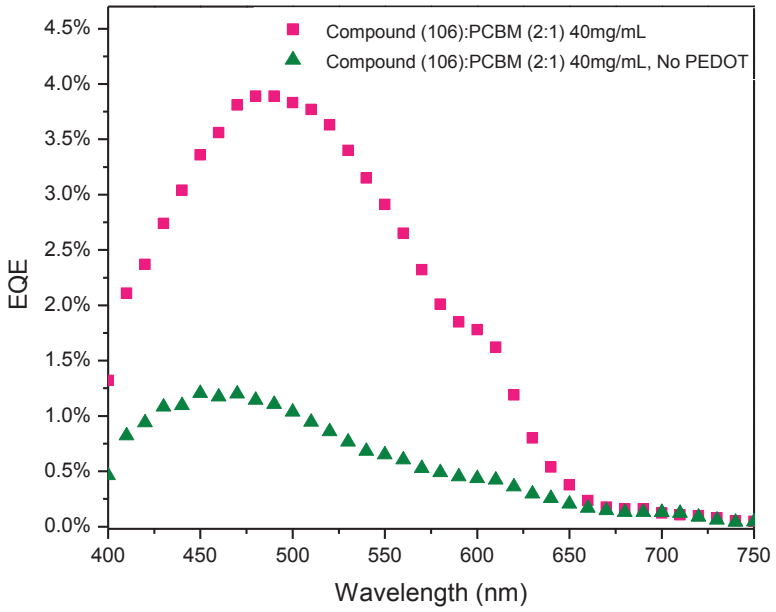

Figure 4.5 Spectrally resolved photocurrent for devices employing compound (106), examining the effect of the PEDOT:PSS interfacial layer.

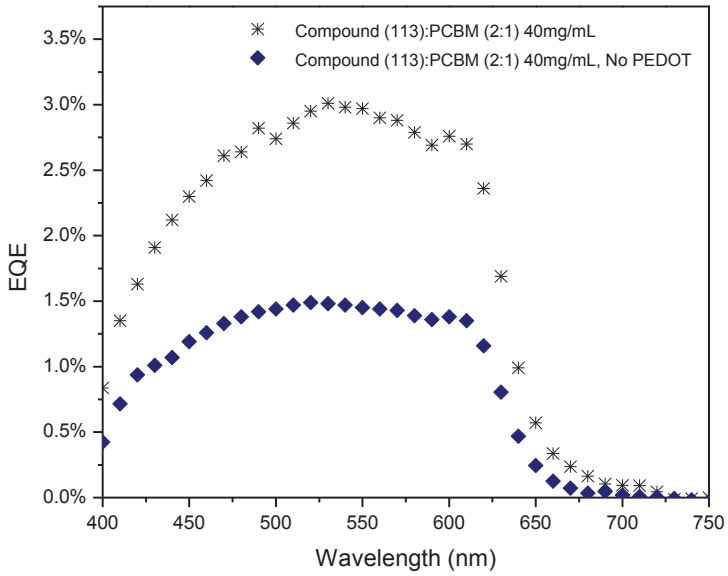

Figure 4.6 Spectrally resolved photocurrent for devices employing compound (113), examining the effect of the PEDOT:PSS interfacial layer.

4.3.2.1.3 Effect of Active Layer Thickness

To assess the effects of active layer thickness, the EQE of devices 12, 13, 14 and 15 were compared for compound (106) (Fig. (4.7)). A thickness of the order of 80 nm gave optimal quantum efficiencies of photocurrent generation. This was achieved with more dilute solutions (20 mg/mL) of active layers than previously used. The preference for thinner layers, in spite of their lower absorption, suggested that thicker layers suffered from significant charge recombination. The fact that thin devices transmitted much of the incident light limited the measured EQE's. Normalizing to absorbed photons (i.e., internal quantum efficiency) would have resulted in efficiencies 2-3 times higher for the thinnest devices.

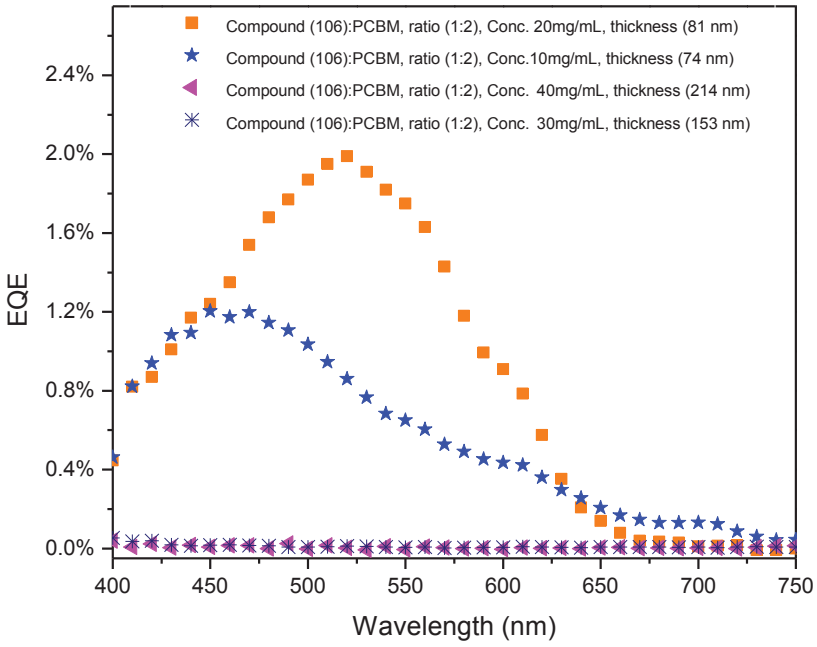

Figure 4.7 Effect of active layer thickness (compound (106):PCBM) in nm, as controlled by total blend concentration.

4.3.2.1.4 Effect of Donor:Acceptor Blend Ratio in Active Layer

The blend ratio had a significant effect on the performances of the solar cell devices. Fig. (4.8) and Fig. (4.9) show the effect of the blend ratio on the EQE of devices with compounds (106) and (113) as donor materials. For both compounds shown in Fig. (4.8) and Fig. (4.9), the 2:1 blends resulted in the highest quantum efficiencies. There was no discernable efficiency trend for other ratios with either compound.

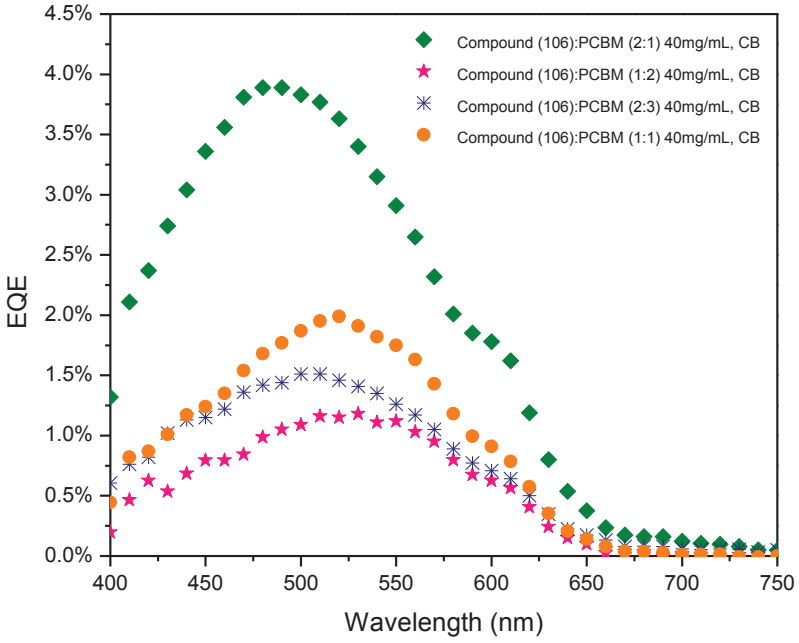

Figure 4.8 Effect of compound (106):$PC_{60}BM$ blend ratio. CB is chlorobenzene used to cast the active layer.

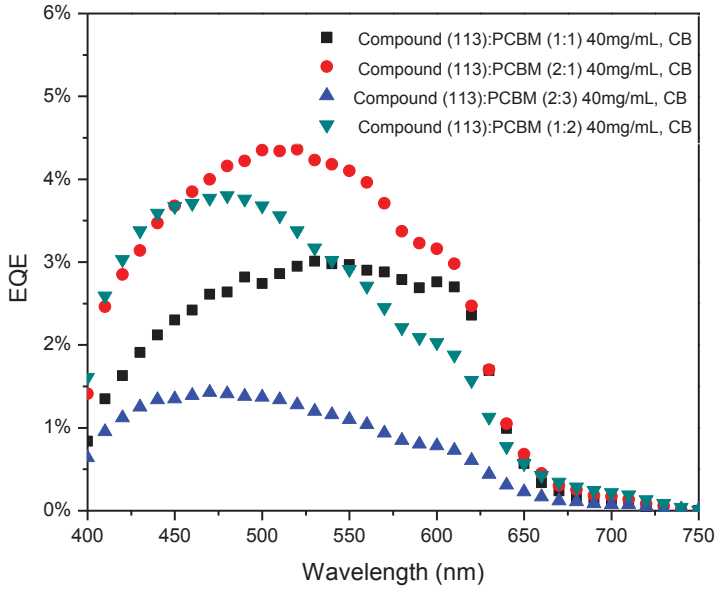

Figure 4.9 Effect of compound (113):$PC_{60}BM$ blend ratio. CB is chlorobenzene used to cast the active layer.

4.3.2.1.5 Effect of Casting Solvent

The effect of the solvent used to deposit the active layer was investigated. Fig. (4.10) shows how casting active layer films from dry chlorobenzene resulted in the most efficient devices. Chlorobenzene is often used with active layer blends in organic solar cells. The relatively poor performance of chloroform is most likely a result of too little phase separation during the rapid solvent evaporation.

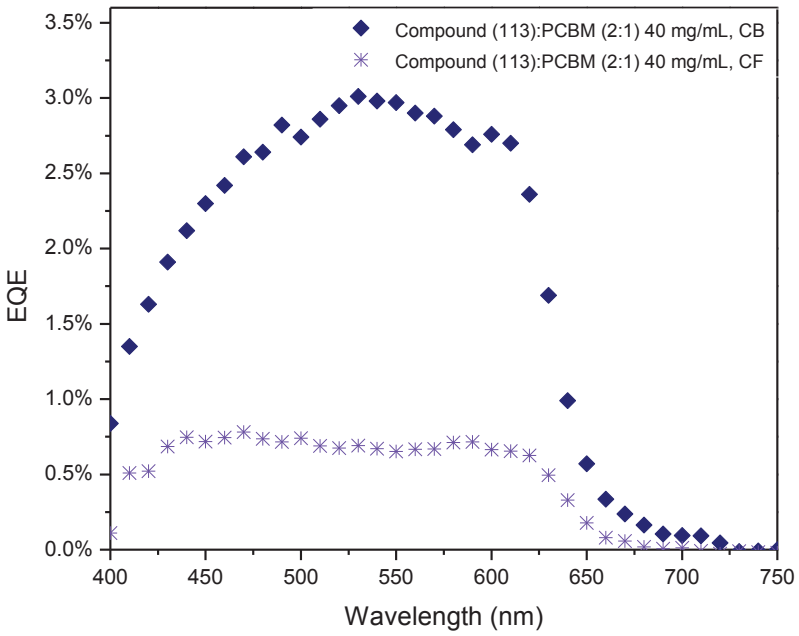

Figure 4.10 Effect of casting solvent, where $PC_{60}BM$ blends with compound (113) were cast from chlorobenzene (CB) and chloroform (CF).

4.3.2.2 Current Density-Voltage (*J-V*) Characteristics

Current density-voltage (*J-V*) characteristics were investigated in order to determine the power conversion efficiency (η) under standard test condition (STC) of Air Mass 1.5 spectrum using a xenon arc lamp as a solar simulator. The *J-V* characteristics determine important parameters of solar cell devices, in particular open-circuit voltage (V_{OC}) and fill factor (FF). Current density-voltage (*J-V*) characteristics were measured for these six compounds (88), (106), (112), (113), (132) and (151).

Fig. (4.11), Fig. (4.12), Fig. (4.13), Fig. (4.14), Fig. (4.15), Fig. (4.16), Fig. (4.17), Fig. (4.18), Fig. (4.19) and Fig. (4.20) show J-V curves for some of the better performing devices (for compounds (106), (112), (113), (132) and (151)). Other devices measured either shared this general shape, often with lower short-circuit currents and lower open-

circuit voltages, or they exhibited an Ohmic response (see Fig. (A2), Fig. (A3), Fig. (A4), Fig. (A5), Fig. (A6), Fig. (A7), Fig. (A8), Fig. (A9), Fig. (A10), Fig. (A11), Fig. (A12), Fig. (A13), Fig. (A14) and Fig. (A15) in Appendix).

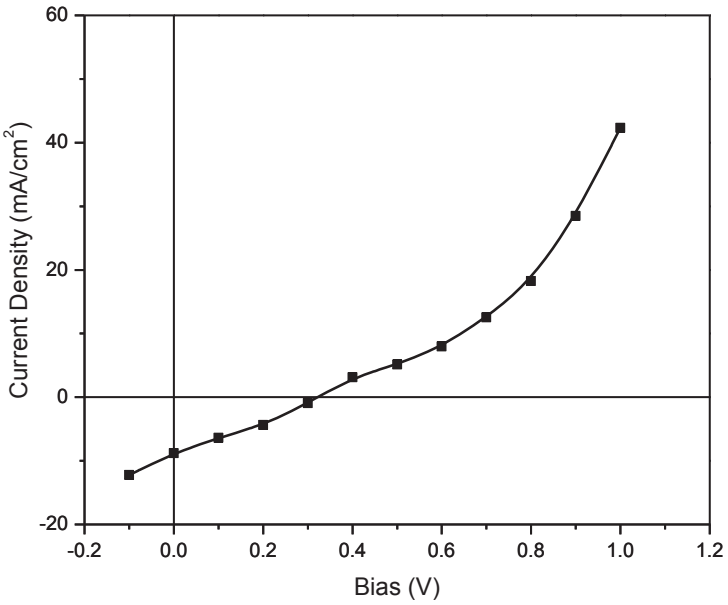

Figure 4.11 The current density-voltage (*J*-*V*) characteristics of device number (7) (made from compound (106)) under Air Mass 1.5 spectrum using a xenon arc lamp as a solar simulator.

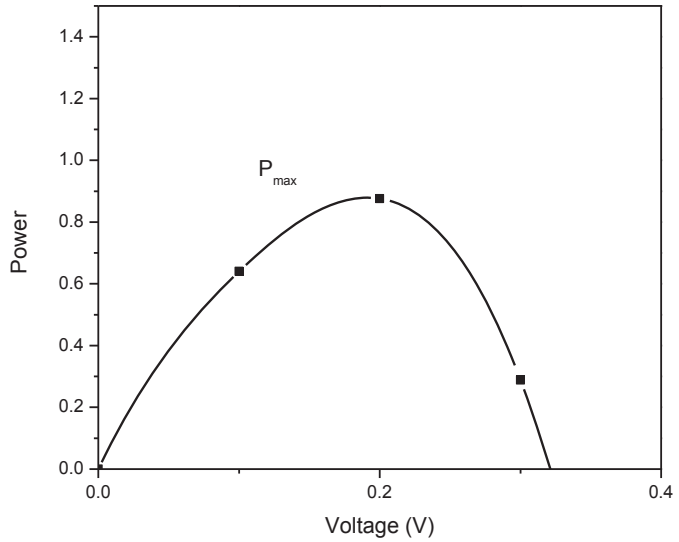

Figure 4.12 The power (J×V) versus V for device number (7) (made from compound (106))

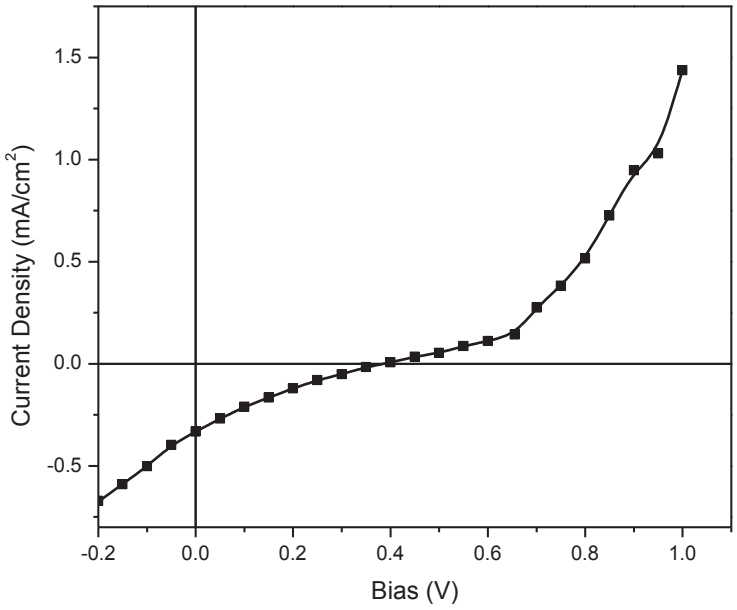

Figure 4.13 The current density-voltage (*J-V*) characteristics of device number (3) (made from compound (151)) under Air Mass 1.5 spectrum using a xenon arc lamp as a solar simulator.

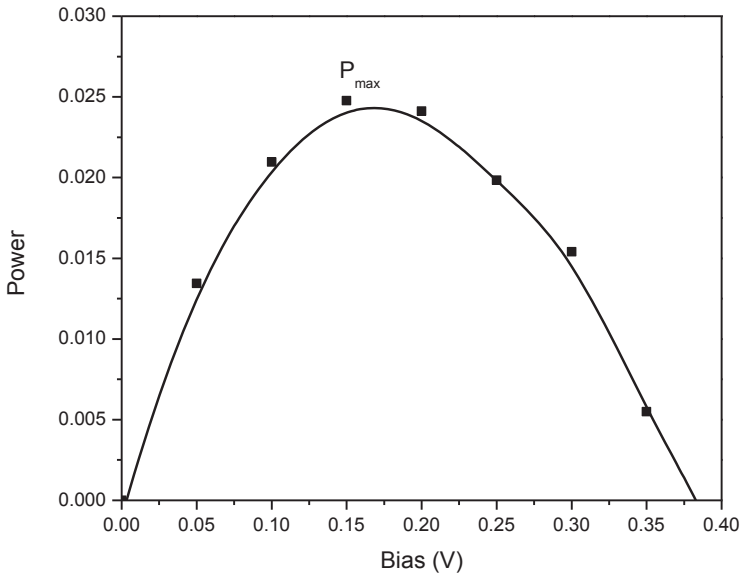

Figure 4.14 The power (J×V) versus V for device number (3) (made from compound (151))

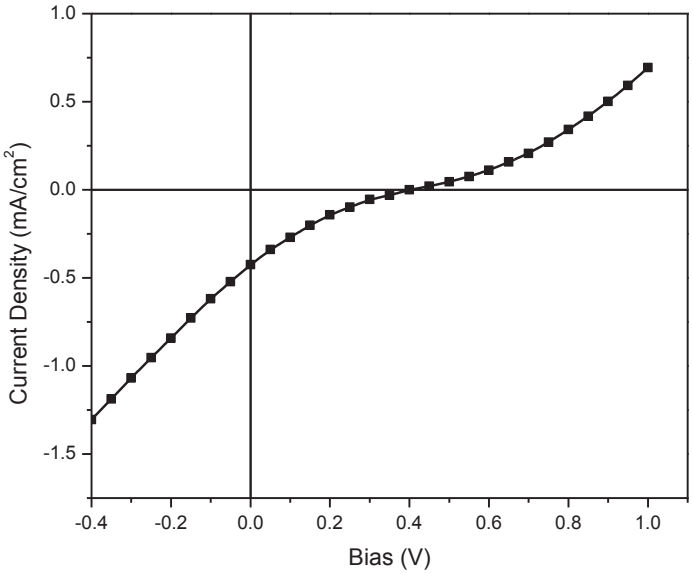

Figure 4.15 The current density-voltage (*J*-*V*) characteristics of device number (4) (made from compound (112)) under Air Mass 1.5 spectrum using a xenon arc lamp as a solar simulator.

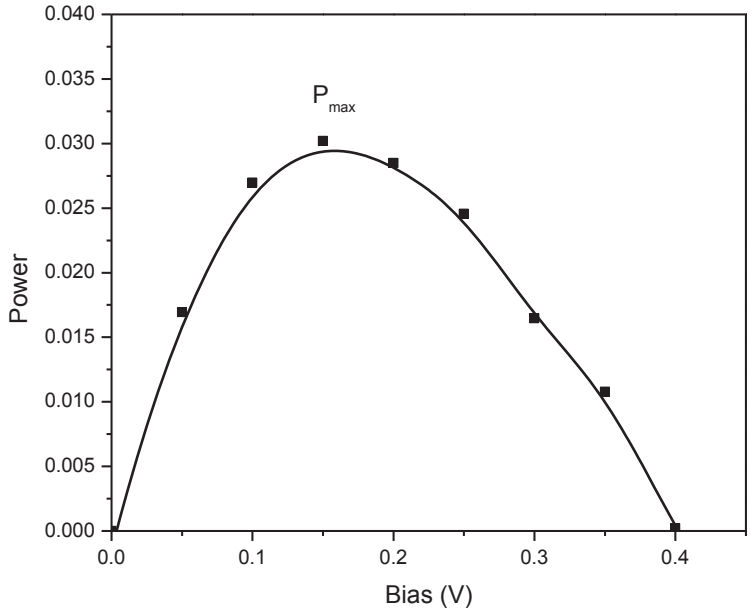

Figure 4.16 The power (J×V) versus V for device number (4) (made from compound (106))

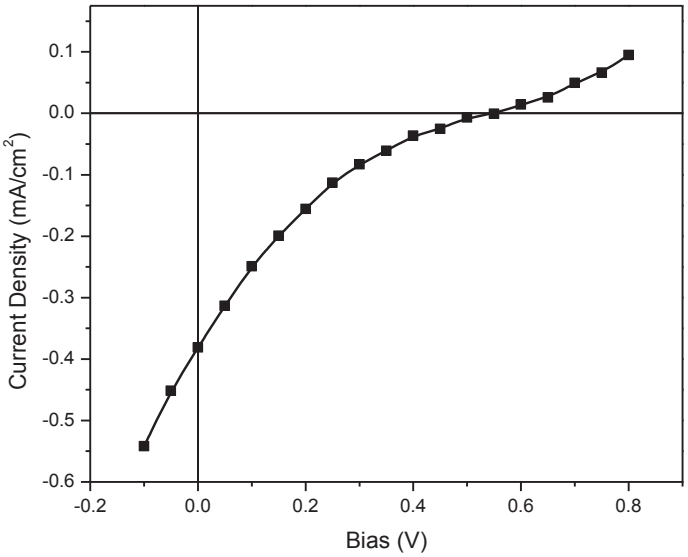

Figure 4.17 The current density-voltage (*J*-*V*) characteristics of device number (23) (made from compound (113)) under Air Mass 1.5 spectrum using a xenon arc lamp as a solar simulator.

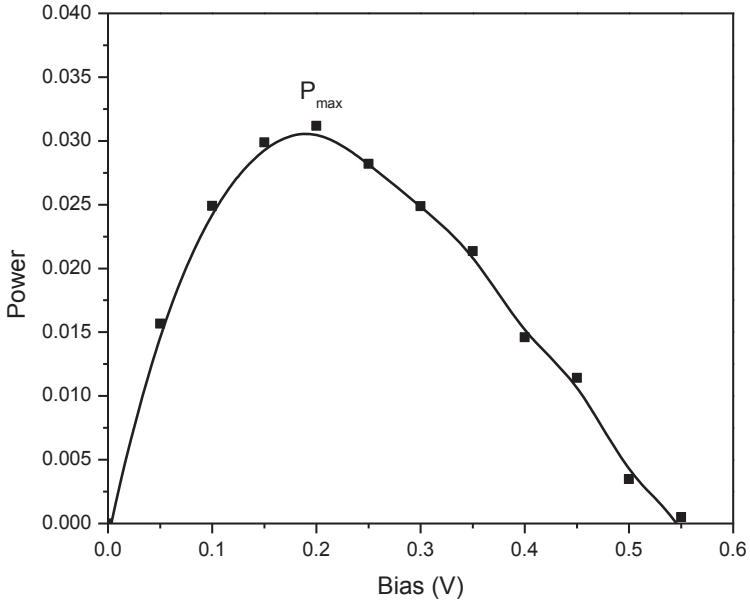

Figure 4.18 The power (J×V) versus V for device number (23) (made from compound (113))

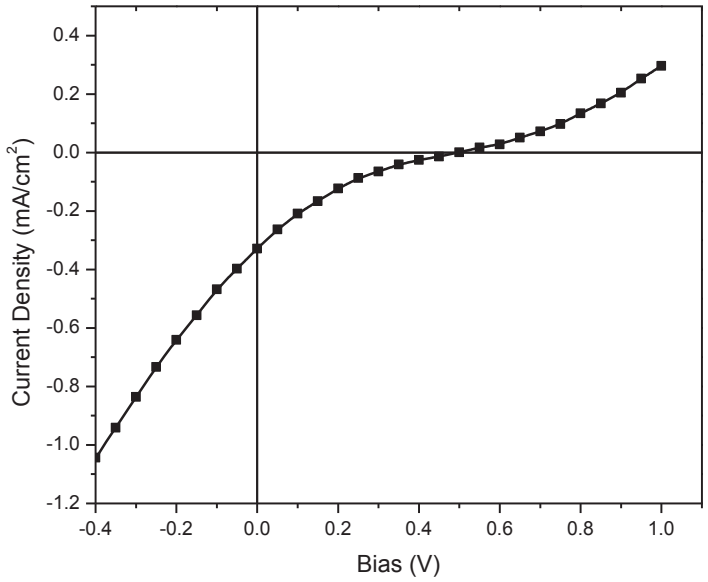

Figure 4.19 The current density-voltage (*J-V*) characteristics of device number (2) (made from compound (132)) under Air Mass 1.5 spectrum using a xenon arc lamp as a solar simulator.

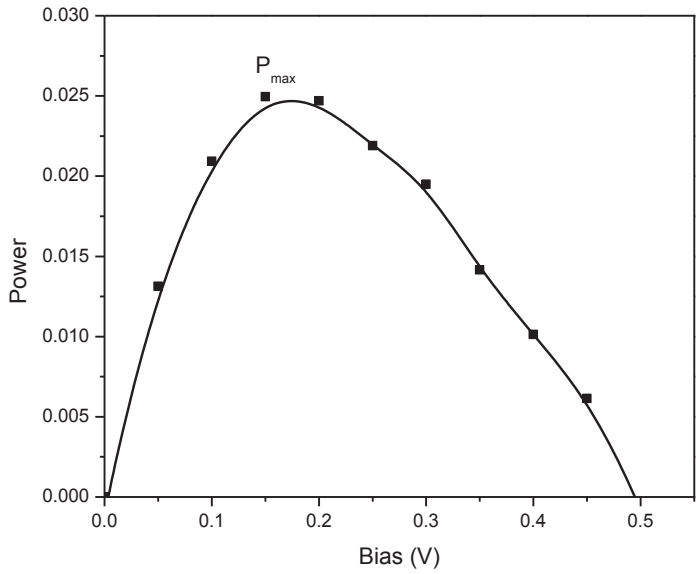

Figure 4.20 The power (J×V) versus V for device number (2) (made from compound (132))

Table (4.2) shows the performance characteristics for some of the better performing devices, which were extracted from the J-V curves. Fill factor (FF) is the ratio of the maximum power (P_{max}) produced by a solar cell to the product of V_{OC} and J_{SC}. FF is a measure of the integrity of the solar cell. Results from devices made with compound (151) as donor should be discarded from further discussion, as the characterization of this compound was not reliable and the material could have been impure.

Table 4.2 Device performance characteristics for the better performing devices.

Compound number	Device number	V_{OC} (V)	J_{SC} (mA/cm^2)	FF	Power conversion efficiency (%)
(106)	7	0.32	8.83	0.312	0.88%
(151)	3	0.40	0.33	0.0189	0.025%
(112)	4	0.40	0.43	0.0174	0.03%
(113)	23	0.55	0.38	0.0147	0.031%
(132)	2	0.50	0.33	0.0151	0.025%

The *J-V* curves revealed the following issues suffered by all of the devices measured. Solar cell devices based on compounds (113) and (132) exhibited a relatively high V_{OC} (0.55 V and 0.50 V respectively), which might be attributable to the HOMO energy levels of these small molecules. This being the case, an effective method for obtaining a high V_{OC} (0.55 V) might be by adjusting the electron-donating abilities of benzothiadiazole, thiophene, phenothiazine and triphenylamine moieties on the aza-BODIPY core. A high values of V_{OC} are required for solar cell devices based on aza-BODIPY derivatives, and the V_{OC} values of (113) and (132) were similar to that in the literature[19-22] compound V_{OC}=0.65 V (see Section (1.5.4) in Chapter 1).

i) Low open-circuit voltages. The higher V_{OC}'s were on the order of 0.4-0.55 V. These low voltages could be related to an interfacial charge extraction barrier (see below). A V_{OC} over 1 V has been reported recently in the literature[23] for an organic solar cell with a FF of 0.63 and a power conversion efficiency of 6.17%.

ii) Low fill factors. The fill factor (defined as ratio of the maximum power to the product $J_{SC} \times V_{OC}$) was extremely poor for these devices (~0.01-0.3, compared with ~0.6-0.8 for high performing OPV devices).[23] The ideal PV response would produce a rectangular curve between V_{OC} and J_{SC} in the PV quadrant (positive bias and negative current in this polarity, see Fig. (4.21) for an ideal *J-V* curve). The curves in Fig. (4.11), Fig. (4.13), Fig. (4.15), Fig. (4.17) and Fig. (4.19) exhibit a severe inflection, which is reflected in the low fill factors. This was most likely caused by an interfacial extraction barrier at one of the active layer interfaces - probably between the active layer and the metal cathode. A possible origin of this barrier would have been a thin layer of aluminium oxide, which cannot easily be prevented without the capability to encapsulate the devices in an inert environment (by carrying out the evaporation in a glovebox prior to direct encapsulation).

iii) Low short-circuit currents. The low J_{SC} values essentially reflected the modest EQE's (particularly in the red part of the solar spectrum) combined with the charge extraction and recombination problems noted above. It can be seen that photocurrents increased at high reverse bias, where the supposed extraction barrier and recombination could be

overwhelmed. This suggests that there was plenty of charge in the devices which could be extracted without applying a strong reverse bias.

Efficiencies would be improved by at least a factor of 30 if a reasonable fill-factor of 0.5 could be obtained. It is likely that resolving the issue of the charge extraction barrier would also have improved J_{SC} and V_{OC}, meaning that overall power conversion efficiencies approaching 2% might be attainable.

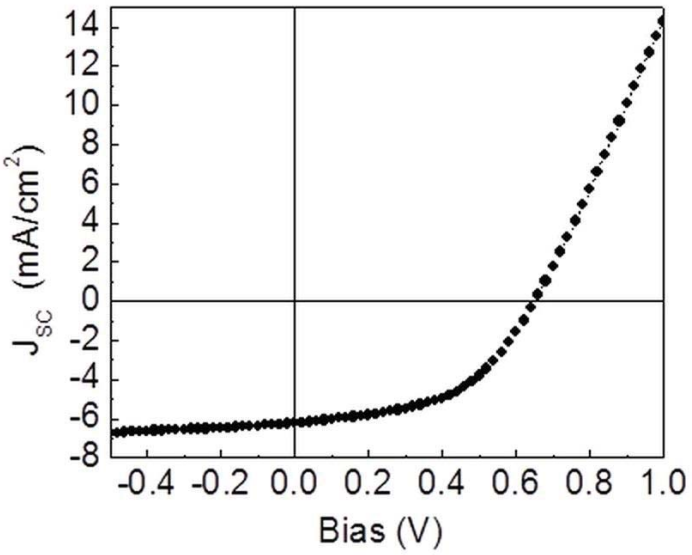

Figure 4.21 The current density-voltage (*J-V*) characteristics of standard solar cell reported in the literature[24] with the architecture ITO/PEDOT/P3HT:PCBM/Al under AM 1.5G simulated 1 sun solar illumination

A solar cell device with a structure of ITO(indium tin oxide)/PEDOT/small molecule (compound (106))/$PC_{60}BM$/Al exhibited a V_{OC} of 0.32 V, a short-circuit current (J_{SC}) of 8.83 mA/cm^2, a fill factor (FF) of 0.312, and a power conversion efficiency (η) of 0.88%, which was the highest η value respectively observed in this study. Devices based on compounds (112), (113) and (132) showed values of V_{OC} of 0.40 V, 0.55 V and 0.50 V; short-circuit current (J_{SC}) of 0.43 mA/cm^2, 0.38 mA/cm^2, 0.33 mA/cm^2; fill factor (FF) of 0.0174, 0.0147 and 0.0151; and η of 0.03%, 0.0031% and 0.025%.

The highest J_{SC} was obtained for a solar cell device based on compound (106):$PC_{60}BM$ (8.83 mA/cm^2), and exceeded J_{SC}'s of the devices based on compound (112):$PC_{60}BM$, compound (113):$PC_{60}BM$ or compound (132):$PC_{60}BM$. This perhaps could be explained by the broad absorption of this compound (106) and the high λ_{max} (λ_{max}= 818 nm). The J_{SC} of the device based on compound (113) was lower (0.38 mA/cm^2) than that of compound (106) (8.83 mA/cm^2), even though compound (113) exhibited nearly the same absorption range (λ_{max}= 855 nm) as that of compound (106).

4.4 Conclusion

Working OPV devices were fabricated from selected aza-BODIPYs. A broad range of device composition and processing conditions were surveyed, leading to a procedure that produced external quantum efficiencies of 4.3% and 3.9% for compounds (106) and (113) respectively. The generally low overall power conversion efficiencies were a result of poor open circuit voltages and fill factors. The shape of the J-V curves suggested the presence of charge extraction barriers, while the lower efficiencies of thicker devices implied significant charge recombination within the films. Future work might involve fabrication of inverted devices (with a high work function metallic cathode) to circumvent the possibility of oxidation of the metal electrode. Two of the dyes exhibited significant photocurrent at the red end of the spectrum.

4.5 References

(1) Sun, Y.; Welch, G. C.; Leong, W. L.; Takacs, C. J.; Bazan, G. C.; Heeger, A. J. *Nat*. *Mater*. **2012**, *11*, 44.

(2) Jen, A. K.; American Chemical Society: 2012, p PMSE.

(3) Shi, M.; Chen, H.; Chen, L.; Chen, J.; Wang, M.; Zhejiang University, Peop. Rep. China . 2010, p 9pp.

(4) Tan, H.; Zhang, X.; Gao, H.; Bai, Y.; Zhang, X.; Yin, Z.; Institute of Semiconductors, Chinese Academy of Sciences, Peop. Rep. China . 2011, p 9pp.

(5) Tang, Z.; George, Z.; Ma, Z.; Bergqvist, J.; Tvingstedt, K.; Vandewal, K.; Wang, E.; Andersson, L. M.; Andersson, M. R.; Zhang, F.; Inganaes, O. *Adv*. *Energy Mater*. **2012**, *2*, 1467.

(6) Zhou, M.; Wang, P.; Huang, H.; Chen, J.; Ocean's King Lighting Science & Technology Co., Ltd., Peop. Rep. China; Shenzhen Ocean's King Lighting Science & Technology Co., Ltd. . 2013, p 11pp.

(7) Cheng, Y.-J.; Cao, F.-Y.; Lin, W.-C.; Chen, C.-H.; Hsieh, C.-H. *Chem*. *Mater*. **2011**, *23*, 1512.

(8) Xie, Z.; Guo, X.; Liu, F.; Geng, Y.; Yue, W.; Qu, Y.; Wang, L.; Changchun Institute of Applied Chemistry, Chinese Academy of Sciences, Peop. Rep. China . 2009, p 18pp.

(9) Xie, Z.; Guo, X.; Wang, L.; Liu, F.; Changchun Institute of Applied Chemistry, Chinese Academy of Sciences, Peop. Rep. China . 2008, p 28pp.

(10) Schmidt, H.; Winkler, T.; Tilgner, M.; Fluegge, H.; Schmale, S.; Buelow, T.; Meyer, J.; Johannes, H. H.; Riedl, T.; Kowalsky, W. *Proc*. *SPIE* **2009**, *7416*, 741611/1.

(11) Brenner, T. J. K.; Yaynzof, Y.; Li, Z.; Kabra, D.; Friend, R. H.; McNeill, C. R. *J*. *Phys*. *D: Appl*. *Phys*. **2012**, *45*, 415101/1.

(12) Horie, M.; Shen, I. W.; Tuladhar, S. M.; Leventis, H.; Haque, S. A.; Nelson, J.; Saunders, B. R.; Turner, M. L. *Polymer* **2010**, *51*, 1541.

(13) Dennler, G.; Scharber, M. C.; Brabec, C. J. *Adv*. *Mater*. *(Weinheim, Ger.)* **2009**, *21*, 1323.

(14) Marsh, R. A.; Hodgkiss, J. M.; Albert-Seifried, S.; Friend, R. H. *Nano Lett*. **2010**, *10*, 923.

(15) Kim, J. Y.; Kim, S. H.; Lee, H. H.; Lee, K.; Ma, W.; Gong, X.; Heeger, A. J. *Advanced Materials* **2006**, *18*, 572.

(16) Yang, X.; Loos, J.; Veenstra, S. C.; Verhees, W. J. H.; Wienk, M. M.; Kroon, J. M.; Michels, M. A. J.; Janssen, R. A. J. *Nano Letters* **2005**, *5*, 579.

(17) Kekuda, D.; Huang, J.-H.; Ho, K.-C.; Chu, C.-W. *The Journal of Physical Chemistry C* **2010**, *114*, 2764.

(18) Leblebici, S. Y.; Catane, L.; Barclay, D. E.; Olson, T.; Chen, T. L.; Ma, B. *ACS Applied Materials & Interfaces* **2011**, *3*, 4469.

(19) Mueller, T.; Gresser, R.; Leo, K.; Riede, M. *Solar Energy Materials and Solar Cells* **2012**, *99*, 176.

(20) Rousseau, T.; Cravino, A.; Bura, T.; Ulrich, G.; Ziessel, R.; Roncali, J. *Chem*. *Commun*. *(Cambridge, U*. *K*.*)* **2009**, 1673.

(21) Min, J.; Ameri, T.; Gresser, R.; Lorenz-Rothe, M.; Baran, D.; Troeger, A.; Sgobba, V.; Leo, K.; Riede, M.; Guldi, D. M.; Brabec, C. J. *ACS Appl*. *Mater*. *Interfaces* **2013**, *5*, 5609.

(22) Mueller, T.; Gresser, R.; Leo, K.; Riede, M. *Sol*. *Energy Mater*. *Sol*. *Cells* **2012**, *99*, 176.

(23) Yuan, J.; Zhai, Z.; Dong, H.; Li, J.; Jiang, Z.; Li, Y.; Ma, W. *Advanced Functional Materials* **2013**, *23*, 885.

(24) Li, G.; Shrotriya, V.; Huang, J.; Yao, Y.; Moriarty, T.; Emery, K.; Yang, Y. *Nat*. *Mater*. **2005**, *4*, 864.

Chapter 5

Conclusions and Future Directions

Chapter 5

5.1 Conclusions and Future Directions

Many of the aza-BODIPYs designed and selected for synthesis have been successfully synthesised, and number have been incorporated with fullerene-based acceptors in photovoltaic devices. These novel symmetrical aza-BODIPYs, which included terthiophene-BF_2-aza-dipyrromethene (87), methoxy-terthiophene-BF_2-aza-dipyrromethene (88), triphenylamine-BF_2-aza-dipyrromethene (100), thiophene-triphenylamine-BF_2-aza-dipyrromethene (106), benzothiadiazole-BF_2-aza-dipyrromethene (111), benzothiadiazole-thiophene-BF_2-aza-dipyrromethene (112), benzothiadiazole-triphenylamine-BF_2-aza-dipyrromethene (113), ethylenedioxythiophene-BF_2-aza-dipyrromethene (125),thiophene-phenothiazine-BF_2-aza-dipyrromethene (132), thiophene-methylpyrrole-BF_2-aza-dipyrromethene (139), thiophene-carbazole-BF_2-aza-dipyrromethene (145), fluorenone-BF_2-aza-dipyrromethene (150), and thiophene-fluorenone-BF_2-aza-dipyrromethene (151) (Fig. 5.1), spanned a broad range of electron donating and electron withdrawing tendencies, as was the original intention. Substituents created additional conjugation and shifts to significantly longer wavelengths were realized in both absorption and emission spectra. The red shift in absorption and emission observed for compound (113) was perhaps remarkable. Compound (113) (benzothiadiazole-triphenylamine-BF_2-aza-dipyrromethene) showed an absorption maximum at 855 nm, which represents the highest absorption maximum known for an aza-BODIPY compound. Introduction of the electron-deficient groups (benzothiadiazole groups) at positions 1 and 7 resulted in a red shift of about 205 nm in the absorption maximum in comparison with the standard aza-BODIPY (compound (4)), or 284 nm in comparison with compound (111) (Fig. 5.2). It has thus been possible to synthesize aza-BODIPY fluorophores with markedly altered absorption and emission properties by changing the substituents on the aza-BODIPY core.

Fluorescence and time-correlated single-photon counting (TCSPC) spectroscopy confirmed interactions between the aza-BODIPYs and $PC_{60}BM$. The fluorescence quenching indicated

how strong the interaction was between aza-BODIPYs and $PC_{60}BM$. Lifetime measurements suggested static quenching.

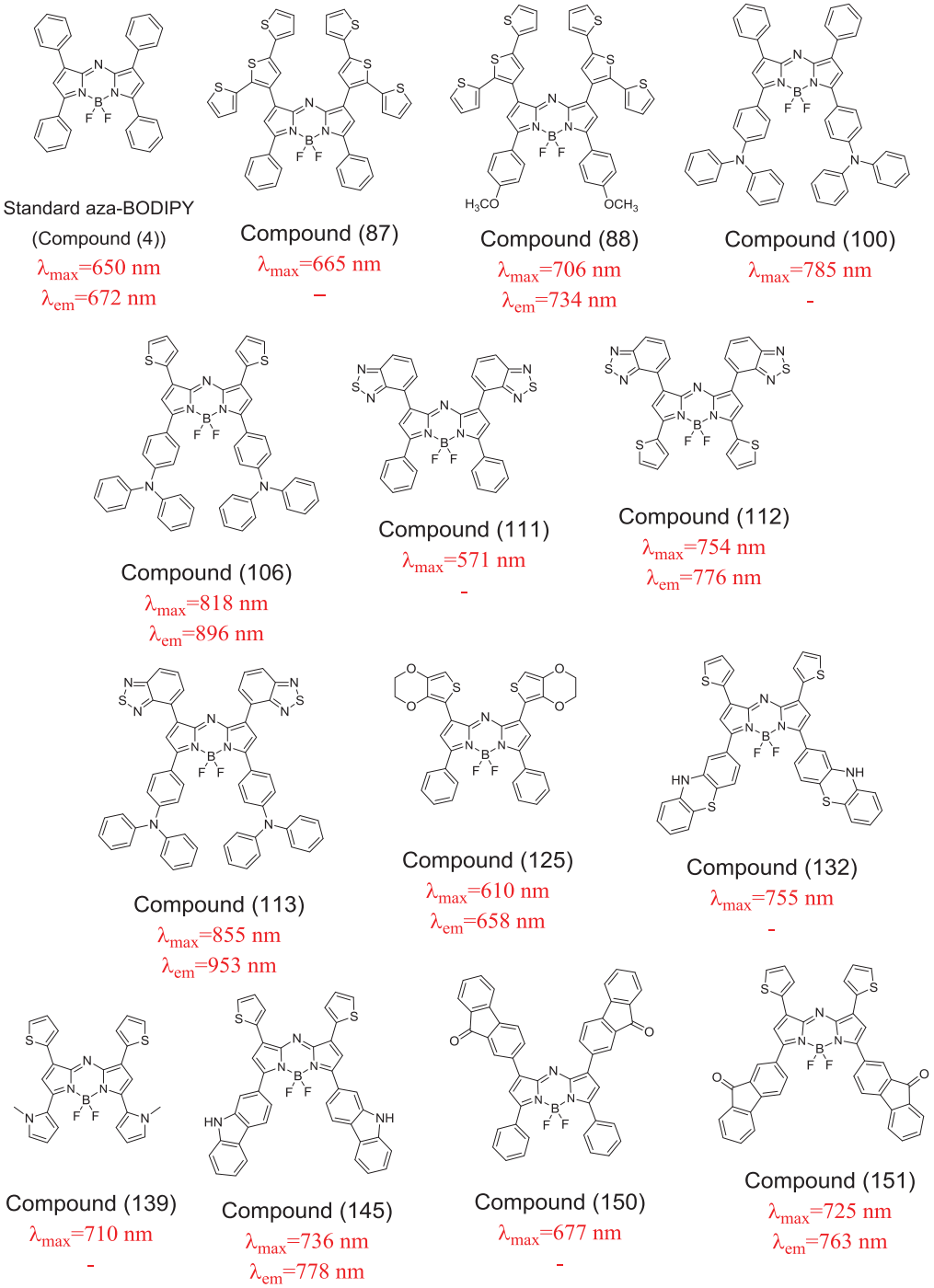

Figure 5.1 The new synthesised aza-BODIPYs ((87), (88), (100), (106), (111), (112), (113), (125), (132), (139), (145), (150) and (151)) along with the standard aza-BODIPY (compound (4)).

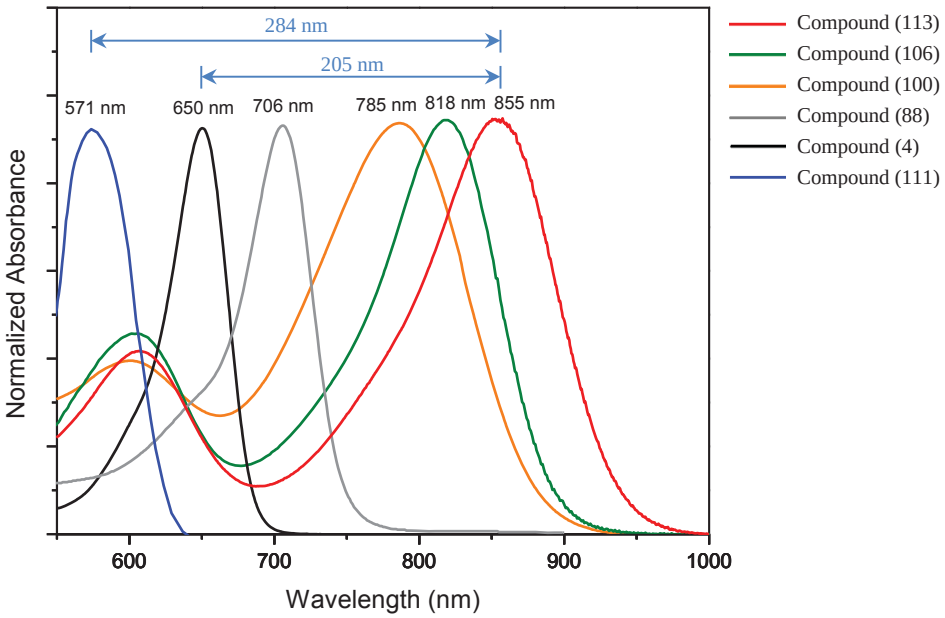

Figure 5.2 The experimental UV-VIS spectra of selected aza-BODIPYs (compound (4), λ_{max}=650 nm (black line), compound (88), λ_{max}= 706 nm (grey line), compound (100), λ_{max}= 785 nm (orange line), compound (106), λ_{max}= 818 nm (green line), compound (111), λ_{max}= 571 nm (blue line) and compound (113), λ_{max}= 855 nm (red line)) in chloroform.

The six of these novel aza-BODIPYs selected for incorporation in solar cells were found to have low external quantum efficiencies (EQE).[1-4] EQE was less than 4.23% (maximum observed which was for (106)). Compounds (106), (112), (113), (132) and (151) were considered to exhibit promising efficiencies (Fig. (5.3)). The optimum thickness of the active layer in these devices was found to be in the order of 80 nm (Fig. 5.4). The lower quantum efficiencies of thicker devices are attributable to charge recombination.

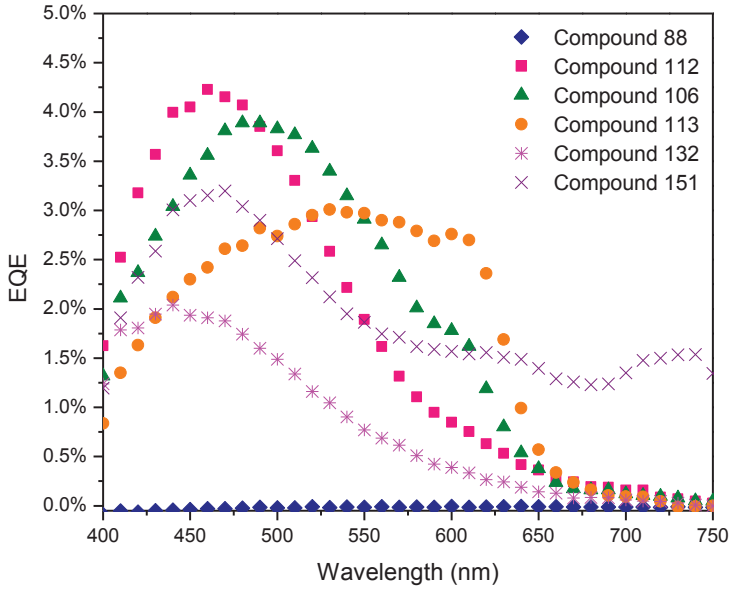

Figure 5.3 Effect of the electron donor (aza-BODIPY) for a series of devices with the same blend ratio and total concentration.

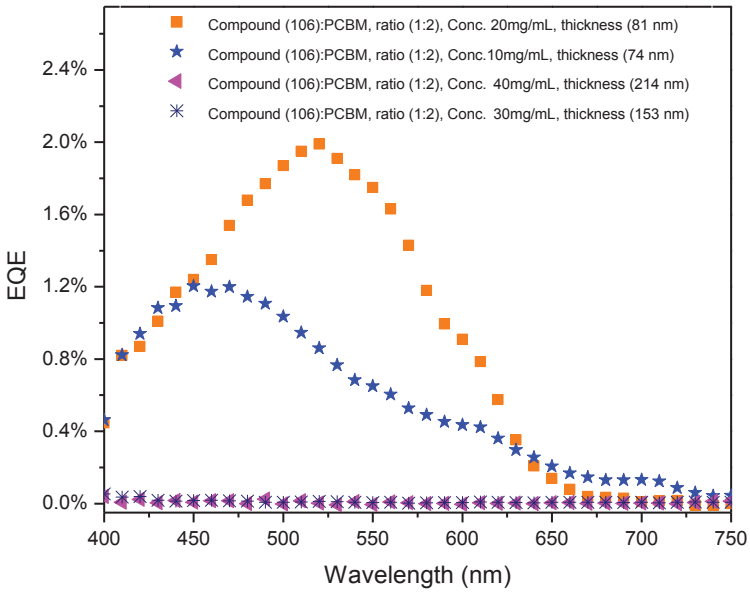

Figure 5.4 Effect of active layer thickness (compound (106):PCBM) in nm, as controlled by total blend concentration.

Current density-voltage characteristics were measured under standard test condition (STC) of Air Mass 1.5 spectrum using a xenon arc lamp as a solar simulator. The J-V curves in all of the measured devices suffered from low open-circuit voltages, low fill factors and low short-circuit currents. Significantly, the J-V curves exhibited severe inflections, which are tentatively attributed to the presence of charge extraction barriers. Respectable power conversion efficiencies would be attainable if a reasonable fill-factor of 0.5 could be obtained. Resolving the charge extraction barrier problem should improve J_{SC} and V_{OC}. Overall power conversion efficiencies approaching 2% might be attainable. The suspected charge barrier could have been due to an oxide layer on the aluminum electrode. Device fabrication is most easily carried out in glove boxes for this very reason, namely to preclude chemical effects from the presence of water and oxygen. Several of the novel compounds (notably (113) and (106)) merit further investigation for use in solar cells.

Ongoing future research could focus on fabrication of inverted devices to circumvent the possibility of oxidation of the metal electrode. Energy levels and band gaps of the novel aza-BODIPYs should be investigated (e.g. via electrochemistry) in order to clarify the variations in performance of these materials in OPV devices and to help design the next generation of efficient donor materials. Finally, an investigation of charge carrier generation and recombination in aza-BODIPY based OPV devices would be the key to understanding how these compounds operate and how improved solar cells based on aza-BODIPY could be realized. Attention must also be paid to the broad question of stability of materials in solar cells. With appropriate designs of photovoltaic cells, and appropriate methods of device fabrication, solar cells based on organic materials such as aza-BODIPY could indeed make a significant contribution in the generation of clean energy and the reduction of greenhouse gas emission.

5.2 References

(1) Dennler, G.; Scharber, M. C.; Brabec, C. J. *Adv. Mater. (Weinheim, Ger.)* **2009**, *21*, 1323.

(2) Marsh, R. A.; Hodgkiss, J. M.; Albert-Seifried, S.; Friend, R. H. *Nano Lett*. **2010**, *10*, 923.

(3) Kim, J. Y.; Kim, S. H.; Lee, H. H.; Lee, K.; Ma, W.; Gong, X.; Heeger, A. J. *Advanced Materials* **2006**, *18*, 572.

(4) Yang, X.; Loos, J.; Veenstra, S. C.; Verhees, W. J. H.; Wienk, M. M.; Kroon, J. M.; Michels, M. A. J.; Janssen, R. A. J. *Nano Letters* **2005**, *5*, 579.

Appendix

Appendix

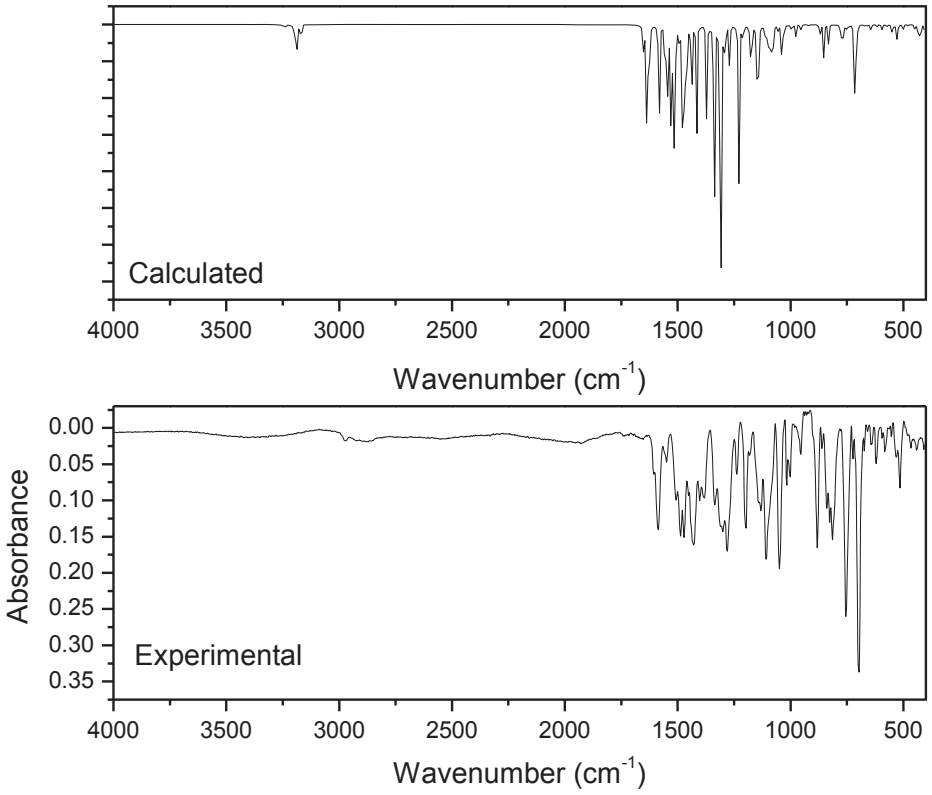

Figure A1 Comparison between the experimental and calculated Fourier transform infrared (FTIR) spectrum of compound (106).

Table A1 Experimental and calculated vibrational frequencies of compound (106) (Vibrational scaling factors = 0.96).

	υ (cm^{-1}) Experimental	**υ (cm^{-1}) Calculated**	**Difference**	**Assignment**
1	514	519	5	Very delocalized in-plane rocking
2	696	683	13	Phenyl rings out-of-plane rocking
3	754	747	7	Very delocalized in-plane rocking
4	813	814	1	Very delocalized in-plane rocking
5	879	880	1	Phenyl rings out-of-plane rocking
6	1016	1007	9	Phenyl rings out-of-plane rocking
7	1049	1031	18	Thiophene rings out-of-plane rocking
8	1105	1094	11	Thiophene-aza-BODIPY core in-plane rocking
9	1197	1191	6	Thiophene-aza-BODIPY core in-plane rocking
10	1236	1234	2	Triphenyl rings out-of-plane rocking
11	1278	1278	0	Very delocalized in-plane rocking
12	1402	1399	3	Thiophene-aza-BODIPY core in-plane rocking
13	1429	1428	1	Triphenyl rings out-of-plane rocking
14	1471	1481	10	aza-BODIPY core in-plane rocking
15	1587	1580	7	Phenyl rings in-plane rocking

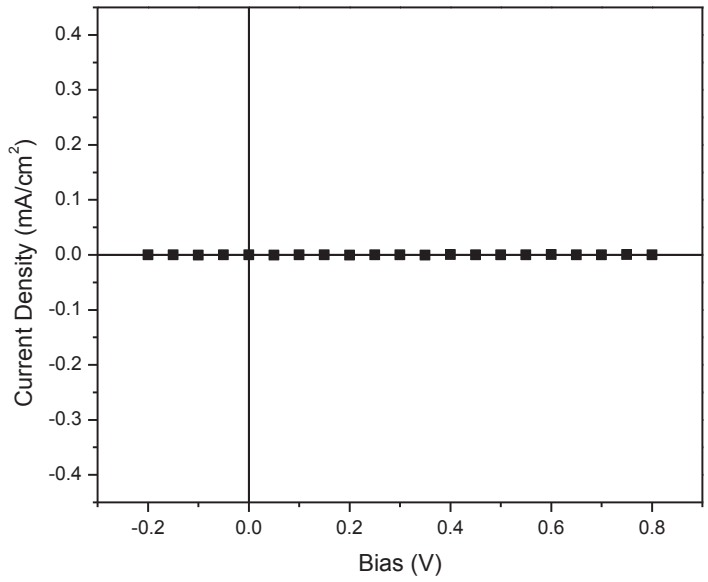

Figure A2 The current density-voltage (*J*-*V*) characteristics of device number (1) under AM 1.5G simulated 1 sun solar illumination.

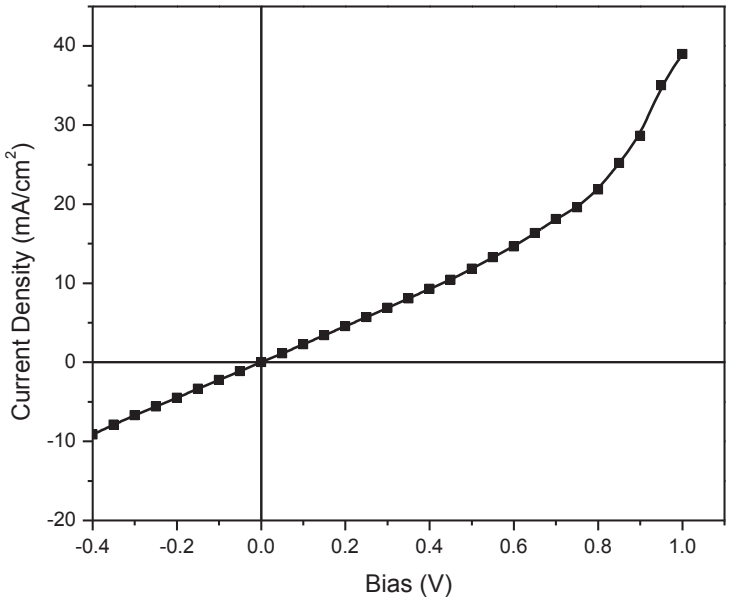

Figure A3 The current density-voltage (*J*-*V*) characteristics of device number (5) under AM 1.5G simulated 1 sun solar illumination.

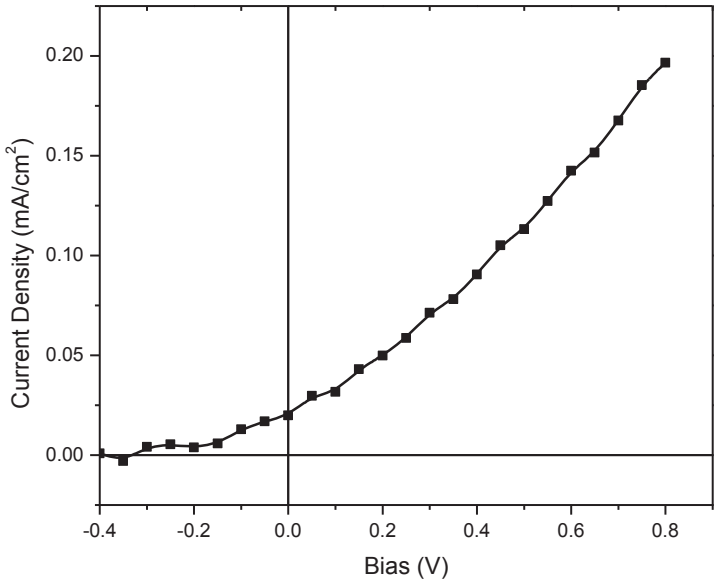

Figure A4 The current density-voltage (*J*-*V*) characteristics of device number (6) under AM 1.5G simulated 1 sun solar illumination.

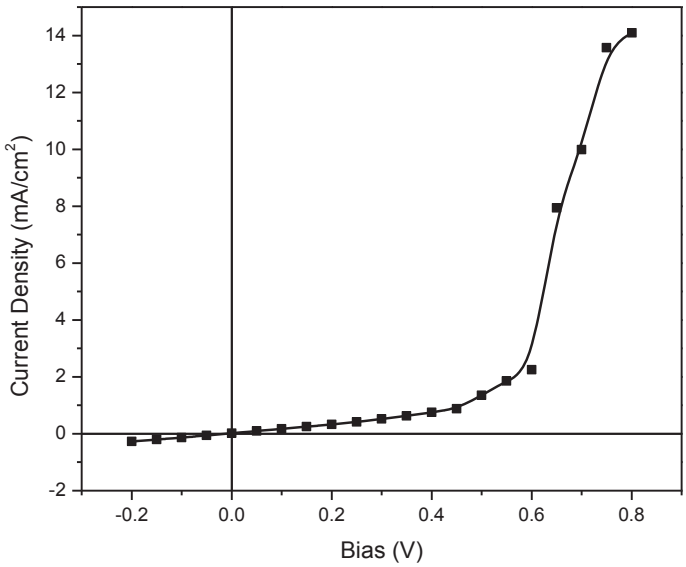

Figure A5 The current density-voltage (*J*-*V*) characteristics of device number (8) under AM 1.5G simulated 1 sun solar illumination.

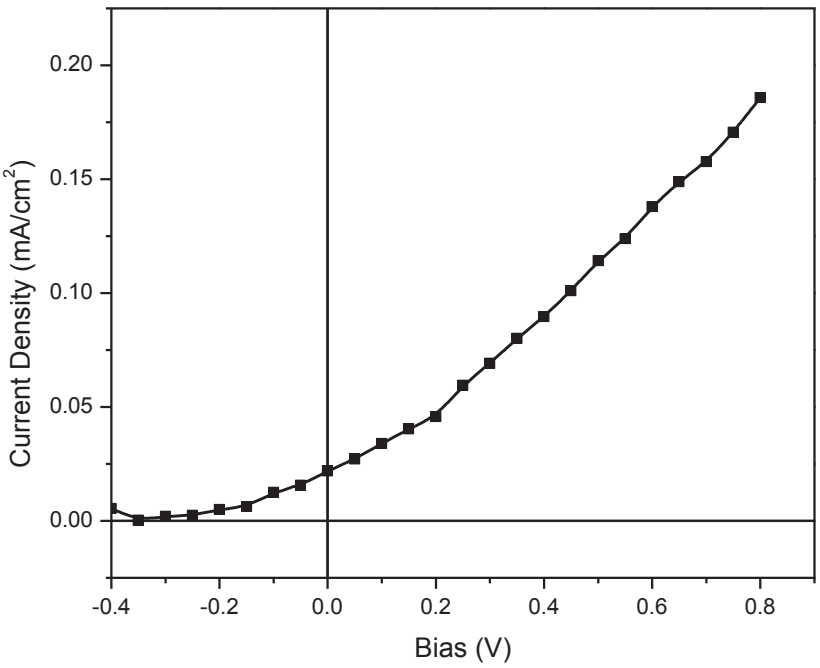

Figure A6 The current density-voltage (*J*-*V*) characteristics of device number (9) under AM 1.5G simulated 1 sun solar illumination.

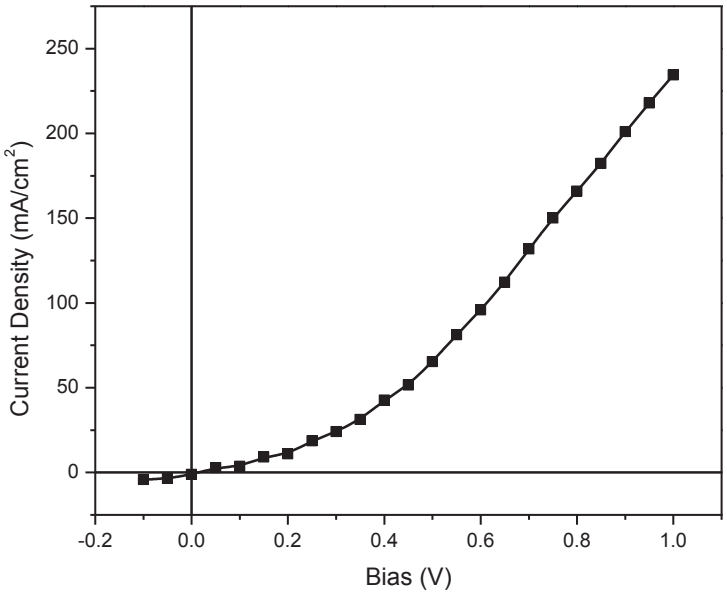

Figure A7 The current density-voltage (*J*-*V*) characteristics of device number (10) under AM 1.5G simulated 1 sun solar illumination.

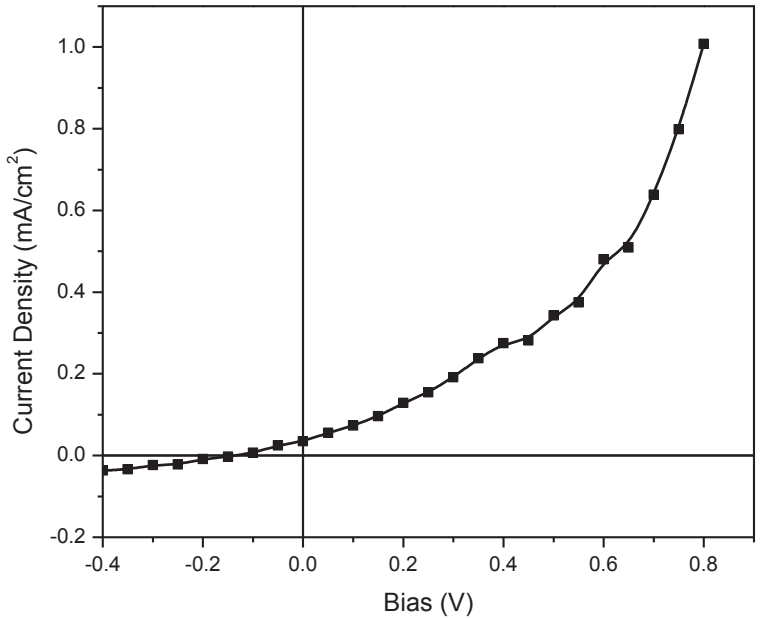

Figure A8 The current density-voltage (*J*-*V*) characteristics of device number (13) under AM 1.5G simulated 1 sun solar illumination.

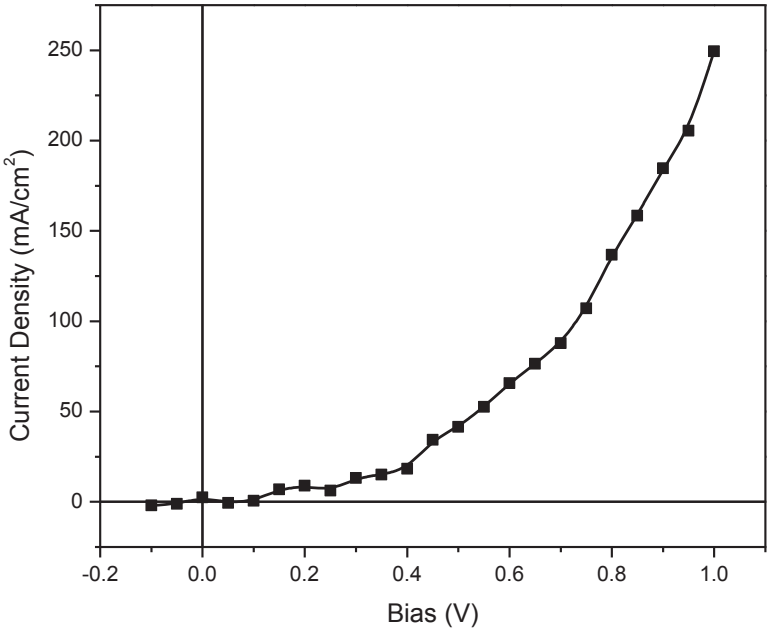

Figure A9 The current density-voltage (*J*-*V*) characteristics of device number (14) under AM 1.5G simulated 1 sun solar illumination.

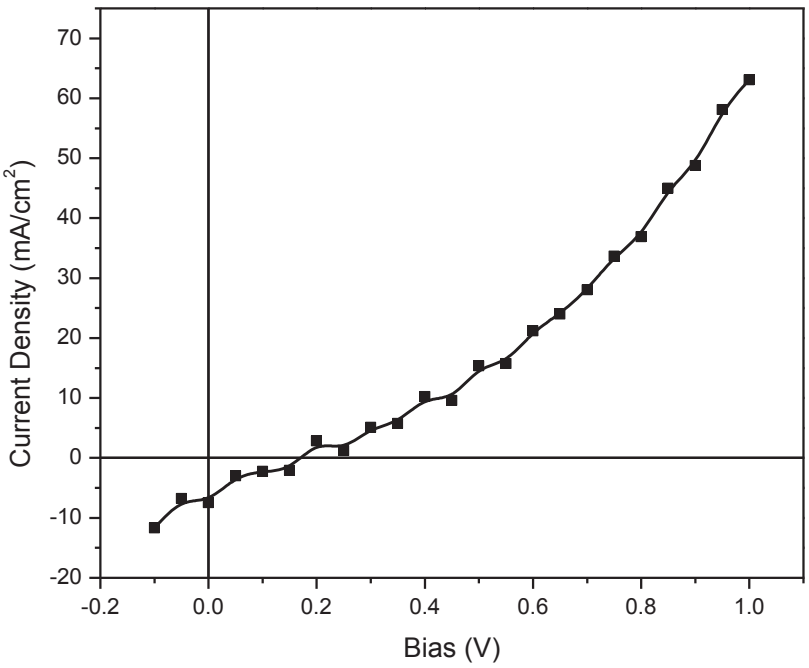

Figure A10 The current density-voltage (*J*-*V*) characteristics of device number (15) under AM 1.5G simulated 1 sun solar illumination.

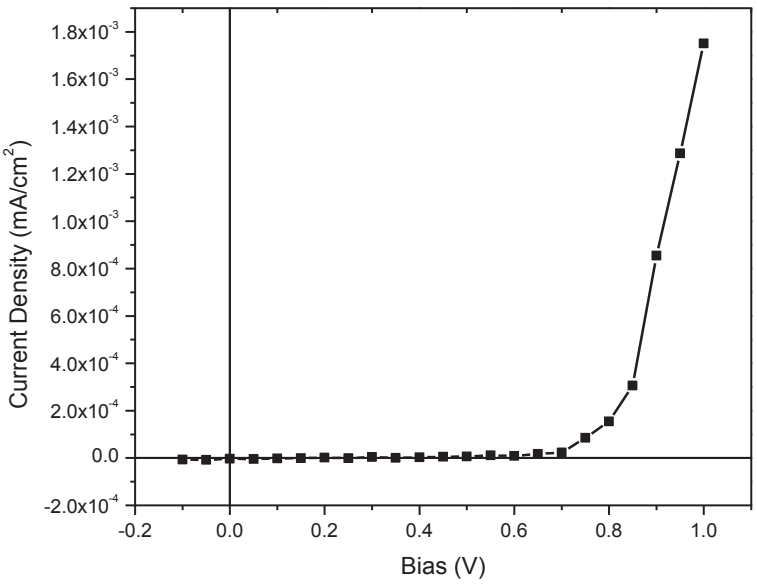

Figure A11 The current density-voltage (*J*-*V*) characteristics of device number (19) under AM 1.5G simulated 1 sun solar illumination.

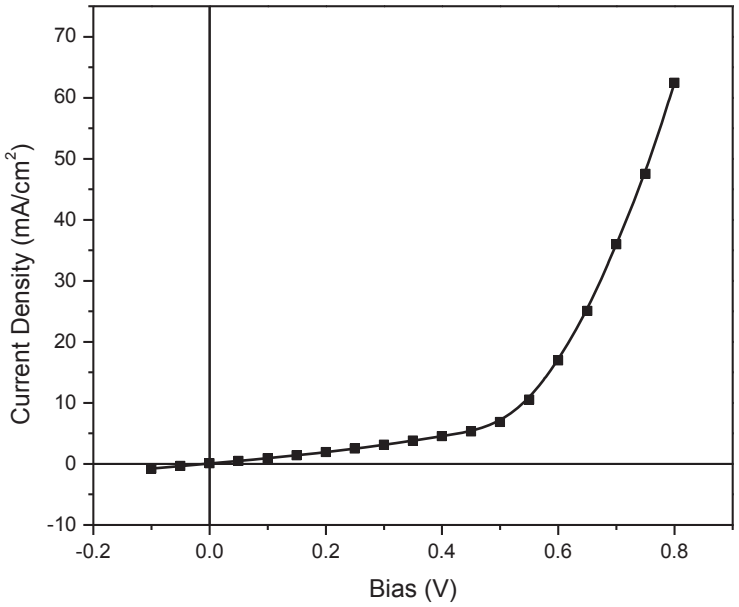

Figure A12 The current density-voltage (*J*-*V*) characteristics of device number (22) under AM 1.5G simulated 1 sun solar illumination.

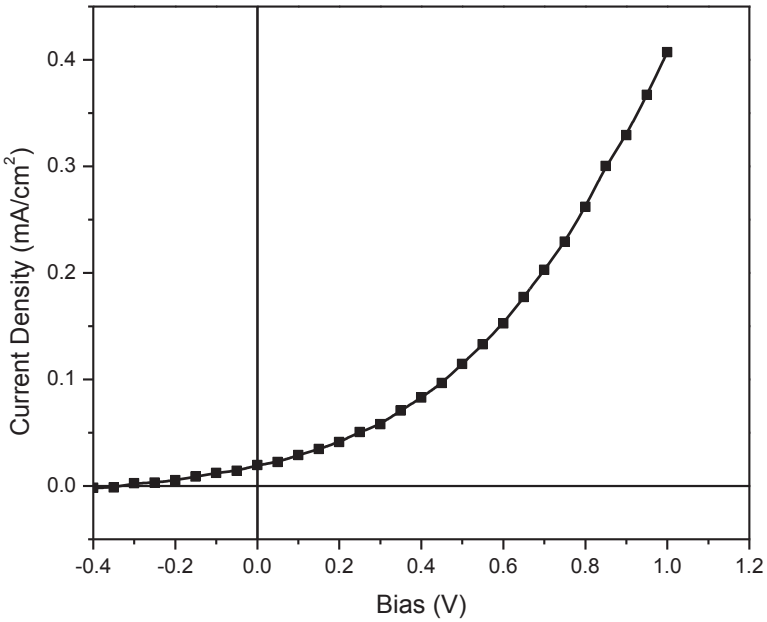

Figure A13 The current density-voltage (*J*-*V*) characteristics of device number (25) under AM 1.5G simulated 1 sun solar illumination.

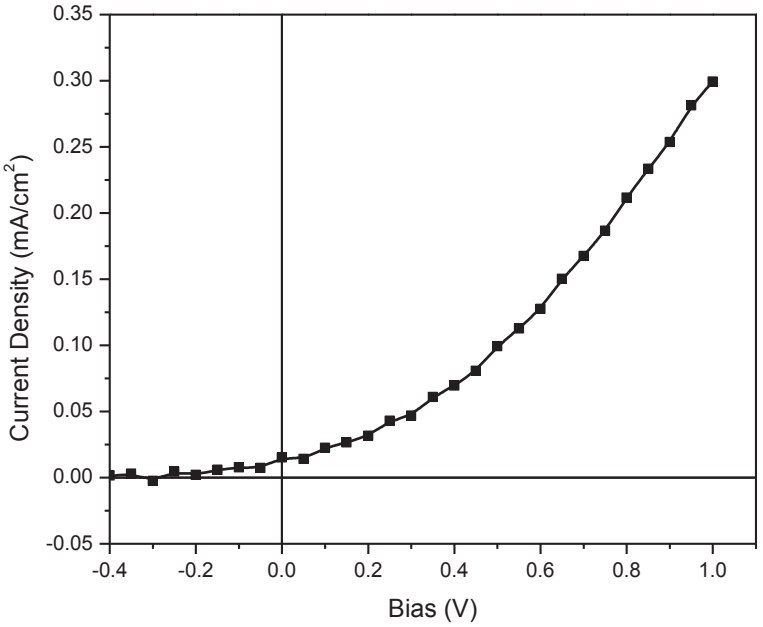

Figure A14 The current density-voltage (*J*-*V*) characteristics of device number (26) under AM 1.5G simulated 1 sun solar illumination.

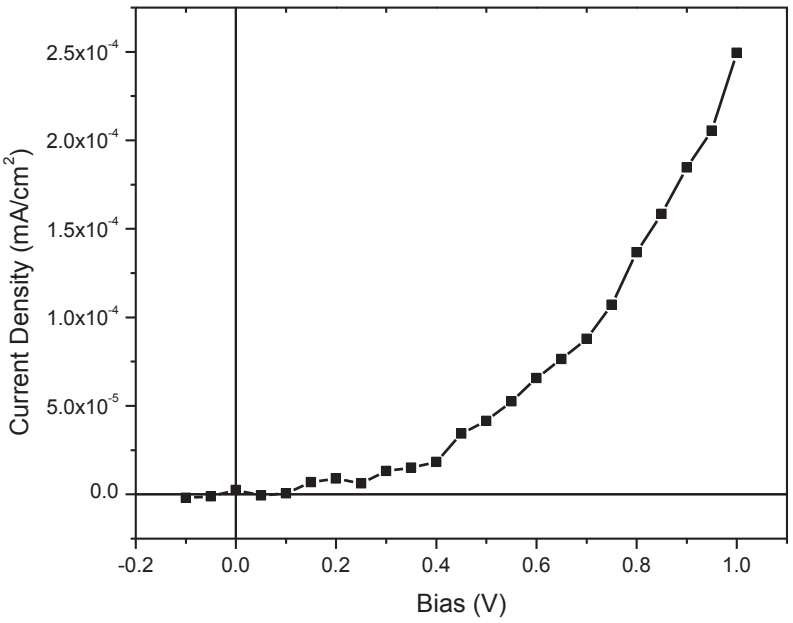

Figure A15 The current density-voltage (*J*-*V*) characteristics of device number (28) under AM 1.5G simulated 1 sun solar illumination.